STRESS IN ION-BEAM ASSISTED SILICON DIOXIDE AND TANTALUM PENTOXIDE THIN FILMS

Natalia SIROTKINA

The Institute for Materials Research,
School of Sciences,
University of Salford, Salford, UK

A thesis submitted for the degree of
Doctor of Philosophy, 2003

Table of Contents

List of Tables

Chapter II

Chapter III

Chapter V

List of Figures

Chapter III

Chapter IV

Chapter V

Appendix I

Acknowledgements

I would like to thank my supervisor, Professor John S. Colligon, for his guidance, help and encouragement throughout my studies. His scientific advice, emotional support and good sense of humour were very important for me.

I would also like to acknowledge the financial support of the Overseas Research Students Award Scheme and of Oxford Plasma Technology.

I am grateful to Dr. Reza Valizadeh for his help in experiment and the RBS measurements, Dr. Vlad Vishnyakov for the XTEM measurements and guidance thought the XTEM sample preparation, Dr. Gerd Lippold for the Raman measurements, Miss Katherine Whitehead for the AFM measurements, Dr. Michael Kuznetsov for the XPS measurements, Dr. Hamid Kheyrandish and Dr. Richard Pilkington for the opportunity of profilometry measurements.

I would like to thank my family and friends for their help and support.

And finally, I would like to express my deepest gratitude to my husband, Dr. Michael Yakushev, for his understanding and encouragement, support and belief in me. Without him this work would be impossible.

Declaration

The results of the stress and compositional measurements of the films, studied in this research, were also presented in the Reports (no. 1-4) for Oxford Plasma Technology by N.Sirotkina, R.Valizadeh and J.S. Colligon, Centre for Materials Science Research, Manchester Metropolitan University. All the data, included in these reports (such as reviews, experimental results and discussion), except RBS spectra collection and externally performed analysis (for example, Raman spectrometry), are the author's individual contribution.

Abstract

Ta_2O_5 and SiO_2 thin films, deposited at room temperature by ion-beam sputtering (IBS) and dual ion-beam sputtering (DIBS), and SiO_2 films, deposited by reactive e-beam evaporation and ion-assisted deposition, were studied. The energy (150-600 eV) and ion-to-atom arrival ratio (0.27-2.0) of assisting argon and oxygen ions were varied. Influence of deposition conditions (deposition system geometry, nature and amount of gas in the chamber, substrate cleaning and ion-assistance parameters) on films properties (stress, composition, refractive index n_{500nm} and extinction coefficient k_{500nm}) was investigated.

A scanning method, based on substrate curvature measurements by laser reflection and stress calculation using the Stoney equation, was employed.

RBS showed that stoichiometric Ta_2O_5 films contain impurities of Ar, Fe and Mo. Stoichiometric SiO_2 films also contain Ta impurity. Argon content increases with ion bombardment and, at maximum incorporation, argon bubbles are registered by TEM. XPS studies are complicated by surface contaminations and preferential sputtering.

Evaporated SiO_2 films show +100 MPa stress (+ is tensile, - compressive). With 300 eV Ar^+ bombardment, stress changes to -200 MPa, n_{500nm} decreases (1.56-1.49) and k_{500nm} increases (1.4×10^{-4}-1.8×10^{-3}).

Of all studied IBS conditions, stress in SiO_2 (-560 MPa) and Ta_2O_5 (-350 MPa) films depends only on sputtering gas species and oxygen entry point into the chamber.

With argon and oxygen bombardment stress in IBS SiO_2 films decreases to -380 MPa and below the stress measurement system resolution, respectively. While Ar^+ bombardment of Ta_2O_5 films leads to increase in stress to -490 MPa, the effect of oxygen assistance depends on ion energy. The observed behaviour was related to the total recoil density.

In DIBS SiO_2 and Ta_2O_5 films n_{500nm} varies in the region of 1.5-1.59 and 2.13-2.20 and k_{500nm} is below 5.5×10^{-3} and 8.5×10^{-3}, respectively. The refractive index exhibits complex behaviour, while k_{500nm} increases after initially decreasing to a minimum. The origins of the observed behaviour are unclear.

Chapter I

Introduction

Thin films and coatings are now widely used in different areas of industry. Desirable properties of thin films vary with every particular application. It is common to refer to each specific application as being a part of one (or more) of the several groups [Colligon, 1999]. A good example of one of such groups is the application of films and coatings for decorative purposes. The aim is to provide an attractive appearance of many modern products, including bath taps, watch cases and spectacles. Apart from noble metals, TiN, TiCN and TiZrN with an attractive golden colour, black-looking DLC and metallic CrN are commonly used. Another example is probably the most well-established group of thin film applications: coatings for the mechanical industry. TiN, TiC and Al_2O_3 are used as hard coatings for a variety of drills and cutters. Low friction films of oxynitrides and carbonitrides find their use in bearings and films of TaC and WC serve as wear-resistant coatings. Thin films can also be utilized in electronics and the electrical industry (contacts, components of electronic devices and as media storage in compact discs), the chemical industry (corrosion-resistant and catalytic coatings) and in biomedicine (biologically compatible coatings and films, favouring or prohibiting bacterial growth).

The main interest of the present study lies with the last group of applications: coatings for the optical industry. The use of optical properties of thin films probably started with the production of metallic films for mirrors and interferometers [Heavens, 1970; Heavens, 1991]. These simple designs have progressed to elaborate multilayered structures tailored to meet almost any special requirements. Narrow- and wide-band antireflection coatings, high reflection designs, edge and band-pass filters are only some of the examples of a wide variety of optical products, available today. The materials, used in modern designs, include not only metals, but also better performing and more durable dielectrics. Common dielectric design normally consists of a multilayered structure of alternating layers of low and high refractive index materials. One of the

examples of such designs is given by Wang et al. [Wang, 2000] and consists of 33 layers (TiO_2 and SiO_2 are used). Although the deposition of similar structures may not be a significant challenge [Heavens, 1991], there are other factors that need to be taken into account during the design stage [Rancourt, 1987], such as mechanical, environmental and chemical constraints.

It is known that the thin film deposition process leads to coatings, which are residually stressed. Quite often, the magnitude of these stresses is in the region of several hundreds to several thousands of MPa. Most properties, vital for future application of thin films, such as adhesion, integrity or temperature stability, are strongly influenced by film stresses. For example, excessive tensile stress can lead to crack formation in the coatings, while high-level compressive stress often causes film delamination. The influence of film stress is even more important in the case of "thick" multilayered structures, such as those used in optical applications. High stress in such a coating may result in its cracking or delamination not only during use, but also even at the production stage. Such stress can also change coating optical performance [Chen et al, 2001]. Another example of an undesirable effect of stress in films is the influence on the flatness of the substrate surface [Cao et al, 2001]. In optical applications alterations of the substrate shape are often unacceptable, as they can significantly change the performance of the designed products. In order to be able to avoid problems, caused by residual stresses in thin films, the origins and factors controlling stress evolution must be clearly understood.

The question of film stress analysis is almost a century old. The fundamental paper on film stress calculation from a curvature of the substrate was published in 1909 by Stoney [Stoney, 1909]. Since then many researchers have tried to improve, modify and adapt this equation to various particular cases. However, a slightly modified version of the Stoney equation, which takes into account the change in size transverse to the plane of substrate deflection, is still one of the easiest, most popular and quite accurate expressions for evaluation of thin film stress from the substrate curvature.

Using the Stoney equation (or modified Stoney equation) many researchers obtained a lot of data on residual stresses in thin films and analysed this data in order to find out the reasons behind residual stress generation. It was found that stress, as well as other film properties, depends on many parameters and, most importantly, can vary not only with the deposition process, but also with the particular conditions used during deposition (see, for example, [Ritter, 1981]). Up to now, no unified model is accepted, which would explain stress, its origins, magnitude and behaviour in any thin film

deposited by any given technique. Instead, several models are used, depending on film thickness (ranging from extremely thin non-continuous to thick films), film nature (metallic or not, crystalline or amorphous, dense or voided) or deposition process (evaporation, sputtering, various assisted depositions).

Two materials: silicon dioxide and tantalum pentoxide, have been studied in this research. These materials are commonly used in the optical industry. However, this is not their only application and these materials also find wide use for corrosion resistance layers and in the electronics and electrical, chemical and biological industries.

Silicon dioxide is probably the most abundant material for amorphous films with low refractive index. Tantalum pentoxide is a high refractive index material with a high (>20) dielectric constant, high chemical stability and weak absorption properties. Deposited under low temperatures, tantalum pentoxide is also amorphous [Chaneliere et al, 1998]. These properties are highly valued in the optical industry. For example, at present in the design of waveguides, an amorphous material is generally preferred. The reason of such choice is simple. In a waveguide a guided mode can be scattered due to imperfections and impurities in the high-refractive index coating, due to coating surface roughness or due to optical anisotropy of the grain boundaries, if a polycrystalline material is used [Mir et al, 1994]. Thus, if amorphous material is used, scatter due to optical anisotropy of the grain boundaries is avoided.

Thin films of silicon dioxide and tantalum pentoxide are often used together in various multilayered structures. Depending on the design, such structures can have various practical applications, for example, as WDM (Wave Division Multiplexing) and DWDM (Dense WDM) filters. Such filters are used in the telecommunication industry to increase the transmission capacity of fibre optic cables. In order to meet modern requirements, these filters should consist of in excess of a 100 layers (see, for example, Web 1), which increases the importance of mechanical constraints put in by the residual stresses in each layer on the total filter design and production. In the optical industry Ta_2O_5 films are primarily used in conjunction with SiO_2 films. However, SiO_2 is also often used with other materials, for example, TiO_2 [Chen et al, 2001] in narrow bandpass filters or HfO_2 [Torchio et al, 2002] in UV mirrors.

Thin films of silicon dioxide and tantalum pentoxide can be deposited using various techniques, such as CVD, RF sputtering or reactive low voltage ion plating. In optical industry popular deposition methods include evaporation and sputtering. It is known (see, for example, [Martin and Netterfield, 1986]) that films, deposited by evaporation, often have poor properties (low density, large number of voids, deviations from desired

refractive index) and exhibit poor performance (reduced lifetimes, environmental instability), all of which is often related to the low mobility and low energy (0.05-0.1 eV) of arriving film atoms. Therefore, improvements in the film characteristics are needed. Often these improvements are carried out by assisting the deposition process, for example, by an ion beam. In this case, a range of deposition parameters can be found, which leads to the coating with optimal characteristics, such as low stress levels, or high film density.

In order to improve film characteristics, a different deposition method, namely, ion-beam sputtering, may be used. Ion-beam sputtered films often exhibit properties and performance, superior to that of evaporated films due to much higher mobility and energy (order of 7 eV) of arriving film atoms. However, even in this case ion beam assistance during deposition may be beneficial. Here ion assistance may serve as an additional tool for achievement of and control over the desired film properties and thus, film performance.

In certain cases film properties can be modified not only by ion bombardment, but also by changes in other deposition conditions, such as pressure or geometry of the deposition system. For example, changes in deposition pressure can lead to increase in the porosity of the coating, which, in turn, can lead to changes in the refractive index of the material and decrease in environmental stability of the coating. Therefore, the influence of these parameters on film also has to be assessed.

The aim of the present study is to develop an experimental method, which will allow *in-situ* stress measurements to be made during film deposition. Using this method, stress in thin silicon dioxide and tantalum pentoxide thin films, deposited by evaporation, ion-beam sputtering and ion-beam assisted variations of these techniques, and stress behaviour with deposition conditions will be studied. From the results obtained, a model, linking parameters of ion assisted ion-beam sputtering deposition, with the resultant stress, will be developed. In addition, other film properties, especially composition and optical performance, will be determined.

This thesis consists of seven chapters and an appendix. In Chapter II a literature overview of work done in the last 20 years by other researchers on SiO_2 and Ta_2O_5 optical thin films is presented. The results of both stress and optical constants measurements are reviewed. Although films, deposited by various techniques are considered, attention is drawn to coatings, produced with ion beam sputtering, e-beam evaporation and ion-assisted deposition as these are the methods used in this research.

Chapter III of this thesis is a literature overview on the question of stresses in thin films and their origins, stress measurement techniques and different formulae for stress evaluation. Various models, explaining stress behaviour in sputtered, evaporated and ion-assisted films are reviewed.

In Chapter IV the theory of interaction of ions with the surface of a solid is briefly presented. Background information on the physical processes taking place during sputtering and ion bombardment is given in this chapter.

In Chapter V a detailed description of the experimental part of the work is given. This includes information on the experimental apparatus for deposition and stress measurements, on sample preparation and on conditions during analysis.

Results of the experimental measurements, their analysis and a model of stress behaviour with ion bombardment are presented in Chapter VI. Conclusions and recommendations for future work are presented in Chapter VII. In the Appendix section background information and a brief description of analysis techniques, used in this research, are given.

References

Cao K., Liu W., Talghader J.J., J. Microelectromech. Systems, **10 (3)**, 409, (2001)

Chaneliere C., Autran J.L., Devine R.A.B., Balland B., Mater. Sci. Eng., **R 22**, 269, (1998)

Chen T.C., Kuo J.-I., Lee W.-L., and Lee C.-C., Jpn. J. Appl. Phys., part I, **40 (6A)**, 4087, (2001)

Colligon J.S., *Physical Vapor Deposition* In *Non-Equilibrium Processing of Materials*, ed. by C. Suryanarayana, Pergamon Materials Series, **2**, 1999

Heavens O.S., *Optical Properties of Thin Solid Films*, Dover Publications, New York, 1991

Heavens O.S., *Thin Film Physics*, Methuen & Co., Ltd., London, 1970

Martin P.J. and Netterfield R.P., *Optical Films Produced by Ion-Based Techniques*, in *Progress in Optics XXIII*, ed. by E. Wolf, Elsevier Sci. Publishers B.V., 1986

Mir J.M., Agostinelli J.A., J. Vac. Sci. Technol., **A 12 (4)**, 1439, (1994)

Rancourt J.D., *Optical Thin Films: Users' Handbook*, Macmillan Publishing Company, New York, London, 1987

Ritter E., Appl. Opt., **20 (1)**, 21, (1981)

Stoney G.G., Proc. R. Soc. London, **A 82**, 172, (1909)

Torchio P., Gatto A., Alvisi M., Albrand G., Kaiser N., Amra C., Applied Optics, **41 (16)**, 3256, (2002)

Wang, J. Vac. Sci. Technol., **A 18 (3)**, 933, (2000)

Web 1: http://www.sspectra.com/designs/wdm_family.html

Chapter II

Stresses and Optical Properties of Silicon Dioxide and Tantalum Pentoxide Films

This chapter is devoted to an overview of published works on stress and optical properties of thin silicon dioxide and tantalum pentoxide films, deposited by various techniques. The review is limited to work, published within the last 20 years. Values of optical constants and stress are given together with the proposed explanations and models of the behaviour of these properties.

The first part of this chapter treats silicon dioxide films. In the second part of this chapter optical properties and stress in tantalum pentoxide films are reviewed.

2.1. Silicon Dioxide Films

Silicon dioxide (SiO_2) is one of the most popular and, probably, one of the most well studied materials in the electronics and optical industries. In electronics, thin films of SiO_2 are used as insulating layers in many components. In the optical industry films of SiO_2 are used as low refractive index layers in filters, mirrors, polarisers, etc.

Probably the first and easiest way of obtaining SiO_2 films is thermal oxidation. Films, acquired in this manner, usually have such high quality that the properties of films, deposited by other techniques are compared to those prepared by thermal oxidation. However, this process normally requires the use of temperatures in excess of 1000 ^{0}C [Blech and Cohen, 1982]. With the advances in the field of polymer substrate materials, such levels of temperature are often unacceptable. Therefore, many attempts have been made to deposit high quality silicon dioxide films at reduced or low temperatures. Various deposition methods were used for this purpose. A lot of work has been done on chemical vapour deposition (CVD), evaporation, sputtering and ion plating. Properties of the films, deposited by each technique, will be reviewed in the following pages.

In CVD, gases containing silicon (e.g., SiH_4) and oxygen (e.g., N_2O), undiluted or diluted with a carrier gas (e.g., He or H_2), are supplied into the chamber, where they react to produce a film on a substrate, which often needs to be heated up to approximately 350 ^{0}C [Gupta and Parsons, 2000]. In order to influence film properties plasma-enhanced CVD (PECVD) techniques are often used. Here plasma is generated and the growing film is subjected to energetic particle bombardment. Film properties will strongly depend on the precursors used in the deposition (this defines the composition) and the plasma-surface interactions (this defines properties such as stress and density) [Martinu and Poitras, 2000]. Among other effects, the PECVD process can lead to changes in stress from tensile to compressive [Rats et al, 1999]. However, even films deposited by PECVD, sometimes have poor quality, low density and a high number of voids. This often manifests itself in the film behaviour during transition from vacuum to ambient air and ageing. Stress levels and optical properties, measured in air, and the difference between the values, measured in air and in vacuum, can be related to the surface reactivity [Haque et al, 1997] or amount of water vapour, incorporated into the film bulk. Also, several studies [Haque et al, 1997; Park et al, 1999] showed that the compressive component of stress increases with ageing. It is believed that the stress behaviour during ageing or annealing is related to the film surface structure and behaviour of hydrogen-bonded water and Si-H and Si-OH bonds. It was found that ageing stress consists of reversible and irreversible components. The influence of water dipole interactions and water absorption and desorption leads to a reversible stress component, which depends on the humidity of the environment. The irreversible stress component is linked to the changes in oxide internal bonding [Park et al, 1999].

Another way of influencing CVD and PECVD film properties is by doping. Several elements, for example, hydrogen [Martinu and Poitras, 2000] or fluorine [Bazylenko et al, 1996], can be used. In many cases refractive index of hydrogen-doped films is higher that that of bulk silicon dioxide or thermally grown films [Martinu and Poitras, 2000]. Optical properties of these films are commonly linked to film density, hydrogen incorporation, and mean bonding angle for Si-O-Si bonds. Small-angle Si-O-Si bonds are often associated with high stress levels in the films. The stress can be relieved by breaking these bonds, which further can be used for reactions with water present in the ambient [Martinu and Poitras, 2000]. In case of SiO_2:F low-refractive index films can be obtained. Film properties will depend on the fluorine flow rate into the reaction chamber. In their work, Bazylenko et al [Bazylenko et al, 1996] found that addition of fluorine leads to an initial decrease in refractive index to 1.44 followed by a

sharp increase to approx. 1.5. Stress initially decreases with fluorine incorporation into the film. At high fluorine flow rate in the deposition chamber stress again increases, which is explained by a deviation from the stoichiometry in the SiO_2 films. In general, it is believed that the decrease in refractive index is due to relaxation of Si-O-Si bonds, a decrease in density and an increase in void population in the film [Martinu and Poitras, 2000]. A summary of properties of SiO_2 films, deposited by thermal oxidation, CVD and PECVD, is given in Table 2.1.

Another well-established and widely used technique of SiO_2 film deposition is evaporation. The popularity of this technique is based on its relative ease and high film growth rates. Films of SiO_2 can be obtained either by evaporating SiO_2 material or by a reactive process of Si metal or SiO evaporation in the presence of oxygen. However, it is known that evaporated films usually have low density and voided structure [see, for example, Souche et al, 1998]. Upon contact with air such films tend to absorb a lot of moisture, which changes their optical properties and stress. For example, water absorption causes refractive index of the films and film stress to increase [Leplan et al, 1995]. Water incorporation into the film leads to the increase in film refractive index, because water has a higher index of 1.33 relative to air [Sankur and Gunning, 1989]. In fact, it was proposed that for SiO_2 films the total stress should consist of extrinsic, intrinsic and water-absorption induced components [Leplan et al, 1996]. Water-absorption-induced stress, in turn, consists of two components. The first component is the stress due to the water dipole incorporation into the film pores and their interactions. This stress may be reversible when the sample is placed in the vacuum. Moreover, as the film pore size decreases, the efficiency of absorbed water molecule interactions increases, reaches its maximum and then decreases [Leplan et al, 1995]. The second component is irreversible and is due to the chemical reaction between film material and incorporated water vapour (formation of Si-OH bonds in the case of SiO_2 films). Si-OH bonds can be formed either by saturation of dangling bonds or by breaking Si-O-Si bonds. It is believed that evaporated SiO_2 films can consist of a Si-O-Si bond lattice, with some amount of dissociated or weakened bonds. Reaction with hydrogen results in the formation of silicic acids, which results in lattice shrinkage and thus in compressive residual stress reduction. Silicic acids contain HO-Si-OH dipole groups, and their interaction can further lead to the formation of tensile stress. Another explanation for water-absorption-induced stress was proposed by Sankur and Gunning [Sankur and Gunning, 1989], who stated that this type of stress depends on the chemical state, pore size and surface area of the film columns. The main driving mechanism is believed to be

Table 2.1. Properties of SiO_2 films, prepared by thermal oxidation, CVD and PECVD.

Deposition Technique	Subst-rate	Refractive Index, n	Extinct. Coeff., k	Wave-length, nm	Stress, MPa	References
Thermal oxidation		1.459				[Bazylenko et al, 1996]
Thermal oxidation	Si				340-370 in compression	[Blech and Cohen, 1982]
CVD	Si				120 in compression	[Park et al, 1999]
CVD at 250 ^{0}C	Si				130 in tension	[Blech and Cohen, 1982]
CVD	Si				600 in compression	[Ambree et al, 1993]
CVD	GaAs				450 in compression	[Ambree et al, 1993]
PECVD	Fused silica or BK7	1.455 ± 0.002	<0.001	633		[Beck et al, 1998]
PECVD	Si	1.465-1.466		633	Approx. 195 in compression	[Bazylenko et al. 1996]
PECVD, at 100-350 ^{0}C	Si	1.43-1.50, depending on gases and temp.		632.8		[Gupta and Parsons, 2000]
PECVD, at 250-350 ^{0}C	Si				Approx. 5 to 50 in compression, depending on temp. and decreasing with film thickness	[Haque et al, 1997]
PECVD	Si	1.456			70 ± 15 in compression	[Hofrichter et al, 2000]
PECVD		1.35-1.5		550		[Martinu and Poitras, 2000]

PECVD,incr. E_i	Si			
PECVD,hydrogen-doped films		Approx. 1.42-1.49		550
PECVD, fluorine-doped films	Si	1.44-1.5, depending on fluorine flow		633
PECVD, fluorine-doped films		1.41-1.43		550

	from 50 in tension to 80 in compr. Approx. 125 in tension to 125 in compression From 45 to 190 in compression, depending on fluorine flow	[Rats et al, 1999] [Martinu and Poitras, 2000] [Bazylenko et al. 1996] [Martinu and Poitras, 2000]

the decrease in the total energy (strain, surface and dipole components) of the stressed film/substrate system.

Several other models of intrinsic stress generation have been proposed for explanation of stresses in SiO_2 films [Leplan et al, 1995]. The oxidation model (oxidation of SiO and Si) explains formation of compressive stress, as oxidation results in a volume increase. Compressive stress may also be generated by strongly bound water molecules. The model by Klockholm (the "buried layer" model) has been criticised, since the deposition to melting point temperature ratio is low.

It was found that stress in thin films of SiO_2 does not depend on evaporation flux angle or film thickness [Leplan et al, 1995; Leplan et al, 1996]. However, stress and other film properties can be significantly modified by changes in pressure in the deposition chamber, substrate temperature and concurrent ion bombardment, all of which can lead to improvements in film microstructure [Martin et al, 1983]. It was found [Leplan et al, 1995] that with increase in oxygen partial pressure in the chamber stress becomes more tensile, which was related to decrease in film density. However, a study by Sankur and Gunning [Sankur and Gunning, 1989] showed that for water absorption into the film it is not the oxygen partial pressure, but the total pressure during deposition, which is a factor of importance. It was also concluded that, apart from film atom mobility and thus film density, film stoichiometry and film surface chemical state are important. Increase in substrate temperature up to approx. 300 ^{0}C, leads to decrease in water absorption into the film [Sankur and Gunning, 1989] and increase in film compressive stress [Leplan et al, 1995].

Growth of evaporated films can be assisted during deposition with a flux of energetic ions or radicals. Usually, Ar or oxygen gases or their mixtures are chosen for such purposes. Studies show, that Ar ion bombardment can lead to increased stability of film optical properties, but also to an increase in the extinction coefficient due to preferential oxygen sputtering from the film [Martin et al, 1983]. Such problems can be avoided by deposition in the presence of oxygen. Oxygen bombardment also leads to a decrease of the influence of the ambient humidity or annealing on the film optical properties due to the increase in film density, while also causing increased values of compressive stress in the coatings [Sankur and Gunning, 1989]. The influence of O_2 and Ar bombardment was also studied by Robic et al [Robic et al, 1996]. It was found that, with increase in normalised momentum of bombardment, film density, refractive index and compressive stress increase linearly. The initial state of compressive stress (10 MPa) for non-assisted films is believed to result from oxidation of SiO species, produced during evaporation

of SiO_2 material. As the density of the initial film is low, bombardment-induced defects are not the main compressive stress generation mechanism. Instead, it is believed that higher stress levels in assisted films (364 MPa for O_2 bombardment and 470 MPa for Ar bombardment) are due to film densification.

The behaviour of SiO_2 films, deposited by e-beam evaporation of Si material and simultaneous substrate irradiation with atomic oxygen radical flux or atomic oxygen radical and oxygen ions flux, was studied by Harada et al [Harada et al, 2001]. It was found that SiO_2 film refractive index and extinction coefficient did not depend on the type of irradiation during deposition, irradiation flux or ion energy.

Film stress and properties will depend on the amount of ion bombardment the film experiences. Souche et al [Souche et al, 1998] studied SiO_2 films bombarded with a mixture of Ar and oxygen ions and found that, due to ion bombardment, there are two regions of densification behaviour with increase in average deposited energy. In the first region, porous film structure is destroyed, which leads to denser films and an increase in the film refractive index. However, in this region some pores still remain in the film, so changes in the refractive index are observed upon contact with air. With further increase in average deposition energy a threshold value (approx. 35-40 eV) is reached. Above this value densification processes saturate. Refractive index in this region increases slowly and is linearly dependent on the average deposition energy. Upon exposure to air for a large amount of average deposition energy supplied to the film, no changes in the refractive index are observed. Such behaviour may be explained if the notion of oriented capillary pores extending throughout the layer, similar to the notion of columns in the case of a crystalline medium, is presumed. Then, it can be said that, below the threshold energy, capillary pores are destroyed. However, small pores remain to be filled by water after exposure to air. The distribution of small pores is believed to be found in films, deposited at energies above threshold but these pores remain empty in air. Above threshold energy another mechanism, namely, forward recoil implantation, starts to dominate, causing small changes in refractive index and density. Thus, for deposition above the threshold energy SiO_2 films in air can be represented by a dense layer with a certain number of small empty pores.

It is known that ion bombardment can lead to improvements in film properties. However, excessive ion bombardment can etch or mill the coating, thus resulting in decreased film thickness, increased surface roughness and modification of the layer by preferential sputtering or decomposition. The question of optimum bombardment conditions for obtaining films with best properties, is treated by McNeil et al [McNeil et

al, 1984]. McNeil et al treated SiO_2 films, deposited onto fused silica substrates by resistively heated SiO evaporation, with 30-500 eV O^+/O_2^+ ions of 0-1 mA/cm^2 current density. It has been found that a threshold current density exists. Below this value of current density the film optical properties improved. As the current density reached the threshold value, optical properties of the SiO_2 layer reached a maximum which approached those of the fused silica substrate. Above the threshold value the optical properties of the film degraded. Such behaviour was explained by a balance of two mechanisms, both depending on the amount of ion bombardment. First is the mechanism of full oxidation of sub-oxides, present in the film, resulting in improvement of optical properties. Second, is the mechanism of oxygen preferential sputtering, resulting in degradation of optical properties. However, at lower energies the effect of the second mechanism it less than expected on the basis of preferential sputtering. The value of the threshold current density depends on the energy of bombarding ions, so that with increase in energy the threshold value of current density decreases. For low-energy bombardment optical properties are closer to those of the substrate and, with increase in current density, degrade slower than in the case of high-energy bombardment. Experiments on the effects of an increased substrate temperature showed that optical properties of films, deposited under ion bombardment and under substrate temperatures of 250 ^0C, are comparable. SiO_2 films were found to incorporate more hydrogen with increase in ion bombardment. Stress measurements, performed by the interferometry technique showed SiO_2 films to be under compressive stress, which is reduced by ion bombardment. It was also concluded that substrate temperature and ion energy have little effect on stress values, which ranged from 600 to 1900 MPa. A summary of SiO_2 film properties, deposited by evaporation and ion-assisted deposition, can be found in Table 2.2.

Many evaporated films possess low stress levels [Takahashi et al, 1994]. However, this is explained by the low density of such films, which leads to degradation of their properties and poor environmental stability. Therefore, high-quality high-density films are preferred. Such films can be deposited by sputtering. Different types of sputtering have been employed in SiO_2 film deposition. Probably the most popular is RF magnetron sputtering [see, for example, Wu and Chiou, 1996], although other methods, like ion-beam [Nomura and Ogawa, 1992], mid-frequency or direct current reactive sputtering [Vergoehl et al, 1999], sputtering-type electron cyclotron resonance microwave plasma deposition [Jia et al, 2000] or indirectly reactive sputtering technique, involving pure Si sputtering followed by oxidation [Song et al, 2000], can

Table 2.2. Properties of SiO_2 films, prepared by evaporation and ion-assisted deposition.

Deposition Technique	Deposition Conditions	Refractive Index, n	Extinct. Coeff., k	Wave-length, nm	Stress, MPa	References
Evaporation	SiO_2 source	1.478		550	200 in compression	[Selhofer Mueller, 1999]
Evaporation	SiO_2 source; O_2 (0.2-4)x10^{-4} mbar				177-192 in compr. at 2x10^{-5} mbar; 25-37 in compr. at O_2 part. press. 2x10^{-4} mbar	[Leplan et al, 1995]
Evaporation	Si substr. temp. from 20 to 285 ^{0}C; O_2 (0.2-4)x10^{-4} mbar				from 500 in compr. to 100 in tension, depending on oxygen pressure, substr. temp. and ageing time	[Leplan et al, 1996]; [Leplan et al, 1995]
IAD	Atomic oxygen radical flux, or atomic oxygen radical and O ions (0-800 eV) flux	1.48	1.3x10^{-3}	600		[Harada et al, 2001]
IAD	SiO_2 source; oxygen or argon ion bombardment	1.44-1.48	<10^{-4}	600	10 in compr. for non-assisted films; up to 364 in compr. for oxygen-bomb. films; up to 470 in compr. for Ar bomb.	[Robic et al, 1996]

IAD	600 eV Ar bombardment		$<2x10^{-4}$ non-assist.; $<2x10^{-4}$ to 10^{-3} assist.
IAD	SiO_2 source; Ar and O_2 mixture for ion bomb. at 150 to 300 eV	1.4-1.49, depending on depos. conditions	
IAD	SiO source, presence of O_2; limited number of films under oxygen ion bomb.300-500 eV;glass substr. at 100-300 ^0C	1.45	
IAD	SiO source, fused silica substr.; bomb. with 30-500 eV O^+/O_2^+ ions		

		[Martin et al, 1983]
600		[Souche et al, 1998]
	0 to approx. 150 in compression, depending on deposition conditions and ambient	[Sankur and Gunning, 1989]
	600-1900 in compr.	[McNeil et al, 1984]

also be used. Both oxide targets and Si targets (for reactive processes) can be used. Substrate temperature, substrate bias voltage [see, for example, Kupfer et al, 1999] or gases, present in the chamber [Takahashi et al, 1994; Takahashi et al, 1996] can also be changed.

A study of interfacial stresses in SiO_2 films on Si was presented by Jia et al [Jia et al, 2000]. It is believed that interfacial stress in thin SiO_2 layers on Si are due to the difference in lengths (3.01 A for Si-Si and 1.62 A for Si-O) and angles of bonds. Moreover, oxygen presence results in the formation of Si-O bonds, which leads to positive polarisation of Si-Si bonds and thus, distortions at the film-substrate interface. The influence of these distortions and thus, interfacial stress, decreases with increase in film thickness. It was found that for a critical film thickness of 22.7 nm the interfacial stress becomes negligible and other effects, like densification, become responsible for the stress levels, measured in the films.

The study [Kupfer et al, 1999] of SiO_2 films, RF magnetron sputtered from a SiO_2 target onto a Si substrate, held at 100 to 400 ^{0}C, showed that total film stress does not vary significantly under these conditions. If thermal stresses are taken into account and only intrinsic stresses are studied, it can be concluded that with the increase in substrate temperature the intrinsic stress decreases. It is proposed that such behaviour is due to reduction of water incorporation into the films at high temperatures.

Total pressure during deposition, as well as composition of gases, present in the chamber, is a factor of importance in the SiO_2 film growth. For example [Song et al, 2000], for films, deposited by an indirect reactive sputtering technique, it was found that the refractive index changes from 1.449 to 1.472 with changes in pressure from 0.36 to 0.23 Pa. Such behaviour was related to the density and amount of voids in the films. Another study [Wu and Chiou, 1996] was performed for films, deposited at the same total pressure and sputtering power, but different levels of oxygen, present in the chamber ($O_2/(Ar+O_2)$ was varied between 10 and 20 %). It was found that, with changes in oxygen concentration in the sputtering gas mixture (10 and 20 %), the film refractive index changes from 1.453 to 1.460. Such an effect can be attributed either to stoichiometry or density changes. It is known that Si-rich films have higher refractive index. This can be understood, if one takes into account, that the refractive index of amorphous silicon is greater than 2, thus indices of Si-rich and O-deficient layers increase [Nomura and Ogawa, 1992]. However, Wu and Chiou [Wu and Chiou, 1996] found that all films are stoichiometric. Thus, the refractive index changes must result

from density changes. Therefore, it was concluded that increased oxygen presence in the chamber leads to an increase in film density and refractive index.

It is known that during most types of sputtering, the growing film is subjected to a considerable amount of energetic particle bombardment, which will not only influence film properties, such as stress or optical constants, but also can lead to total film re-sputtering [Kupfer et al, 1999]. One of the examples of ion bombardment influence on film properties is seen from the work by Howson et al [Howson et al, 1997], who have found that, depending on the amount of argon bombardment, compressive stress in SiO_2 films changes from approx. 200 to approx. 400 MPa. It was also found that the same deposition conditions are required in order to obtain films with maximum stress and maximum refractive index (equal to bulk) and such behaviour was ascribed to film densification processes. Konopka et al [Konopka et al, 1999] deposited films by bipolar pulsed DC sputtering under various total pressures (7.5 to 15 mTorr) and sputtering powers (350-700 Watt). It was found that with increase in total pressure the refractive index decreased within the range of 1.38-1.46. With an increase in power at 7.5 and 10 mTorr pressures the refractive index decreased, while at 15 mTorr the refractive index increased. For SiO_2 films the compressive stress ranged from less than 100 to approx. 1200 MPa. The stress became more tensile with increase in total pressure or sputtering power.

Sputtered films can have high quality and reasonable growth rates, but also can possess high stress levels. One of the ways to decrease the stress levels in sputtered coatings without reduction of growth rate is to use a mixture of Ar and other gases for sputtering. Takahashi et al [Takahashi et al, 1994] studied SiO_2 films on Si substrates deposited by RF magnetron sputtering of a fused SiO_2 target in Ar/H_2, Ar/O_2 or N_2 ambient. For films, deposited in an Ar/H_2 environment, slightly under-stoichiometric composition, presence of hydrogen due to Si-H bonds and absence of Si-OH bonds were found. It was found that for an Ar/O_2 mixture stress does not depend on sputtering gas composition. In the case of an Ar/H_2 mixture stress levels decreases with increasing H_2 content up to approx. 20%. Further increase in hydrogen content did not influence the stress levels, but resulted in decreasing growth rates. Overall, stress levels in films, sputtered in an Ar/H_2 mixture were lower than in those, sputtered in an Ar/O_2 mixture. On the other hand, for the same conditions the growth rate increased when hydrogen was used instead of oxygen in the mixture. It was found and supported by later experiments [Takahashi et al, 1996], that stress in the films increased with increase in sputtering power and decreased with increase in total working pressure (0.2-1.5 Pa).

It is believed that incorporation of Ar into the film can influence film stress levels. Takahashi et al [Takahashi et al, 1994] found that, apart from some films, where the decrease of stress levels with increase in Ar incorporation was observed, for most of the samples stress increases with increase in number of Ar, incorporated into the films. It was stated that such dependence of stress on the impurity incorporation is supported by the results of experiments in an N_2 atmosphere. It is known that nitrogen normally incorporates into the film in the molecular form and that the size of the N_2 molecule is similar to the size of Ar atoms, so a similar effect on the film is expected. Indeed, it was found that the high amount of N_2, trapped in the films during deposition, corresponded to high compressive stress levels. However, later studies [Takahashi et al, 1996] of SiO_2 films, deposited in Ar/H_2 and Ar/O_2 atmospheres showed that, for both types of films, the Ar concentration is approximately the same. Moreover, Ar/H_2 sputter-deposited films were more dense than Ar/O_2 sputter-deposited ones. Therefore, it was concluded that it is not the amount of Ar incorporation or densification, which are the driving mechanisms for stress behaviour. Instead, it was proposed that stress is related to the Si-O-Si network, the amount of Si-O-Si bonds and their properties. Hydrogen atoms can terminate some of the Si bonds and also can break Si-O-Si bonds, which leads to stress relaxation. Indeed, it was found [Takahashi et al, 1994] that an increase in the number of Si-H bonds leads to decreased stress levels.

A more recent study of ion-plated SiO_2 films was performed by Strauss et al [Strauss et al, 1997]. Films were deposited from Si source in the presence of Ar and O_2 gases. Several deposition parameters, such as arc current, total working pressure or amount of O_2 in the gas mixture, which can influence film properties, were varied. All films deposited were found to be stoichiometric, amorphous and compressively stressed. Thin films (less than 100 nm thick) exhibited stress levels of 1100 MPa, but with increase in film thickness stress decreased and saturated at approx. 670 MPa. Such behaviour was explained by increased adatom mobility at the initial stages of film growth due to heating from the source and momentum transfer. This causes relaxation processes in the film. Some time after the start of the deposition these processes stabilise and no more stress changes are observed. In ion plating an increase in arc current leads to an increase in bombarding ion current density and a very slight increase in energy of bombarding ions. Silicon dioxide films showed only a slight increase in stress with increase in arc current. It is believed that stress changes with changes in arc current are due to the densification mechanisms in the films. As the densification saturates, so does the stress. Variation of the total working pressure from 0.4 to 4.0×10^{-3} mbar during deposition was

performed by increasing the amount of oxygen in the chamber. It was found that the SiO_2 film stress reached a maximum level of 1100 MPa ($1.5x10^{-3}$ mbar) and then decreased to 700 MPa ($4.0x10^{-3}$ mbar). If the total working pressure was kept constant and the Ar to O_2 ratio was varied then, for an increase in oxygen content and decrease in argon content, the stress in SiO_2 films increased to about 1100 MPa, then decreased and saturated at approx. 800 MPa. Increase in total pressure during deposition can lead first to an increase in the number of ions and neutrals bombarding the surface and thus an increase in energy supply to the film. Further pressure increase leads to a decrease in number and energy of bombarding species due to increased gas density and reduced mean free path which means more collisions occur in the gas phase and the ion energy does not reach the film surface. A summary of properties of SiO_2 films, deposited by various types of sputtering and by ion plating, is presented in Table 2.3.

2.2. Tantalum Pentoxide Films

Tantalum pentoxide (Ta_2O_5) is an increasingly popular material. A lot of researchers [see, for example, Four et al, 2000] mention its high dielectric constant, which makes Ta_2O_5 important in microelectronics and the semiconductor industry. In fact, in many scaled-down products Ta_2O_5 replaces SiO_2 due to its superior performance [Chaneliere et al, 1998]. On the contrary, in the optical industry, Ta_2O_5 and SiO_2 films are often used together in many applications, such as wavelength division multiplex filters [Ukechi et al, 2000] or anti-resonant reflecting optical waveguide (ARROW) type vertical coupler filters [Chu et al, 1999], to mention a few. These materials can also be used to form a composite film with desired refractive index or a graded film [Cevro, 1995]. Many modern thin film optical components represent complex designs, consisting of alternating layers of low and high refractive index materials. Tantalum pentoxide, having a high refractive index and wide transmission range (300 nm – 10 μm) [Tien et al, 2000], often represents a popular choice. Another common application of Ta_2O_5 coatings is in the chemical industry. It is known that Ta_2O_5 is chemically very inert and, therefore, can be used as a protective coating for sensors, designed to work in aggressive media [Christensen et al, 1999]. If deposited at high temperatures (above 650 ^{0}C), Ta_2O_5 films can grow in orthorhombic or hexagonal phases [Chaneliere et al, 1998]. The crystalline phase of Ta_2O_5 is known to exhibit anisotropic behaviour: its dielectric constant changes with change in crystal orientation. Moreover, the dielectric

Table 2.3. Properties of SiO_2 films, prepared by sputtering and ion plating.

Deposition Technique	Deposition Conditions	Refractive Index, n	Extinct. Coeff., k	Wave-length, nm	Stress, MPa	References
RF magnetron sputtering	Various Ar/H_2 or Ar/O_2 ratios, N_2 ambient, various total pressures and sputtering power values	1.5063-1.6970 (Ar/H_2); 1.4683-1.4698 (Ar/O_2); 1.6460-1.7847 (N_2)		633	In compression 47.5-157.5 (Ar/H_2); 171.3-187.0 (Ar/O_2); 184.7-739.0 (N_2)	[Takahashi et al, 1994]
RF magnetron sputtering	Various Ar/H_2 or Ar/O_2 ratios and RF power values	Approx. 1.47-1.62		633	Approx. 40-180 in compresstion	[Takahashi et al, 1996]
RF magnetron sputtering	Substr. temp. 100-400^{0}C, substr. bias 0 to –125 V	1.5	$<10^{-5}$	300-800	100-250 in compression	[Kupfer et al, 1999]
RF magnetron sputtering	Various O_2/Ar ratios	1.453-1.460				[Wu and Chiou, 1996]
Asymmetric bipolar pulsed DC sputtering	Total pressure of O_2/Ar mixture 7.5-15 mTorr, sputtering power 350-700 Watt	1.38-1.46		560	100-1200 in compression	[Morton et al, bipolar]
Mid-frequency or DC reactive sputtering	Various O_2 partial pressures (metallic to oxide modes) and target voltages	Approx. 1.5 (oxide and transition mode)	$<2.x10^{-3}$ (oxide/tr. mode)	600		[Vergoehl et al, 1999]

Reactive unipolar or bipolar pulse mode magnetron sputtering		1.47	$2x10^{-4}$	550		[Frach et al, 2001]
Indirectly reactive sputtering	Total pressure 0.19-0.36 Pa	1.449-1.477,				[Song et al, 2000]
Time-resolved successive plasma anodisation		1.4000-1.490			200-400 in compression	[Howson et al, 1997]
Reactive ion-beam sputtering	UV light irradiation for increased growth rates	Approx. 1.435-1.46				[Nomura and Ogawa, 1992]
Arc ion plating	Ion current density 0.1-0.5 mA/cm^2, total pressure (0.4-4.0)$x10^{-3}$ mbar; various O_2/Ar concentrations				600-1100 in compression	[Strauss et al, 1997]

constant of crystalline Ta_2O_5 is higher than that of amorphous layers. Below 650 ^{0}C, Ta_2O_5 grows in the amorphous state. Amorphous films are preferred, especially in the chemical industry, as grain boundaries can be weak points in the protective coatings [Christensen et al, 1999]. Such coatings should also be stoichiometric and have a low degree of porosity. It should be noted as well that low stress films are preferred, as highly-stressed coatings can change the stiffness of the sensor, thus degrading its performance. Other examples of Ta_2O_5 film applications can be found in a review by Chaneliere et al [Chaneliere et al, 1998].

Tantalum pentoxide thin films can be deposited by various techniques, for example, pulsed laser deposition [Mingfei et al, 1997; Zhang and Boyd, 2002], asymmetric bipolar pulsed DC sputtering [Konopka et al, 1999] or an indirect reactive sputtering technique [Song et al, 2000]. Ta_2O_5 films can also be deposited by various CVD methods. However, as noted by [Chaneliere et al, 1998], although CVD has many advantages, such as applicability over a wide pressure range, deposition of uniform coatings with good step coverage and high growth rates, its disadvantages include operation with harmful or toxic chemicals, high substrate temperatures and, often, a high level of impurities. Excellent reviews with the emphasis on various CVD techniques are available [Chaneliere et al, 1998; Martinu and Poitras, 2000], so here properties of Ta_2O_5 films, deposited by some PVD techniques only, will be reviewed.

Al-Jumaily and Edlou [Al-Jumaily and Edlou, 1992] studied the properties of Ta_2O_5 films, deposited by e-beam evaporation of Ta_2O_5, IAD and reactive magnetron sputtering from a pure Ta target. A mixture of oxygen and argon gases was used for bombardment. Optical constants of the films were calculated from transmittance spectra, measured in air and in vacuum, using the envelope method and Cauchy dispersion relation. Simple evaporated Ta_2O_5 films showed a shift towards the longer wavelengths in transmittance values, measured under air, which is representative of a low film density and quality. Experiments on IAD and reactive sputtering yielded films with higher refractive indices. The increase in absorption for the IAD coating was explained by preferential sputtering of oxygen, which leads to Ta-rich films. This is supported by Franke et al [Franke et al, 2001], who state that for stoichiometric Ta_2O_5 the film extinction coefficient k is very small, but with increase in the Ta concentration in the film k also increases. Such deficiency can be corrected by post-baking the coatings, which leads to full oxidation and thus improvement of coating stoichiometry. Ion-assisted and sputtered coatings exhibited no changes with humidity cycling, which shows their high quality [Al-Jumaily and Edlou, 1992]. Increase in refractive index of

ion-assisted films was also reported by Morton and Fridman [Morton and Fridman], who evaporated Ta_2O_5 films under concurrent oxygen ion bombardment onto a 120 ^{0}C heated substrate. No clear correlation was found between the refractive index and ion bombardment conditions in this case.

Another study of IAD Ta_2O_5 films was performed by Martin et al [Martin et al, 1994]. Ta_2O_5 films were deposited onto glass and Si substrates by e-beam evaporation of Ta_2O_5 material and concurrent bombardment with a flux of oxygen ions ranging from 0 to 200 μA/cm^2. Stress levels were calculated from the interferometry measurements. Film thickness was measured by DekTak profilometer and density was then calculated from RBS spectra.

The Ta_2O_5 films were found to be stoichiometric and amorphous. The refractive index of these films measured at 633 nm increases from 1.93 for purely evaporated films to 2.14 for 100 eV $\approx$100 μA/cm^2 oxygen-bombarded films and then decreases to approx. 2.0 for 100 eV 200 μA/cm^2 oxygen-bombarded films. For bombardment with 1 keV ions a maximum of 2.14 for the refractive index is reached at $\approx$30 μA/cm^2. Such behaviour was explained by the increase in oxygen incorporation into the film due to high ion bombardment. The extinction coefficient changed from the range of $3x10^{-3}$ to $2x10^{-2}$ for 1 keV bombardment to the range of $3x10^{-4}$ to $4x10^{-4}$ for 100 eV ion bombardment. Film stress was found to vary from low tensile (approx. 85 MPa) for evaporated films to approx. 400 MPa in compression for 100 eV 200 μA/cm^2 bombarded films and approx. 200 MPa in compression for 60-120 μA/cm^2 1 keV bombarded films. No correlations of stress behaviour with ion energy or saturation stress value were found. Stress changes observed were related to the collapse of the voided structure of the film with ion bombardment and associated increase in the film density.

It was found that with increase in ion current density, the film density increases, reaches its maximum value and then decreases. For 1 keV oxygen ions a maximum value of density of 7.5 g/cm^3 (93% of bulk value of 8.2 g/cm^3) was reached at 26 μA/cm^2 ion bombardment. For 100 eV oxygen ions the maximum value of density was achieved at 100 μA/cm^2 ion bombardment. The maximum density coincides with the maximum in refractive index. For 1 keV bombarded films this also corresponds to a tensile-compressive stress transition. For 100 eV bombardment films with maximum density are found to be in compression.

For low-energy bombarded films the refractive index was found to linearly relate to film packing density. For high-energy bombardment this relation is not linear.

Ta_2O_5 can also be deposited by various sputtering techniques, including RF [Cheng et al, 1999; Franke et al, 2000] or reactive DC [Christensen et al, 1999] magnetron sputtering and ion-beam sputtering [Tien et al, 2000]. In ion-beam sputtering flux of argon ions or mixed flux of argon and oxygen ions can be used. The influence of the flux composition on the deposition process was studied by Demiryont et al [Demiryont et al, 1985]. It was found, that a critical value of oxygen content is needed in the ion beam. Below this value an oxide is not formed on the target. Above this value the rate of formation of the oxide layer on the target exceeds the rate of sputtering of this layer, so the stoichiometric oxide can be formed and the growth rate decreases dramatically. It was found, that stoichiometric Ta_2O_5 films are non-dispersive and non-absorbing in the region of 365-2000 nm. The refractive index was calculated to be equal to 2.18. Both refractive index and extinction coefficient sharply increase, when wavelengths of 300 and shorter are considered. Such behaviour is linked to the fundamental bad gap absorption in the films. For sub-oxides the decrease in oxygen content in the film leads to an increase in n and k values. It was also concluded that optical properties of the films are strongly related to the amount of oxygen, present in the samples.

A study of reactively ion-beam sputtered and dual-ion-beam sputtered Ta_2O_5 films was performed by Cevro and Carter [Cevro and Carter, 1995]. For dual ion-beam sputtering Ar or oxygen ions of 0-300 eV energy and 0-80 $\mu A/cm^2$ were used. Some films were also deposited by evaporation. It was found that with an increase in oxygen partial pressure in the chamber from $0.8x10^{-4}$ -$2.0x10^{-4}$ mbar the film refractive index (region of 2.12-2.17 at 550 nm) and extinction coefficient (region of $(2\text{-}6)x10^{-4}$ at 550 nm) decrease. It was found that the energy of sputtering ions (800-1500 eV) does not influence film optical properties. For films, evaporated onto substrates, held at 300 ^0C, refractive index and extinction coefficient were found to be 2.06 and $2x10^{-4}$ respectively. Bombardment of Ta_2O_5 films with 300 eV oxygen ions of 0-40 $\mu A/cm^2$ current density leads to a decrease in n values from 2.15 to 2.11, with k values unchanged. Bombardment with 300 eV Ar ions (0-30 $\mu A/cm^2$) did not change n values, but led to an increase in k values (maximum of $3x10^{-2}$ at 30 $\mu A/cm^2$). Higher levels of bombardment led to an increase in k, which is due to stoichiometry loss. It was found that the compressive stress increased with increase in current density of Ar ions, was independent of ion energy (200-300 eV) and was in the region of approx. 300-600

MPa. Changes in n values during oxygen bombardment are believed to be due to the small damage made to the film. Changes in k values with Ar bombardment may be due to either preferential oxygen sputtering, or changes in tantalum-oxygen bonding, or argon incorporation (typically 2.5%).

A study of various deposition parameters and their influence on film properties was performed by Strauss et al [Strauss et al, 1997; Strauss et al, 1999]. Ta_2O_5 films were deposited by reactive low voltage ion plating from Ta_2O_5 material onto glass substrates. Both Ar and O_2 were present in the chamber during deposition. All films were compressively stressed. Experiments on films of different thicknesses showed that for very thin films (<100 nm) stress levels are high (1700 MPa), but with increase in film thickness stress decreases and saturates at approx. 550 MPa. With variation in arc current (thus, in ion current density) stress increased from 50 MPa to 500 MPa, which was explained by film densification. With increase of total working pressure ((0.4-4.0)$x10^{-3}$ mbar by increase in oxygen content) stress levels decreased to approx. 200 MPa. If the total pressure was kept constant, but the Ar/O_2 ratio was varied, then within an increase in oxygen content then stress increased, reached its maximum at 600 MPa and then decreased. Variation of Ar gas pressure, while keeping O_2 pressure and ion current density constant did not have any significant effect on absorption in the film (k at 550 nm = $9x10^{-4}$). However, both refractive index and density decreased with increase in Ar pressure in the chamber. Best quality films with relative density of 1 and n at 550 nm = 2.250 were obtained at an oxygen pressure of $1.1x10^{-3}$ mbar and argon pressure of $0.4x10^{-3}$ mbar. Films with lowest relative density of 0.95 and n at 550 nm = 2.225 were deposited at the same oxygen pressure and argon pressure of $2.9x10^{-3}$ mbar. Under the conditions of constant argon pressure of $0.8x10^{-3}$ mbar, constant ion current density and variable oxygen pressure ($0.1\text{-}2.0x10^{-3}$ mbar) absorption decreased from k at 550 nm =$10.5x10^{-4}$ to $4x10^{-4}$. Both film density and refractive index decreased with increase in oxygen pressure and, at 550 nm, the refractive index changed from 2.253 to 2.237. It was proposed that absorption increases when local defects in chemical bonds are generated by ion bombardment. Increased oxygen presence in the chamber leads to lower levels of defects in the film.

It was found that post-deposition heat treatment (either 1 h at 120 ^{0}C or 4h at 350 ^{0}C) results in stoichiometric films with low absorption levels. It is believed that these results can be explained by higher atom mobility and diffusion, which repairs film defects. High values of refractive index are explained by high-density structure of the films,

which results from ion bombardment. As the pressure increases, the level of ion bombardment decreases, leading to a degradation of film properties.

The drawback of high-quality films is their high state of compressive stress. With an increase in total deposition pressure the stress decreases from 700 to 300 MPa. Post-deposition heat treatment at 350 ^{0}C in atmosphere decreases absorption, refractive index and stress levels and increases film thickness due to structural relaxation.

Attempts have been made to compare the behaviour of SiO_2 and Ta_2O_5 film properties [Strauss et al, 1997]. It was concluded, that differences in stress and its behaviour in films of two materials can be explained by the differences in the energy transfer during energetic particle – film interactions.

Properties of Ta_2O_5 films, deposited by various techniques, are summarised in Table 2.4. A summary of optical properties of Ta_2O_5 films can be also found in papers by Demiryont et al and Chaneliere et al [Demiryont et al, 1985,Chaneliere et al, 1998].

In conclusion, it can be said that film properties strongly depend on film stoichiometry, density and composition. For example, Si-rich films will have higher refractive index and extinction coefficient. In the case of Ta_2O_5 films oxygen deficiency will lead to an increase in film absorption.

As a rule of thumb, it can be said that if the film atom mobility is low, the resulting films will have low density, low stress, high instability in ambient and poor optical performance. With increase in atom mobility films tend to become denser and more stable in air. These films are able to support high stress levels and film optical properties approach those of the bulk materials. If at this stage the film experiences even more energetic particle bombardment, its properties start to decline (for example, film absorption increases due to preferential oxygen sputtering).

Therefore, knowledge of conditions, resulting in films with best performance, is important for design and production of high quality industrial components and products.

Table 2.4. Properties of Ta_2O_5 films, prepared by various techniques.

Deposition Technique	Deposition Conditions	Refractive Index, n	Extinct. Coeff., k	Wave-length, nm	Stress, MPa	References
PECVD		2.12-2.17		550		[Martinu and Poitras, 2000]
PECVD		2.12; 2.232 re-cryst.		632.8		[Four et al, 2000]
PVD		2.15-2.25		550	250-600 in compr.	[Martinu and Poitras, 2000]
Evaporation	Ta_2O_5 source, substr. at 300 ^{0}C	2.1-2.25	0-5x10^{-3}	300-800		[Al-Jumaily and Edlou, 1992]
Evaporation	Substr. at 300 ^{0}C	2.06	2x10^{-4}	550		[Cevro, Carter, 1995]
IAD	O_2/Ar=10/1 at 400 eV 130 mA, substr. at 300 ^{0}C	2.17-2.8	5x10^{-3}	300-800		[Al-Jumaily and Edlou, 1992]
IAD	Oxygen ion flux 0-200 μA/cm^2, energies a) 100 eV; b) 1000 eV	1.93-2.14	a) (3-4)x10^{-4}; b) (0.3-2)x10^{-2}	633	85 in tension to 400 in compr., depending on ion energy/flux	[Martin et al, 1994]

IAD	Growth rate 6 A/sec, O_2 pressure $2x10^{-4}$ Torr ion current density 0-148 μ A/cm^2, substr. at 120 ^{0}C	2.041-2.179
Asymmetric bipolar pulsed DC sputtering	Total pressure 7.5-15 mTorr, sputtering power 350-700 Watt	2.1-2.2
Reactive DC sputtering	Annealing at O_2 ambient at 100-700 ^{0}C	
React. magnetr. sputtering	O_2/Ar mixture	2.15-2.41
RF magnetron sputtering	Temperature varied 25-100 ^{0}C; variation of n with temperature was studied a)with account of thermal stresses and b)without account of thermal stresses	2.3 ± 0.2,varies (25-55 ^{0}C) as a) $7.89x10^{-6}/^0$C;b)$3.64x10^{-6}/^0$C
Reactive RF magnetron sputtering	Ar/O_2 mixtures, varying O_2/Ar ratio 22-40 %, varying total pressure, substr. temp. 20-200 ^{0}C	2.04-2.16

	560		[Morton and Fridman, ionbeam]
	560	500-1500 in compr.	[Morton et al, bipolar]
		200 in compr. to 250 in tension; no sudden changes with re-crystallisation	[Christensen et al, 1999]
0-3.5x10^{-3}	300-800		[Al-Jumaily and Edlou, 1992]
	632.8	310-350 in compr., depending on temperature	[Cheng et al, 1999]
	550		[Franke et al, 2000]

Pulsed laser deposition		2.15
Ion beam sputtering	Varying O_2/Ar ratio 0-56 %	2.18
Ion beam sputtering	O_2 near substrate at $3x10^{-5}$ Torr, total pressure $1x10^{-4}$ Torr; Temp. varied 25-70 ^{0}C, BK-7 and Pyrex glass substrates	2.16
Ion beam sputtering/DIBS	Some bombarded with 300 eV oxygen of Ar ions (0-40 μ A/cm^2)	2.11-2.17
Ion Plating	Total pressure $(0.4\text{-}4.0)x10^{-3}$ mbar; various Ar/O_2 ratios, ion current density 0.1-0.5 mA/cm^2	
Ion Plating	Ion current density 0.27 mA/cm^2, O_2 $1.1x10^{-3}$ mbar and Ar $(0.4\text{-}2.9)x10^{-3}$ mbar OR Ar $0.8x10^{-3}$ mbar and O_2 $(0.1\text{-}2.5)x10^{-3}$ mbar; annealing at 120-350 ^{0}C	2.224-2.256, depending on depos. cond. and annealing

	632.8		[Mingfei et al, 1997]
$<10^{-4}$	365-2000		[Demiryont et al, 1985]
$1.15x10^{-3}$		Temp. varied 25-70 ^{0}C; Stress varied accordingly from 398 to 64 in compr. on BK-7 and from 399 to 340 in compr. on Pyrex	[Tien et al, 2000]
Max. $3x10^{-2}$	550	300-600 in compr.	[Cevro and Carter, 1995]
		50-1700 in compr., depending on depos. cond. and film thickness	[Strauss et al, 1997]
$<1.2x10^{-3}$	550	Approx. 0-800 in compression, depending on depos. cond. and annealing	[Strauss et al, 1999]

References

Al-Jumaily G., Edlou S.M., Thin Solid Films, **209,** 223, (1992)

Ambree P., Kreller F., Wolf R., and Wandel K., J. Vac. Sci. Technol., **B 11 (3)**, 614, (1993)

Bazylenko M.V., Gross M., Simonian A., and Chu P.L., J. Vac. Sci. Technol., **A 14 (2)**, 336, (1996)

Beck U., Smith D.T., Reiners G., Dapkunas S.J., Thin Solid Films, **332**, 164, (1998)

Blech I., and Cohen U., J. Appl. Phys., **53 (6)**, 4202, (1982)

Cevro M., Thin Solid Films, **258**, 91, (1995)

Cevro M., Carter G., Optical Engineering, **34 (2)**, 596, (1995)

Chaneliere C., Autran J.L., Devine R.A.B., Balland B., Mater. Sci. Eng., **R 22**, 269, (1998)

Cheng W.H., Chi S.F., Chu A.K., Thin Solid Films, **347**, 233, (1999)

Christensen C., de Reus R., and Bouwstra S., J. Micromech. Microeng., **9**, 113, (1999)

Chu S.T., Pan W., Sato S., Little B.E., Kaneko T., and Kokubun Y., J. Lightwave Technol., **17 (4)**, 652, (1999)

Demiryont H., Sites J.R., and Geib K., Applied Optics, **24 (4)**, 490, (1985)

Four S., Devine R.A.B., Brunel M., J. Vac. Sci. Technol., **A 18 (2)**, 554, (2000)

Frach P., Goedicke K., Gottfried C., Bartzsch H., Surf. Coat. Technol., **142-144**, 628, (2001)

Franke E., Schubert M., Trimble C.L., DeVries M.J., Woollam J.A., Thin Solid Films, **388**, 283, (2001)

Franke E., Trimble C.L., DeVries M.J., and Woollam J.A., J. Appl. Phys., **88 (9)**, 5166, (2000)

Gupta A., and Parsons G.N., J. Vac. Sci. Technol., **B 18 (3)**, 1764, (2000)

Haque M.S., Naseem H.A., and Brown W.D., J. Appl. Phys., **82 (6)**, 2922, (1997)

Harada T., Yamada Y., Uyama H., Murata T., Nozoye H., Thin Solid Films, **392**, 191, (2001)

Hofrichter A., Constantinescu A., Bulkin P. and Drevillon B., J. Vac. Sci. Technol., **A 18 (4)**, 2012, (2000)

Howson R.P., Danson N., Hall G.W., Nucl. Instr. Meth. Phys. Res., **B 121**, 90, (1997)

Jia Y., Liang Y., Liu Y., Liu Y., Shen D., Thin Solid Films, **370**, 199, (2000)

Konopka D., Morton D.E. and Zimone F.T., in: Proc. of the Soc. of Vacuum Coaters, 42nd Annual Techn. Conference, (1999)

Kupfer H., Fluegel T., Richter F., Schlott P., Surf. Coat. Technol., **116-119**, 116, (1999)

Leplan H., and Geenen B., Robic J.Y., Pauleau Y., J.Appl. Phys., **78 (2)**, 962, (1995)

Leplan H., Robic J.Y., Pauleau Y., J. Appl. Phys., **79 (9)**, 6926, (1996)

Martin P.J., Bendavid A., Swain M., Netterfield R.P., Kinder T.J., Sainty W.G., Drage D., Wielunski L., Thin Solid Films, **239**, 181, (1994)

Martin P.J., Macleod H.A., Netterfield R.P., Pacey C.G., and Sainty W.G., Applied Optics, **22 (1)**, 178, (1983)

Martinu L., Poitras D., J. Vac. Sci. Technol., **A 18 (6)**, 2619, (2000)

McNeil J.R., Barron A.C., Wilson S.R. and Herrmann Jr. W.C., Appl. Optics, **23 (4)**, 552, (1984)

Mingfei Z., Zhengwen F., Haijun Y., Zhuangjian Z., Qizong Q., Appl. Surf. Sci., **108**, 399, (1997)

Morton D.E., and Fridman V., Denton Vacuum Technical Papers, Moorestown, NJ, http://www.dentonvacuum.com/news/tech.html

Nomura K., and Ogawa H., J. Appl. Phys., **71 (3)**, 1469, (1992)

Park Y., Lee J.K., Jung I., Heo S.-B., Lee J.-Y., Appl. Phys. Lett., **75 (24)**, 3811, (1999)

Rats D., Hajek V., Martinu L., Thin Solid Films, **340**, 33, (1999)

Robic J.Y., Leplan H., Pauleau Y., Rafin B., Thin Solid Films, **290-291**, 34, (1996)

Sankur H., and Gunning W., J. Appl. Phys., **66 (2)**, 807, (1989)

Selhofer H., Mueller R., Thin Solid Films, **351**, 180, (1999)

Song Y., Sakurai T., Maruta K., Matusita A., Matsumoto S., Saisho S., Kikuchi K., Vacuum, **59**, 755, (2000)

Souche D., Brunet-Bruneau A., Fisson S., Nguyen Van V., Vuye G., Abeles F., Rivory J., Thin Solid Films, **313-314**, 676, (1998)

Strauss G.N., Danh N.Q., Pulker H.K., J. Non-Cryst. Solids, **218**, 256, (1997)

Strauss G.N., Lechner W., Pulker H.K., Thin Solid Films, **351**, 53, (1999)

Takahashi H., Nagata H., and Kataoka H., Takai H., J.Appl. Phys., **75 (5)**, 2667, (1994)

Takahashi H., Nishiguchi A., Nagata H., and Kataoka H., Fujishima M., J. Appl. Phys., **79 (5)**, 2787, (1996)

Tien C.-L., Jaing C.-C., Lee C.-C., and Chuang K.-P., J. Mod. Opt., **47 (10)**, 1681, (2000)

Ukechi M., Miyashita T., Takahasgi A., Kaku R., Komine Y., Mase T., Nishimura T., Hirayama S., Kameda K., and Ito K., IEICE trans. Electron., **E 83-C (9)**, 1458, (2000)

Vergoehl M., Malkomes N., Staedler T., Matthee T., Richter U., Thin Solid Films, **351**, 42, (1999)

Wu W.-F., and Chiou B.-S., Semicond. Sci. Technol., **11**, 1317, (1996); Wu W.-F., and Chiou B.-S., Applied Surface Science, **99**, 237, (1996)

Zhang J.-Y., Boyd I.W., Appl. Surf. Sci., **186**, 40, (2002)

Chapter III

Stresses in Thin Films

Thin films of SiO_2 and Ta_2O_5 are now widely used in the optical industry. Residual stresses, arising during the deposition, can strongly influence not only performance of these films, but also the flatness of the surface of the substrate. In order to be able to avoid the problems, caused by residual stresses in these films, their origins and factors controlling their evolution must be clearly understood.

This chapter is devoted to the questions of stress origins in thin films, experimental methods of stress measurement and calculation of stress values from the measured data. The first part of this chapter treats different origins of stress in thin films, both intrinsic and extrinsic and gives a review of models of stress behaviour in non ion-assisted and ion-assisted films. It should be noted, that this field is vast, and therefore, only most recent and most popular models are included in this review. In the second part of this chapter various stress measurement methods are reviewed. Again, the accent is made on most popular and newer techniques. The last part of this chapter is devoted to consideration of the Stoney formula for the evaluation of the experimental data, conditions of its applicability and its limitations.

3.1. Stresses in Thin Films and Their Origins

Stress, arising in a thin film, can be represented by the sum of three components [Tamulevicius, 1998]:

$$\sigma_{total} = \sigma_{ext} + \sigma_{th} + \sigma_{in}, \tag{3.1}$$

where σ_{ext}, σ_{th} and σ_{in} are the external, thermal and intrinsic stresses, respectively. In the absence of external forces, applied to the sample, residual stress is usually used to identify the stress state in a thin film grown on a substrate. This stress also consists of

two parts: extrinsic and intrinsic. Because the films are usually used under thermal conditions that are different from those under which the films were grown, the extrinsic or thermal stress arise due to the difference in thermal expansion of the film and the substrate material.

The origin of the intrinsic stress is not clearly understood [Ohring, 1992]. This stress can be defined as the stress that is not related to thermal processes, but to the film growth process. The stress magnitude is strongly dependent on the growth process. Thermal stresses will be considered in the first part of this section; theories on origins of intrinsic stress in non-ion assisted thin films will be reviewed in the second part of this section. The third part of this section will be devoted to theories on stress behaviour in films, deposited under bombardment with energetic ions. The summary of stress origins can be found in Table 3.1.

3.1.1. Thermal stresses

Thermal bending of the substrate arises from three main sources [Hoffman, 1976], all of which are important if the thermal expansion coefficients of the film and the substrate, and/or between the layers in a multilayer coating, differ significantly. The first of the sources is the difference in the temperatures during deposition or film device operation and during measurements. Second is a thermal gradient through the length of the sample. Third is a thermal gradient through the thickness of the sample. All three sources can influence the resulting radius of curvature of the sample. The part of the stress arising from a difference in temperatures (first source) may be easily calculated if the temperature of the sample and the linear expansion coefficients of the materials in bulk form are known. However one should keep in mind that it is difficult to measure the exact temperature of the sample during the experiment and the expansion coefficient for the film may not be the same as that for the bulk material.

The most widely used formula for the thermal stress calculation is

$$\sigma_{thermal} = \frac{E_f}{1-\nu_f}\left(\alpha_f - \alpha_s\right)\left(T_s - T\right), \tag{3.2}$$

where $\left(\frac{E_f}{1-\nu_f}\right)$ is the biaxial modulus of the film, and α_f and α_s are the bulk linear thermal expansion coefficients for the film and the substrate materials, respectively,

Table 3.1. Origins of thin film stress.

Total film stress			
External	Thermal	Intrinsic	
	a) Temperature difference, e.g. between device fabrication and operation; b) Thermal gradient through sample length; c) Thermal gradient through thickness	Ion-assisted films	Non ion-assisted films
		a) Inert gas incorporation b) Recoil implantation c) Thermal spikes	a) Impurity incorporation and chemical reactions b) Lattice mismatch c) Film crystallite size, its' influence on film lattice constant d) Re-crystallisation processes e) Film densification, influence of voids f) Phase transformation

T_s is the temperature of the substrate during the deposition and T is the temperature of the specimen during the measurement. The obvious difficulty with this calculation is that the elastic properties of the film have to be known.

The stress due to the influence of the thermal gradient along the sample can be calculated using the following equation, from Hoffman [Hoffman, 1976]

$$\sigma = \frac{1}{6}\frac{E_f}{(1-\nu_f)}(\alpha_f - \alpha_s)\Delta T, \tag{3.3}$$

if the temperature difference ΔT between the free and clamped ends of the sample is measured before the film deposition. In the case of materials with approximately the same thermal expansion coefficients this effect can be neglected. However, it is difficult experimentally to obtain the temperature measurements required for such calculation.

It was initially believed [Murbach and Wilman, 1953], that there could exist a gradient through the film thickness, caused by the heat of condensation. However, careful consideration of the time of lattice vibration damping does not support this hypothesis [Windischmann, 1992]. The maximum influence of the thermal gradient through the substrate thickness can be estimated from [Hoffman, 1976]

$$\sigma_s = \frac{1}{6}\frac{E_s}{(1-\nu_s)}\alpha_s\frac{Pd}{K}, \tag{3.4}$$

where P is the power input per unit area of the substrate and K is the substrate thermal conductivity.

Several other approaches to the studies of the thermal stresses in various thin film coatings exist in modern research ([Cherepanov and Martinez,1997], [Yamada-Kaneta et al, 1987], [Kim et al, 1999] or [Klein, 2000] to mention a few). However, in many practical cases of single-layer ion-beam deposition without additional substrate heating, simple equations, presented in this section, give satisfactorily estimates of thermal stresses.

3.1.2. Intrinsic stresses in non ion-assisted thin films

The question of origins of stresses in non ion-assisted thin films is long debated and is subject to many excellent reviews and classifications [e.g. Hoffman, 1976; Windischmann, 1992; Spaepen and Shull, 1996, etc.]. In our treatment of this topic, the classification, given by Hoffman [Hoffman, 1976] is followed. Here all mechanisms of intrinsic stress generation in non ion-assisted films are arranged into six main groups. Each of these groups will be considered in more detail.

The first group includes the influence of incorporation of impurities (for example, inert gases or water vapour) and chemical reactions within the film on film stress levels. These processes were first proposed for explanation of stress in metallic films, but their use can be extended to the non-metallic films studied in this research.

Impurities may be incorporated into the film in different ways: they may be absorbed at the surface of the film and then diffuse into the bulk, causing stress, or be buried under a monolayer of film atoms [d'Heurle and Harper, 1989]. Gas impurities can also be either contained in the matrix of the film or form gas-filled voids [Was et al, 1996].

Impurities can influence films in several ways [Windischmann, 1992]. The impurity can react with the film material, leading to volume changes, and thus, to stress generation. Impurities can also lead to interatomic potential energy reduction, which can lead to stress changes (for example, oxygen incorporation at the grain boundaries may mask the attractive forces, acting between the film atoms in the neighbouring grains, and thus lead to decrease in tensile stress [Misra and Nastasi, 2000]).

The nature of the impurity is a factor of importance. The influence of different types of common film impurities was reviewed by Windischmann [Windischmann, 1992]. For example, consider water vapour incorporation. Here, a model has been developed [Hirsh, 1980], linking stress in the film to the dipole interaction, which exists when water molecules are absorbed into the pores in the film. For very small and very large pore sizes the effect of the dipoles are negligible, but for pores of 1-10 nm size the effect is most pronounced. The sign of the generated stress is dependent on the dipole orientation in the pores. Other commonly considered impurities are oxygen, hydrogen and inert gases. In case of hydrogen it is believed that stress may be linked to the material-hydrogen bond length and saturation of dangling bonds in the film material. Not all authors agree on the special case of impurity incorporation, i.e. inert gas incorporation, as an origin of intrinsic stress. Some experimental results [Thornton et al, 1979] show, that there is no link between inert gas incorporation and stress in the film.

This issue remains open for discussion, as other opinions exist, where incorporation of a differently sized atom into the film bulk is considered as a source of stress in itself.

This question was treated by Kamminga et al [Kamminga et al, 1998], who proposed a model, based on the effect of misfitting particles, incorporated into the film. It is assumed that the initial film can be represented by a free unstressed layer with holes in it. Incorporation of particles into holes results not only in stress, but also in volume changes, thus the film has to be even more stressed to fit the substrate. The stress, resulting from the incorporation of the misfitting particles, can be calculated as

$$\sigma_M = \frac{2}{3}\frac{E_f}{(1+\nu_f)} 4\pi n \frac{3(r_p - r_M) r_M^2 K_p}{3K_p + \frac{2E_f}{1+\nu_f}\frac{r_M^3}{r_{M+p}^3}}, \tag{3.5}$$

and stress, resulting from the requirement of bonding to the substrate, as

$$\sigma_{fix} = -\frac{3}{2}\sigma_M, \tag{3.6}$$

where n is the number of misfitting particles, incorporated into the unit volume of the film, r_M is the radius of the hole before the particle has been inserted, r_{M+p} is the radius of the hole after the particle has been inserted, r_p is the radius of the particle before it has been inserted and K_p is the bulk modulus of the misfitting particle. The authors note, that the last equation does not apply in all cases, as the assumption of the spherical symmetry of the problem does not always hold.

If impurities form gas bubbles (gas-filled voids), the following formula may be used [Parfitt et al, 1995]

$$\sigma = \frac{3p(2\mu+\lambda)}{4\mu\left(1/f\right)+(2\mu+3\lambda)}, \tag{3.7}$$

where μ and λ are shear modulus and Lame coefficient of the film material, f is the volume fraction of voids and p is the gas pressure in the voids.

Part of recent molecular-dynamics simulations studies [Fang et al, 1993] focused on impurity incorporation into the non ion-assisted films due to the presence of inert gas in

the deposition chamber. In the low adatom energy region (approx. 0.1 eV) inert gas becomes absorbed and loosely trapped in the film, leading to decreased film density. As the adatom energy increases, inert gas incorporation decreases and film density increases. It should be noted that, although the effect on the average stress in the film is small, it was found, that a local compressive stress field develops around the gas atom, if it is tightly trapped in the film.

The second reason for stress generation [Hoffman, 1976] is believed to be the lattice mismatch between the film and the substrate during epitaxial or heteroepitaxial film growth. An example of stresses of this type is the stress, produced during accommodation of the lattice mismatch between the silicon substrate and the porous silicon film [Manotas et al, 2001]. If the lattice parameters for the film (d_0) and for the unconstrained film material (for porous silicon films and epitaxial films) or substrate (d) are known, the stress can be calculated as [Ramaswamy et al, 2001]

$$\sigma = \frac{E_f}{1-\nu_f}\frac{d-d_0}{d}. \tag{3.8}$$

In the case of epitaxial films a critical film thickness exists, below which the film is under an elastic stress state, but above which misfit is accommodated and the stress in the film is relaxed by the formation of interfacial dislocations. This question, as well as stress models for heteroepitaxial films, is well reviewed by Hoffman [Hoffman, 1976] and Nix [Nix, 1989] and, therefore, shall not be considered here in more detail.

The third group of stress origins includes the influence of the crystallite size of the film material on the lattice constant of the film, and thus on the stress. The concept of surface energy plays an important part in the explanation of the result in this group. Although the influence of the surface energy on the stress in films in their initial growth stage (island growth) has long been recognised [Windischmann, 1992], the influence of this parameter on stress in thick coatings has not been established up until lately. Here only the latest works on the subject will be reviewed.

Two quantities are often used for surface characterisation: the surface tension or surface energy and the surface stress. These quantities can be defined in several ways. Here the definition of Spaepen [Spaepen, 1996] is quoted. The surface tension γ is defined as "the work, required to create a unit area of a new interface at constant strain in a solid".

The surface stress f_{ij} is a "2x2 tensor such that the surface work required to strain a unit surface elastically by $d\varepsilon_{ij}$ is $f_{ij}d\varepsilon_{ij}$". These quantities are related by

$$f_{ij} = \gamma\delta_{ij} + {}^{d\gamma}/_{d\varepsilon_{ij}}. \tag{3.9}$$

For fluids f is identical to γ, whereas for solids these quantities are different.

With the advance of measurement techniques and increase in their sensitivity, reliable curvature measurements have become available for films as thin as 0.1-0.5 nm. In this region stress evolution in Volmer-Weber (V-W) films currently attracts most attention. (The V-W growth mode is characterised by the nucleation of small islands, their growth and subsequent formation of a continuous percolating network on the substrate. As the deposition progresses, a continuous coating is formed which grows further by thickening.) An excellent review by Floro et al [Floro et al, 2002] on this subject is available. The main results of this review, together with some results of other relevant research, will be given here.

It can be said, that stress always arises in films, which undergo any density changes, while still firmly attached to the substrate. In polycrystalline films, growing in V-W mode, stress changes from compressive to tensile and back to compressive with increase in film thickness or the amount of material deposited onto the substrate. This behaviour is sometimes referred to as CTC behaviour and is directly linked to the evolution of the film microstructure during film growth. Initial compressive stress stage is attributed to the effect of discrete islands, nucleating on the substrate surface at the first steps of film growth. The stress becomes tensile with the growth and coalescence of these islands and reaches its maximum when the continuous film is formed. Finally, stress enters the second compressive stage due to the subsequent film growth by thickening. The second compressive stage has a very pronounced characteristic: if the growth is interrupted, the stress relaxes. With the continuation of the film growth, stress returns to its original value and develops further without the "memory" of growth interruption. Films only exhibit CTC stress behaviour if their atoms are highly mobile. "Low-mobility" films can only reach tensile stress.

The first stage of film growth and stress evolution is the compressive stress stage during island nucleation. Here the concept of surface stress is used to explain stress behaviour. Surface stress is believed to arise from the fact, that atoms at the surface of a solid have

fewer neighbours than atoms in the bulk, therefore, their equilibrium neighbouring distances will be different and this mismatch will lead to the stress formation. Considering growth of a cylindrical island on a thick substrate, it is possible to predict the stress using the following [Floro et al, 2002]

$$\sigma = (f_1 + f_2)\left(\frac{1}{h} - \frac{1}{h_0}\right) + \frac{1-3\nu_f}{1-\nu_f} f_3 \left(\frac{1}{r} - \frac{1}{r_0}\right), \tag{3.10}$$

where h_0 and h are initial and final height of an island, r_0 and r are initial and final radius of an island, f_1 is the surface stress at the island-vacuum interface, f_2 is the stress at island-substrate interface and f_3 is "the surface stress associated with the cylindrical perimeter of the island". This expression describes the following physical process: when initial island attaches to the surface of the substrate, its interior and surface stresses balance, leading to some equilibrium spacing between the atoms. As this island grows, its surface stresses change, but the island is constrained from equilibrating its surface and interior stress. Thus, the new equilibrium interatomic spacing cannot be reached, which leads to compressive stress generation.

Several other models of film behaviour in this region have been proposed. Spaepen [Spaepen, 1996] considered curvature of a substrate, resulting from the presence of a droplet on a substrate surface, surrounded by a vapour phase (see Figure 3.1). It is known that around the droplet the curvature is zero, but underneath the droplet the curvature varies from maximum in the middle to zero at the ends. The mean or average curvature, often measured in experiments, is found to be

$$\frac{1}{R} = -\frac{4\gamma_{lv} R_{dr} \sin^2\theta}{d^3 E_s}, \tag{3.11}$$

where γ_{lv} is the surface tension at the droplet-vapour interface, R_{dr} is the radius of curvature of the droplet-vapour interface and θ is the half-angle between the radii to the end points of the droplet.

If the horizontal capillary forces, acting on the substrate are considered,

$$\frac{1}{R} = \frac{6(f_{sv} - f_{sl} - \gamma_{sl}\cos\theta)}{d^2 E_s} \tag{3.12}$$

where f_{sv} and f_{sl} are stresses at substrate-vapour and substrate-droplet interfaces.

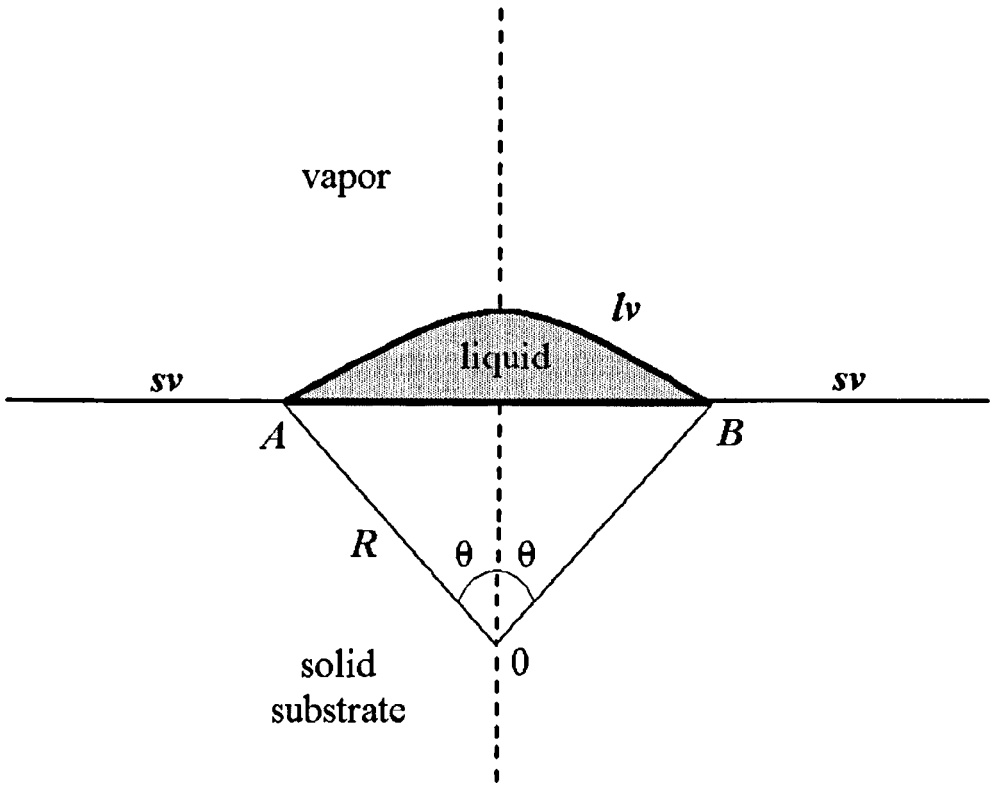

Figure 3.1 Schematic representation of the droplet on substrate surface. [Spaepen, 1996]

Three different models have been proposed by Gill et al [Gill et al, 2002]. First is a spherical layer model. Here it is presumed that the island grows by addition of hemispherical monolayers, which are subjected to the capillary forces due to surface stress. As the island grows, atoms near the surface attempt to relax to their bulk positions and thus, stresses are generated

$$\sigma_R^T = \frac{2f}{R}; \quad \sigma_\Theta^T = \sigma_\Phi^T = \frac{f}{R}, \tag{3.13}$$

where f is the surface stress, R is the radius of the spherical island. The expressions are written down for the spherical coordinate system (R, Θ, Φ), where R is the spherical radial distance, Θ is the angle between the x-axis and the projection of R onto x-y plane and Φ is the angle between R and x-y plane.

The second model is the cylindrical layer model. Here the island grows by incorporation of atoms at the perimeter of its base in such a manner that, after initial formation of a ring around the island base, further growth proceeds by addition of atoms on top of the atoms already forming a ring. In this case the stress can be calculated as

$$\sigma_r^T = \frac{f}{r}; \quad \sigma_\theta^T = \sigma_z^T = 0, \tag{3.14}$$

where r is the radius of the ring and the expressions are written down in the cylindrical coordinate system (r, θ, z), where θ is the angle between r and the x-axis.

The third model is called the local transformation model. In this model the origin of the capillary pressure in the island is believed to be in the difference between the lattice parameter of the surface and bulk atoms. Thus,

$$\sigma_r^T = \sigma_\Theta^T = \sigma_\Phi^T = \frac{(1-\nu)}{(1-2\nu)}\frac{f}{b}, \tag{3.15}$$

where b is the thickness of the surface monolayer.

The substrate curvature, induced by the islands, described in each model, can then be calculated as

$$C_I = -(\alpha_A + 2\alpha_E + \alpha_F + \alpha_G)A_A C_0; \tag{3.16}$$

$$C_{II} = -(\alpha_A + \alpha_B)A_A C_0; \tag{3.17}$$

$$C_{III} = -(\alpha_k + \alpha_L + \alpha_M)\frac{(1-\nu)}{1-2\nu}\frac{R_0}{b}A_A C_0, \tag{3.18}$$

where R_0 is the radius of the island, b is the thickness of the surface layer of the island, A_A is the areal fraction of islands, $C_0 = \frac{6\gamma(1-\nu_s)}{E_s d^2}$, γ is the surface energy and α_i are the geometrical parameters, which depend on the type of loading and can be determined numerically. The values of these parameters are given by Gill et al [Gill et al, 2002].

Models I and II are different from the model III in that the first two models assume substrate curvature to be a result of the effect of "transformation stress accumulated inside crystallite layers during deposition and that due to the capillary forces acting on the surface of the crystallite" [Gill et al, 2002]. In model III surface-to-bulk transformation strain is assumed. Despite of the differences in model assumptions, all three models predict substrate curvature satisfactorily. Yet, more work has to be done in order to clarify the differences between all the approaches and find out the conditions under which each approach should be used.

The second stage in CTC behaviour is tensile stress stage due to island coalescence/grain growth. A concept of surface energy also plays an important role in the models, explaining stress behaviour in this regime. However, it can be debated that these models should belong to the fourth group of stress origins, which take into account different re-crystallisation processes in the film. One model, belonging to this group, is that of densification by grain growth and grain boundary elimination. These processes are believed to be driven by the need of the growing system to minimise the elastic and surface energies. Island coalescence, treated by several authors, can also be considered a result of a balancing act between the surface and elastic energies.

According to Hoffman [Hoffman, 1976], contact of surfaces of neighbouring grains results in the generation of tensile stress. As the film grows and forms grains, attractive forces act between the atoms at the neighbouring grain boundaries, causing them to relax. At the same time tensile forces inside the grains balance grain boundary relaxation and the film experiences tensile stress. The strain energy is related to the difference between the energy of a free surface of the neighbouring grains and energy of a grain boundary. The stress can then be calculated as [Windischmann, 1992]

$$\sigma \sim \frac{E_f}{1-\nu_f}\frac{r_0}{\theta}, \tag{3.19}$$

where r_0 is the ionic radius and θ is the final grain size.

Nix and Clemens [Nix and Clemens, 1999] treated grain boundary formation as a closure of cracks in the elastic material, resulting in the reduction of the surface energy and formation of the elastic strain. Freund and Chason [Freund and Chason, 2001] treated elastic islands and the attractive forces between them so that volume-averaged stress

$$\left\langle \frac{\sigma^{(N)}}{E} \right\rangle = A_N \left(\frac{2\gamma_s - \gamma_{gb}}{2rE} \right)^{C_N}. \tag{3.20}$$

Here $N = 1,2,3$ is the model dimension, $C_1 = 1/2$, $C_2 = 2/3$, $C_3 = 1$ and $A_1 = 0.82$, $A_2 = 0.44$, $A_3 = 4$. Another model was proposed by Sheldon et al [Sheldon et al, 2001]. Here it is presumed that films of low-mobility materials grow such, that step edges in neighbouring grains are formed. As these edges become closer, attractive forces between them lead to the formation of tensile stresses. Additional stresses are then formed due to fast grain boundary growth (i.e. grain boundary formation rate is higher than the deposition rate). Freund-Chason model can be used to predict stress in "high-mobility" materials. Hoffman and Nix-Clemens models are more consistent with the stress behaviour in "low-mobility" materials. Hoffman model also gives the maximum stress value for the continuous film with established grain structure, independently of initial coalescence type.

Grain growth is another mechanism, which explains tensile stress in thin films. During this stage grain boundary volume in the film decreases and density increases, leading to a decrease in film volume and thus formation of tensile stress

$$\sigma = 2\frac{E_f}{1-\nu_f}\Delta a\left(\frac{1}{D} - \frac{1}{D_0}\right), \tag{3.21}$$

where D is instantaneous grain diameter, D_0 is as-deposited grain diameter and Δa is "the excess free volume per unit area of grain boundary" [Doerner and Nix, 1988].

The third stage in CTC film behaviour is the compressive stress stage due to film thickening. Here total film stress can be expressed as

$$\sigma = \sigma_0 - (f_1 + f_2)\left(\frac{1}{h_{cont}} - \frac{1}{h}\right), \tag{3.22}$$

where σ_0 is the stress in the film after coalescence of islands, h_{cont} is the initial (i.e. after coalescence) film thickness and $h > h_{cont}$ is the final film thickness. It is believed that the effect of the film surface stress at this stage is thickness-dependent, thus the total stress is changing with changing thickness.

Another explanation for film behaviour in the third stage of growth is based on the assumption of difference in chemical potential of the surface during and in the absence of deposition [Chason et al, 2002]. The schematic of the process is given in Figure 3.2. It is proposed that during deposition film surface is in the non-equilibrium state, which is expressed by the increased chemical potential relative to the equilibrium state. This drives atoms to migrate into and to overpopulate the grain boundaries, which, in turn, creates compressive stress in the film. This causes the increase in the chemical potential of the grain boundary, thus it becomes harder for the newly arriving atoms to migrate to the grain boundary and steady-state is achieved. It is proposed to calculate compressive stress σ in this state as

$$\sigma = \frac{\sigma_{tens}\hat{R} - \sigma_0\left(\left(\Delta\mu_0 + \delta\mu_s\right)/kT\right)}{\hat{R} + \left(\sigma_0\Omega/kT\right)} \tag{3.23}$$

where σ_{tens} is the tensile stress due to the grain boundary growth; $\hat{R} = R/(2aC_s\Gamma)$ is a normalised growth rate, $a = \Omega^{1/3}$ being the atomic spacing; Ω is the atomic volume; Γ is the kinetic parameter linked to the surface-grain boundary transition rate; $C_s = N_s\frac{a}{L}$ is the mobile atoms concentration on the surface, N_s being the number of mobile atoms at the grain surface and L being the length of the grain (in plane of the substrate); $\sigma_0 = E\alpha\frac{a}{L}$ is the compressive stress due to one atom at each atomic plane in the grain boundary added so, that there is no change in the grain size; $\Delta\mu_0$ is the difference in chemical potentials of the surface and the grain boundary at the equilibrium conditions; $\delta\mu_s$ is the difference in the chemical potentials of the surface in equilibrium and non-equilibrium conditions. In case of low surface mobility or high growth rate $\hat{R}$ is small and the steady-state stress is tensile due to the effect of grain boundaries. When there is

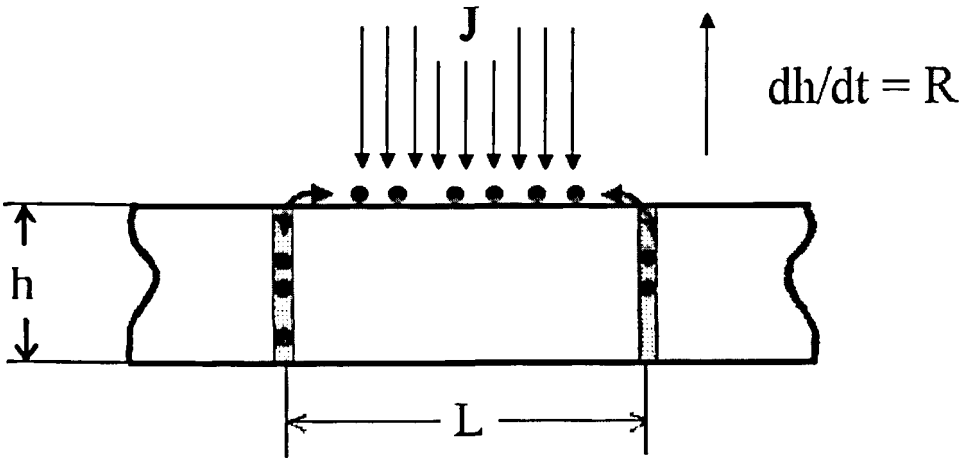

Figure 3.2. Schematic representation of the processes in the film during the deposition. [Chason et al, 2002]

no deposition flux the steady-state stress is predicted to be equal to $-\frac{\mu_0}{\Omega}$. It should be noted that concentration gradients, which may be present at the surface and grain boundary, as well as non-uniform stress in the film, are not taken into account.

The theory of CTC stress behaviour was initially proposed for polycrystalline materials with high mobility. However, the present study is concerned with amorphous films and stress evolution during film growth is also exhibited by evaporated amorphous films [Mayr and Samwer, 2001]. It is observed that evaporated amorphous $Zr_{65}Al_{7.4}Cu_{27.5}$ films pass three distinct stress regions during growth. For very thin films (up to approx. 50 nm) the stress is tensile, changing to compressive with increasing film thickness and finally changing back to tensile for even thicker (200-300 nm and above) films. In very thin films stress, and its changes, are commonly linked to the growth and coalescence of islands. The second stress change (from compressive to tensile) may be linked to the maximum development of the surface roughness by broadening and heightening of the surface structures. It is noted that other binary amorphous metals exhibit similar stress-surface structure behaviour, independent of the substrate features.

Amorphous film growth modelling showed that these films grow by self-shadowing and energy minimisation by atom diffusion. In the model by Mayr and Samwer [Mayr and Samwer, 2001] the stress is linked to non-diffusional morphology independent energy minimisation at the surface of the growing film, which occurs by changes in the surface packing density. For medium film thickness it is estimated that stress σ

$$\sigma = (f - \gamma)/t_0 , \tag{3.24}$$

where f and γ are the surface stress and energy respectively and t_0 is the thickness of the surface layer (can be estimated by the atomic roughness of the film).

In case of thicker films with rough surfaces "continuous liquidlike hill coalescence" is presumed to take place. If the surface can be represented by hexagonally arranged clusters with the radius $R_c/2$, the stress in thick films is given by

$$\sigma = (-6\gamma)/R_c . \tag{3.25}$$

This model was checked on several alloys and it was found that the calculated stress values are in a good agreement with the experimentally measured ones. Thus, after

island coalescence, stress levels in amorphous films will only depend on the shape of the surface.

As already mentioned above, the fourth group of stress origins include all models, which take into account re-crystallisation processes. Apart from those already considered, several other widespread models are worth reviewing.

It is believed that, due to the lack of grain boundaries in case of amorphous films, tensile stress cannot be explained by the grain boundary model [Andersen et al, 1999]. Instead tensile stresses are explained by the "freezing" model [Moske et al, 1989], which states that, on reaching the substrate, atoms transfer their energy and achieve "freezing" temperature. Tensile stress develops as a result of cooling from this characteristic temperature to the substrate temperature.

Another example of the model in this group is the "buried layer" model [Klockholm and Berry, 1968]. The model of a "buried layer" attributes stress formation to the re-arrangement of the atoms, buried below the advancing surface of the film. It is believed that initially the surface of the growing films is in disordered material state. As the film grows, this layer becomes buried under the advancing surface and re-orders itself by one of the thermally activated mechanisms (grain growth or defect annihilation). Such re-ordering causes constrained shrinkage and, thus, tensile stress generation. According to this model, contribution of the stress, caused by the "buried layer" growth to the total film stress will be zero, if the film is deposited under high temperature ($> T_{melting}/4$) or under very low temperature, when the re-arrangement is inhibited and atoms are "frozen" in their positions. This model was further re-developed for amorphous films to state that only "amorphous phases with a short range order similar to that of a liquid (frozen liquids) grow without internal stress" [Buckel, 1969].

Probably the most general model was proposed by d'Heurle and Harper [d'Heurle and Harper, 1989]. It is known that evaporated films, deposited in the absence of ion bombardment or impurity incorporation, are normally in the state of tensile stress. A general thermodynamic model thus states that evaporated films are initially in a state of disorder, which is characterised by increased volume of the material. As the film relaxes towards a more ordered state, the volume decreases, which leads to the formation of the tensile stress in the film. The rate of relaxation should be less then the rate of deposition, otherwise the free surface will relax and the holes will be filled in by newly arrived atoms. Other models, based on the same principle, are believed to be the special cases of this generalised approach.

The fifth group of origins of stress in non ion-assisted thin films includes theories on the influence of voids and dislocations in films. Many authors [e.g. Hudson and Somekh, 1995] link tensile stress, often exhibited by evaporated films, to highly voided, low density microstructure of these films. As the number of voids decreases and density increases, films start to develop compressive stress, which is mostly attributed to the influence of ion bombardment, necessary for production of such films. Generally, it may be more accurate to talk about the adatoms energy, and thus their mobility as a source of changing void population and, therefore, stress, rather than simply about void-stress correlation. In non ion-assisted films adatom energy can be changed by changing deposition process, for example, switching from evaporation to sputtering. Part of recent molecular-dynamics simulations by Fang et al [Fang et al, 1993] were devoted to the subject of adatom energy – microstructure – stress link. Simulations were performed for Ni film deposition onto a Ni substrate. To study the effect of adatom energy (0.1-6.0 eV) experiments were performed in the absence of ion bombardment and background gas. It was found, that for atoms with low energy (approx. 0.1 eV) film stress is tensile, film density is low and film structure is columnar with large open voids. In this region there is a possibility for atoms to relax into the unoccupied spaces, thus tensile stresses are small. Increase in adatom energy (approx. 2.0 eV) leads to disappearance of columns and large voids. The film in this region is characterised by the presence of vacancies and high tensile stresses due to atomic interactions near the vacancy sites. Further increase in adatom energy (approx. 4.0 eV and higher) leads to almost defect and stress-free, dense films. Although with an increase in adatom energy the density exhibits asymptotic behaviour, the stress increases, passes though a maximum point and then decreases.

In the last group phase transformation is linked with the film stress. Again, it can be argued that this group can include group four and thus be a more general case. It is supposed, that phase transformation leads to volume changes in the film, which inevitably leads to stress generation or relaxation, depending on the sign of the volume change. As an example, amorphous as-deposited film, undergoing phase changes by re-crystallisation, say, due to heating, can be taken. However, as it was rightly noted by Windischmann [Windischmann, 1992], observable stress changes may not be solely due to the phase change itself, but also have a contribution due to grain growth and grain boundary formation.

In conclusion, it is worth noting that at the moment there is no single unified theory, explaining stress behaviour of non ion-assisted films. Although origins of stress can be

divided into groups or classified, in real life several mechanisms can be working together, thus several theories may be needed to explain stress at different stages of film growth or total resultant stress in the film.

3.1.3. Intrinsic stresses in ion-assisted thin films

As already mentioned, ion bombardment of the substrate and film can significantly influence the properties of the resulting materials [Colligon, 1995]. Adhesion, corrosion resistance and hardness can be improved by the use of ion implantation before, during or after the deposition. It is also possible to guide the film growth in a preferred crystallographic orientation. A detailed discussion of these effects as well as the influence of ion bombardment on stress can be found in a paper by Wolf et al [Wolf et al, 1991]. These authors consider that the main parameters that influence the film stress, developing during the ion-assisted growth, are the ion to atom arrival ratio, ion energy and residual gas pressure. In most cases an increase in ion-to-atom arrival ratio gives rise to a compressive stress and decreases the tensile one.

The effect of ion beam assistance on the film, its properties and its stress have been studied by many authors with the help of the molecular-dynamics simulations [for example, see review by Muller, 1989]. Here parts of one of the recent studies by Fang et al [Fang et al, 1993], relevant to the subject of ion assistance will be reviewed. It is known that non ion-assisted films with low adatom mobility often exhibit voided porous microstructure and tensile stress values. In the work by Fang et al [Fang et al, 1993] first the effect of 50 eV Ar ion bombardment of Ni film on Ni substrate with the ion-to-atom arrival ratio of 1.33 is considered. It is presumed that there are no gas impurities in the film. It was found that ion bombardment breaks down the columnar film structure and densifies films by knock-on filling of large voids. The peak of tensile stress shifts towards the region of lower adatom energy in comparison to the non ion-assisted films and with further increase in adatom energy stress decreases to almost zero level. However, ion bombardment often leads to incorporation of the bombarding species into the film bulk, thus a study of the combined effect of inert gas incorporation and ion bombardment was performed. Such a study shows an increase in density and decrease in the number of loosely trapped impurities in ion-bombarded films. In the low adatom mobility region this leads to high tensile stress in the film. In the medium adatom mobility region the stress becomes compressive due to the local compressive fields

around tightly incorporated impurity atoms. An increase in the energy of bombarding ions leads to dense films with fewer impurity atoms and higher compressive stress levels. Thus, it is concluded, that the magnitude of compressive stress in ion-assisted sputtered films is strongly dependent not on the total amount of inert gas atoms, but on the amount of impurity atoms, which are tightly trapped in the film and a well-known effect, called "atomic peening".

Although the question of inert gas incorporation into the film as a source of compressive stress generation is still debated, the second reason, namely, "atomic peening" is often used to explain stress behaviour in ion-assisted films [e.g., d'Heurle and Harper, 1989]. The term "atomic peening" takes its origins from the well-known term "shot" peening, which describes compressive stress generation in a material, subjected to repetitive impacts. It is believed, that this mechanism leads to surface atoms being implanted into the film bulk to occupy non-equilibrium positions, which are smaller than those available under equilibrium conditions. This causes film swelling and thus leads to compressive stress, which is an outcome of interaction between the plastically deformed subsurface layer, resulting from the impacts, and its surroundings [Carter, 1994]. It should be noted, that in the present study for ion-beam sputtered films "atomic peening" may result not only from the bombardment with specially directed ions, but also from bombardment with energetic neutralised ions, reflected from the target. High atomic mass metals, which have low mobility, are most influenced by this atomic peening effect [Ramaswamy et al, 2001].

One of the first quantitative models, developed to describe the effect of atomic peening on stress in thin films, was presented by Windischmann [Windischmann, 1987]. The model was derived for polycrystalline films condensing under low deposition temperature from a non-single-crystal target and links stress to the film properties (elastic modulus and molar volume) and deposition conditions (ion bombardment). The materials of the film and the substrate were presumed to obey Hooke's law for a biaxial stress state. It is believed, that both energetic ions, directed to bombard the growing film, and neutralised particles from the sputtering beam, back-reflected from the target, should be taken into consideration. On the basis of Sigmund's knock-on linear cascade theory and presuming that the deposition temperature is less then 0.25 times the melting temperature, the stress is represented as

$$\sigma = 4.79 KI \sqrt{E_i}\, \delta Q / N_0 , \qquad (3.25)$$

where K is a constant, I is ion flux, E_i is the bombarding ion energy, $Q = EM_a/(1-\nu)\rho$ is the elastic energy per mole, $E/(1-\nu)$ is the biaxial modulus of the film material, ρ is the density of the film material, N_0 is the Avogadro's number and $\delta = \sqrt{Z_a Z_i}/U_0\left(1+\frac{M_i}{M_a}\right)^{1/2}\left(Z_i^{2/3}+Z_a^{2/3}\right)^{3/4}$, $Z_{a,i}$ and $M_{a,i}$ being atomic number and mass of atom and ion respectively and U_0 being the target sublimation energy. Simplified, this leads to expression

$$\sigma = 1.91KI\sqrt{E_i}Q/N_0. \tag{3.26}$$

The formula above predicts a square-root dependence of stress on the bombarding ion energy, therefore, it is concluded that the stress is a momentum (or momentum-dose $P = \frac{I}{A}\frac{2M_i}{M_i+M_a}\sqrt{2E_iM_a}$ from [Rizzo et al, 2001]) dependent property. It should be noted, that the Windischmann model is not expected to predict stress correctly for the evaporated films, as during evaporation the energy of arriving target atoms as well as density of the resulting film are low, so bulk values for elastic constants cannot be used in the calculation.

Several other limitations on the use of the Windischmann model exist [Windischmann, 1992]. First, it cannot be used in case of bombardment with light ions. The Windischmann formula is based on Sigmund's theory and the condition $Z_i/Z_a << 1$ invalidates it. Second, the Windischmann formula is valid for a finite range of bombarding ion energies. The lower limit of this range is approximately equal to the threshold or atomic displacement energy, as below this value sputtering theory cannot be applied. The upper limit of this range is set by the energy, at which re-sputtering and plastic flow begins in the film.

Another model, which takes into account the influence of ion bombardment, was proposed by Carter [Carter, 1994]. Here densification and the effect of ion bombardment are considered the main mechanisms behind stress generation process. It is noted, that, according to simulation studies, densification and stress changes are ballistic-driven processes, and not thermal spike driven ones, although thermal spikes can cause re-arrangement of surface atoms.

In the derivation of the model it is presumed that ions impact the substrate normally with a flux density of I. The film is deposited simultaneously with the flux density of atoms of A. The substrate is self ion-bombarded and self-atom deposited and several effects, such as ion implantation or relaxation, are not considered.

The model describes several main processes, happening in the film during growth. First process is the steady state flux of forward recoil atoms, which is directed from the surface into the bulk of the film. This process results in film densification and thus, modification of the tensile stress in the thin film. It can be shown that the fractional densification N_m^1/N can be expressed as

$$\frac{N_m^1}{N} = \frac{I}{A} Y_F \propto \frac{I}{A} \sqrt{E_i} \,. \tag{3.27}$$

Here Y_F is the forward recoil yield, N is the atomic density of the film and N_m^1 is the maximum additional concentration.

However, it is noted that densification is not indefinite. With increase in normalised energy of bombarding ions, packing density of the film increases, i.e. film densification occurs by filling in the voids with forward recoils that are generated by ion bombardment. As the void diameter decreases, the attractive interatomic forces become stronger and thus the tensile stress is increased. With further increase in normalised energy of bombarding ions film packing density saturates, which can be attributed to a decreasing number of surface recoils with increasing bombarding energy and to the fact, that, as the maximum value of density is achieved, further densification is prevented by local relaxation. Thus, the tensile stress decreases and disappears together with the disappearance of the voids.

This part of the model was compared to the model, proposed by Windischmann [Windischmann, 1987]. Windischmann related densification to the formation of compressive stress, but not to the modification of tensile stress. The initial increase in tensile stress with increase in ion bombardment also was not described.

The formation of compressive stress in the Carter model is attributed to the effects of ion bombardment. Ion bombardment of metals leads to formation of dislocations, which is linked to the formation of compressive stress. Compressive stress formation in covalently bonded materials is ascribed to the effect of amorphization under

bombardment and resistance to plastic flow (plastic flow leads to stress relaxation and takes place if film stress levels are higher than the yield level).

The second process, described by the Carter model, is the change in total number of recoil atoms. Steady state density of recoil atoms can be expressed as

$$\frac{N_R}{N} = \frac{0.42}{E_d}\frac{I}{A}F_d \propto \frac{0.42}{E_d}\frac{I}{A}E_i, \tag{3.28}$$

where E_d is the displacement energy and F_d is "the total energy deposited in elastic collision". Under ion bombardment recoils will migrate and some will form dislocations and dislocation loops. The forces between the loops will generate compressive stress, which in this case can be represented by

$$\sigma = K\left(\frac{I}{A}E_i\right)^{1/2}, \tag{3.29}$$

where $K = const$.

For a covalently-bonded film material the Carter model describes the changes in the steady-state amorphous fraction in a film. Here the fractional amorphous volume V_α can be expressed as

$$V_\alpha = \frac{I}{A}\nu_\alpha \propto \frac{I}{A}E_i^{3/2}, \tag{3.30}$$

where ν_α is the "fractional atomic volume amorphized by each ion impact" [Carter, 1994].

Finally, it should be noted that the Carter model is derived for the case, when re-sputtering of the growing material is negligible and modifications need to be made to take into account the opposite effect. It is thought, that in this case stress would be an independent function of *I/A* and ion energy. This model also does not take into account several other effects, such as preferential sputtering or bombarding gas incorporation and accumulation in the film bulk.

A different model, explaining stress behaviour under ion bombardment was proposed by Davis in 1993 [Davis, 1993]. This model takes into account two mechanisms,

responsible for stress behaviour. One of the mechanisms is "atomic peening" and is responsible for the formation of the compressive stress. Davis states that in this case ions and atoms are equivalent for the purpose of stress formation. The second mechanism is based on "thermal spike" mechanisms and it is responsible for stress relaxation. Atoms, implanted below the film surface, are resting in metastable positions. Provided with additional energy they will readily escape to the surface of the film, causing stress relaxation. This additional energy can be supplied by a "thermal spike", i.e. intensive local heating caused by motion of atoms, which have received additional energy from the bombarding ions. The film stress can then be expressed as

$$\sigma \propto \frac{E_f}{1-\nu_f} \frac{E_i^{1/2}}{A/I + kE_i^{5/3}}. \tag{3.31}$$

Here E_i is less than 1 keV and k is a constant depending on the film structure and composition.

As noted by Davis, this model considers both processes of stress generation and stress relaxation. The proportionality factor in the equation above and the constant k are both strongly dependent on the particular film and are thus unknown. They can be used to fit the model to the existing experimental data for the purpose of predictions. Hoang et al [Hoang, 1996] used A/I and k as fitting parameters and, although the Davis model was derived assuming the substrate temperature to be 0 K, Hoang et al have applied it to experimental data at deposition temperatures less than 130°C and seem to have obtained a reasonable fit (see Figure 3.3.).

In the case of low values of the ion to deposition flux ratio (so that A/I is large compared with $kE_i^{5/3}$), The Davis equation can be shortened to the form of the Windischmann formula with the correction of Cd

$$\sigma = \frac{E_f}{1-\nu_f} \frac{AE_i^{1/2}}{dN} = \sigma_{Windischmann\ theory} / Cd, \tag{3.32}$$

where d is the deposition rate, material-dependent constant $C = \frac{1.91KQ\rho(1-\nu_f)}{N_0 E_f}$ and ρ is a film density.

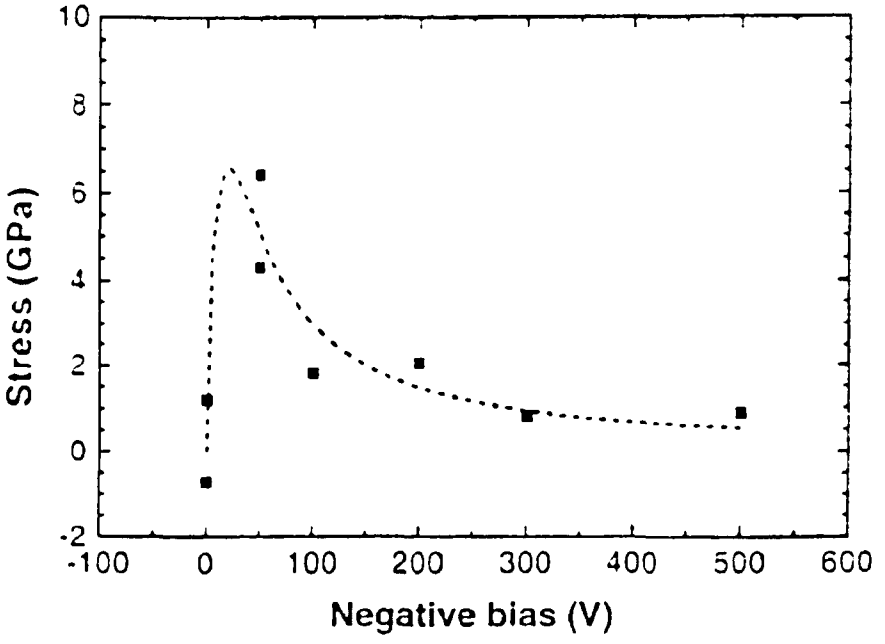

Figure 3.3. Results of the Davis model fitting (dashed line) to experimentally measured stress values (black squares) in TiN films, deposited by RF sputtering with varied bias potential of the substrate. [Hoang, 1996]

In cases, when A/I is very low, i.e. for high normalised flux, the Davis formula can be written in the form

$$\sigma \propto \frac{E_f}{1-\nu_f} \frac{1}{kE_i^{7/6}}. \tag{3.33}$$

Finally, it should be noted, that the Davis formula was derived for structureless films at zero temperature, therefore temperature effects, as well as the influence of, or, changes in film structure, composition or density, are not included into the formula.

Results of recent numerical experiments on the influence of ion bombardment by Koster and Urbassek [Koster and Urbassek, 2002] highlight other deficiencies of the Davis model. In their experiments, Koster and Urbassek studied the influence of impact of silicon ions with energies between 10 and 150 eV onto a stress-free and compressively stressed amorphous silicon target. It is mentioned that atom bombardment produces damage and in case of amorphous materials this damage may be characterised by the amount of over- or under-coordinated atoms. It was found that more over-coordinated atoms are produced as a result of ion bombardment. It was also found, that stress behaviour due to ion bombardment depends on the initial stress state of the target. For the stress-free target, the stress due to ion bombardment is almost zero, with a slight tendency towards the compressive regime. In the initially compressed target, significant stress changes are observed. These changes range from compressive to tensile and depend on the energy of the bombarding ions. In order to explain the origins of such behaviour, two quantities, namely atom energization and recoil implantation, are considered. It was found, that more atoms are energised as the energy of bombarding ions increase, and that these two quantities are related linearly. In a stress-free sample all energised atoms end up in the compressively stressed positions, while in the compressively stressed sample all energised atoms end up in the relaxed state positions. Thus, it is concluded that the hypothesis of stress relaxation by thermal spikes, used in some models, may only be true in case of initially compressively stressed samples.

The studies of recoil implantation showed that, in the case of long-ranged implantations, the initial stress state of the sample does not influence the number of implanted ions. For short-ranged implantations it was found, that atoms find it harder to relax to their original positions in the case of an initially compressively stressed target due to the slight increase in density, thus there are more displaced atoms in this sample. Again, the number of recoil-implanted atoms and energy of bombarding ions are found to relate

linearly. The stress behaviour depends on the path of recoil atoms and ion energy. If the recoils are relocated towards the surface, the stress relaxes. For forward-implanted recoils, compressive stress is generated in the initially stress-free sample. The result of forward recoil implantation into the initially compressively stressed target depends on the energy of bombarding ions. If this energy is quite large, implantation relaxes the stress. If the ion does not have enough energy to relax its surroundings, compressive stress is generated. Thus, it is concluded that, in an initially stress-free target the effect of forward- and backward- recoil implantation is balanced, leading to almost zero net stress. In an initially compressed target and for relatively high energies of bombarding ions, stress is relaxed by both forward- and backward- recoil implantation. In the case of an initially compressed target and low energy of bombarding ions, forward-recoil implantation leads to compressive stress. Again, these results question the validity of some stress behaviour models (including the Davis model), which do not take into account the initial stress state and only assume that forward recoil implantation leads to compressive stress generation.

The Davis model of stress behaviour under ion bombardment only takes into account the influence of ion bombardment and presumes the film is structureless. However, more recent models have started to appear, which also take into account film structure and explain stress behaviour in the transition zone, where stress changes from compressive to tensile. Knuyt et al [Knuyt et al, 2000] propose a semi-quantitative model, predicting the stress behaviour in this zone.

The proposed model presumes columnar growth in the film with depletion zones (zones with lower density) in-between the columns. It is proposed, that the energy density E in the film consists of two contributions. The first is a result of the material's elastic deformation, whereas the second is due to the existence of the depletion zones. As during film growth elastic energy tends to its minimum value, stress can be represented as

$$\sigma = \frac{E_f}{1-\nu_f} \frac{\Delta - \left(d_{depl}\right)_{\min E}}{d_0}, \tag{3.34}$$

where $d_0 = d_{gr} + d_{depl}$, and d_{gr} and d_{depl} are the lateral dimensions of the grain (mean distance between the atoms of the opposite sides of the grain) and depletion zone (mean distance between atoms on the neighbouring sides of the two grains), respectively. The value of $\left(d_{depl}\right)_{\min E}$ is defined as the breadth of the depletion zone, at which the

minimum in energy density is obtained. The parameter Δ is a growth-related parameter and can be represented as

$$\Delta = \Delta_{shad} - \frac{1}{3} d_0 f_{an} n_V \frac{I}{A}, \tag{3.35}$$

where $\Delta_{shad} = d_0 - d_{gr,0}$ expresses the effects of column shadowing, surface diffusion and thermal relaxation of the film material with $d_{gr,0}$ expressing these effects at the grain boundary; f_{an} is an anisotropic volume expansion factor (equal to 1 in the case of isotropic grain expansion due to the effect of ion bombardement); n_V is a parameter, which takes into account the energy of bombarding ions and defects in the film material. Analysing the formula, two cases of stress behaviour can be distinguished. When the contribution to the total elastic energy of the system is mainly due to the elastic deformation of columns, $\left(d_{depl}\right)_{\min.E} \approx \Delta$, so that $\sigma \approx 0$, i.e. the value of stress is negligible. When the contribution is mainly due to the depletion zones, $\left(d_{depl}\right)_{\min.E} \approx d_{depl,0}$ and thus stress can be represented as

$$\sigma \approx \frac{E_f}{1-\nu_f} \frac{\Delta_{shad} - d_{depl,0}}{d_0} - \frac{1}{3} \frac{E_f}{1-\nu_f} f_{an} n_V \frac{I}{A}. \tag{3.36}$$

The first term of this equation expresses tensile stress due to shadowing effects in the film. The second term expresses compressive stress due to the effect of energetic ion bombardment during film growth. Thus, the total stress is the balance of these two contributions, and the formula above can predict transition from compressive to tensile stress and stress behaviour due to the column size or flux of incoming ions.

Another way of prediction of the residual stress arising in thin film is the use of a Finite Element (FE) Simulation [Ward et al, 1999]. This method can be used to study the effect of different deposition parameters on the stress magnitude and has an advantage of a low computational cost. In FE simulation, as well as in other models, it is considered that the residual stress arises due to defects created in coating during deposition and ion bombardment. Although Ward et al [Ward et al, 1999] criticises the Davis hypothesis of stress generation due to the formation of interstitial coating atoms, which would lead to over-dense coatings, not commonly observed, and believes that stress is due to the interstitial bombarding gas atoms incorporation, the FE simulation is

still based on the Davis theory, as it is believed that the nature of stress-generating particles does not affect computer model validity. Thus, the rate of compressive stress creation ε is accounted by

$$\varepsilon = -k_1 I\sqrt{E_i}\ , \tag{3.37}$$

where k_1 is a material dependent parameter, I is the flux of ions and E_i is the ion energy. The rate of stress relaxation ε' is accounted by

$$\varepsilon' = -k_2 \varepsilon I\left(\frac{E_i}{I_{0(INT)}}\right)^{5/3}, \tag{3.38}$$

where k_2 is a proportionality constant and $I_{0(INT)}$ is the effective excitation energy for the knock-on implantation of coating atoms.

The residual stress is numerically calculated after treating a small layer of added coating material with energetic ions impact. As additional layer thickness is small and the time step tends to zero, the processes of deposition and bombardment can be considered as simultaneous. The results of the calculation can possibly be used to develop a failure criterion for a coating or to explain some trends of stress evolution. As it is, the model does not include temperature dependence, which can introduce corrections in the resulting stress value. Further literature on finite element simulation and its application to the studies of stress in thin films can be found elsewhere [Mackerle, 2001].

3.2. Stress measurement methods

In order to evaluate stress state of products and components and further understanding of stress origins and behaviour, various stress measurement techniques have been developed over the years. Older, destructive or somewhat cumbersome methods, for example, hole drilling or material removing methods, (A brief overview of these methods, as well as many others, has been reported [Withers and Bhadeshia, 2001].) are now being succeeded by modern techniques, which were specially developed or adjusted for thin film measurements, possess exceptional sensitivity and in many cases do not require any special sample preparation.

It has become customary that all modern techniques are classified and arranged into two main groups [see, for example, Ruud et al [1993]]. The first group covers various methods, which are based on substrate curvature measurement. The second group utilises the diffraction of X-rays by the interplanar spacing in the film. Other methods of stress measurement, such as electron or neutron diffraction or properties monitoring (stress can influence, for example, values of critical temperature or ferromagnetic resonance), exist, but they are not as common due to low availability, high measurement costs or low sensitivity [Maissel and Glang, 1970].

Techniques, based on X-ray diffraction, are described in detail by Noyan et al [Noyan et al, 1995]. Widespread X-ray techniques are based on measurements of the plane lattice spacing of the film and correlation of changes in the measured values to the strain in the film. Thus, the behaviour of the film crystal structure is often compared to that of a common strain gauge. It is known, that in crystals and polycrystalline materials X-rays are diffracted according to the Bragg's law ($n\lambda = 2d\sin\theta$, n=1,2,..., λ is the radiation wavelength, d is the measured lattice plane spacing and θ is the angle diffracted peak makes with the lattice plane). Analysis of the shape of the diffracted peak itself can yield some information: the shift in the position of the peak shows the presence of elastic deformation, broadening of the peak may be a sign of a plastic deformation. However, data interpretation can sometimes be complicated by the fact, that peak broadening can also result from the reduction of crystallite dimensions. The strain in the direction normal to the diffracting plane is calculated as $\varepsilon = (d - d_0)/d_0$, d_0 being the plane lattice spacing of the unstrained film material. Usually several measurements are taken and values of strain for up to 6 different families of lattice planes are calculated. This allows transformation to the sample coordinate system and calculation of stress according to the Hooke's law.

Several major disadvantages of the approach described above prevent the use of X-ray diffraction methods in the present research. First, the presence of crystal structure in the coating is required, i.e. only crystalline films can be studied. Second, X-ray methods are not so well suited for *in-situ* measurements and are usually used to carry out *ex-situ* analysis.

Most methods, based on non X-ray substrate curvature measurements, could be applied both *ex-situ* and *in-situ*, and therefore allow observation of the stress evolution during film growth [Gerlach et al, 1998]. This is one of the main advantages, which, together with several other features, makes substrate curvature methods increasingly popular. Substrate curvature methods can be used for films with different properties, such as

thickness [Sander et al, 1995], magnetic features [Weber et al, 1994] and the number of layers in multilayer systems [Fayeulle et al, 1997; Townsend et al, 1987]. These techniques are also viable for films deposited by different methods, such as CVD [Hearne et al, 1999], thermal spraying [Gill et al, 1994; Kuroda et al, 1988], magnetron sputtering [Malhotra et al, 1997] and ion-beam-assisted deposition [Gerlach et al, 1998] to mention a few. Generally, these techniques work with any process, as long as there is a clear optical path to the substrate and the substrate is coated on one side only.

Substrate curvature techniques are based on observation of the film-substrate system behaviour. It is known that a stressed film with good adhesion to the substrate will bend the substrate in order for the system to reach an equilibrium state. Stress in the film is then calculated from the measured amount of the substrate deflection relative to the initial shape.

Two kinds of substrate shape are commonly used in stress measurement experiments. The choice of the substrate shape relies on the expected properties of the film stress field. If the stress in the plane of the film is anisotropic, a circular substrate should be used. For mean isotropic stress it is sufficient to use a substrate in the form of a cantilever beam rigidly clamped at one end and free at the other [Hoffman, 1976]. The film has to cover only one side of the substrate.

The measurement of substrate deflection may be performed in several ways. One of the simplest methods is to obtain the information on the substrate shape before and after the deposition by profilometry [Thomas et al, 1988]. This method, which can be easily used and implemented in almost any laboratory, has a disadvantage of being an *ex-situ* method. Another simple method is an interference method [Maissel and Glang, 1970]. Here a sample is placed onto an optical flat and substrate deflection is measured from the changes in the interference fringe positions for the substrate with and without a film. The disadvantages of this method include the fact that it is an *ex-situ* technique and requirement of a relatively thick substrate, so that electrostatic forces between the sample and the optical flat can be ignored. Among many others (for surveys see e.g. [Maissel and Glang, 1970]), examples of more elaborate substrate deflection measurement methods include use of an electrobalance [Klokholm, 1969]; monitoring changes in capacitance [EerNisse, 1971; Gerlach et al, 1998] between the sensor plates and the sample or using a commercially available strain gauge [Cremona et al, 2000]. However, it seems that the most easily implemented *in-situ* methods are various reflection methods.

Reflection methods include laser reflection [Sander et al, 1995; Flinn et al, 1987], surface-stress-induced optical deflection (SSIOD) [Bicker et al, 1998; Shell-Sorokin and Tromp, 1990; Martinez et al, 1990] or commercial variations of these techniques (multiple-beam optical stress sensor (MOSS) [designed and supplied by K-Space Associates, Inc., Ann Arbor, MI] and a dual wavelength technique [designed and supplied by KLA-Tencor] systems).

The principles of operation of the laser reflection method are illustrated in Fig. 3.4. An incident laser beam is reflected by the substrate and its position is recorded (for example, sensed by a position-sensing detector (PSD)). If, during deposition, the substrate shape stays the same, the position of the "reflected" beam is also constant. With a change in the substrate curvature, the position of the "reflected" beam on the sensor changes. This difference in the position of the beam is related to the substrate curvature according to the geometry of the experiment. For a cantilever-beam substrate the radius of curvature R can be calculated as

$$R = -2lx/d \tag{3.39}$$

where l is the distance from substrate to detector, x is the distance from the clamped end of the substrate to the point, where the measurements are taken, and d is the deflection of the laser bream from its initial position, measured at the detector [Moulard et al, 1998]. From the measured radius of curvature it is possible to calculate the mean stress through the thickness of the film using the Stoney formula [Stoney, 1909], discussed in the next section.

The method of laser reflection has many advantages, for instance, the stress measurement equipment is located outside the vacuum chamber and thus would not be influenced by any reactive or otherwise harmful environment present in the chamber during deposition [Taylor et al, 1998]. However, it is susceptible to introduction of significant errors into stress values due to the influence of vibrations or changes in substrate position resulting, for example, from the thermal expansion of the substrate clamp. The sensitivity of the method can also be reduced as a result of the decrease in length of the optical path, therefore it is always better to use a fairly long optical path to improve the sensitivity of the device.

The problem of undesired clamp movements can be avoided by using SSIOD (Figure 3.5) or scanning (Figure 3.6) techniques [Flinn et al, 1987]. In SSIOD the incident laser

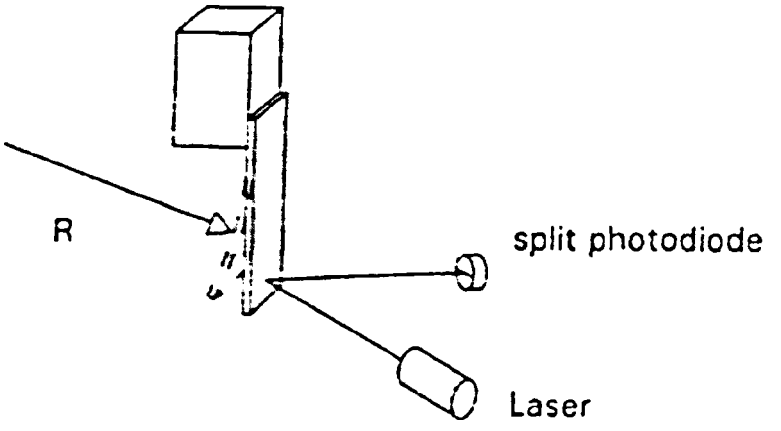

Figure 3.4. Principles of operation of the laser reflection method. Note that substrate dimensions and deflection are exaggerated for clear representation of the principle. [Sander et al, 1995]

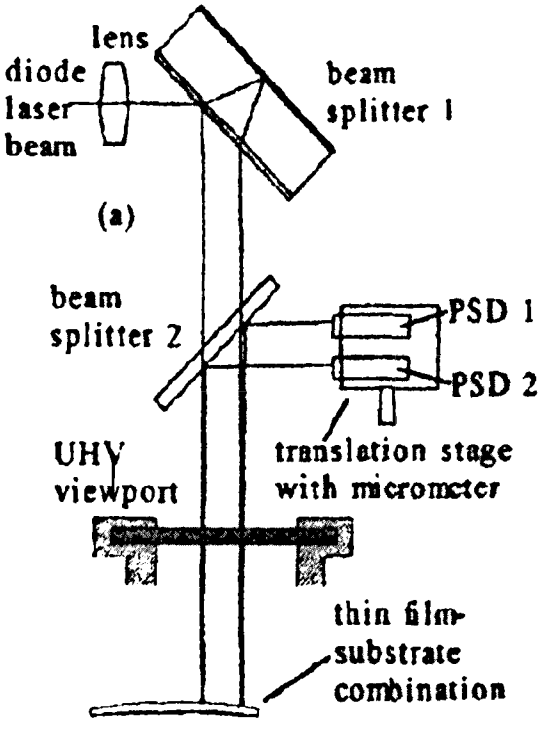

Figure 3.5. Principles of operation of SSIOD method [Bicker et al, 1998].

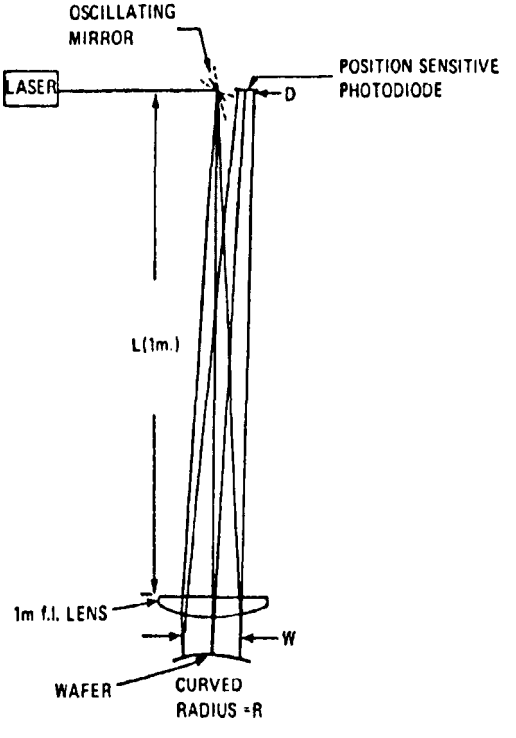

Figure 3.6. Principles of operation of scanning method of stress measurements [Flinn et al, 1987].

beam is split in two and directed onto the substrate so, that one beam hits the free end of the cantilever sample, while the other beam hits the clamped end. In scanning techniques the substrate is scanned through its length and measurements are taken in several points along the length, thus the substrate profile can be obtained. In both techniques information on the movements of the clamped end is available and this source of error can be accounted for. Also, it is possible to minimise the influence of vibrations by mounting the laser and detector housing directly onto an optical flange of a vacuum system [Sander et al, 1995] or taking measurements of several points on the sample simultaneously [Taylor et al, 1998].

Two groups of stress measurement techniques (substrate curvature-based and X-ray diffraction-based) have been compared by Malhotra et al [Malhotra et al, 1997]. Generally, for the case of magnetron sputtered Mo films magnitudes of average biaxial stress, obtained by different techniques, were comparable, but the substrate curvature based technique yielded the lowest stress value. This can be explained by the fundamental differences in the measurement techniques. Often stresses are referred to either as macroscopic or microscopic. Macroscopic stresses vary gradually over macroscopic length, while microscopic stresses (such as intragrain stress or stress due to phase precipitation) have a strong point-to-point variation. X-ray methods are sampling the film itself and in the final result often may include contributions from both macroscopic and microscopic stresses. Thus, results obtained from X-ray diffraction methods, will to a certain degree depend on the internal state of the diffracting grains [Noyan et al, 1995]. Substrate curvature-based techniques, on the other hand, are sensitive to macroscopic stress only and the result can also include contributions due to extrinsic stress or stress existing entirely due to the presence of the substrate [Malhotra et al, 1997].

3.3. Formulae for evaluation of stress level

Techniques, discussed in the previous section, measure the radius of curvature of the stressed composite system of substrate and film. This measurement can be directly related to the stress, arising in the film, by the Stoney formula, which was introduced in 1909 by Stoney and modified in the middle of the century to its present form

$$\sigma = \frac{E_s}{1-\nu_s}\frac{d^2}{6Rt}, \tag{3.40}$$

where σ is the stress of the film, t is the thickness of the film, R is the radius of curvature of the strip, d is the substrate thickness, E_s is the Young's modulus and ν_s is the Poisson ratio of the substrate. The factor $\left(\frac{E}{1-\nu}\right)$, is also known as a biaxial modulus of the material.

This expression is known under the name of the modified Stoney formula and is often cited, since it requires knowledge of only the substrate properties, but not those of the film. Hoffman [Hoffman, 1966] has proposed that, since the film stress is related only to the measured substrate strain, the elastic properties of the film can be neglected in calculations. The formula is also independent of the film microstructure and composition. The other advantage of this formula is that, in the case of a multilayered film, the final stress can be represented by the sum of the stresses induced by each film layer independently. This formula may be derived on the basis of minimising the energy of the system [Flinn et al, 1987] or using the results of a beam bending theory [Nix, 1989; Clyne, 1996].

It is presumed that the substrate is initially flat, which is not always true. To avoid the error, caused by any initial curvature of the substrate, the following formula is used

$$\sigma = \frac{E_s}{1-\nu_s}\frac{d^2}{6t}\left(\frac{1}{R}-\frac{1}{R_0}\right), \tag{3.41}$$

where R_0 is the initial curvature of the uncoated substrate.

Modified Stoney formulae are only valid under certain conditions:

- the adhesion between the substrate and the film is good,
- the film has a uniform thickness,
- the film is thin in comparison to the substrate thickness. According to Moulard et al [Moulard et al, 1998], the thickness of the film should be not more then 5% of that of the substrate,
- the substrate should be elastically isotropic in the plane of the film,
- the stress is isotropic and uniform in the plane of the film,

- the radius of curvature of the specimen is much larger than the substrate thickness or maximum deflection of the sample is smaller than half the substrate thickness [von Preissig, 1989],
- the conditions for Hooke's law are fulfilled both for the substrate and the film, and,
- the length of the substrate is relatively large compared to its width. A ratio of 3 is acceptable.

There are two points of view on the value of Young's modulus that should be used in the modified Stoney formula. According to Gillet et al [Gillet et al, 1998], the modulus of elasticity of the substrate and the film should be of the same order of magnitude, while Nix [Nix, 1989] stated that, for thin films, it is possible to neglect the influence of the difference in elastic properties of the film and the substrate.

Many authors [for example, Hoffman, 1966; Brenner et al, 1949; Davidenkov, 1960] pointed out deficiencies and limitations of the Stoney formula. Attempts were made to increase the accuracy of the formula by taking into account the difference in the Young's modulus of the materials, the change in stiffness of the specimen and the stress relief during the deposition due to the change in the radius of curvature of the coated substrate. However, authors themselves have noted that corrections introduced by more accurate formulas usually did not exceed 5 percent.

Recent attempts have been made to modify the Stoney formula, so that it will be applicable in case of thick coatings or large deformations (for example, see [Dobrynin, 1997], [Freund et al, 1999] or [Klein, 2000]). However, the comparison of the calculations according to the recent formulae and the modified Stoney formula has shown that, for thin films on relatively thick substrates and ranges of deformation, observed in the work reported in this thesis, it is possible to use the simple Stoney equation without introducing any significant error.

The assumption of the existence of the neutral axis in the substrate, where the bending moment is equal to zero, made in the derivation of the Stoney formula, were questioned by Chu [Chu, 1998]. Chu states that in the case of simple bending of a bi-layer structure by externally or internally applied moments, which results in convex or concave only shape, non-zero net bending moment exists. Zero net bending and thus neutral axis, where the bending curvature is equal to zero, can exist only in specially designed structures with number of layers more or equal to three, or in case of complex *sin*-like bending configuration. Thus, Chu considers neutral axis for stress, i.e. axis, where the stress is equal to zero. In a bi-layer structure, subjected to internal stresses, for example, due to the difference in thermal expansion coefficient or difference in lattice constants

of the film and the substrate, instead of single neutral axis of the composite, two neutral axis, one for each layer, exist. Basing his arguments on this assumption, considering the stress fields in each layer and satisfying the requirements of zero net force, Chu derives new expressions for the substrate curvature. In case of $t/d < 0.01$

$$\frac{1}{R} = \frac{12\frac{K_f}{K_s}\frac{t}{d}\Delta\varepsilon}{d\left[1+6\frac{K_f}{K_s}\frac{t}{d}\right]}, \tag{3.42}$$

where K_f, K_s are the biaxial moduli of film and substrate material, respectively, and $\Delta\varepsilon$ is the differential strain, which can be of different origins.

The value of stress, calculated from the radius of curvature following the approach by Chu, is half the value, calculated using the Stoney equation. However, Chu himself notes that, as the influence of interfacial relaxation is often uncertain, the error in using the Stoney equation is tolerable. In view of this the Stoney equation has been used in the present study.

Formulae given relate the radius of curvature of the sample to the total residual stress in the film. In order to obtain the intrinsic component of the stress, the influences of other parameters such as temperature and gravitational forces must be considered.

The effects of gravitational force, non-uniform thickness of the film, crystallinity and shape have been thoroughly discussed by von Pressig [von Preissig, 1989] and Kitahara [Kitahara, 1994]. However, it should be noted that consideration of all the effects is not always possible and most published results only discuss the influence of thermal stresses.

References

Andersen P., Moske M., Dyrbye K., Bottinger J., Thin Solid Films, **340**, 205, (1999)

Bicker, U. von Hulsen, Laudahn U., Pundt A. and Geyer U., Rev.Sci.Instr., **2**, 460, (1998)

Brenner, S. Senderoff, J. Nat. Bur. Stand., **42**, 105, (1949)

Buckel W., J. Vac. Sci. Technol., **6**, 606, (1969)

Carter G., J. Phys. **D 27 (5)**, 1046, (1994)

Chason E., Sheldon B.W., and Freund L.B., Floro J.A., and Hearne S.J., Phys. Rev. Lett., **88 (15)**, no. 156103, (2002)

Cherepanov G.P., and Martinez L., Computers and Structures, **63 (6)**, 1095, (1997)

Chu S.N.G., J. Electrochem. Soc., **145 (10)**, 3621, (1998)

Clyne T.W., Key Engineering Materials, **116-117**, 307, (1996)

Colligon J.S., J.Vac.Sci.Technol. **A 13(3)**, 1649, (1995)

Cremona M., Gazola L.M., Scavarda do Carmo L.c., Castro J.T.P., Achete C.A., Thin Solid Films, **377**, 436, (2000)

Davidenkov N.N., Fizika Tverdogo Tela, **2(11)**, 2919, (1960)

Davis C.A., Thin Solid Films, **226**, 30, (1993)

Dobrynin A.V., Techn. Phys. Lett., **23 (9)**, 709, (1997)

Doerner M.F. and Nix W.D., CRC Crit. Rev. Solid State and Mater. Sci., **14 (3)**, 225, (1988)

d'Heurle F.M. Harper J.M.E., Thin Solid Films, **171**, 84 (1989)

EerNisse E.P., Appl. Phys. Lett., **18 (12)**, 581, (1971)

Fang C.C., Jones F., Prasad V., J. Appl. Phys., **74 (7)**, 4472, (1993)

Fayeulle S., Nastasi M., J. Appl. Phys., **81 (10)**, 6703, (1997)

Flinn P.A., Gardner D.S. and Nix W.D., IEEE Trans.on Electron Dev., **ED-34(3)**, 689, (1987)

Floro J.A., Chason E., Cammarata R.C., and Srolovitz D.J., MRS Bulletin, January, 19, (2002)

Freund L.B., Floro J.A., Chason E., Appl. Phys. Lett., **74 (14)**, 1987 (1999)

Freund L.B., and Chason E., J. Appl. Phys. **89**, 4866, (2001)

Gerlach J.W., Kraus T., Sienz S., Moske M., Zeitler M., Rauschenbach B., Surf.Coat.Technol. **103-104**, 281, (1998)

Gill S.C., Clyne T.W., Thin Solid Films, **250**, 172, (1994)

Gill S.P.A., Gao H., Ramaswamy V., Nix W.D., J. Appl. Mech., **69**, 425 (2002)

Handbook of Thin Film Technology, ed. by L.I.Maissel and R. Glang, McGraw-Hill, (New York) Inc., (1970)

Gillet M., Assaban A.; and Mikaelian G., Vacuum, **50 (1-2)**, 73, (1998)

Hearne S., Chason E., Han J., Floro J.A., Figiel J., Hunter J., Amano H., Tsong I.S.T., Appl. Phys. Lett., **74(3)**, 356, (1999)

Hirsh E.H., J. Phys. D: Appl. Phys., **13**, 2081, (1980)

Hoang N.H., McKenzie D.R., McFall W.D., Yin Y., J.Appl.Phys. **80 (11)**, 6279, (1996)

Hoffman R.W., Physics of Thin Films, **3**, 221, (1966)

Hoffman R.W., *Mechanical Properties of Non-Metallic Thin Films* in *Physics of Nonmetallic Thin Films,* ed. By C.H.S. Dupuy and A. Cachard, Plenum Press, N.Y. and London, 1976

Hoffman R.W., Thin Solid Films, **34**, 185, (1976)

Hudson C. and Somekh R.E., J. Vac. Sci. Technol. **A 14(4)**, 2169, (1996)

Kamminga J.-D., de Keijser Th. H., Delhez R., Mittemeijer E.J., Thin Solid Films, **317**, 169 (1998)

Kim J.S., and Paik K.W., Lim J.H., and Earmme Y.Y., Appl. Phys. Lett., **74 (23)**, 3507, (1999)

Kim J.S., and Paik K.W., Oh S.H., J. Appl. Phys., **86 (10)**, 5474, (1999)

Kitahara K., Jpn. J. Appl. Phys., **33**, Pt. 1., no. 6B, 3673, (1994)

Klein C.A., J. Appl. Phys. **88 (9)**, 5487, (2000)

Klein C.A., J. Appl. Phys. **88 (9)**, 5499, (2000)

Klokholm E., Rev. Sci. Instr., **40 (8)**, 1054, (1969)

Klockholm E., and Berry B.S., J. Electrochem. Soc., **225**, 823, (1968)

Knuyt G., Lauwerens W., Stals L.M., Thin Solid Films, **370 (1-2)**, 232, (2000)

Koster M., Urbassek H.M., Surf. Sci., **496**, 196 (2002)

Kuroda S., Fukushima T., Kitahara S., Thin Solid Films, **164**, 157, (1988)

Mackerle J., Finite Elem. In Analysis and Design, **37(3)**, 253, (2001)

Malhotra S.G., Rek Z.U., Yalisove S.M., Bilello J.C., Thin Solid Films, **301**, 45, (1997)

Manotas S., Agullo-Rueda F., Moreno J.D., Ben-Hander F., Martinez-Duart J.M., Thin Solid Films, **401**, 306 (2001)

Martinez R.E.,Augustyniak W.A., Golovchenko J.A., Phys.Rev.Lett., **64 (9)**, 1035, (1990)

Mayr S.G. and Samwer K., Phys. Rev. Lett., **87(3)**, no. 036105, (2001)

Misra A. and Nastasi M., J. Vac. Sci. Technol., **A 18 (5)**, 2517, (2000)

Moske M., Samwer K., Z. Phys. B 77, 3, (1989)

Moulard G., Contoux G., Motyl G., Gardet G., and Courbon M., J. Vac. Sci. Technol., **A 16 (2)**, 736, (1998)

Muller K.-H., *Film Growth Modification by Concurrent Ion Bombardment: Theory and Simulation*, in *Handbook of Ion Beam Processing Technology: Principles, Deposition, Film Modification and Synthesis*, ed. By Cuomo J.J. and Rossnagel S.M., Kaufman H.R., Noyes Publications, U.S.A., (1989)

Murbach H.P., and Wilman H., Proc. Phys. Soc, **66 B**, 905, (1953)

Nix W.D., Metall. Trans. **A 20A**, 2217, (1989)

Nix W.D., and Clemens B.M., J. Mater. Res. 14, 3467, (1999)

Noyan I.C., Huang T.C., and York B.R., Crit. Rev. Solid State and Mater. Sci., **20 (2)**, 125 (1995)

Ohring M., *The Materials Science of Thin Films*, Academic Press, Inc. (1992)

Parfitt L., Goldiner M., Jones J.W. and Was G.S., J. Appl. Phys. **77 (7)**, 3029, (1995)

Ramaswamy V., Phillips M.A., Nix W.D., Clemens B.M., Mater. Sci. Eng., **A 319-321**, 887, (2001)

Rizzo A., Alvisi M, Sarto F., Scaglione S., Thin Solid Films, **384**, 215 (2001)

Ruud J.A., Witvrouw A., Spaepen F., J. Appl. Phys., **74 (4)**, 2517, (1993)

Sander D., Enders A., and Kirschner J., Rev. Sci. Instrum., **66 (9)**, 4734, (1995)

Sander D., Enders A., Kirschner J., Appl. Phys. Lett., **67 (13)**, 1833, (1995)

Schell-Sorokin A.J. and Tromp R.M, Phys. Review Letters, **64 (9)**, 1039, (1990)

Sheldon B.W., Lau A., and Rajamani A., J. Appl. Phys., **90**, 5097, (2001)

Spaepen F., J. Mech. Phys. Solids, **44 (5)**, 675, (1996)

Spaepen F., and Shull A.L., Current Opinion in Solid State and Mater. Sci., **1**, 679, (1996)

Stoney G.G., Proc. R. Soc. London, **A 82**, 172, (1909)

Tamulevisius, Vacuum, **51(2)**, 127, (1998)

Taylor Ch., Barlett D., Chason E., and Floro J., The Industrial Physicist, March, 25, (1998)

Thomas M.E., Harnett M.P. and McKay J.E., J. Vac. Sci. Technol., **A6(4)**, 2570, (1988)

Thornton J.A., Tabock J., and Hoffman D.W., Thin Solid Films, **64**, 111, (1979)

Townsend P.H., and Barnett D.M., Brunner T.A., J. Appl. Phys., **62 (11)**, 4438, (1987)

von Preissig F.J., J. Appl. Phys., **66(9)**, 4262, (1989)

Ward D.J., Williams A.F., Thin Solid Films, **356**, 311, (1999)

Was G.S., Jones J.W., Parfitt L.J., Goldiner M. and Kalnas C.E., Proc. Mater. Res. Soc., MRS, Pittsburgh, **396**, 479 (1996)

Weber M., Koch R., Rieder K.H., Phys. Rev. Lett., **73 (8)**, 1166, (1994)

Windischmann H., J.Appl.Phys. **62 (5)**, 1800, (1987)

Windischmann H., Crit. Rev. Solid State Mater. Sci., **17 (6)**, 547, (1992)

Withers P.J., and Bhadeshia H.K.D.H., Mater. Sci. and Technol., **17 (4)**, 355, (2001)

Wolf G.K., Ensinger W., Nucl.Instr.and Methods in Phys.Res. **B59/60**, 173, (1991)

Yamada-Kaneta H., Ogawa T., and Wada K., J. Appl. Phys., **62 (1)**, 62, (1987)

Chapter IV

Ion-Solid Interactions

In this study thin films of silicon dioxide and tantalum pentoxide were deposited by dual ion-beam sputtering and ion-assisted deposition. Both techniques are based on one of the possible interactions between an energetic ion and the surface of a solid material. Therefore, a general knowledge of processes that take place during surface bombardment with energetic ions is important for the understanding of deposition and analysis methods, resulting film properties and parameters that may influence these properties.

The aim of the first part of this chapter is to give a brief overview of the phenomenon of ion-solid interaction with special attention given to sputtering. In the second part the physical basis for sputtering will be explained and parameters, important for the practical application of sputtering for thin film deposition (such as ion energy, yield, energy and angular distribution of sputtered species) will be reviewed. Processes, that take place during sputtering in the presence of a reactive gas, will also be considered. And finally, in the third part of this chapter, the effect and reasons for application of energetic ion bombardment during film deposition will be examined.

4.1. Introduction to Ion-Solid Interactions

When a beam of energetic ions is directed onto the surface of a solid material, ions undergo collisions with atoms and electrons of this material. Their interactions depend largely on the energy and mass of the incoming ion and also on the properties of the solid material used. Some of these interactions are presented in Figure 4.1.

When the energy of arriving ion is low, a chemical reaction may take place at the surface of the solid material. At higher energies ion bombardment can lead to increased surface mobility of species on the solid surface. Highly energetic particles can transfer their energy not only to surface atoms, but also to the atoms just below the surface, causing their displacement from original sites and ejection of the surface atoms, known

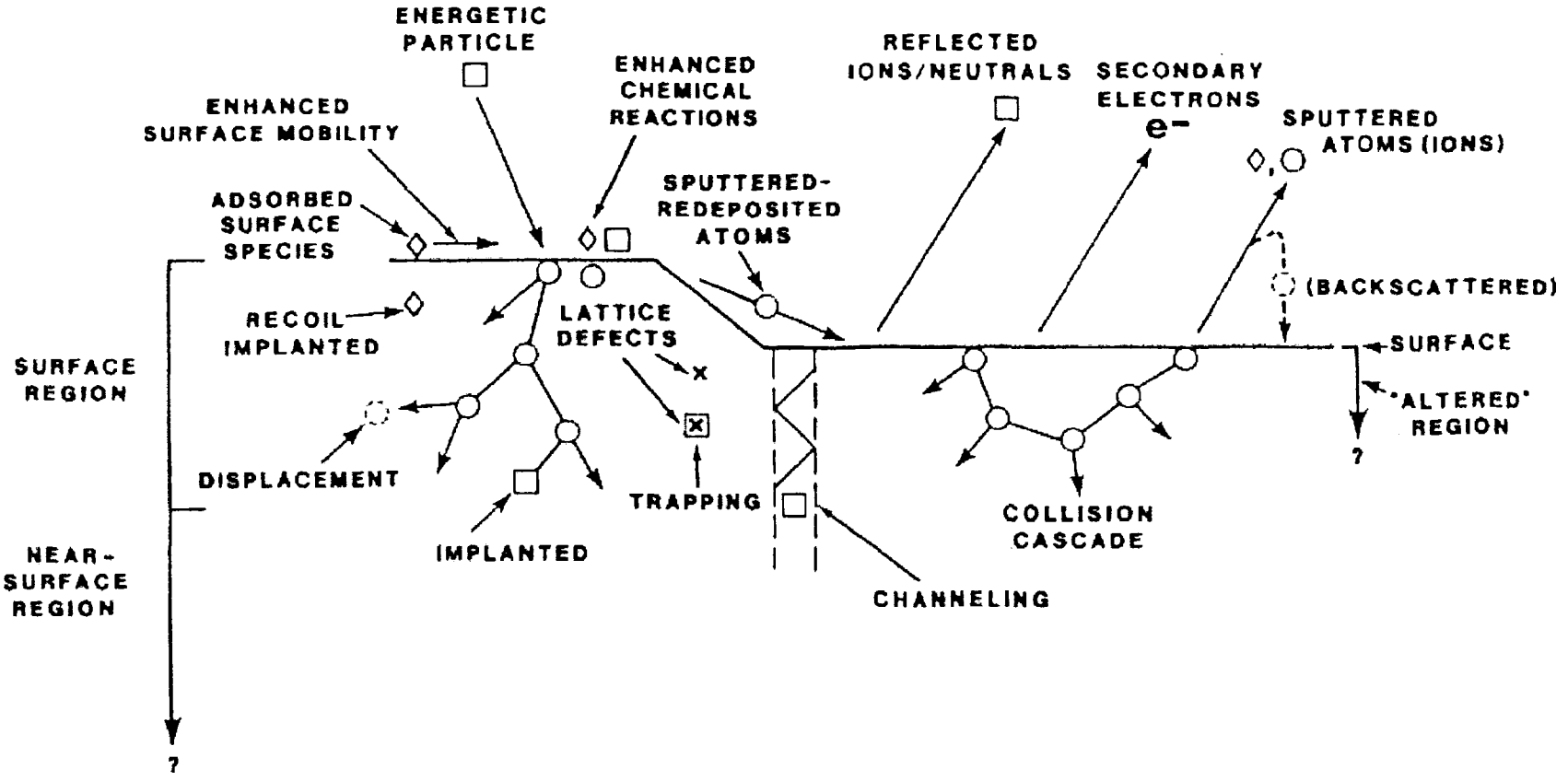

Figure 4.1. Processes, resulting from an ion collision with a solid surface [Mattox, 1989].

as sputtering. Some of the bombarding ions can eventually become embedded in the near-surface region of the solid material. Other processes, such as ejection of ions, photons and secondary electrons, can also be a result of ion bombardment.

As mentioned above, the bombarding ion can lose its energy in a series of collisions with atoms and electrons of a solid material. Depending on the method of energy transfer, collisions are usually referred to either as being "inelastic" (or electronic) or being "elastic" (or nuclear).

In "inelastic" collisions ions interact with electrons of the atoms of the bombarded material, causing excitation and ionisation and sometimes leading to radiation emission. As the mass of an electron is much smaller then the mass of an ion, the energy transfer at each collision will be very small and the ion trajectory will not undergo any significant changes. However, each collision will remove some of ion energy and, as electron density is large, and, therefore, the amount of such collisions is high, electronic stopping $(dE/dx)_e$ (i.e. ion retardation caused by "inelastic" collisions) can become a dominant mechanism of ion-surface interaction.

In "elastic" collisions ions interact not with the target electrons, but with the nuclei of the bombarded material atoms. In this case the masses of interacting particles are comparable, therefore, energy transfer is much more effective, than in case of electron-ion interaction and thus "elastic" collisions can result in large angular changes of the ion trajectory. Such a process of ion energy loss is known as nuclear stopping $(dE/dx)_n$. Nuclear collision is the mechanism, that can result in sputtering of the surface atoms. The duration of a nuclear collision is very small, which allows researchers to treat "elastic" collision as a two-body elastic event, governed by the laws of classical mechanics (i.e. by the laws of conservation of momentum and energy).

Depending on the trajectory of the incoming ion and its energy, two types of ion-atom interaction are possible. At high ion energies or velocities, the ion approaches the nucleus of the stationary atom at the distance r less than a_0 - the first Bohr radius of the hydrogen (i.e. $0<r<<a_0$, a_0=0.53 Å). In this case repulsive nuclear forces dominate the interaction and a Coulomb potential $V(r)$ is often used in process description and modelling:

$$V(r) = \frac{Z_i Z_a e^2}{4\pi\varepsilon_0 r}. \qquad (4.1)$$

Here Z_a is the atomic number of the target atom, Z_i is the atomic number of the incoming ion, r is the distance between atom and ion, ε_0 ($0.885 \cdot 10^{-11}$ F/m) is the permittivity in vacuum and e ($=1.6 \cdot 10^{-19}$ C) is the electronic charge.

If the energy or velocity of the projectile is lower, the ion approaches target atom to a distance greater than a_0. In this case the effect of attractive nuclei-electron forces become important. This screening effect has to be taken into account during collision calculations and various screened potentials (for example, the power potential $V(r) = \frac{Z_i Z_a e^2 a_s^{s-1}}{4\pi\varepsilon_0 s r^s}$, proposed by Lindhard et al [Lindhard et al, 1963] or the Thomas-Fermi-Firsov $V(r) = \frac{Z_i Z_a e^2}{4\pi\varepsilon_0 r}\phi(r/a)$ [Biersack et al, 1982; O'Connor et al, 1986] potential) are used. Here $a_s \propto (Z_i^{2/3}+Z_a^{2/3})^{-1/3}$, s is inversely proportional to the energy of the projectile and the exponential function $\phi(r/a)$ is known as a screening function with $a=a_0 Z_a^{-1/3}$ being the screening length.

The differential energy loss (also called stopping power) dE/dx, experienced by the ion with energy E, travelling through the small thickness dx of the bombarded material, can be represented according to the Lindhard-Scharff-Schiøtt theory [Lindhard et al, 1963] as a sum of a nuclear stopping and an electronic stopping component, i.e.

$$\frac{dE}{dx} = \left(\frac{dE}{dx}\right)_n + \left(\frac{dE}{dx}\right)_e = N\left[S_n(E) + S_e(E)\right]. \qquad (4.2)$$

Here $S_n(E)$ and $S_e(E)$ are nuclear and electronic stopping cross-sections, which depend on the bombarded material, N is the number of bombarded material atoms per unit volume or atomic density of the bombarded material. For practical purposes of application of sputtering to thin film deposition, it is important to know the balance between the "elastic" and "inelastic" compounds of ion energy loss for each particular combination of target material, ion and its energy. In the general case this balance can be presented as in Figure 4.2 with both components increasing, going through a maximum and then decreasing with increased ion energy. As can be seen, nuclear stopping dominates at low ion energies and electronic stopping is the main energy loss mechanism for ions of higher energies.

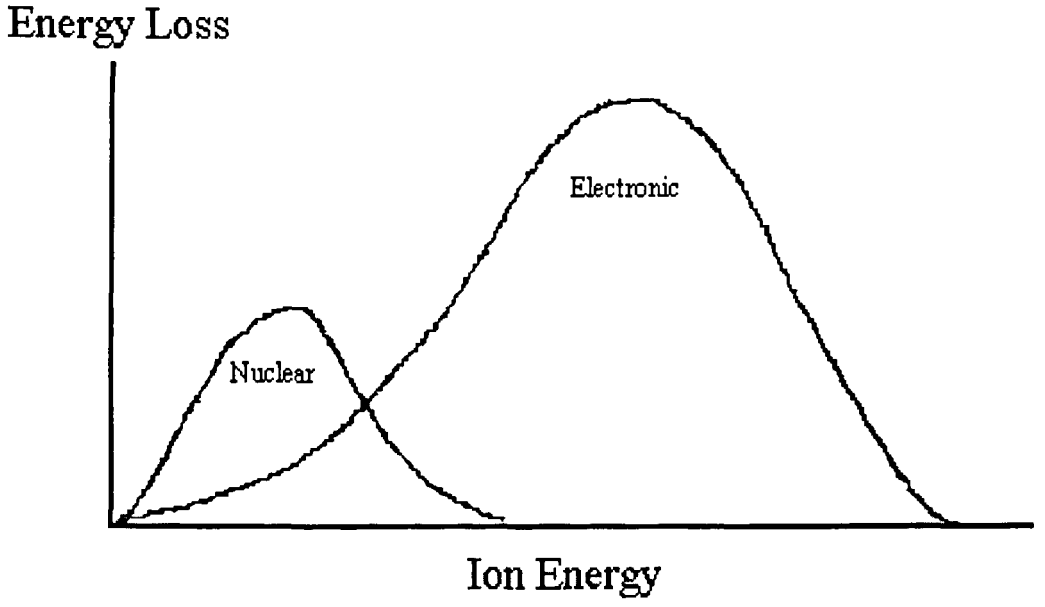

Figure 4.2. Balance between nuclear and electronic stopping. [Pringle, 1994]

4.2. A Short Overview of the Theory of Sputtering

As mentioned above, one of the possible events during ion bombardment of solid material is ejection of surface atoms. When an energetic ion strikes a solid material, it can transfer some of its momentum in a series of collisions to the atoms of the target. Some of this momentum is transferred back to the surface atoms and, if they receive additional energy in excess of the binding energy, these surface atoms will be ejected from the target. This process is called sputtering.

Sputtering is now widely used in different areas of research and industry for thin film deposition, by collecting sputtered species on a suitable substrate, for substrate surface pre-cleaning by re-sputtering of the surface layer, for fabrication of miniature devices by pattern etching and for thin film analysis.

The main characteristic of the sputtering process is the sputtering coefficient or sputtering yield Y, which is defined as a ratio of a number of the atoms of solid material, removed from the surface to the number of ions, bombarding the material:

$$Y = \frac{Number\ \ of\ \ removed\ \ atoms}{Number\ \ of\ \ incident\ \ ions}. \tag{4.3}$$

The sputtering yield depends on many variables, one of which is the energy of the incoming ion E_i. Sputtering yield behaviour with ion energy is well established now and is illustrated in Figure 4.3. Up to a certain level of ion energy, called the threshold value E_t, there is no sputtering. The threshold value will be different for each material-ion combination and will also depend on the state of the material surface. With further increase in ion energy, the yield increases first quadratically and then, linearly, and then the sputtering yield goes through a maximum and decreases, with the latter effect caused by ions, penetrating so deep into the solid material, that their energy is not transferred as successfully to the atoms at the solid surface.

In general, the sputtering yield is determined not only by ion energy, but also by many other parameters, which include ion mass M_i and atomic number Z_i; mass M_a and atomic number Z_a of the target atom; angle of incidence θ of the ion onto the solid surface and structure and orientation of the target material. Depending on all these

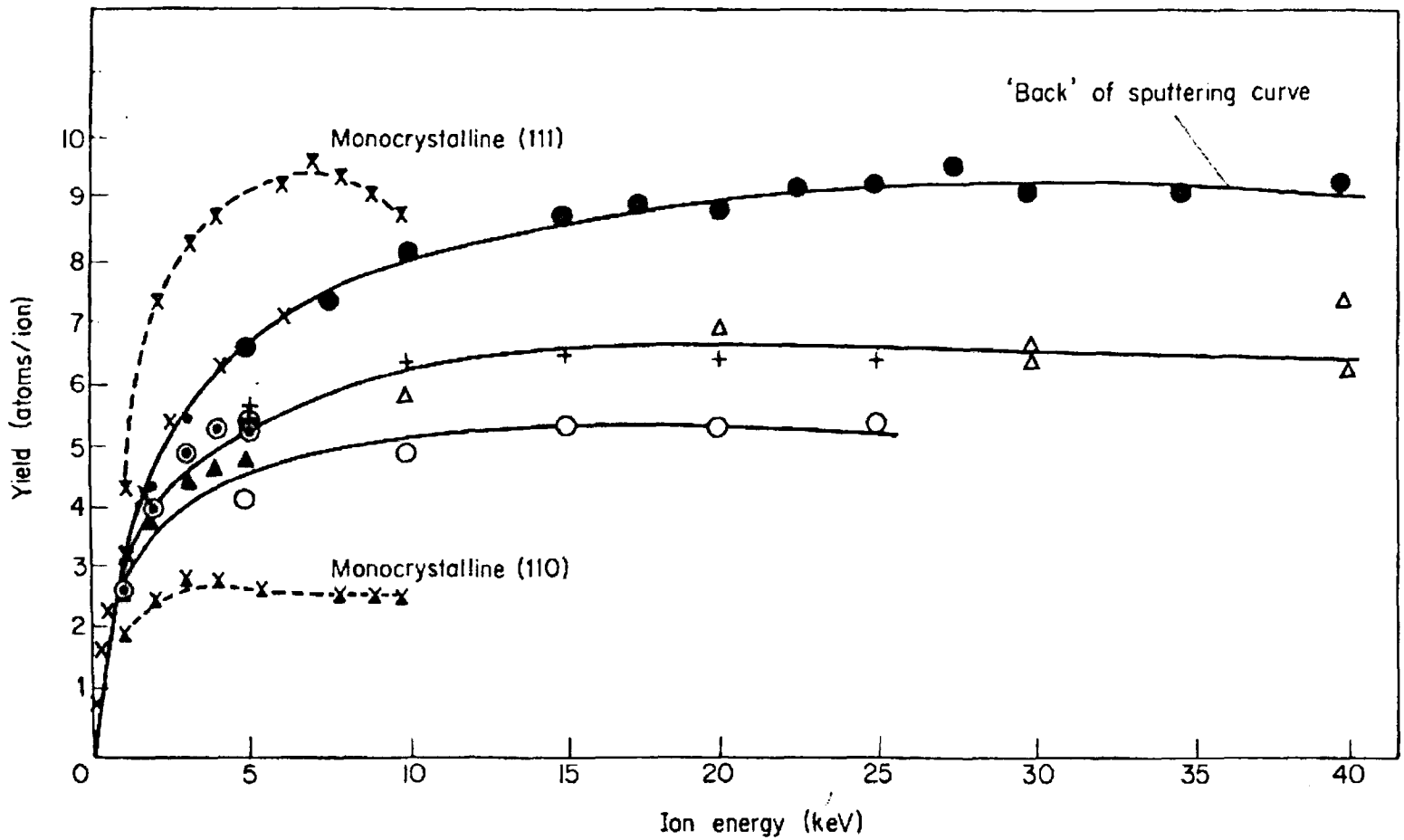

Figure 4.3. Sputtering yield of Cu target as a function of Ar ion energy. Different shapes and colours (e.g., solid circles or crosses) correspond to experimental data points, obtained by different researchers. [Carter and Colligon, 1969].

parameters, the sputtering event can be described by one of the following models [Behrisch, 1981]:

- single knock-on model,
- linear collision cascade model, and
- thermal spike model.

Schematically, these models are presented in Figure 4.4.

The linear collision cascade model was developed by Sigmund [Sigmund, 1969; see also Behrisch 1981] for the case of amorphous and polycrystalline targets. This model is based on the assumption that an energetic incoming ion (or neutral) will transfer some of its kinetic energy to the stationary atom (or atoms) of the bombarded material, so that this atom will be displaced from its original site and become a recoil. This recoil will, in turn, transfer some of its energy to other stationary atoms of the target and a collision cascade will be generated. It should be noted that, in this model, only two bodies can take part in one collision, i.e. collision may only happen between ion and stationary atom or recoil and stationary atom. The cascade will be diminished by energy dissipation (phonon-assisted processes) and, eventually, the energy, transferred to the stationary atom, will be less than the energy, which is required to displace this atom from its original site. If, during such collisions, sufficient energy is transferred to the surface atoms, they will be sputtered and the sputtering yield in this case can be calculated from:

$$Y = 0.042 \frac{\alpha}{E_b} S_n(E_i). \tag{4.4}$$

Here α is a function of the ion energy, the angle of incidence and the ratio of masses of atom and ion and can be found from works of Sigmund [Sigmund, 1969] and Winterbon [Winterbon, 1975]; E_b is the surface binding energy and $S_n(E_i)$ is the nuclear stopping cross-section.

At low energies of bombarding ions (approx. 50-1000 eV) or low energy transfer (as in the case of low mass sputtering ions on heavy targets) extensive collision cascades, described by Sigmund, may not be generated. The main contribution to the sputtering yield in this case will be by primary recoils. The mechanisms of such events are presented in Figure 4.5. The empirical analytical formula, predicting sputtering yield in

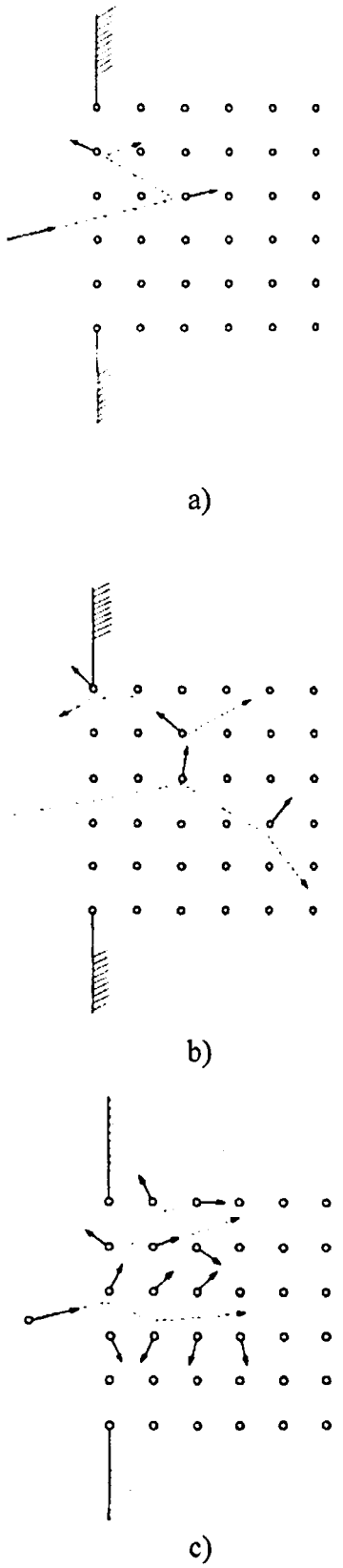

Figure 4.4. Sputtering models: a) single knock-on regime; b) collision cascade regime; c) thermal spike regime. [Behrisch, 1981].

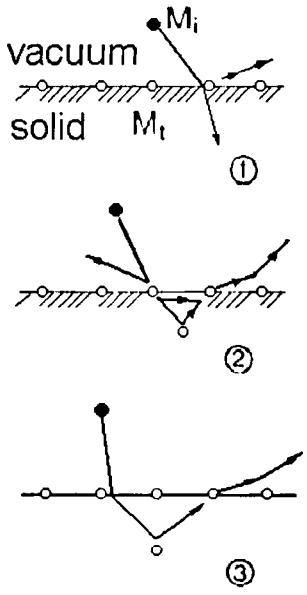

Figure 4.5. Examples of knock-on sputtering. Cases (1) – atom is ejected directly as a result of collision with ion; (2) – atom is ejected after collision with primary (i.e. the atom, displaced as a result of collision with ion); (3) – atom is ejected as a result of collision with ion, which undergoes multiple collisions. [Cuomo et al, 1989].

this regime for all ion-target combinations and normal ion incidence, was proposed by Bohdansky et al [Bohdansky et al, 1980] and can be written in the form:

$$Y = 6.4 \times 10^{-3} M_a \gamma^{5/3} E_i^{1/4} \left(1 - E'^{-1}\right)^{7/2}. \qquad (4.5)$$

Here $\gamma = 4 M_a M_i / \left(M_a + M_i\right)^2$, $E' = E_i / E_{thr}$ is the normalised energy, $E_{thr} = \begin{cases} E_b / \gamma\left(1-\gamma\right), & if \quad M_i/M_a \le 0.3 \\ E_b 8 \left(M_i/M_a\right)^{5/2}, & if \quad M_i/M_a > 0.3 \end{cases}$ is the threshold energy, E_b is the surface binding energy. This relation is in good agreement with the experimentally obtained data and can be used for prediction of the sputtering yield in the knock-on sputtering regime "with reasonable confidence" [Bohdansky et al, 1980].

The basis for the theory of thermal spikes was first outlined by Seitz and Koehler in 1956 [Seitz and Koehler, 1956]. This theory was further developed by Sigmund [Sigmund, 1974]. The theory of thermal spikes was originally used to explain effects during sputtering, which could not be accounted for by the known ballistic models. These effects included changes in sputtering yield with target temperature, which were attributed to rapid vapourisation of the target surface material in the area of ion impact. However, according to Kelly [Kelly, 1997], no experimental results on thermal-spike sputtering are available, so the effect of thermal spikes should, probably, be considered negligible during ion-beam sputtering, where ballistic processed are thought to predominate. Moreover, the thermal spike model should not be used to explain the results, obtained during experiments on targets made of low vapour pressure materials, such as SiO_2 [Kelly, 1997].

In this work sputtering is used for thin film deposition, therefore, practical questions of angular distribution and energy of sputtered species, of multi-component sputtering and of sputtering in the presence of reactive gas should also be considered.

If the sputtering event occurs according to the linear collision cascade or thermal spike models and the target under bombardment is either amorphous or polycrystalline, the angular distribution of sputtered species is predicted to be cosine-like. Indeed, from Sigmund's theory the differential yield $\frac{dY}{d\Omega} \sim \cos^{\nu_a} \theta_a$, $1 \le \nu_a < 2$ (Ω is the direction of emission and θ_a is the polar angle of the emitted target particle), which agrees with the experimental data (see, for example, Figure 4.6). It should be noted that, in this case,

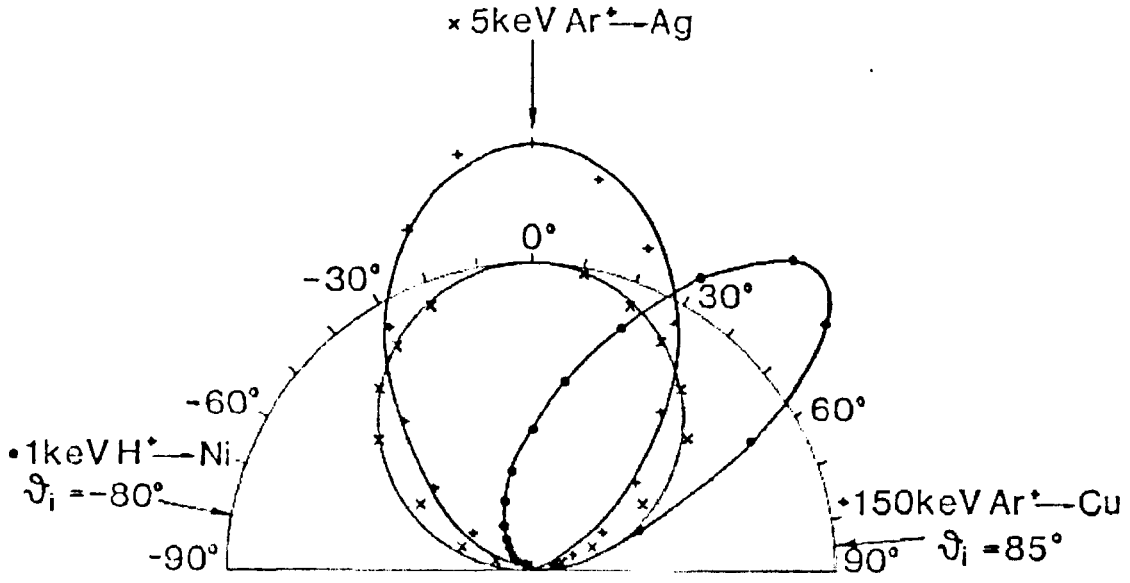

Figure 4.6. Angular distribution of sputtered particles. Glancing angle Ni (circles) shows behaviour typical for knock-on sputtered particles; Ag (crosses) shows cosine distribution; Cu (diagonal crosses) shows effect of high-energy ion bombardment. [Cuomo et al, 1989].

the emitted particle distribution is independent of the angle of incidence of the incoming ion, except for glancing incidence angles, when other effects (for example, the influence of surface structure) become more important. Such behaviour may be explained by the mechanisms of sputtered particle creation – the energy to the target surface atoms is transferred through a long chain of collision events, so that randomisation occurs and the ejected atom does not have a "memory" of the ion angle of incidence.

In cases where the knock-on model is applicable, energy, required by the surface atom to leave the target, is transferred through a few collisions, hence the atom will retain the information about the ion angle of incidence and atoms will be ejected in the forward direction with respect to incoming ions. An example of such a distribution is also presented in Figure 4.6.

It should be noted that other parameters, such as surface topography, surface contamination or favoured chemical reactions (such as in case of reactive sputtering) can significantly change the yield and angular distribution of sputtered species. Another very important effect, first discovered by Wehner [Wehner, 1955], is observed in the case of single crystal targets, where the yield and angular distribution of sputtered species is strongly anisotropic and emission is enhanced along the closed packed lattice directions.

The energy of sputtered species is another parameter of interest for thin film deposition, a parameter that marks one of the most important differences between sputtering and other physical vapour deposition techniques. It is known that, on average, the energy of sputtered species is of the order of 10 eV, while for evaporated particles this value is only of the order of 0.1 eV. The simplest theoretical prediction for the energy distribution of atoms, ejected in the direction of the target normal, follows from the linear collision cascade theory and can be written in the following form [Thompson, 1969; Cuomo et al, 1989]:

$$\frac{dY}{dE_a} = \frac{E_a}{\left(E_a + U_0\right)^{3-2m}}. \tag{4.6}$$

Here $m \approx 0$ when $0 < E_a \leq U_0$ and approaches $m \approx 1/4$ when $E_a \approx 1\,\text{keV}$, U_0 is the surface binding energy. This formula is often known under the name of the Thompson formula. The experimental results have shown that the energy distribution can be reasonably accurately described by the Thompson formula when m=0, i.e. experimental

data agrees well with predictions for a linear collision cascade. However, in case of knock-on sputtering events, other formulae have been found to be more appropriate [Cuomo et al, 1989]. Some care should be taken and adjustments have to be made when using the Thompson formula for the case of high energy transfer, as the inequality

$$E_a < T_m = E_i \frac{4M_a M_i}{(M_a + M_i)^2} \tag{4.7}$$

should always be satisfied.

The Thompson formula predicts that, with increase in sputtered particle energy to $U_0/2$, the distribution increases and reaches its peak value, for energies in excess of $U_0/2$ the distribution falls as $1/E_a^2$. This is supported by experimental results (see, for example, Figure 4.7).

Some deviations from the behaviour, predicted by the Thompson formula, occur at low ejection energies of the sputtered atoms [Dullni, 1984; Dullni, 1985; Husinsky et al, 1983, Husinsky et al, 1984]. Such behaviour is believed to be caused by the presence of reactive gas during sputtering or by sputtering with chemically active species.

Sputtering in the presence of a reactive gas is becoming an increasingly important tool for deposition of compound films, such as oxides or nitrides. The necessity for such a process, usually termed reactive sputtering, can be seen after a consideration of complications, experienced during sputtering of alloys and compounds.

The main and most commonly observed complication during alloy or compound sputtering is that in this case the composition of the resulting film may differ significantly from that of the initial target composition, as different target components may be sputtered in different amount. This process is called "preferential sputtering". Several models have been proposed over the years to account for such behaviour during deposition. The reasons offered include differences in mass, chemical bonding and volatility of the target compounds, thermal and bombardment-induced (Gibbsian) segregation, bombardment-induced mixing and decomposition [Rossnagel et al, 1990].

Several quantities are used to describe the sputtering yield of a multi-element target. First, the total sputtering yield Y, i.e. the ratio of the number of ejected atoms irrespective of their mass to the number of incident ions, is used. Then, a ratio of the number of ejected atoms of a particular component i of a target to the number of incident ions is defined and called the partial sputtering yield Y_i. The total sputtering

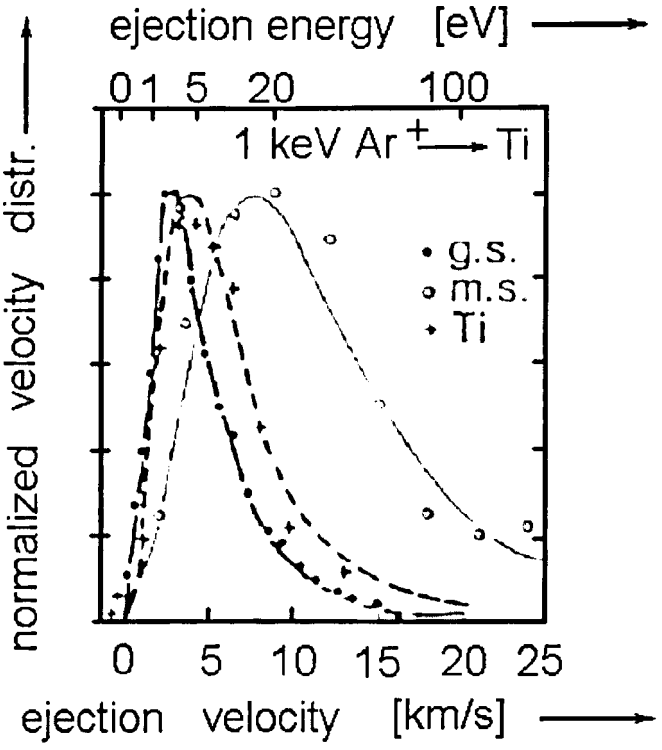

Figure 4.7. Energy distribution of sputtered particles. Ground state (g.s.), metastable (m.s.) and ionised (Ti) are shown. Curves are fitted with the Thompson formula. [Cuomo et al, 1989].

yield of the target will be represented by the sum of partial sputtering yields of each target component:

$$Y = \sum_i Y_i . \tag{4.8}$$

Another widely used quantity is component sputtering yield Y_i^c, i.e. the ratio of one component's partial sputtering yield to the equilibrium surface concentration c_i^s of this component:

$$Y_i^c = {Y_i}/{c_i^s} . \tag{4.9}$$

It should be noted that, during the initial period of target bombardment, the element which has a higher partial sputtering yield is removed from the target surface first. This leads to a formation of so-called "altered layer" with thickness of the order of the ion range. In the absence of significant thermal diffusion in the target the "altered layer" stays at a finite thickness and steady-state sputtering conditions are established, where the target components are sputtered according to their bulk concentration. For the case of a binary compound AB this can be expressed as

$${n_a}/{n_b} = {c_a}/{c_b} , \tag{4.10}$$

where n_a and n_b are the number of ejected atoms of compound components A and B respectively and c_a and c_b are their bulk concentrations. It is obvious, that ${n_a}/{n_b} = {Y_a}/{Y_b}$, therefore

$$\frac{Y_a^c}{Y_b^c} = \frac{c_a}{c_b}\frac{c_a^s}{c_b^s} . \tag{4.11}$$

The equation above is important for experiments on determination of ${Y_a^c}/{Y_b^c}$ by measuring surface and bulk concentrations of target components and comparison of component yields with those of the pure elements.

Up to the 1980s three models were established, that explained "preferential sputtering". One of them was based on the differences in mass of the elements in an alloy or

compound target. Although somewhat disputed in the case of oxides and halides, it has been established since then, that the mass plays an important role only for sputtering with low-energy ions (i.e. in the near-threshold conditions) and in isotope sputtering (preferential sputtering of a lighter isotope) [Rossnagel et al, 1990].

Chemical binding is the basis for the second model. Differences in chemical binding have been employed for an explanation why a heavier element can be sometimes preferentially sputtered from the target surface. However, if considered as the only mechanism present, this method tends to underestimate the observed compositional changes.

The basis for the third model is differences in volatility of target components. It is accepted now that, if one of the elements composing a target is more volatile than others (for example, in case of oxides), the grown film would be deficient in this component due to its preferential loss.

Since the 1980s several other models have been proposed, including bombardment-induced Gibbsian segregation (BIGS), mixing and bombardment-induced compositional changes. BIGS is similar to equilibrium or thermal segregation in that the surface of the target becomes enriched in one component and depleted in another. But, in contrast to equilibrium segregation BIGS happens not under the influence of increased temperature, but under the influence of ion bombardment. The driving force for BIGS is low and is generally accepted to be approx. 0.06-0.52 eV.

Bombardment-induced mixing is a process, similar to BIGS. The driving force for bombardment-induced mixing is also low ($\leq$1.3 eV) in comparison with the energy of the bombarding ion and is based on the differences in chemical energy of the target components.

The last reason for bombardment-induced compositional changes in the target is decomposition. It was proposed by several authors [see, for example, Rossnagel et al, 1990; Christie et al, 1983; Contarini et al, 1985] that, during bombardment, an energetic ion generates a collision cascade and this cascade in itself should be considered as a source of new stoichiometries. Thus, for an oxide target after ion bombardment several new stoichiometries can be observed with significant loss of oxygen from the compound.

Reactive sputtering is a process, which is now widely used to deposit compound films. It has an additional advantage, that compounds, impossible to form by other means at ambient temperature, can be deposited in this manner [Colligon, 1995]. In reactive sputtering the target is sputtered by inert or reactive gas ions in the presence of the

reactive gas in the deposition chamber. Depending on the partial pressure of the reactive gas, several processes can occur. If the flow is insufficient, the film will only be partially reacted. At higher levels of reactive gas films with the desired composition will be deposited. Very high flows will result in compound formation directly on the surface of the target. In this case the reactive gas flow should be significantly reduced to allow the sputtering process to expose the metallic target underneath the compound layer. This process is usually described with the help of the hysteresis curve (see Figure 4.8). This curve represents two stable states of the system; metallic target and compound target states with a swift transition between them. In the absence of reactive gas in the chamber the pressure in the system will vary linearly with the inert gas flow (dashed line in Figure 4.8) and follow the relation

$$Total\ \ flow\ \ rate\ \ of\ \ gas = Pumping\ \ speed\ \times\ pressure.$$

With increasing reactive gas flow into the chamber the total pressure change will be negligible at first, as all of the gas will be consumed by the growing film. When the flow is high enough to form a compound on the target surface, the pressure behaviour will be similar to that in the absence of the reactive gas, but with a lower total value. It should be noted, that compound formation on the target surface usually results in reduced sputtering yield and thus reduced growth rate of the film. The presence and exact shape of the hysteresis curve will strongly depend on the pumping speed of the system [Rossnagel, 1990; Okamota et al, 1986; Danroc et al, 1987]. In general, reactive gas will not only be consumed by the target and the pump. The third way of reactive gas consumption is by gettering. Gettering leads to an unknown value of the reactive gas partial pressure during deposition, as after the compound formation on the target surface reduced sputtering yields will lead to reduced influence of gettering and, therefore, to an increased reactive gas pressure. Models exist, which take gettering into account [see, for example, Heller, 1973; Goranchev et al, 1970; Larsson et al, 1988], but it is also common to find the conditions for the deposition of a stable compound with the desired stoichiometry experimentally.

4.3. Ion-assisted Deposition

In order to fully understand the importance of ion-assisted techniques and the effects of ion bombardment, properties of films, deposited by non ion-assisted methods (evaporation and sputtering), should be considered first.

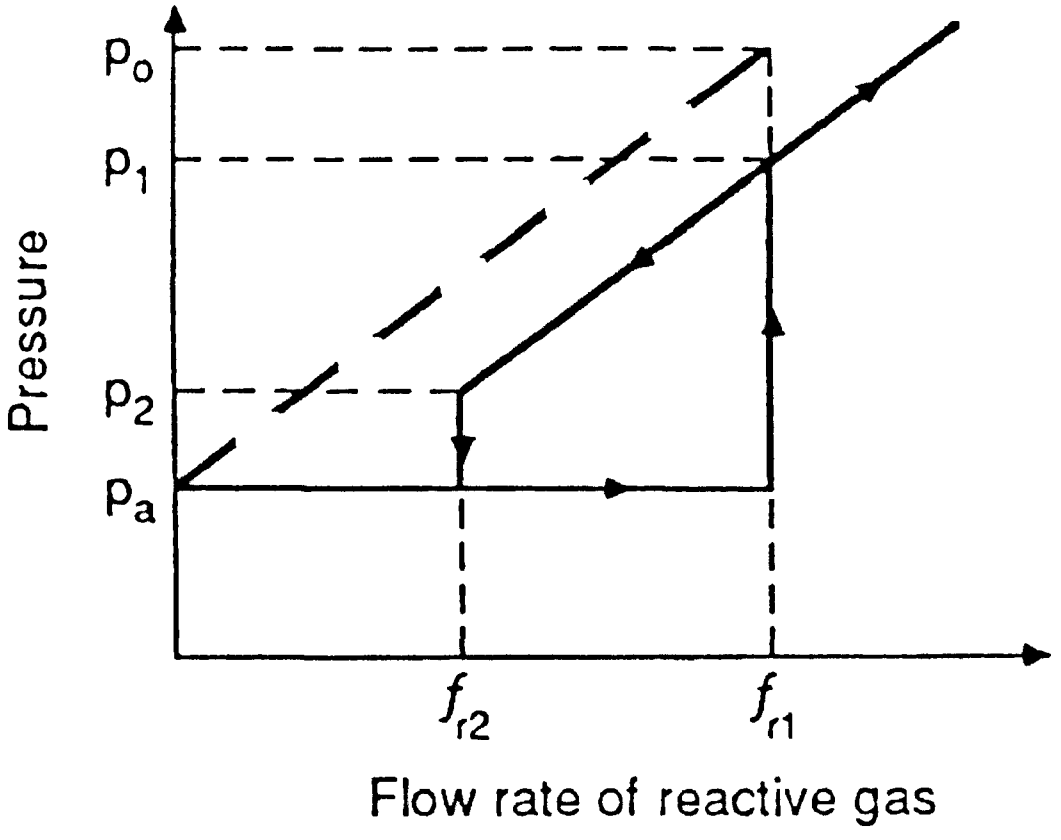

Figure 4.8. Hysteresis curve for reactive sputtering. [Rossnagel et al, 1990].

It is known that the energy of evaporated species is only of the order of 0.05-0.1 eV and is very low in comparison with the energy of atoms, arriving to the substrate during ion beam sputtering (order of 7 eV). The energy of film atoms is directly related to their mobility, which has long been established as one of the keys to the good density and morphology of the coatings. The mechanism was established by Henderson et al [Henderson et al, 1974] and states that atoms, deposited onto the substrate to form a film, have limited mobility, so the uncoated parts of the substrate can become shadowed by the previously deposited species, which leads to a porous structure.

Mobility of film atoms can be increased by variation of several deposition parameters, most important of which are substrate temperature and ion bombardment of the growing film. The influence of these parameters is thoroughly described by structure zone model (structure phase diagram). This model was first proposed by Movchan and Demchishin in 1969 [Movchan and Demchishin, 1969] and later on developed by Thornton (see Figure 4.9) [Thornton, 1974] and Messier et al [Messier et al, 1984] to include films, deposited by sputtering. According to the classical model, thin film microstructure is dependent on the reduced temperature T/T_m where T is the substrate temperature during deposition and T_m is the film material melting point. With increase in the reduced temperature film microstructure changes from zone 1 (narrowing crystallites forming at $T/T_m<0.3$) to zone 2 (columnar grains forming at $0.3< T/T_m<0.45$) and then zone 3 (equiaxed grains forming at $0.45< T/T_m$). Thornton introduced transitional zone T (fibrous grains, tightly packed and not extending through film thickness) between zones 1 and 2 and accounted for the pressure of argon during deposition. Messier et al revised this model to take into account bombardment-induced mobility of film atoms. It was also proposed, that transitional zone is a subzone of zone 1 and that zone 1 can be divided into 5 distinct regions (see Figure 4.10) depending on the size of columns/voids, which in turn is dependent on thermal-induced and bombardment-induced mobility of film atoms and film thickness and can range from 1-3 nm to 200-400 nm.

Films, deposited by evaporation, usually have low density and poor morphology and are placed in the Zone 1 of the structure phase diagram. Although having improved characteristics in comparison with evaporated films, sputtered coatings can also be under-dense and are usually placed in the Zone 2 of structure phase diagram. It is known, that poor microstructure can not only influence film properties in an undesirable manner (for example, it can lead to reduced refractive index in high-refractive-index coatings), but also can give rise to instability of the coating. However, increase in atom mobility by substrate heating is not always possible as, for example, many plastic

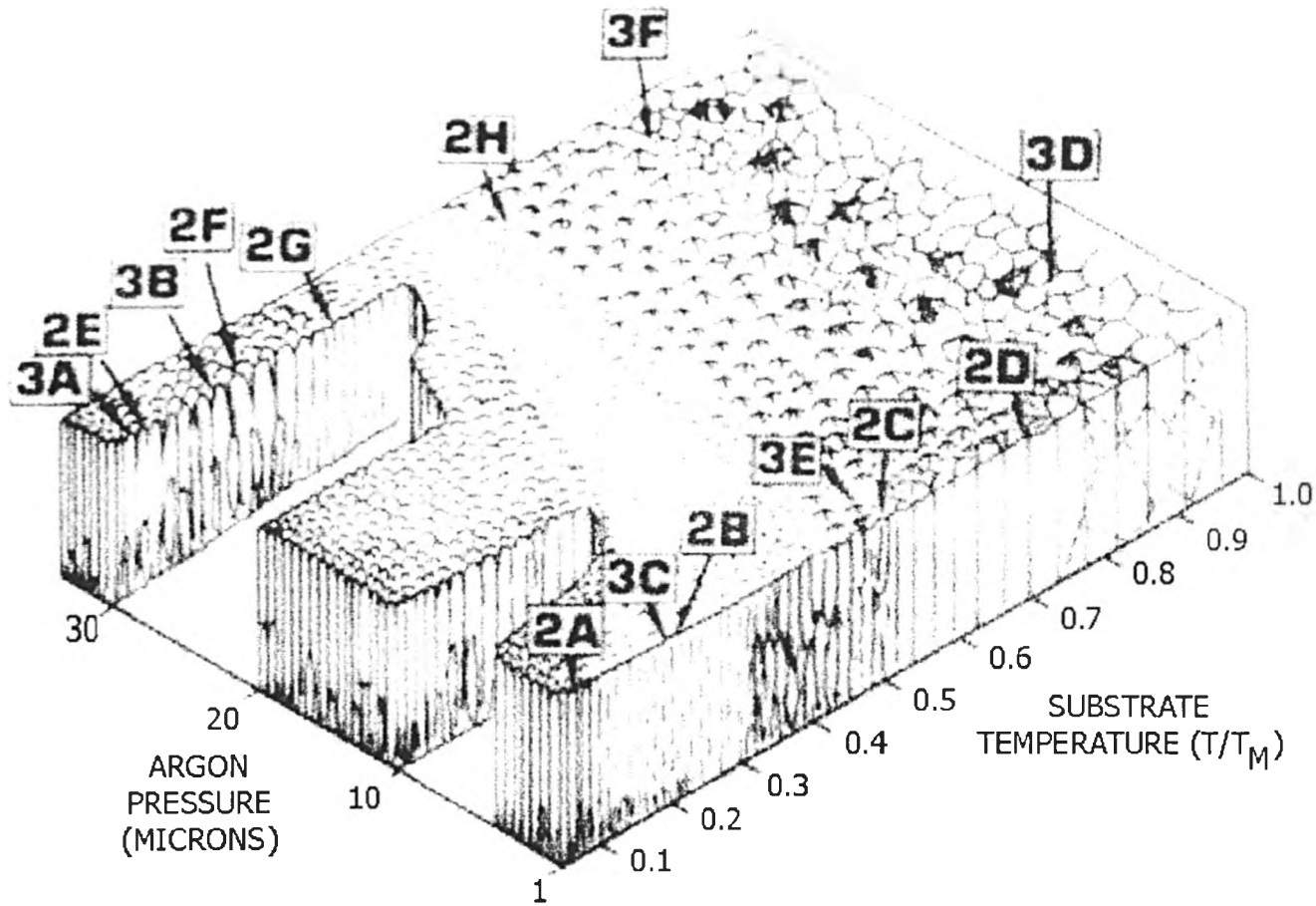

Figure 4.9. Structure zone model by Thornton [Thornton, 1974]. The notation 2A, 2B, etc. are used by Thornton to refer to SEM micrographs of the studied films.

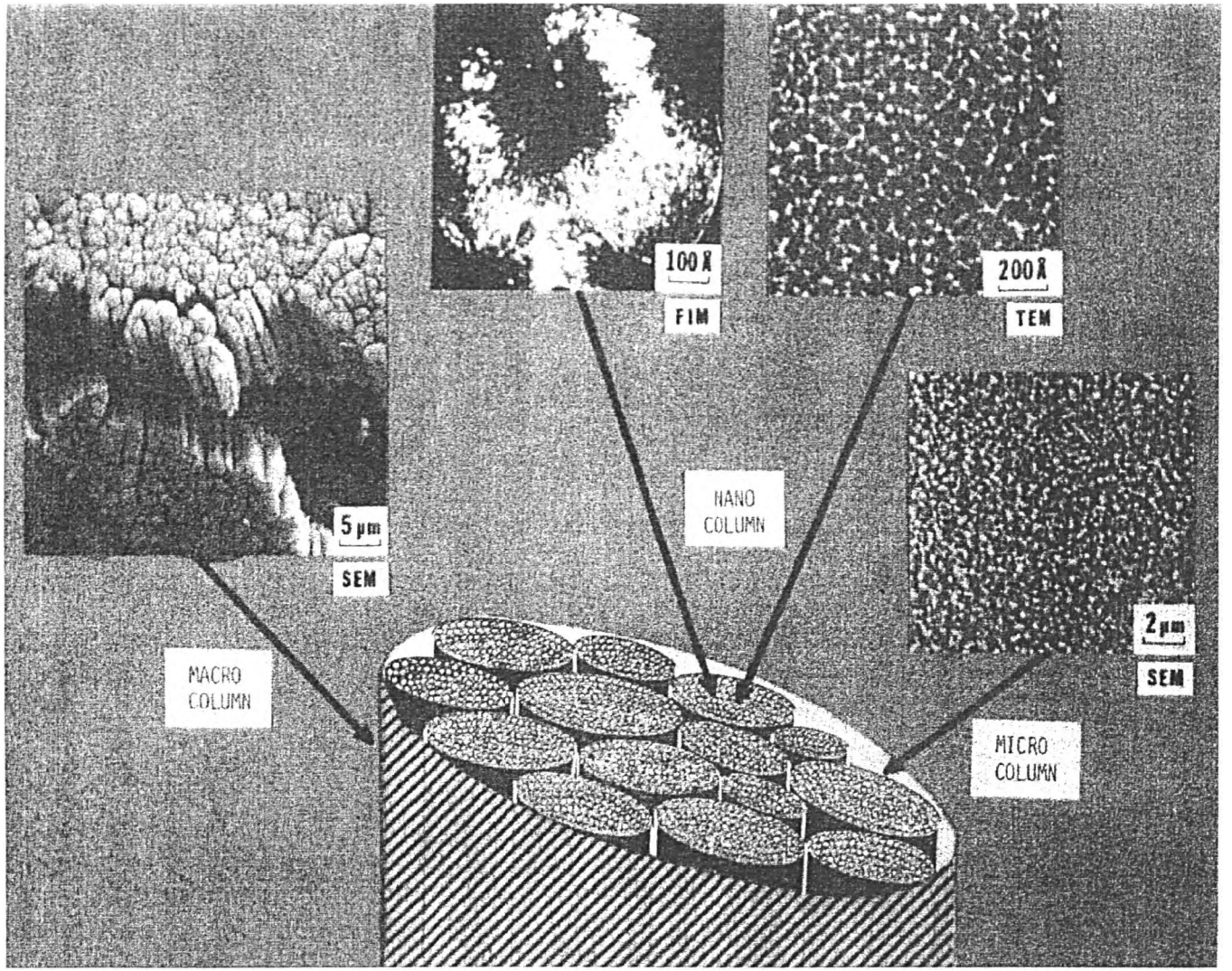

Figure 4.10. Subdivision of zone 1 of the structure zone model by Messier et al [Messier et al, 1984].

substrates do not withstand high temperatures. The practical solution of this problem is the use of various enhanced and ion-assisted deposition methods, which are based on bringing additional energy to the growing film without significant heating of the whole sample.

One of the consequences of additional ion bombardment is enhanced mobility of atoms at the surface and near-surface of the growing film. It was shown [Hultman et al, 1988], that when energy of assisting ions is low, enhanced mobility of atoms plays an important part in decrease of defect population in the film. This results in changing of the growth pattern of the film and leads to improved morphology and density of the coating. In case of bombardment with ions of higher energy, although the mobility of atoms is increased, the rate of defect production due to the ion-solid interaction is also high. The defects are created faster, than they can be annealed, which may lead to reduced quality of the coating. Therefore, care should be taken when specifying particular requirements for ion-assistance and several experiments may be needed to find out optimum deposition conditions.

Additional ion bombardment results not only in improved morphology, but also in improved density, stoichiometry and adhesion [Colligon, 1995; Ensinger, 1997]. Ion-assistance can also lead to changes in other film properties, including stress and optical properties.

The effect of ion bombardment on the growing films has been modelled by many authors. Depending on the approach used, these models can be based on thermal spikes, collision cascades or molecular-dynamics simulations [Cuomo et al, 1989].

In the thermal spike approach [Müller, 1986] it is presumed that atoms of a growing porous film are re-arranged during thermal spikes, which are caused by the bombarding ions. It is assumed, that the film is homogeneous and that the temperature pulses are spherically symmetric. Spikes originate at a distance from film surface, equal to the average damage depth. Atomic re-arrangement during a thermal spike is produced by atoms moving between different lattice sites with temperature-dependent rate. Although with this model predictions on the development of closed voids agree well with experimental results, the presumption of an isotropic re-arrangement of film atoms prevents the thermal spike model from predicting densification correctly.

The latter deficiency is avoided when the collision-cascade approach is used. In his model Müller [Müller, 1986] considers that bombarding ions lose their energy by both elastic and inelastic interactions with atoms of a growing film. These ions can either be back-reflected from the surface of the film or become incorporated into the film. One of

the possible interactions results in the production of knock-on atoms, which in turn can be either re-sputtered or incorporated deeper into the film. This type of interaction leads to a strongly voided surface layer, which is eventually filled by the newly arriving atoms. Thus, the resulting film will be more dense, than the film, deposited without ion bombardment. The first model, based on the collision-cascade approach did not predict one of the important characteristics, well-observed in the densification behaviour of thin films, namely, densification saturation with increasing bombardment. This was because the mechanism responsible (repulsion between film atoms after reaching saturation density value) was not included in the model. This effect was overcome later [Müller, 1987] with the decreasing densification explained by a decrease in the probability of surface vacancy generation with increase in ion energy (i.e. the higher the ion energy, the deeper the vacancy generation occurs, therefore these vacancies cannot be filled with newly coming atoms).

The latest approach used is a molecular-dynamics (MD) approach. All models based on this approach require a numerical solution for a system of coupled classical equations of motion. The solution will represent the result of interactions in the bombarding ion-growing film system, which changes with time and in space. The ion-film system is modelled by a many body atomic system undergoing mutual atomic interactions and collisions. Depending on the material under study, two- or two- and three-body potentials should be used for materials with metallic or covalent bonds respectively.

MD simulations performed by Müller [Müller, 1987] for the case of ion-assisted deposition, yielded several important results. It was found, that bombardment with energetic ions does indeed cause densification by removing overhanging atoms, keeping surface voids open to be filled with newly arriving and re-sputtered film atoms and by inducing collapse of voids. Bombarding ions can also increase the surface mobility of atoms, induce localised heating and cause recrystallisation of film material.

It should be noted, that results of investigations reviewed above are generally applicable to the case of porous films with poor microstructure if deposited in the absence of ion bombardment and the enhancement of these deposition conditions with ion bombardment. This would correspond, for example, to a practical case of films, deposited by evaporation onto a cold substrate. In the case of initially dense films and/or bombardment with large energy ions the film density may actually decrease due to formation of a voided area at the film surface [Davis, 1993].

Bombardment with energetic ions does not only modify microstructure and density of the deposited film, as was discussed above, but also influence other film properties,

such as optical characteristics, stress or preferred crystallographic orientation. The influence of ion bombardment on optical properties and stress in thin films is thoroughly discussed in the first chapters of this work. In the case of a crystalline film, ion bombardment can also influence the grain size of the film material with a general tendency towards a decrease in grain size with increasing ion bombardment. Ion assistance during deposition can favour a preferred crystallographic orientation of the film and can become an important tool for crystal growth control [Petrov et al, 1993]. Recent research has shown that defect arrangement in TiN films does indeed depend on the energy of bombarding ions and it is possible to find optimum conditions such as to minimise the defect levels [Hultman et al, 1988; Kheyrandish et al, 1994]. Ion bombardment can strongly improve film adhesion to the substrate [see, for example, Cotell, Hirvonen, 1996], although the main mechanism of this process is not yet clearly established with atomic mixing at the interface and improved bonding caused by enhanced atom mobility being the two possible causes of such behaviour.

These are only some of the examples of film property modification by ion bombardment. Among others, there is another very important parameter, modified by ion assistance, i.e. film composition in general or film stoichiometry as a special case. Bombardment of the growing metallic film with energetic reactive gas ions can result in production of not only high-quality compounds of known stoichiometry, but also of novel materials, which are not known to exist in the bulk form [see, for example, Hentzell et al, 1985; Rossnagel et al, 1988]. Not only reactive gas ions, but also noble gas ions, so widely used in many energetic ion processes and techniques, can become embedded into the bulk of the film. Therefore, knowledge of gas trapping into solid under bombardment is important for understanding film properties and their modification.

Many studies of gas trapping phenomena are limited to high-energy low-mass ion implantation into crystals and crystalline materials [Scherzer, 1983; Luukkainen et al, 1985]. Four regions of structure, developed as a result of ion bombardment, can be distinguished in this case. These regions are divided according to the ion fluence and are presented here following the work by Scherzer [Scherzer, 1983].

The first region is a very low fluence range with fluences of $\leq 10^{18}$ions/m^2. No surface effects are observed in this case. Gas atoms are usually trapped individually at the damage sites (vacancies, interstitials or dislocations) of a crystal target and in low concentrations, so that interaction between damage sites can be neglected. However, as

fluences increase towards the limit of this range, clusters of several trapped atoms may form.

The second region is an intermediate fluence range with fluences of 10^{18}-10^{21} ions/m^2. Here all gas atoms, which are implanted into the target, are trapped with several gas atoms trapped into one damage site. This leads to gas bubble formation, which can cause expansion of the bombarded area and thus provoke compressive stress formation. Gas bubbles may then grow by accumulation of vacancies, with several models put forward in order to explain growth mechanisms [Scherzer, 1983 and references there].

In the high fluence region (10^{21}-10^{23} ions/m^2) gas trapping reaches its saturation point of 0.3-1 gas/target atoms. Surface effects, such as blisters, flakes and pinholes, are observed in this range. The formation of a particular effect depends on the nature of bombarding gas and target material, on temperature and, for non-metals, on the diffusivity of gas in target material.

The last region is very high fluence range (>10^{23} ions/m^2). Here sputtering of the surface region becomes important, which results in a spongy surface structure. Surface effects, such as grooves, ridges or steps may also form.

In the case of low energy ion bombardment trapped gas can be incorporated either into the matrix of the target or into bubbles, formed in the target [Carter and Colligon, 1968]. The positions of trapped gas in the target matrix can be such, that activation energies for gas migration are either governed by, or less than, the diffusion energy. In the case of bubble formation, their size will increase with increase of target temperature. Bubble growth will then be governed by the same mechanism, as in the case of high-energy intermediate fluence ion implantation, i.e. by the collection of vacancies.

Another very important question which arises in connection with ion bombardment during deposition is its influence on the thin film stress. It is known, that energetic ions can cause thermal spikes in the bombarded medium. Although, as outlined above, the effect of thermal spikes is somewhat disputed in the case of sputtering and their influence on sputtering yield is negligible, thermal spikes can certainly cause re-arrangement of the deposited material, which was accounted for in the Davis model [Davis, 1993] of stress behaviour. The characteristics of importance in our case are the conditions for the formation and existence of a thermal spike and its "temperature".

A thermal spike is traditionally defined as "a limited volume with the majority of atoms temporarily in motion" [Sigmund, 1974; Seitz and Koehler, 1956]. The bombarding ion transfers some of its energy to the lattice atoms and this energy causes lattice vibrations in a localised area surrounding the point of impact. This results in "heating" of this area

and the material within the spike becomes liquid-like, which leads to a permanent re-arrangement of the target atoms [Seitz and Koehler, 1956]. The thermal spike then "cools down" by conducting heat to its surroundings [Kelly, 1977] and, possibly, by losing some part of its energy to the wave, generated by lattice strain caused by thermal stresses [Martynenko, 1994].

One of the first treatments of thermal spikes was that of Seitz and Koehler [Seitz and Koehler, 1956], however, the conditions of thermal spike formation are not strictly outlined there. It can be summarised that the solid (i.e. target) under consideration should consist of atoms with atomic number ≥ 10 and the energy E_{th}, transferred to an atom by the ion, should be high enough to generate the thermal spike, but low enough to generate just one thermal spike, but not a number of localised hot spots ($50\ \text{eV} \leq E_{th} \leq 300\ \text{eV}$). Slightly modified conditions were introduced by Brinkman [Brinkman, 1954; Brinkman, 1956], where atoms in thermal spike area were assumed to have mean free paths, which are less than or equal to the interatomic distance in the solid and energy E_{th}<150-250 eV. Probably the most well-defined condition of thermal spike formation was postulated by Cheng [Cheng, 1990], who applies fractal geometry to ion-solid interactions. Cheng defines the critical energy E_{crit} of an atom and states, that in case of

(1) $E_{crit} < E_d$ (E_d is the threshold displacement energy) the spike will not form;

(2) $E_{crit} > E_i > E_d$ the spike may form, and

(3) $E_i > E_{crit} > E_d$ the incident ion will form several displaced atoms. If the displaced atom has an energy just below E_{crit}, it can generate a local thermal spike.

The value of E_{crit} will depend on the species involved in the collision. If the "universal interatomec potential" of Ziegler, Biersack and Littmark [Ziegler et al, 1985] is chosen, then the condition for E_{crit} becomes

$$E_{crit} = \frac{2Z_1 Z_2 e^2 x_c}{\alpha} \sqrt{\frac{2M_1}{M_2}}, \tag{4.12}$$

where $x_c = 0.903 \times 10^{-3}$, $\alpha = 0.8854\alpha_0 / \left(Z_1^{0.23} + Z_2^{0.23}\right)$, α_0 is the Bohr radius, Z_1 and Z_2, M_1 and M_1 are atomic numbers and masses of the ion and the target atom. The main disadvantage of the conditions, proposed by Cheng, is that they apply to single-component systems.

Apart from the duration of the thermal spike, its main characteristic is energy density. The most common equation for energy density calculations is the relation, derived by Sigmund [Sigmund, 1974]. This equation is based on the assumptions that scattering is elastic and the potential of interaction is an inverse-power potential ($V \propto r^{-1/m}$, r is the internuclear distance, $0 \le m < 1$). The "effective maximum energy density θ_0 (energy per atom)" in this case is

$$\theta_0 = \begin{cases} G_2 N^2 / E_i^2 & for \quad m = 1/2 \\ G_3 N^2 / E_i & for \quad m = 1/3 \end{cases}, \tag{4.13}$$

where N is number density of a target material (number of atoms per unit volume), E_i is an initial energy of the projectile and G_2 and G_3 are functions of masses of projectile and target atom, which can be found from Figure 4.11. The conditions for the choice of the value of m, outlined by Winterbon [Winterbon et al, 1970], strongly depend on the value of a parameter t

$$t = \left(\left(\frac{M_2 E_i}{M_1 + M_2} \right) \left(\frac{Z_1 Z_2 e^2}{\alpha} \right)^{-1} \right)^2 \frac{T}{T_m}, \tag{4.14}$$

where T is the recoil energy and T_m is defined accoring to Equation (4.7). If t is small, m = 1/3 can be taken, while for a "reasonable all-over approximation" [Winterbon et al, 1970] the value of m = ½ should be chosen.

Sigmund's approach was criticized by Cheng, who states that the assumption that all atoms involved in the cascade volume share energy E_i is invalid for the chosen values of m and thus the formation of local spikes in this case may be overlooked. According to Cheng,

$$\theta_0(E) = G(m) N^2 E^{1-6m}, \tag{4.15}$$

where $0 < m \le 1/6$ (condition for spike formation), $G(m)$ is a function of projectile and target masses, E is the energy of target atom, that initiates a cascade.

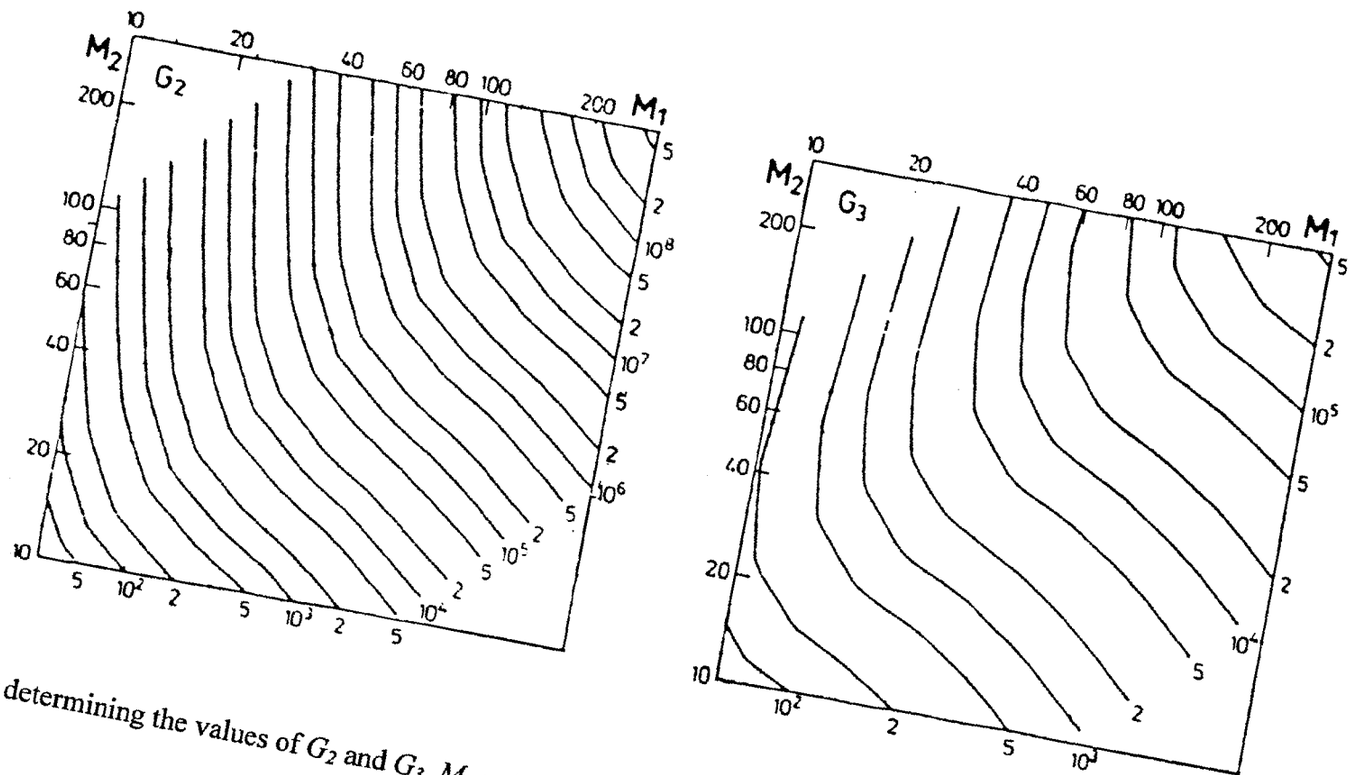

Figure 4.11.Plots for determining the values of G_2 and G_3. M_1 and M_2 are ion and target atom masses in atomic units respectively.[Sigmund,1974].

In conclusion to this chapter it can be said that all the questions, treated here, are important for practical application of sputtering and ion bombardment for thin film deposition. Consideration of various processes, resulting from ion bombardment of the solid surface, of the theories of compound sputtering, thermal spikes or gas trapping, can help in understanding of the processes, taking place in the growing films, subjected to concurrent ion bombardment. The background knowledge of the questions on sputtering yield, angular and energetic distribution of sputtered particles are also important and can help in the identification and choice of correct experimental procedure and parameters. For example, in many experiments in this research sputtering targets were positioned at 35° to the sputtering beam of 1 keV ions. These conditions are expected to lead to knock-on sputtering regime, so the sputtered particles will have the "memory" of the angle of incidence of bombarding ions onto target and will be ejected in the forward direction. Other examples of theory application include expectation of gettering in reactive processes (especially with the Ta target) or of gas trapping in ion-assisted films.

References

Biersack J.P. and Ziegler J.F., Nucl. Instr. Meth., **194**, 93, (1982)

Bohdansky J. and Roth J., Bay H.L., J. Appl. Phys., **51(5)**, 2861, (1980)

Brinkman J.A., Am. J. Phys., **24**, 246, (1956)

Brinkman J.A., J. Appl. Phys., **25**, 961, (1954)

Carter G. and Colligon J.S., *Ion Bombardment of Solids*, Heinemann Educational Books Ltd., London, 1968

Cheng Y.-T., Materials Science Reports, **5(2)**, 45, (1990)

Christie A.B., Lee J., Sutherland I. and Walls, J.M., Appl. Surf. Sci., **15**, 224, (1983)

Colligon J.S., J. Vac. Sci. Technol., **A 13(3)**, 1649, (1995)

Contarini S. and Rabalais J.W., J. Electron Spect. And Rel. Phenom. **35**, 191, (1985)

Cotell C.M., Hirvonen J.K., Surf. Coat. Technol., **81**, 118, (1996)

Danroc J., Aubert A. and Gillet R., Surf. Coat. Technol. **33**, 83, (1987)

Davis C.A., Thin Solid Films, **226**, 30, (1993)

Dullni E., Appl. Phys., **A38**, 131, (1985)

Dullni E., Nucl. Instr. and Meth., **B2**, 610, (1982)

Ensinger W., Nucl. Instr. Meth. Phys. Res., **B 127-128**, 796, (1997)

Goranchev B., Orlinov V. and Popova V., Thin Solid Films **33**, 173, (1976)

Handbook of Ion Beam Processing Technology: Principles, Deposition, Film Modification and Synthesis/ed. by Cuomo J.J. and Rossnagel S.M., Kaufman H.R.,, Noyes Publications, U.S.A., 1989

Handbook of Plasma Processing Technology: fundamentals, etching, deposition and surface interactions/ ed. by S.M. Rossnagel, J.J. Cuomo, W.D. Westwood, Noyes Publications, U.S.A., 1990

Heller J., Thin Solid Films, **17**, 163, (1973)

Henderson D.J., Brodsky M.H. and Chaudhari P., Appl. Phys. Lett. **25**, 641, (1974)

Hentzell H.T.G., Harper J.M.E. and Cuomo J.J., J. Appl. Phys., **58**, 556, (1985)

Hultman L., Barnett S.A., Sundgren J.-E. and Greene J.E., J. Cryst. Growth **92**, 639, (1988)

Husinsky W., Betz G. and Gigris I., J. Vac. Sci. Technol., **A2**, 698, (1984)

Husinsky W., Betz G. and Gigris I., Phys. Rev. Lett., **50**, 1689, (1983)

Kelly R., Miotello A., Nucl. Instr. Meth. Phys. Res., **B 122**, 374, (1997)

Kelly R., Rad. Eff., **32**, 91, (1977)

Kheyrandish H., Colligon J.S. and Kim J.-K., J. Vac. Sci. Technol., **A12**, 2723, (1994)

Larsson T., Blom H.-O., Nender C. and Berg S., J. Vac. Sci. Technol., **A 6 (3)**, 1832, (1988)

Lindhard J., Scharff M. and Schiott H.E., Mat. Fys. Medd. Dan. Vid. Selsk, **33**, 1963

Luukkainen A., Keinonen J. and Erola M., Phys. Rev., **B32(7)**, 4814, (1985)

Martynenko Yu.V. and Umasky M.V., Radiation Effects And Defects in Solids, **132**, 31, (1994)

Mattox D.M., J. Vac. Sci. Technol., **A 7(3)**, 1105, (1989)

Messier R., Giri A.P. & Roy R., J. Vac. Sci. Technol., **A 2**, 500, (1984)

Movchan B.A. and Demchishin A.V., Fiz. Metall. Metalloved., **28**, 653, (1969)

Müller K.-H., J. Appl. Phys., **59**, 2803, (1986)

Müller K.-H., J. Vac. Sci. Technol., **A4**, 184, (1986)

Müller K.-H., J. Vac. Sci. Technol., **A5**, 2161, (1987)

Müller K.-H., Phys. Rev., **B35**, 7906, (1987)

O'Connor D.J. and Biersack J.P, Nucl. Instr. Meth., **B15**, 14, (1986)

Okamota A. and Serikawa T., Thin Solid Films **137**, 143, (1986)

Petrov I., Adibi F., and Greene J.E., Hultman L. and Sundgren J.E., Appl. Phys. Lett., **63** (1), 36, (1993)

Pringle S.D., *A Study of the Formation of Silicon Oxide Thin Films Using Dual Ion Beam Reactive Sputtering*, Ph.D. thesis, Dept. of Electronic and Electrical Engineering, University of Salford, Salford, U.K., 1994

Rossnagel S.M. and Cuomo J.J., Vacuum, **38**, 73, (1988)

Scherzer B.M.U., *Development of Surface Topography due to Gas Ion Implantation* in *Sputtering by particle bombardment. – 2:Sputtering of Alloys and Compounds, Electron and Neutron Sputtering, Surface Topography* ed. by R.Behrisch– Berlin: Springer-Verlag, 1983. – (Topics in applied physics; vol. 52)

Seitz F. and Koehler J.S., Solid State Physics, **2**, 305, (1956)

Sigmund P., Phys. Rev. **184**, 383 (1969)

Sigmund P., Appl. Phys. Lett., **25 (3)**, 169, (1974), Appl. Phys. Lett. **27**, 52, (1975)

Sputtering by particle bombardment. – 1:Physical Sputtering of Single-Element Solids/ ed. by R.Behrisch– Berlin: Springer-Verlag, 1981. – (Topics in applied physics; vol. 47)

Thompson M.W., Phil. Mag., **18**, 377, (1969)

Thornton J.A., J. Vac. Sci. Technol., **11**, 666, (1974)

Wehner G.K., J. Appl. Phys., **26**, 1056, (1955)

Winterbon K.B., Sigmund P. and Sanders J.B., Mat. Fys. Medd. Dan. Vid. Selsk, **37(14)**, 1, (1970)

Winterbon K.B., *Ion Implantation Range and Energy Deposition Distribution*, Vol. 2, Plenum Press, 1975

Ziegler J.F., Biersack J.P. and Littmark U., *The Stopping and Range of Ions in Solids*, vol. 1, Pergamon Press, New York, 1985

Chapter V

Experimental

This chapter contains a detailed description of a deposition and stress measurement apparatus and the exact experimental conditions used. The experiments were designed to find the conditions for deposition of stoichiometric Ta_2O_5 and SiO_2 films and to study the effect of deposition parameters on stress in these films. Also described in this chapter are the exact conditions during the analysis of thin film properties. Background information on thin film analysis techniques, used in this research, is provided in Appendix 1.

5.1. Stress measurement

Independently of the deposition method used, the stress measurement part of the experimental apparatus was set up as follows. A He-Ne laser beam was directed onto a mirror positioned so that the reflected laser beam was passing through the optical port of the main chamber and directed onto the back side of the substrate. The substrate reflected this incoming beam and directed the reflected beam back through the optical port to the SiTeK position-sensing detector (PSD), where the reflected beam position was measured. The geometry of the system, together with the distances between the components used, is presented in Figure 5.1. The sensitivity of this system, measured in terms of detectable radius of curvature is 170 m, or, in terms of minimum detectable force per unit width, 29 Pa·m.

Substrates used in this study were clean Si wafers cleaved to form a cantilever beam of 1 cm width and 4.5-5 cm length with 3.4 cm exposed to the atom flux. Double side polished test silicon wafers (<100>, p/boron doped, 400μm thickness) were used. The substrate, clamped at one edge with all other edges free, was rotated between the deposition and the stress measurement positions and could be moved sideways, thus

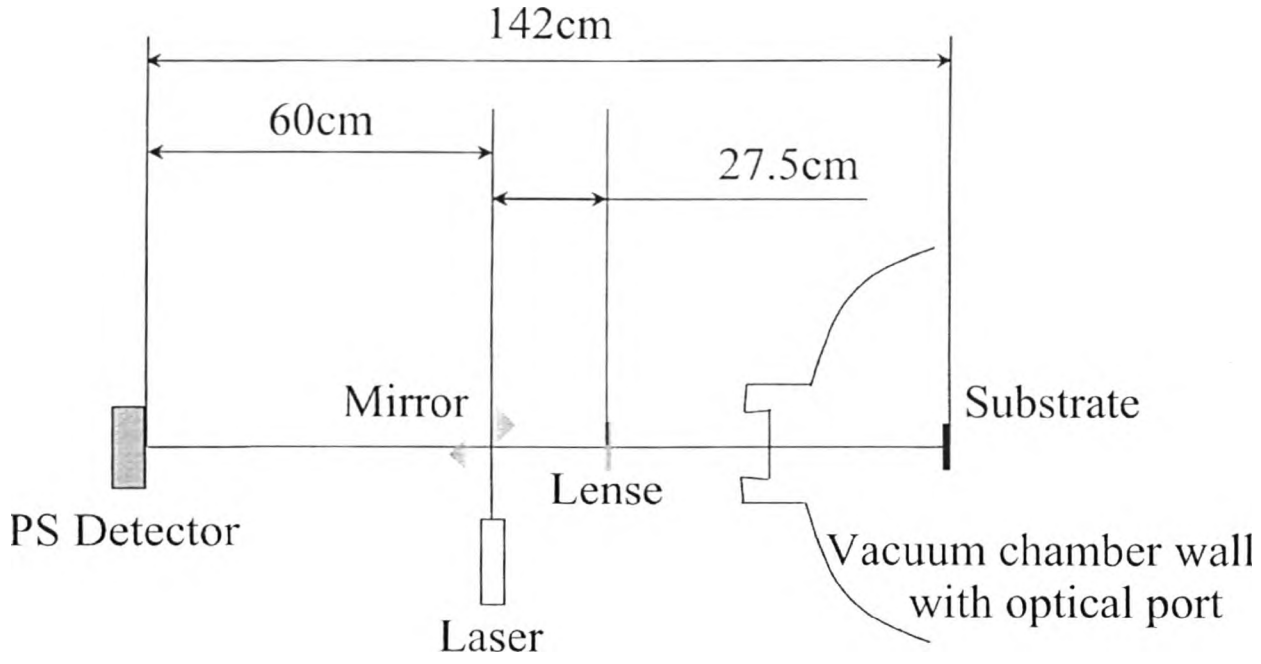

Figure 5.1. Geometry and dimensions of the stress measurement part of experimental rig.

allowing the readings to be taken at several points along its length. Substrate elastic constants (Young's modulus and Poisson's ratio) were taken from the work by Brantley [Brantley, 1973].

The stress measurement system was bench-tested in order to find out the effect of various parameters on the measured curvature of the substrate.

A set of experiments has been completed in air, investigating the influence of the angle of incidence of the laser on the measured curvature of the substrate. A fixed stationary substrate with a detectable curvature was used. The angle of incidence of the laser beam onto the substrate was varied and the sample was scanned after each change in angle. The results of these experiments showed that different angles of incidence of the laser beam influence the position of the reflected beam on the detector. However, the results of calculation of the radius of curvature from the difference in movement of the beam, reflected from clamped end and free end of substrate, do not change. This is important, as it confirms that the measured radius of curvature does not depend on the angle of incidence of the laser beam when it is evaluated from data obtained at any two points on the beam.

The effect of substrate and substrate holder heating during deposition was also considered. The substrates were not intentionally heated during deposition. However, the temperature during sputtering could reach up to 85-100°C. An experiment was performed where an aluminium foil was clamped in front of the silicon substrate, protecting it from the flux of particles forming the film. In this case only the effect of temperature would be measured. The results of this experiment, presented in Figure 5.2, show that, the measured position of the reflected laser beam changes, which can indicate angular movements of the substrate with respect to the laser beam. However, calculations, which take into account movements of the clamped end as well as the free end, indicate that the substrate curvature did not change. The substrate returned to its initial position one hour after the deposition.

Although the temperature does not affect the bare substrate, it can have an influence on a coated substrate curvature via the effect of thermal stresses. Such influence can be estimated from the properties of film and substrate materials and changes in temperature during deposition. If 1549.4 GPa [Tien et al, 2000], 73 GPa [Web 1] and 180.5 GPa [Brantley, 1973] are taken as the values of biaxial moduli and 3.6×10^{-6} $(^0C)^{-1}$ [Tien et al, 2000], 0.55×10^{-6} $(^0C)^{-1}$ [Web 1] and 3×10^{-6} $(^0C)^{-1}$ [Weast, 1974] are taken as the values of thermal expansion coefficient for Ta_2O_5, SiO_2 and Si, respectively and the temperature change is assumed to be approx. 80 ^0C, then the thermal stress can be

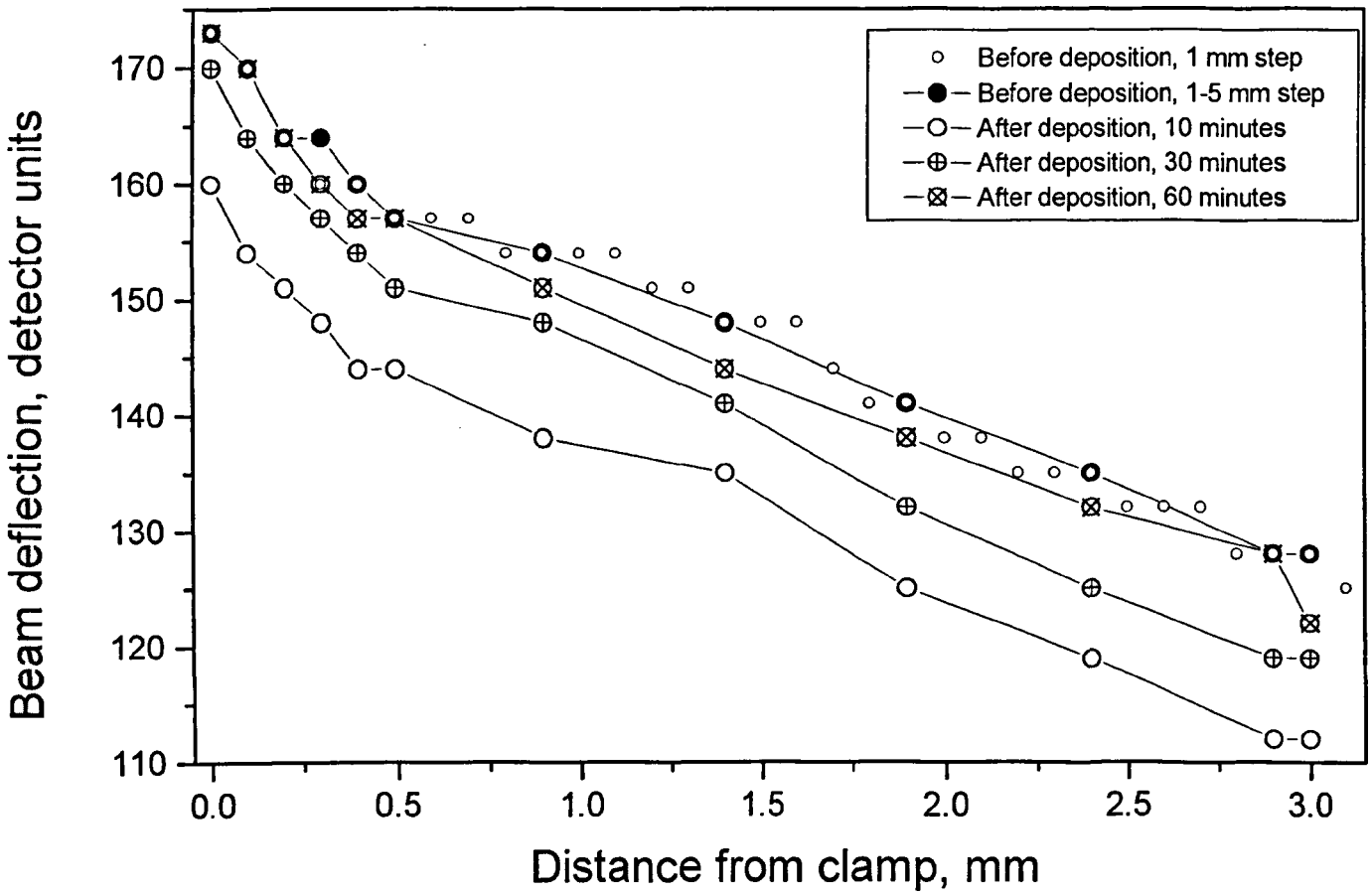

Figure 5.2. Effect of substrate and substrate holder temperature on measured laser beam position (1 detector unit = 50 μm).

estimated using formula (3.2) in chapter III. Thus, for a Ta_2O_5 film on a Si substrate the magnitude of thermal stress is estimated to be 74 MPa. For a SiO_2 film on a Si substrate the magnitude of thermal stress is 14 MPa. The value of 14 MPa is below the sensitivity range of the stress measurement rig, thus thermal stress in SiO_2 films on Si substrates will not influence the results in the range of temperatures studied. In the case of Ta_2O_5 films on a Si substrate additional measurements were performed. The substrate curvature was measured once straight after the deposition and after several timed intervals after the deposition (10 minutes, 30 minutes, 1 hour, 2 hours, approx. 12 hours). It was found that, after an initial 10 minutes of substrate cooling (no special measures were used), sample curvature does not change. Therefore, it was concluded that, if curvature measurements are performed after the substrate is allowed to cool down for approx. 10 minutes, the effect of thermal stress on the substrate curvature is negligible even for Ta_2O_5 films on Si substrates.

When using the scanning method it is possible to plot the profile of the sample. Consider an example of a typical sputtered stoichiometric Ta_2O_5 film on a Si substrate, deposited for 2.5 hours with measurements taken every ½ hour. The stress measurement rig yields the information, presented in Figure 5.3. Using this information and accounting for the movement of the clamped end of the sample in the calculation, the profile of the sample, presented in Figure 5.4, may be obtained. As it is assumed, that the stress is isotropic and uniform in the plane of the film, its value can be calculated from the data from any two points of the sample, provided that the distance between them is known and any movements of the point, considered as fixed, are taken into account. Figure 5.5 shows that the values of stress, calculated using data on several different points of the sample, although they vary slightly, are still within the error margin of the method. It should be noticed, however, that it is not advisable to use points, which are too close to each other as this significantly reduces the accuracy of the technique.

Figures 5.2-5.3 also show the scale of the accuracy in the measurement of laser beam position on the detector. It was estimated that maximum error in this case is 10 detector units. If the film thickness is known, it is possible to calculate film stress, required to cause sample deflection, leading to laser beam movement of 10 detector units. This value was taken as the error in film stress measurements.

Thus, unless specified otherwise, stress measurements were taken in scanning configuration. Measurements were taken before deposition and 10 minutes after the deposition (or a part of deposition). The radius of curvature R of the sample was

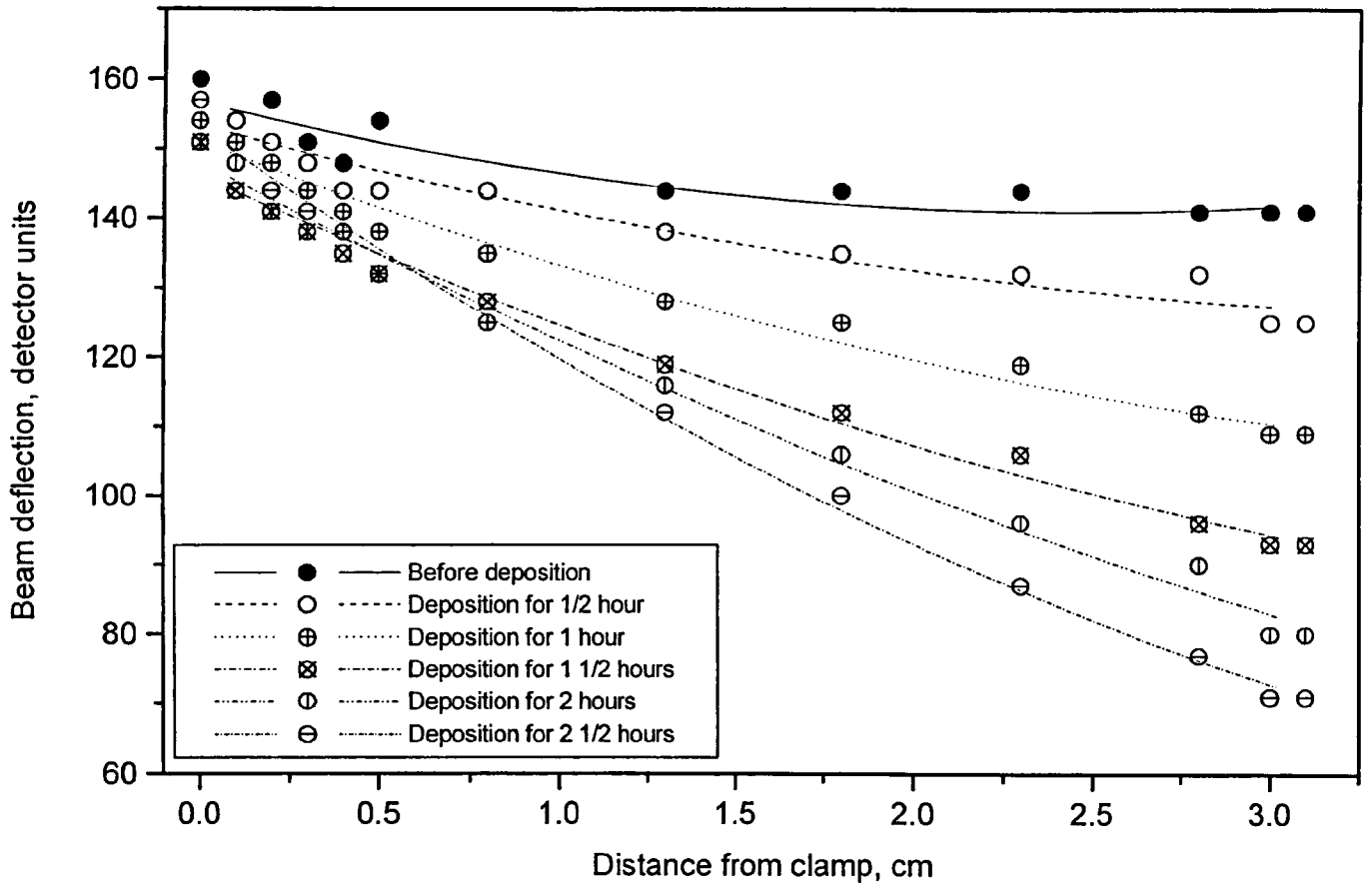

Figure 5.3. Measured laser beam deflection for sputtered stoichiometric Ta_2O_5 film, in detector units (1 detector unit = 50 μm). Lines are drawn to guide the eye.

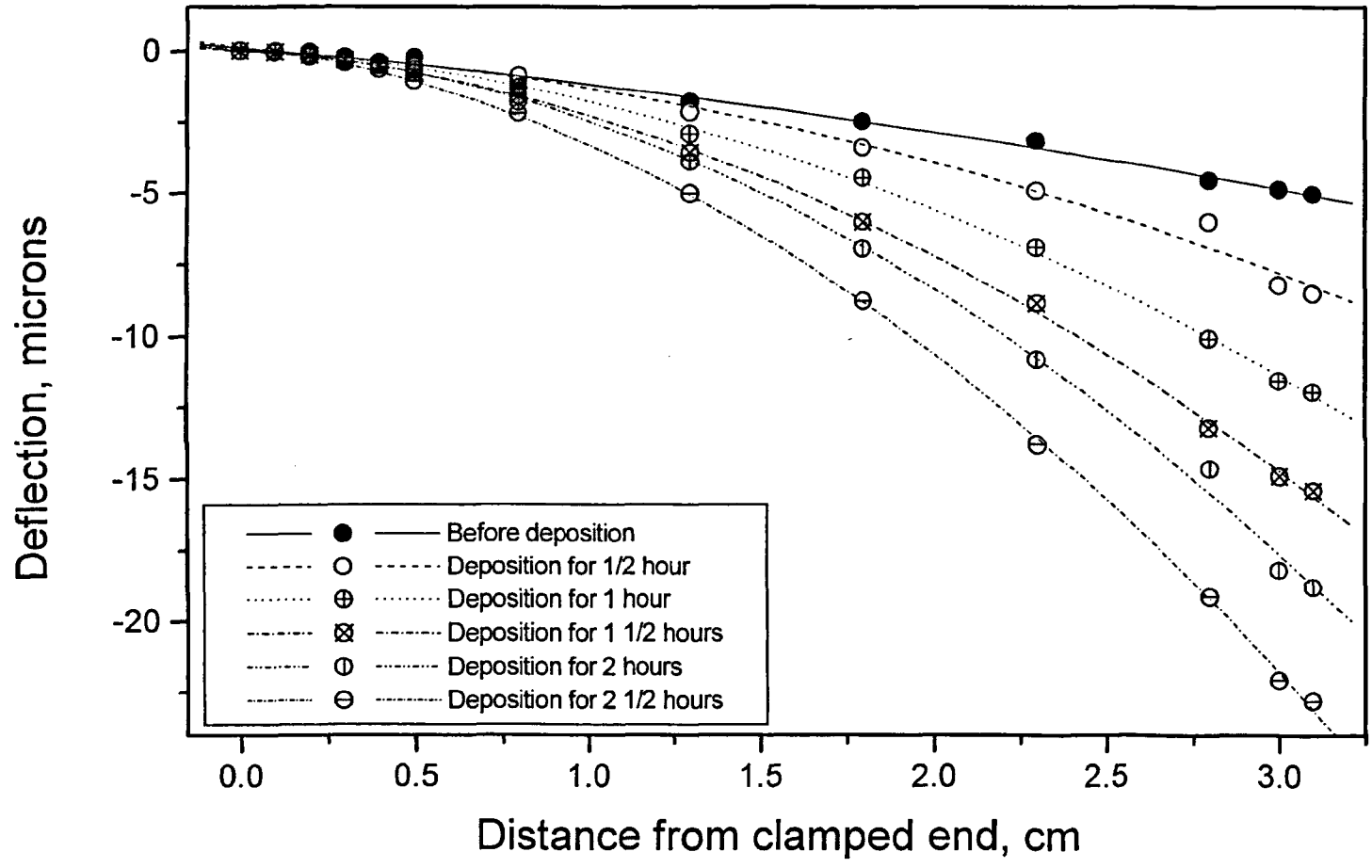

Figure 5.4. Measured substrate deflection for sputtered stoichiometric Ta_2O_5 film, in microns. Lines are drawn to guide the eye.

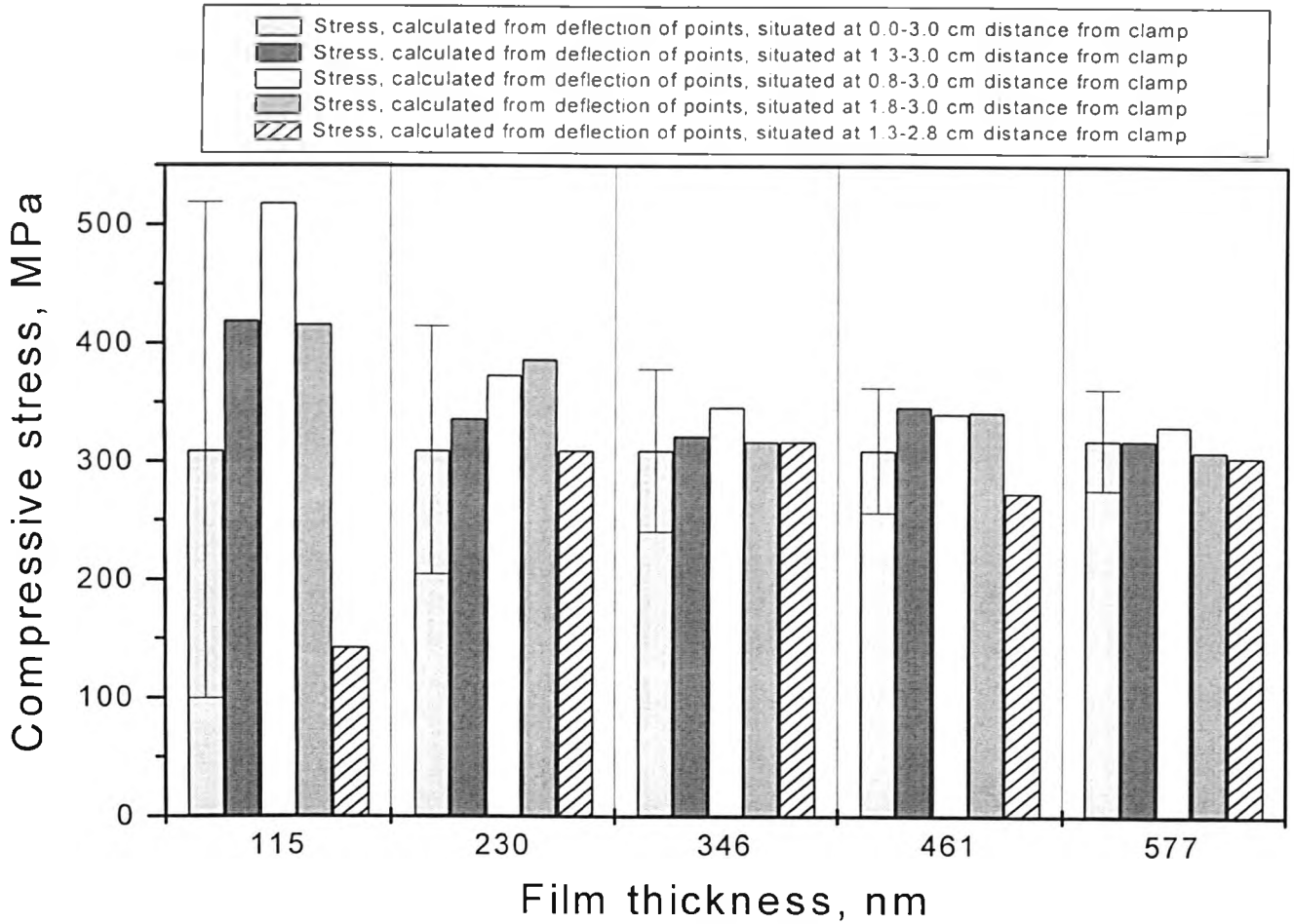

Figure 5.5. Film stress, calculated using different data points on the sample.

calculated using the formula [Moulard et al, 1998] $R = -\frac{2l_{opt}l_s}{m}$, where l_{opt} is the length of optical path, i.e. the distance from sample to detector, l_s is the distance from the clamped end to measurement position and m is the deflection of the laser beam (with account for any movement of clamped end). To minimise the error, film stress was calculated from the data points, separated by 3 cm from each other. The errors were calculated according to the procedure, described above. The final value of film stress was calculated using the Stoney equation (Equation (3.40) chapter III).

5.2. Ion-beam sputtered films

5.2.1 Deposition chamber configuration

Thin films of silicon dioxide and tantalum pentoxide were deposited using a custom-built ultra-high vacuum (UHV) system. This system consists of a main and a loading chamber separated by a gate valve to allow sample entry.

The loading chamber is a stainless steel vessel, pumped with a turbo-molecular pump and a rotary pump to a base pressure, similar to that of the main chamber. The use of a loading chamber allows sample entry without breaking vacuum in the main chamber.

The main chamber is a 40 cm diameter stainless steel vessel, pumped by turbo-molecular and rotary pumps to a typical base pressure of 8×10^{-5} Pa. This chamber is equipped with an e-beam evaporator, two Kaufman type ion sources for sputtering and ion assisting, respectively, a Penning gauge for pressure measurements, rotatable target and substrate holders and an optical port for the laser beam used for stress measurements. The geometrical arrangements for film deposition by ion-beam sputtering is presented in Figure 5.6.

A 3 cm IonTech (flange-mounted) ion source with carbon or molybdenum grids was used for sputtering the target. A beam of assisting ions was produced by a custom-built 3 cm ion source with carbon or molybdenum grids. In some experiments oxygen had to be introduced into the chamber through the main or assisting ion sources. This had an adverse effect on standard carbon grids, fitted to the sources, and led to their erosion. To increase the lifetime of the sources grid systems, the carbon grids were replaced by molybdenum grids.

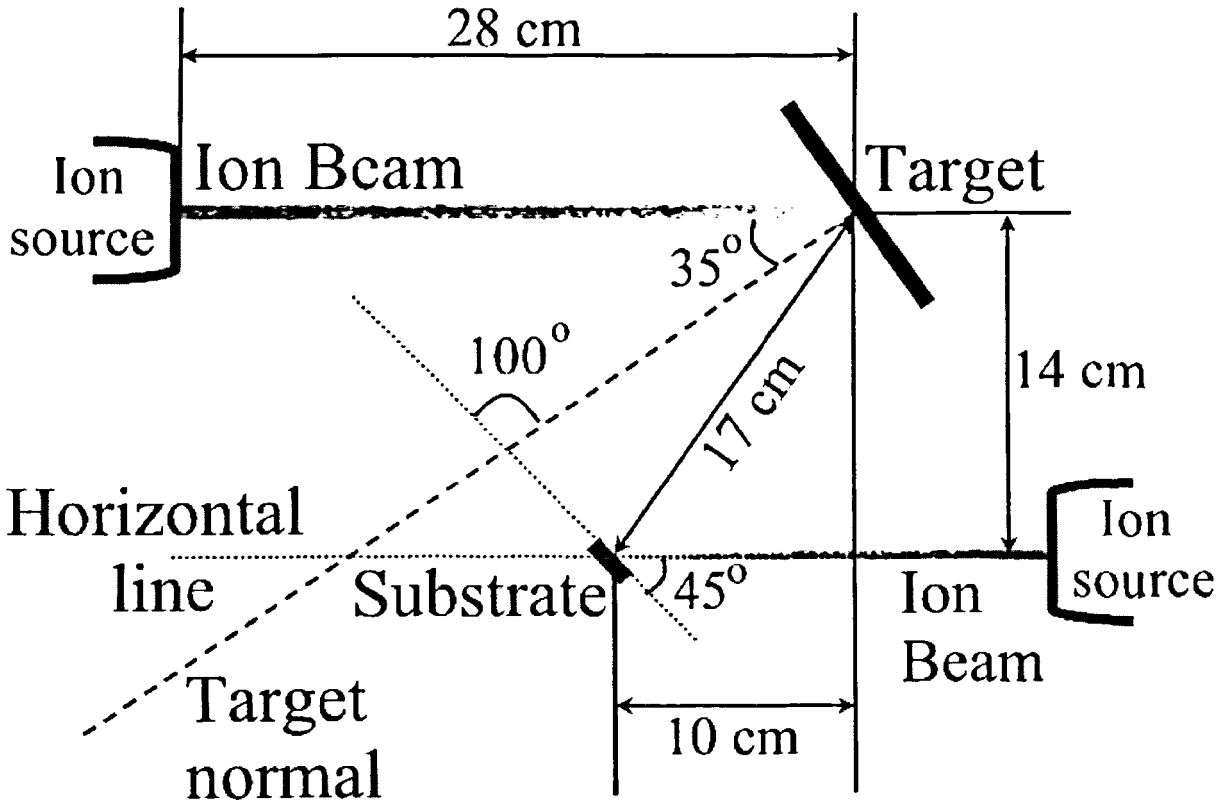

Figure 5.6. Internal geometry and dimensions of the deposition chamber, set for ion-beam sputtering.

Measurements of current density of assisting ion beam were carried out using a Faraday cup, placed close to the substrate position during the deposition. The measurements were taken before each run with the Faraday cup facing the beam of assisting ions. For film growth the substrate was positioned at an angle (45^0 for sputtered ion-assisted films) to the beam of assisting ions (see Fig. 5.2). At this position the readings on the Faraday cup cannot be taken, so instead of current density, total beam current, corresponding to the required current density, was monitored and held constant during deposition.

Film materials, used in this study, are insulators, so neutralisation is required to avoid charge-up of the targets and substrates. An immersed wire neutraliser, supplied with the IonTech ion source, or a plasma-bridge neutraliser were used. Tungsten or thoriated tungsten wire was used for the source cathode and immersed wire neutraliser filaments. Tantalum wire was used as a filament in the plasma-bridge neutraliser.

Rotatable Ta, Si or SiO_2 targets (10×10cm) were used for film deposition. All targets were pre-cleaned for 30 minutes before deposition under conditions identical to those used for the deposition itself. Substrates were not intentionally heated during the deposition.

5.2.2. Cleaning procedures

To study the influence of the initial state of the substrate on stress in thin films, four Si substrate cleaning procedures were used in this study. The basic cleaning procedure included 5 minutes treatment in acetone in an ultrasonic bath, followed by 5 minutes of methanol treatment in the ultrasonic bath. The substrate was then rinsed with distilled water and dried with nitrogen. The second cleaning procedure consisted of the basic cleaning, followed by a further 20 minutes bombardment with 500 eV argon ions. The third cleaning procedure was similar to the second one, but the bombardment was by oxygen ions. The last cleaning procedure consisted of several steps, outlined below:

1. wipe the substrate with ethanol and polyurethane sponge;
2. ultrasonically clean the substrate in distilled water for 5 minutes;
3. change distilled water and repeat step 2 once;
4. ultrasonically clean for 15 minutes in the solution of "Quadrilene" detergent;
5. clean in the ultrasonic bath in distilled water for 5 minutes;
6. change distilled water and repeat step 5 once;
7. ultrasonically clean in hot distilled water for 3 minutes;

8. spin-clean with a flow of distilled water;
9. stop the flow of distilled water and spin the substrate until dry.

5.2.3. Ion-beam sputtered tantalum pentoxide films

In general, all Ta_2O_5 films were deposited by ion-beam sputtering of a Ta target with 1 keV ions. Unless specified otherwise, argon was used as a sputtering gas and its flow through the main ion source was fixed at 1.8 sccm. Oxygen was let into the chamber near the substrate or through the assisting ion source. Then additional argon, required for the operation of the plasma bridge neutraliser (PBN) (if used) was let into the deposition chamber. If the immersed wire neutraliser was used, additional argon was let through the assisting ion source. Addition of argon permitted the total pressure during deposition to be kept constant at 4×10^{-2} Pa for all runs. For each experiment main deposition conditions are listed in Table 5.1. For some experiments specific conditions, not listed in Table 5.1, are listed in the descriptions below.

a) Film composition

Films were deposited continuously for 1.5 hours. The thin film composition was calculated from Rutherford Backscattering Spectroscopy (RBS) data and the film thickness was measured using a Dektak II profilometer.

b) Substrate cleaning effect

In this experiment deposition conditions were first checked for the deposition of reproducible stoichiometric films by depositing two films for 1.5 hours continuously and two films for 2.5 hours with interruption of the growth process for additional stress measurements. Next, silicon substrates were cleaned according to the procedures, outlined in chapter V section 5.2.2. Films were deposited onto these substrates for 2.5 hours with stress measurements after every ½ hour.

c) Sputtering gas effect

In this experiment no Ar was introduced into the chamber. Instead, Xe was used as a sputtering gas. Additional Xe was allowed into the chamber through the non-operating

Table 5.1. Conditions for deposition of sputtered tantalum pentoxide films.

Experiment	Angle, degrees		Flow of O_2 near the substrate, sccm	Sputtering source		Neutralisation			Assisting source		
	Substrate	Target		Gas	Beam current, mA	Immersed wire	Plasma Bridge		Gas	Ion-to-atom arrival ratio	Ion Energy, eV
						Current, mA	Gas	Current, mA			
Film Composition	**45**	**35**	**1.0-13.0**	**Ar**	**45**	**51**			**Ar**		
Substrate Cleaning Effects	**45**	**35**	**10**	**Ar**	**45**	**51**			**Ar**		
Sputtering Gas Effect	**45**	**35**	**13**	**Xe**	**25**	**31**			**Xe**		
Target Angle Effect	**45**	**15, 35, 55**	**13**	**Xe**	**25**	**31**			**Xe**		
Substrate Angle Effect	**25, 45, 70**	**35**	**10**	**Ar**	**45**	**51**			**Ar**		
Effect of Other Deposition Conditions	**45**	**35**		**Ar**	**45**	**51**	**Ar**		**O_2 10 sccm**		
	45	**35**		**Ar**	**45**		**Ar**	**500**	**O_2 10 sccm**		
	45	**35**		**Ar**	**45**		**Ar**	**500**	**O_2 8 sccm**		
	45	**35**	**10**	**Ar**	**45**		**Ar**	**500**			
Ion Bombardment	**45**	**35**	**10**	**Ar**	**45**	**51**			**Ar**	**0.49-1.4**	**250, 400, 600**
	45	**35**		**Ar**	**45**		**Ar**	**500**	**O_2 10 sccm**	**0.7-2.0**	**150, 250, 400**

assisting source to keep the total deposition pressure at 4×10^{-2} Pa. Under the described deposition conditions stoichiometric films with reproducible stress values were obtained. The results of this experiment were compared to the results of the previous experiment, where Ar was used as the sputtering gas.

d) Effect of angle of incidence of sputtering beam to target normal

Thin films of tantalum pentoxide were deposited for 2.5 hours with intermittent stress measurements after every ½ hour of deposition. The total deposition pressure was attained using the method, described in the experiment on the effect of sputtering gas. The angle between the sputtering beam and target normal (see Fig. 5.2) was varied from 15^0 to 55^0.

e) Effect of angle of arrival of sputtering flux onto the substrate

In this experiment Ar was used as the sputtering gas. The substrate angle, defined as the angle between the substrate current position and the substrate vertical position, was varied from 25^0 to 70^0.

f) Effect of other deposition conditions

This experiment was designed to establish any effect other deposition conditions (namely, material of ion source grids, type of neutralisation, or, the entry point of reactive gas into the chamber) may have on stress in thin Ta_2O_5 films. Here, several runs were performed. First, ion source grids were changed from carbon to molybdenum and reactive gas was introduced through the assisting source. Then the neutralisation method was changed from immersed wire to PBN. Next, the flow of oxygen was reduced from 10.0 sccm to 8.0 sccm. Finally, oxygen was introduced into the chamber near the substrate, rather than through the assisting ion source. The results of these experiments were compared to the results, obtained in the experiment on the influence of substrate cleaning.

g) Argon-assisted sputtered tantalum pentoxide films

Additional energy was brought to the film during its growth by bombardment with energetic argon ions. The energy of these ions was varied from 250 V to 600 V. The dose of bombarding species was determined by the ion-to-atom arrival ratio, i.e. the ratio of arriving argon ions to tantalum atoms and was varied from 0.49 to 1.4. The number of Ta atoms, arriving per cm^2 per second, was calculated from the Rutherford Backscattering Spectrometry (RBS) data.

h) Oxygen-assisted tantalum pentoxide films

The current experiment consisted of a study of the influence of concurrent bombardment by energetic oxygen ions on the stress in tantalum pentoxide films. The energy of bombarding species was varied in the range of 150 eV to 400 eV. It was assumed that the substrate was bombarded by oxygen ions and that all ionised oxygen molecules dissociated into two oxygen ions on arrival to the substrate. Thus, for oxygen-assisted Ta_2O_5 films the ion-to-atom arrival ratio, was defined as the ratio of oxygen ions to tantalum atoms. This ratio was varied from 0.7 to 2.0. As for the experiment on argon-assisted Ta_2O_5 films, the amount of Ta atoms deposited per cm^2 per second, was calculated from Rutherford Backscattering Spectrometry (RBS) data.

5.2.4. Ion-beam sputtered silicon dioxide films

SiO_2 films were deposited by two methods. In the first method a SiO_2 target was sputtered by a mixed Ar and O_2 beam of 1 keV ions. In the second method, a pure Si target was sputtered by a beam of 1 keV Ar ions in the presence of oxygen, fed near the substrate or through assisting ion source. If the plasma bridge neutraliser (PBN) was used, additional argon, required for the operation, was admitted through the PBN. Otherwise, additional argon was introduced through the assisting ion source. This allowed control of the values of total pressure during film deposition. Conditions of each experiment are listed in Table 5.2. Films, deposited under these conditions, were found to be stoichiometric and exhibit reproducible stress values. Experiments on the effects of substrate cleaning and the angle of arrival of sputtering flux onto the substrate in the case of SiO_2 films were performed according to the same methods, as in the case

Table 5.2. Conditions for deposition of sputtered silicon dioxide films.

Experiment	Target	Angle, degrees		Flow of O_2 near the substrate, sccm	Sputtering source		Neutralisation			Assisting source			Total Pressure, Pa
		Substr.	Target		Flow of gas, sccm	Beam current, mA	Immersed wire	Plasma Bridge		Gas	Ion-to-atom arrival ratio	Ion Energy, eV	
							Current, mA	Gas	Current, mA				
Substrate Cleaning Effects	**SiO_2**	**45**	**35**		**Ar 1.8, O_2 3.0**	**45**	**51**						**$1.2x10^{-2}$**
Total Working Pressure	**SiO_2**	**45**	**35**		**Ar 1.8, O_2 3.0**	**45**	**51**			**Ar**			**$1.2x10^{-2}$, $1.9x10^{-2}$, $2.5x10^{-2}$, $1.0x10^{-1}$**
Substrate Angle Effect	**SiO_2**	**25, 45, 70**	**35**		**Ar 1.8, O_2 3.0**	**45**	**51**			**Ar**			**$2.5x10^{-2}$**
Ion Bombardment	**Si**	**45**	**35**	**15**	**Ar 1.2**	**40**	**50**			**Ar**	**0.35-1.4**	**250, 400**	**$3.6x10^{-2}$**
	Si	**45**	**35**		**Ar 1.2**	**40**		**Ar**	**500**	**O_2 15 sccm**	**0.7-2.0**	**150,250, 300,400**	**$5.0x10^{-2}$**

of Ta_2O_5 films. However, it should be noted that, in the experiment on the influence of cleaning procedures, film stress measurements were performed in a single stationary beam configuration. In the experiment on the effect of total working pressure additional Ar was introduced through the assist ion source until the pressure reached 1.2×10^{-2} Pa, 1.9×10^{-2} Pa, 2.5×10^{-2} or 1.0×10^{-1} Pa.

a) Argon-assisted sputtered silicon dioxide films

Stress in thin films, deposited under concurrent argon ion bombardment, was studied in this set of experiments. The Ar^+ energy was varied from 250 V to 600 V, the ion-to-atom arrival ratio (ratio of arriving argon ions to silicon atoms) from 0.35 to 1.4. The amount of Si atoms, arriving per cm^2 per second, was calculated from the Rutherford Backscattering Spectrometry (RBS) data.

Two types of target have been used in this study. First, the experiments were performed with a SiO_2 target (deposition conditions as for the experiment on cleaning procedures were used). However, these conditions led to low film growth rate (arrival rate of silicon atoms of about $9\text{x}10^{13}$ $At_{Si}cm^{-2}s^{-1}$). Moreover, the introduction of the plasma bridge neutralizer resulted in increased deposition pressures and thus a further decrease in growth rates down to approx. $7.6\text{x}10^{13}$ $At_{Si}cm^{-2}s^{-1}$.

Due to the operational constraints for the main sputtering source, it was impossible to increase the beam current and increase the film growth rate. Therefore, the necessary increase in the rate of SiO_2 deposition was facilitated by changing the sputtering target from SiO_2 to pure Si. The immersed wire neutralizer was used since the total operating pressure in this case can be decreased. As a result, the growth rate increased up to approx. $1.5\text{x}10^{14}$ $At_{Si}cm^{-2}s^{-1}$, which allowed the ion current density to be varied to give a range of ion-to-atom arrival ratios from 0.35 to 1.4. For this reason a silicon target was used for this and all subsequent experiments.

b) Oxygen-assisted sputtered silicon dioxide films

In this experiment oxygen ions were used for concurrent bombardment of the film during growth. The energy of bombarding species was in the range of 150 eV to 400 eV. The ion-to-atom arrival ratio, which in this case is the ratio of O^+ ions to silicon

atoms, was varied from 0.7 to 1.5. The amount of Si atoms deposited per cm^2 per second was calculated from the Rutherford Backscattering Spectrometry (RBS) data.

5.3. E-beam evaporated films

5.3.1 Deposition chamber configuration

The deposition chamber, described in chapter V section 5.2.1, was modified for the deposition of e-beam evaporated films. The new internal configuration of this chamber is presented in Figure 5.7. The electron-beam evaporator used was produced by Telemark, Inc. (model 528 with TT-3 power supply).

A beam of assisting ions for ion-assisted deposition was produced by a custom-built 3 cm ion source, fitted with molybdenum grids. However, this source is not equipped with a neutraliser. Gas conditions in the chamber did not allow the plasma-bridge neutraliser to be used. Therefore, neutralisation was provided by the neutraliser filament of a 3 cm IonTech ion source mounted in the vicinity of the ion assisting source. Measurements of assisting ion current were performed according to the procedure, described in section 5.2.1.

For deposition the substrate was positioned at 0^0 (see Fig. 5.3) and was not intentionally heated. The evaporator to substrate distance was 14 cm, the assist source to substrate distance was approx. 28 cm.

It is known that silicon dioxide has a low thermal conductivity (at 300 ^{0}C thermal conductivity of silicon is 0.014 W cm^{-1} C^{-1} in comparison with 1.5 W cm^{-1} C^{-1} for pure solid Si [Web 2]) and high melting temperature (in excess of 1600 ^{0}C [Weast, 1974]). These properties make it hard to obtain a single molten ingot from the granules of SiO_2 material. Furthermore, even evaporation from a readily obtained ingot has additional requirements. The e-beam has to be scanned across the surface of the material source for the uninterrupted deposition of films of required thickness and reproducible properties. In the present evaporator configuration such a facility was not available. Therefore, a reactive method of deposition was employed. The evaporator crucible was loaded with pure Si granules. These granules were carefully melted into a single ingot in the presence of oxygen. Then the deposition was carried out by evaporating material from the obtained ingot in the presence of oxygen gas in the chamber. The e-beam evaporator was routinely used at a voltage of 3.5 kV.

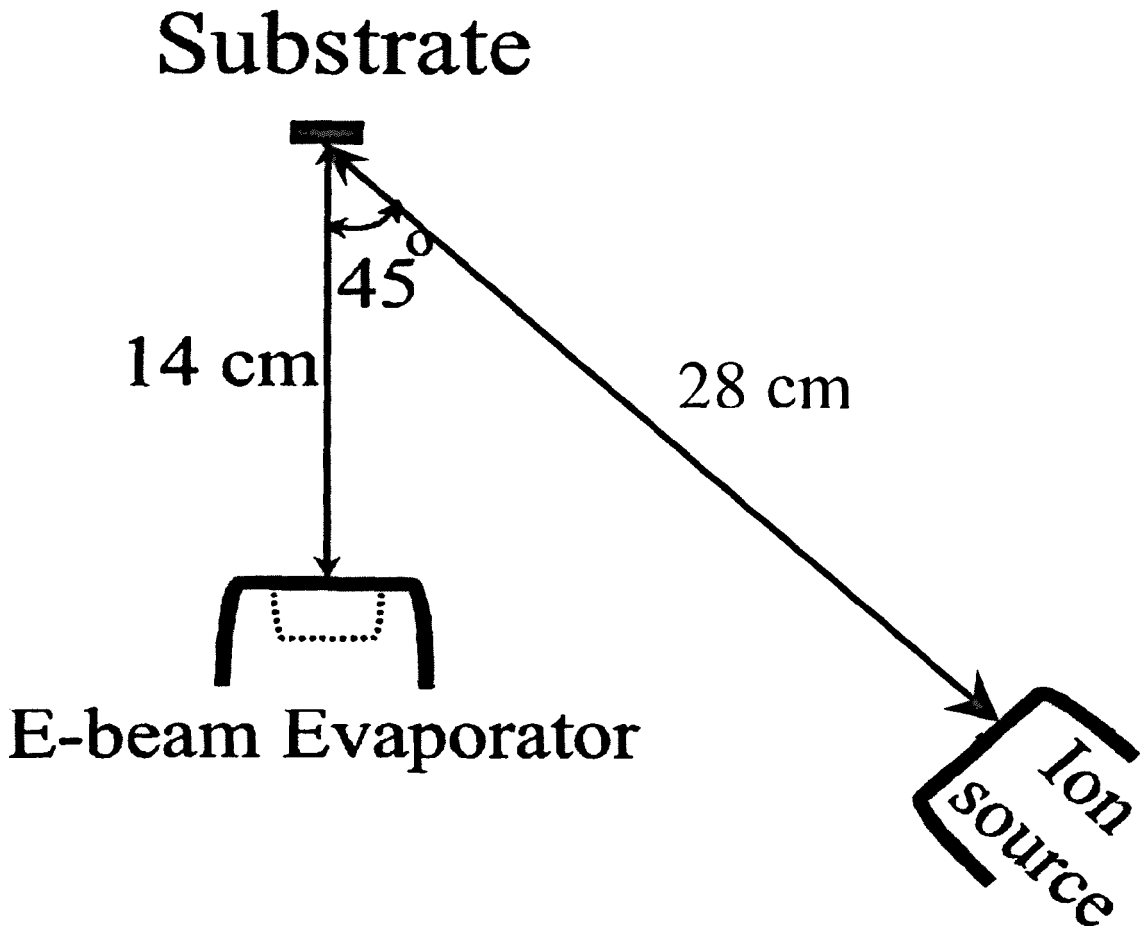

Figure 5.7. Internal geometry and dimensions of the deposition chamber, set for e-beam evaporation and ion-assisted deposition.

The deposition rate was monitored using a quartz crystal monitor (quartz crystal with Intellemetrics model IL800 controller). This monitor was fitted so that a fraction of the evaporated flux was incident on the quartz crystal. The quartz crystal was not in the line of sight of the beam of assisting ions. The film growth rate (i.e. increment in film thickness for a small set time interval) was kept constant by adjusting the current through the filament of e-beam evaporator.

5.3.2. Argon-assisted evaporated silicon dioxide films

The base pressure in the deposition chamber was in the region of $(2.5\text{-}10)\text{x}10^{-4}$ Pa. Oxygen gas was introduced near the substrate with the flow rate of 15.0 sccm. Then argon was introduced into the chamber through the assisting ion source until the total deposition pressure reached $2.3\text{x}10^{-2}$ Pa. Source materials were then evaporated for 5 minutes before the beginning of deposition. These conditions lead to deposition of stoichiometric SiO_2 films.

Each deposition run consisted of two parts. First, a calibration sample was deposited for 30 minutes without any ion bombardment. Then the sample was changed to a bare substrate, the measurements of ion current and initial substrate shape were performed, an ion-assisted film was deposited for 5 hours and measurements of final substrate curvature were taken.

In this experiment argon ions with energy of 300 eV and ion-to-atom arrival ratio varying from approx. 0.27 to 1.4 were used.

5.4. Film analysis

5.4.1. Rutherford backscattering spectrometry (RBS)

The RBS spectra from the film-substrate composite were obtained using a beam of 2 MeV He^+ ions, produced using the Van-de-Graaf accelerator based at the University of Salford, UK. This accelerator is equipped with a facility dedicated to RBS measurements. The RBS data was analysed using the QUARK v1.2 simulation package (Quantitative Analysis of Rutherford Kinematics) [Web 3]. This package allows not

only routine analysis of film composition, but also, gives numerical estimates of the amount of argon trapped in the films.

The RBS measurements were used not only for compositional analysis, but also, for calculations of film thickness. Such type of calculations requires known values of film density. It was assumed that deposited films have a density of 2.203 g/cm^3 for all SiO_2 films [Web 4] and 8.2 g/cm^3 for all Ta_2O_5 films [Web 5].

5.4.2. Spectrophotometry

A nkd-8000 spectrophotometer, produced by Aquila Instruments, was used. It was possible to perform only the measurements of the reflectance of the samples. In order to increase the amount of experimental information and thus the accuracy of the optical constants calculations, measurements were performed for both *s*- and *p*-polarisations and the resulting spectra were merged for analysis. Analysis was performed using numerical fitting methods, built into the nkd-8000 software.

In the beginning, three measurements on the bare Si substrate were performed. The results of these measurements were analysed and mean values of refractive index *n* and extinction coefficient *k* were taken as the values of substrate optical constants for all subsequent measurements.

For the analysis of optical behaviour of thin films, samples of these films, deposited on silicon substrates, were used. In the data analysis Drude-Lorentz and Cauchy dispersion relations were used for SiO_2 and Ta_2O_5 films, respectively. Measurements were performed several (2-5) times on almost every film and the mean value $\bar{X}$ for each constant (*n* or *k*) was calculated. The standard error of the mean ($SEM = \sqrt{\frac{1}{n(n-1)}\sum_{i=1}^{n}(X_i - \bar{X})^2}$, where *n* is the number of measurements, X_i is the measured value and $\bar{X}$ is the mean value) was chosen to represent the measurement error.

5.4.3. Raman Spectrometry

Raman measurements were performed using a Dilor XY 800 Raman spectrometer in backscattering configuration. The facility is based at the University of Leipzig, Germany.

5.4.4. Atomic force microscopy (AFM)

The measurements were performed using a Quesant Instrument Corporation Resolver AFM. The AFM was used in contact mode with a constant force of 0.32 nN applied to the tip. Three scans of 20x20 μm on each studied sample were performed. These scans were processed with the built-in software to give information on surface roughness. The mean of the obtained values was chosen to represent sample roughness, the measurement error is given by the standard error of the mean.

5.4.5. Profilometry

A Sloan DekTak II profilometer based at MATS-UK was used. Film thickness was calculated from the analysis of the trace of the profilometer stylus dragged across the film/substrate step. A typical scan length of 800 μm was used. The substrate was positioned horizontally at the zero-height level (see Figure 5.8). Two readings near the edge of the step were taken and the film thickness was represented by the mean value of those readings.

5.4.6. Transmission electron microscopy (TEM)

Samples for cross-section TEM microscopy were prepared according to the procedure, thoroughly described by McCaffrey [McCaffrey, 1997], Walck and McCaffrey [Walck and McCaffrey, 1997] or Suder et al [Suder et al, 1997] and known under the name of the small angle cleavage technique (SACT). Briefly the technique can be described as follows: the back of a sample is polished down to approx. 100 μm using a special hand tool and a sample grinder with abrasive paper. Then the sample is cleaved along two directions so, that a wedge with a sharp tip (three-face pyramid) is formed. Good quality sharp wedges, chosen under a stereomicroscope, are then mounted on their sides onto a TEM grid and the adhesive is cured. This gives a sample, ready for cross-section TEM studies.

The JEOL 3010 transmission electron microscope based at the University of Salford, UK was used. Images were captured with the overall magnification of 800k and digitally processed for clear representation.

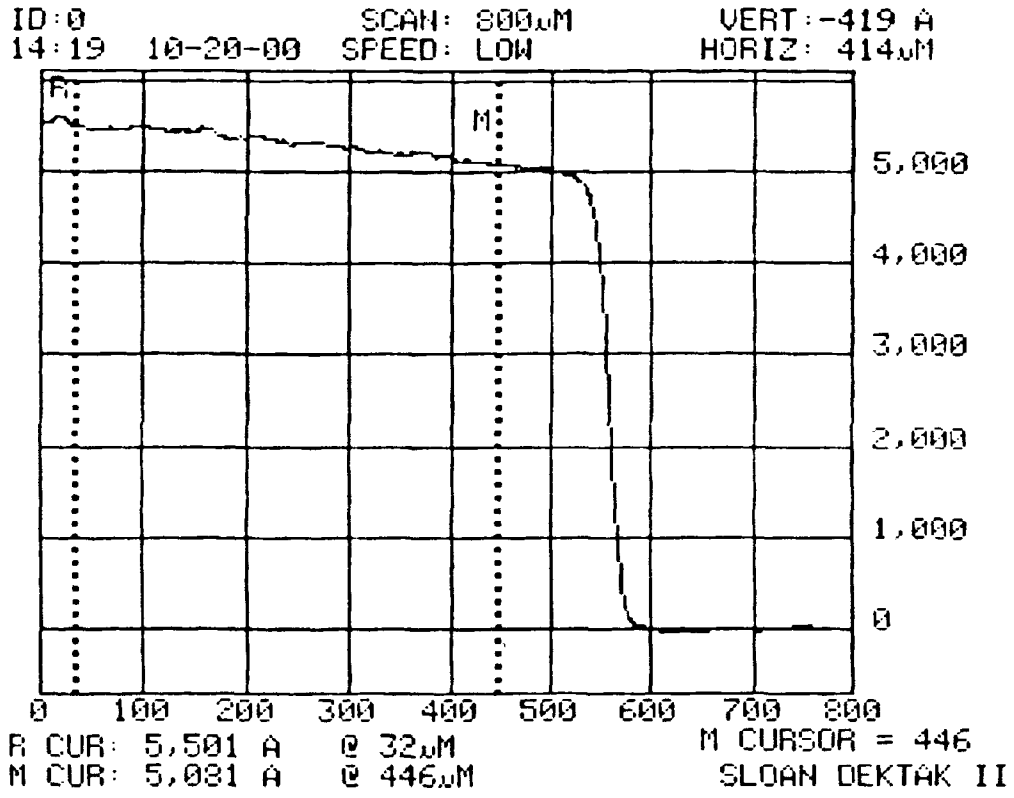

Figure 5.8. Example of a trace, obtained by Dektak II profilometer from a Ta_2O_5 film.

5.4.7. X-ray photoelectron spectroscopy (XPS)

XPS measurements were performed using a VG ESCALAB MK II electron spectrometer with a Mg Kα ($E_{h\nu}$=1253.6 eV) source and electrostatic half-sphere analyser. The spectrometer, based at the Urals Branch of the Russian Academy of Sciences, Russia, operates at a base pressure of 10^{-10} Pa during measurements. The binding energy of electrons E_b is calculated as $E_b = h\nu - E$, where E is the kinetic energy of registered photoelectron (a step of 0.1 eV was used during scanning) and $h\nu$ is the energy of X-ray photons. The spectrometer is calibrated to the Au $4f_{7/2}$ line at 84.0 eV. Current calibration was performed using the C1*s* level of surface carbon contamination at 285.0 eV. The spectrometer resolution, defined as the width of half-maximum of the Ag $3d_{5/2}$ line, is 0.84 eV for an analyser pass energy of 10 eV.

XPS spectra were taken for the surfaces of Ta_2O_5 and SiO_2 films and after 10 minutes of etching of these surfaces with a 6 keV Ar^+ beam (assumed to correspond to 50 nm surface material removal).

References

Brantley W.A., J. Appl. Phys., **44** (1), 534, (1973)

Handbook of Chemistry and Physics 55th edition, ed. by Weast R.C., CRC Press, Inc., 1974

McCaffrey J.P., Micros. Res. Techn., **36**, 372, (1997)

Moulard G., Contoux G., Motyl G., Gardet G.and Courbon M., J. Vac. Sci. Technol. A 16(2), 736, (1998)

Suder S., Faunce C.A., Donnelly S.E., Thin Solid Films, **304**, 157, (1997)

Tien C.-L., Jaing C.-C., Lee C.-C., and Chuang K.-P., J. Mod. Opt., **47** (10), 1681, (2000)

Walck S.D., McCaffrey J.P., Thin Solid Films, **308-309**, 399, (1997)

Web 1: http://www.accuratus.com/fused.html

Web 2: http://www.hut.fi/Units/MEC/documents/Si_SiO2.htm

Web 3: http://www.quarksimulation.com

Web 4: http://www.crystran.co.uk/sio2data.htm

Web 5: http://www.cerac.com/pubs/proddata/ta205.htm

Chapter VI

Results and Discussion

In this chapter experimental results are presented and an explanation of the film property behaviour with changes in the deposition parameters is proposed. The chapter has four sections. The first is devoted to the analysis of oxide film composition. In the second section the results of stress measurements of non-ion-assisted films are presented and analysed, so that possible reasons of observed film stress behaviour could be identified. In the third section the results of the stress measurements of ion-assisted films are presented and a model, explaining stress behaviour with ion bombardment, is proposed. The last section deals with the question of the optical properties of the films, their changes with deposition parameters and possible reasons for such behaviour.

At this point it should be noted that in this research all of the results of measurements on ion-assisted films are going to be presented against normalized added energy (or simply normalized energy) $E_n=E_i(I/A)$, where E_i is the energy of bombarding ions and I/A is the ion-to-atom arrival ratio. The choice of the most appropriate parameter, which would fully express processes in the film and thus film properties behaviour due to ion bombardment, is still debated in the literature. At the moment, many different ways of presentation of experimental results, especially film stress, and the results of theoretical calculations and modelling, are common. To mention a few, consider papers by Davis [Davis, 1993], where ion energy is used as a variable and I/A used as a parameter in the model, by Hudson and Somekh [Hudson and Somekh, 1996], where stress in thin films is plotted against energy of bombarding neutrals, by Martin et al [Martin et al, 1994], where film stress is presented against bombarding ion current with ion energy used as a parameter, by Takahashi et al [Takahashi et al, 1994], where a graph of stress versus rf-magnetron sputtering power is shown, or by Strauss et al [Strauss et al, 1997], where stress in reactive-low-voltage-ion-plated films is presented against arc current (which is mainly related to the changes in ion current density but also has a small (approx. 10%) influence on mean energy of bombarding ions). A commonly used parameter [see, for

example, Parfitt et al, 1995 or Was et al, 1996, etc.], which incorporates the influence of both bombarding ion energy and bombarding ions flux, is normalized added energy. The choice of such variable is debated by Petrov et al [Petrov et al, 1993] who argues that normalised energy is not "a fundamental, or universal, parameter characterizing ion-assisted deposition" and shows that bombardment with ions of different energy and equal normalised energy can lead to crystalline films with different properties. However, Petrov et al [Petrov et al, 1993] also accept that a range of deposition variables exists, where normalised energy "can be correlated with film properties".

In this research stress measurement results are presented versus normalized added energy of bombardment as the most appropriate parameter. Compositional and optical properties of ion-assisted films are also presented versus normalized energy for the ease of properties comparison and consistency in the results presentation. The choice of normalized energy is based on the following considerations. First, normalised energy is the measure of additional energy, brought by bombarding ions to each atom or molecule forming the film. However, this parameter has another very important meaning. It is known that bombardment with ions of sufficient energy can generate atomic displacements in the film. The steady state density N_R/N of displaced atoms, or recoils, in the absence of film re-sputtering can be calculated as [Carter, 1994]

$$\frac{N_R}{N} \propto \frac{0.42}{E_d}\frac{I}{A}E_i, \tag{6.1}$$

where E_d is the displacement energy, N_R is the concentration of recoils and N is the film atomic density. Thus, the total number of recoil atoms will be inversely proportional to the displacement energy of the film material and proportional to film atomic density and normalised energy of bombardment.

6.1. Composition and stoichiometry of oxide films

Before one attempts to study the results of the ion-bombarded films and to explain the mechanisms of stress generation, film composition has to be analysed in detail. In this research two methods have been used. Rutherford Backscattering Spectrometry (RBS) was chosen as a routine method due to its high accuracy in measuring atomic areal density of the film and determining the film composition, especially in case of oxides.

Furthermore, this is a non-destructive method and can provide information on film composition as a function of depth. However, this method does not give any information on the state of chemical bonding of film atoms. A limited number of the films was therefore also studied by XPS.

6.1.1. Rutherford Backscattering Spectrometry (RBS) measurements

In this experimental work two major processes, having an effect on the film composition, can occur during ion bombardment. First, bombarding ions can become embedded into the bulk of the film. Second, preferential sputtering of film components can take place. Therefore, the film composition and level of inert gas incorporation in both Ta_2O_5 and SiO_2 films were studied by RBS in detail.

The results of RBS experiments showed no significant changes in the film composition with changes in substrate cleaning procedures, target or substrate angles or total deposition pressure. All Ta_2O_5 films were found to be stoichiometric, i.e. have approximately the "correct" ratio of elements (5 oxygen for 2 tantalum). It was found that Ta_2O_5 films also have a very low level of iron (0.3-1.4%) and argon (2-3%), incorporated in them.

For ion-beam sputtered SiO_2 films the ratios of elements were found to be approx. 2.25 oxygen to 1 silicon for experiments using concurrent oxygen bombardment and approx. 2.05 oxygen to 1 silicon in all other cases. These changes can be related to the variations in deposition conditions (most probably, entry point of reactive gas and level of film impurities), rather than to the effect of ion bombardment. Such a conclusion follows from the compositional studies of a film deposited without ion assistance, for calibration purposes, before the start of experiments on oxygen bombardment. This film showed the ratio of oxygen to silicon of 2.25, which is in agreement with the other films in the oxygen-assisted set. Some of the additional oxygen, incorporated in the film, can be related to the presence of molybdenum (molybdenum oxide) impurity in these films. Such impurity is absent in the films, deposited in other experiments. The presence of oxygen in the chamber necessitated changes in the grid material for ion-beam sources from carbon to molybdenum. A certain degree of grid sputtering could be the source of such impurity in the films. Within each set of experiments (i.e., argon bombardment or oxygen bombardment) RBS measurements only show variations in the O/Si ratio within the measurement error. Silicon dioxide films also contained impurities of Ta (0.1-0.15%) and Fe (0.5-1.4%), however, for non-assisted films, no argon incorporation was

observed. It should be noted that the level of impurities is very low, so the error in the determination of their amount in the film can be quite high.

Purely evaporated SiO_2 showed no argon incorporation into the film and a ratio of oxygen to silicon of 1.9. These films contain approx. 0.1% of Ta impurity.

The high amount of argon present in Ta_2O_5 films in comparison to the SiO_2 films is due to a much higher degree of Ta_2O_5 film bombardment with energetic back-reflected Ar from the sputtering target. This is further supported by the results of a TRIM simulation, which shows that, for a 1keV Ar beam incident onto the targets at 35^0 to target normal, only approx. 0.6% of Ar is back-reflected from a silicon dioxide target in comparison to 35% reflected from a tantalum target.

It is expected that, with an increase both in the energy of bombarding argon and in the bombardment dose, incorporation of argon into the film would increase. Indeed, it was found for ion-beam sputtered ion beam assisted Ta_2O_5 films that argon incorporation increased from 0.09 (Ar/Ta ratio) for a non-assisted film to 0.128 for a 600 eV Ar^+-assisted film with an ion-to-atom arrival ratio of 1.4 (see Figure 6.1). No significant changes in the Ta-O film stoichiometry have been observed. For ion-beam sputtered ion beam assisted SiO_2 films, argon bombardment leads to an increase in argon concentration from 0 (i.e. below the detectable level) to a maximum value of 0.043 (Ar/Si ratio) (see Figure 6.2). It should also be noted that, unlike argon incorporation in Ta_2O_5 films, the argon concentration in SiO_2 reaches saturation at bombardment with higher normalised added ion energy. From the RBS spectra no changes in Si-O film stoichiometry were observed.

Similar behaviour of argon incorporation with normalized added energy of bombardment was found in evaporated ion-assisted SiO_2 films (see Figure 6.3). It can be seen that, with increase in normalized energy, argon concentration in the film increases up to approx. 0.03 Ar/Si. It should be mentioned that all evaporated SiO_2 films, deposited under concurrent ion bombardment, were found to exhibit an oxygen to silicon ratio of 2.0, which is 5% higher than that of the purely evaporated films.

For ion-beam sputtered films concurrent oxygen bombardment leads to an increase in argon incorporation into Ta_2O_5 films for high doses (see Figure 6.4). For ion-beam sputtered SiO_2 films oxygen bombardment leads to an increase in argon concentration in the coatings up to approx. 0.015-0.02 Ar/Si (see Figure 6.5). No significant compositional changes were detected from the RBS spectra for both Ta_2O_5 and SiO_2 films. During oxygen-assisted deposition argon is still present in the chamber as a working gas and comes

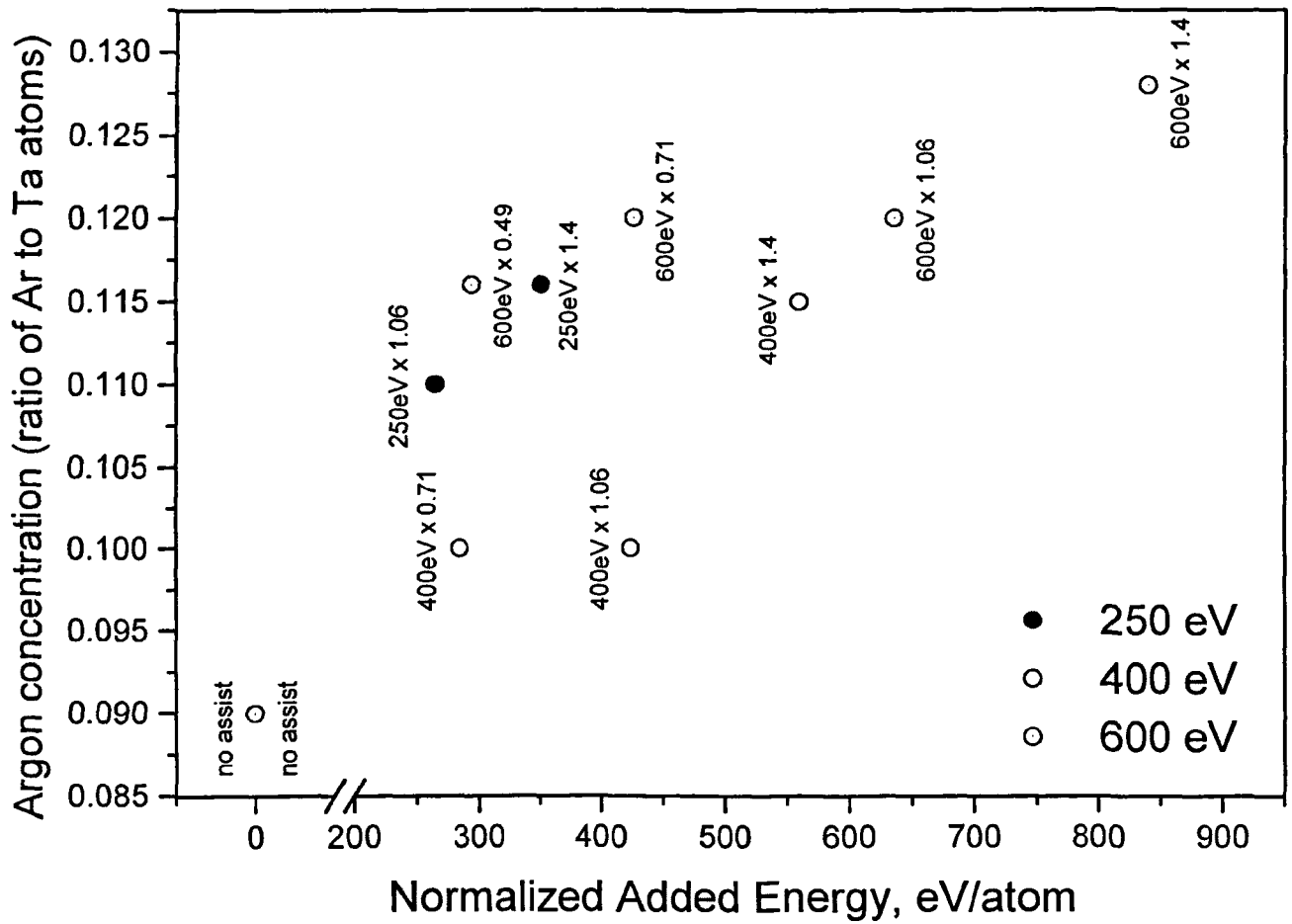

Figure 6.1. Argon incorporation into argon-bombarded Ta_2O_5 films. Numbers after multiplication sign are the ion-to-atom arrival ratios used.

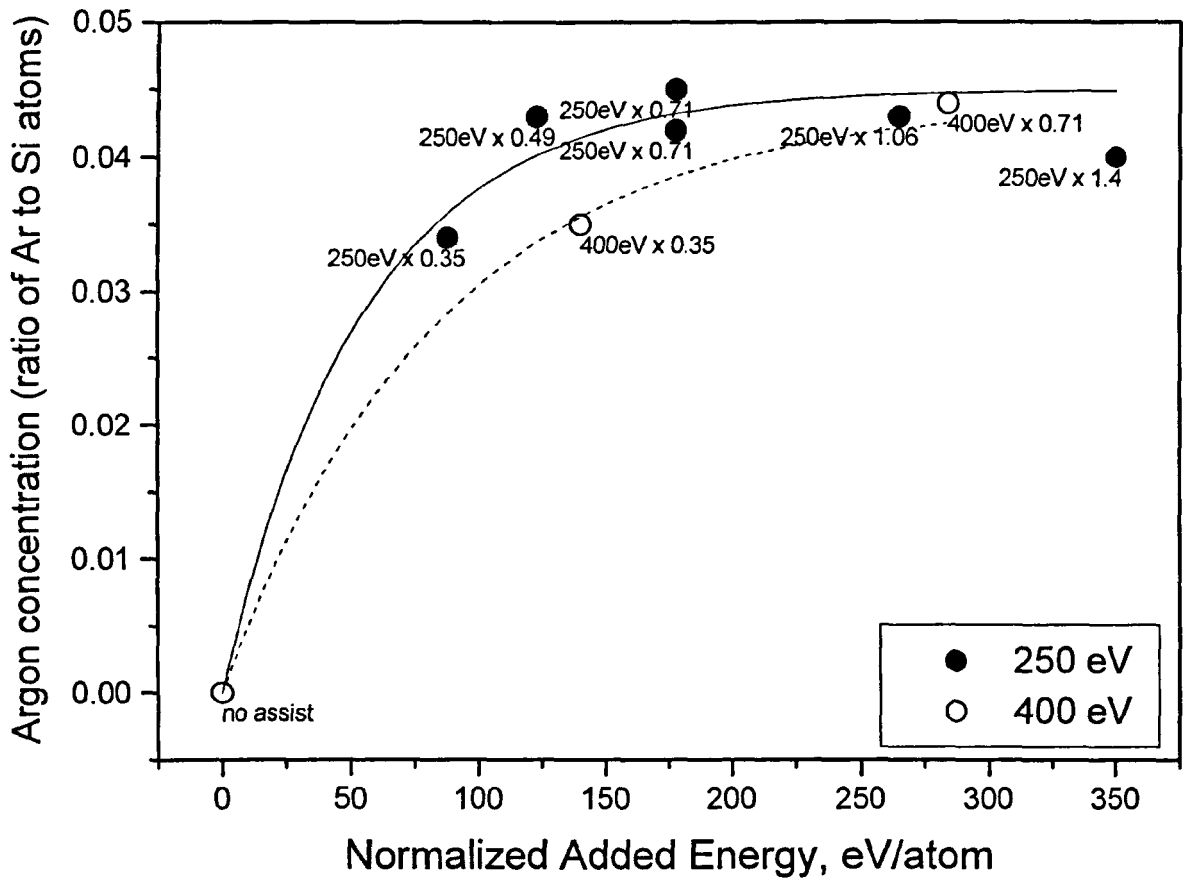

Figure 6.2. Argon incorporation into argon-bombarded SiO_2 films. Lines represent exponential fitting of the experimental data. Numbers after multiplication sign are the ion-to-atom arrival ratios used.

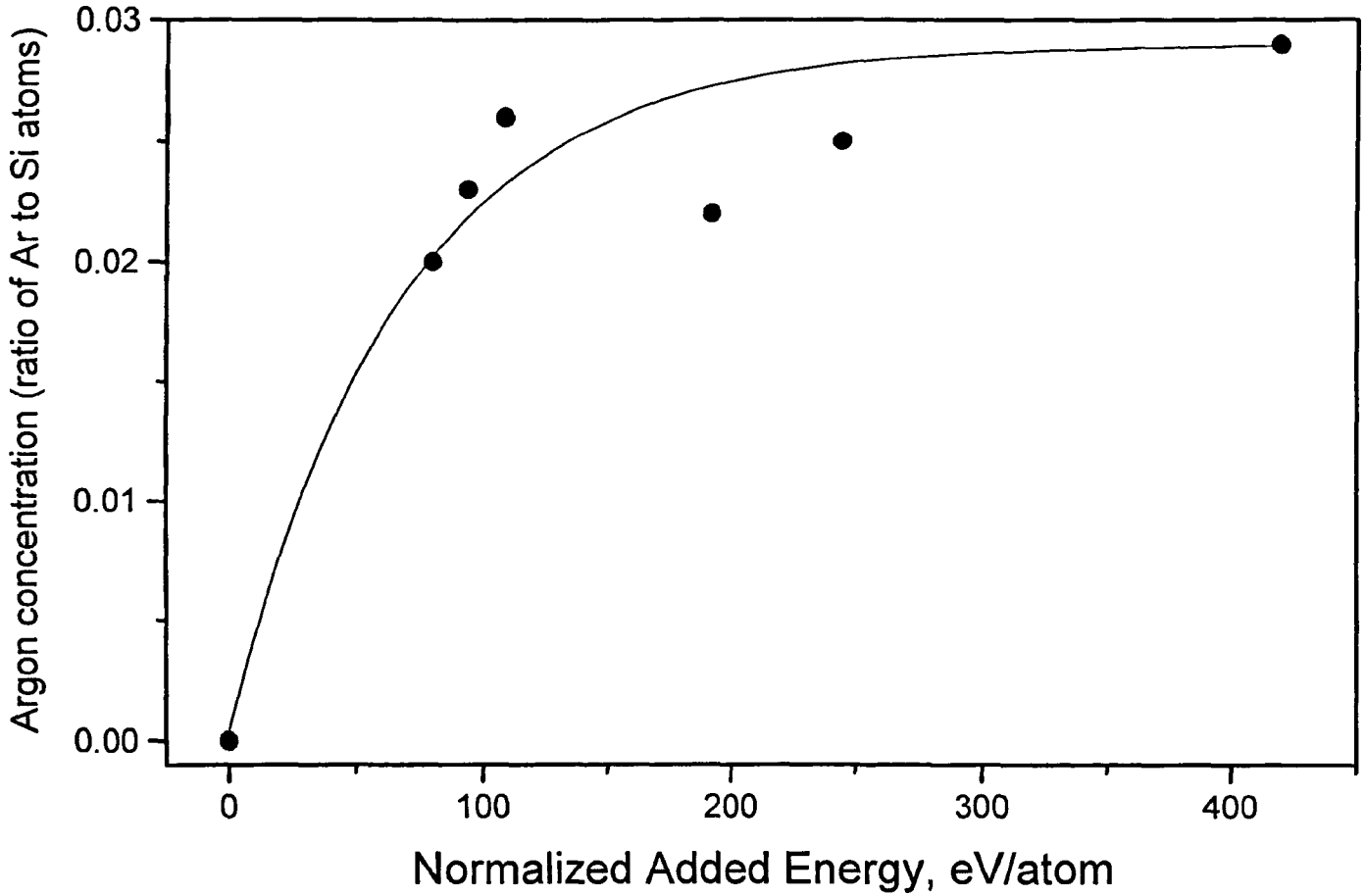

Figure 6.3. Argon incorporation into evaporated argon-assisted SiO_2 films. Line is drawn to guide the eye only.

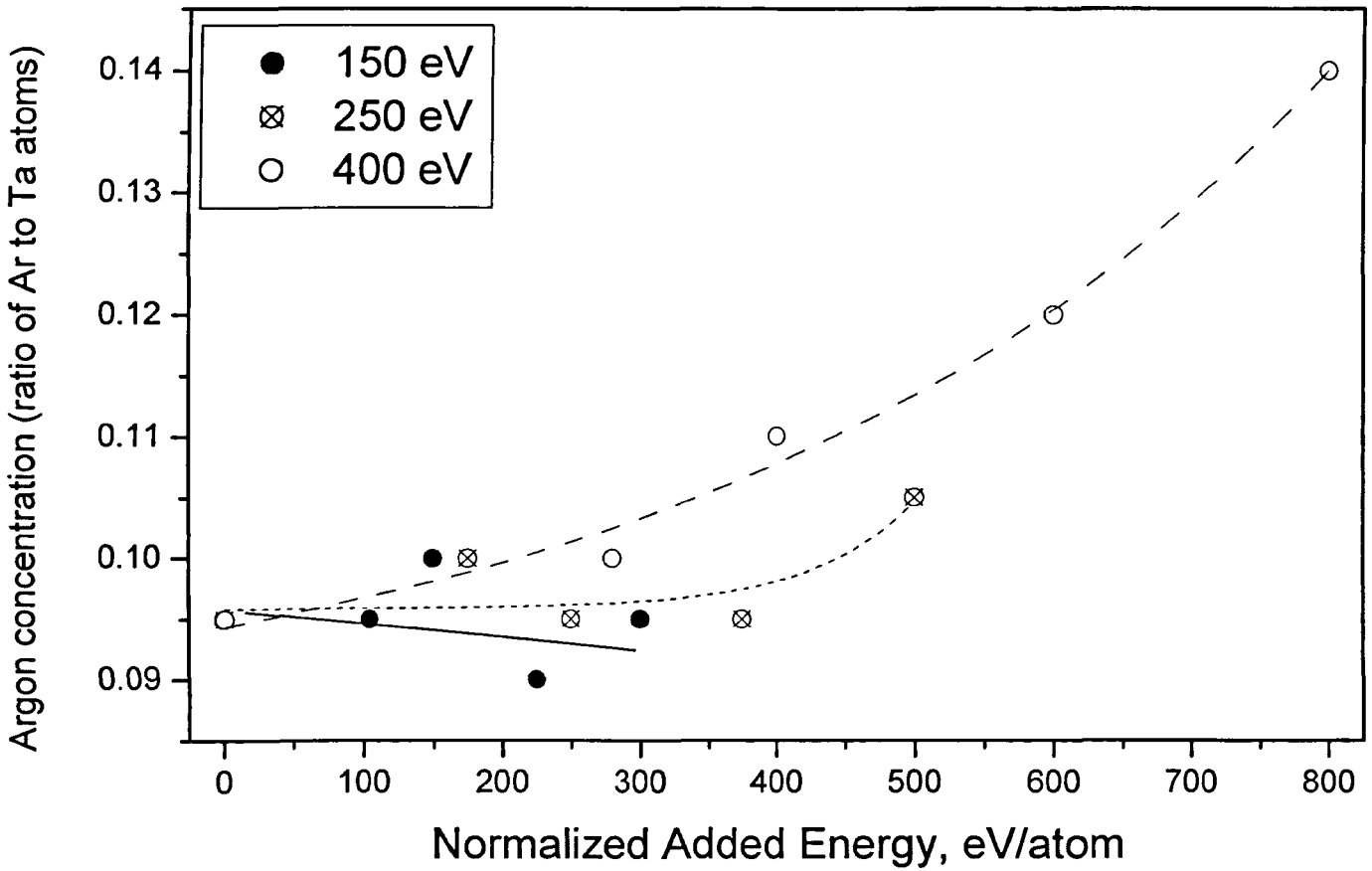

Figure 6.4. Argon incorporation into oxygen-bombarded Ta_2O_5 films. Lines are drawn to guide the eye only.

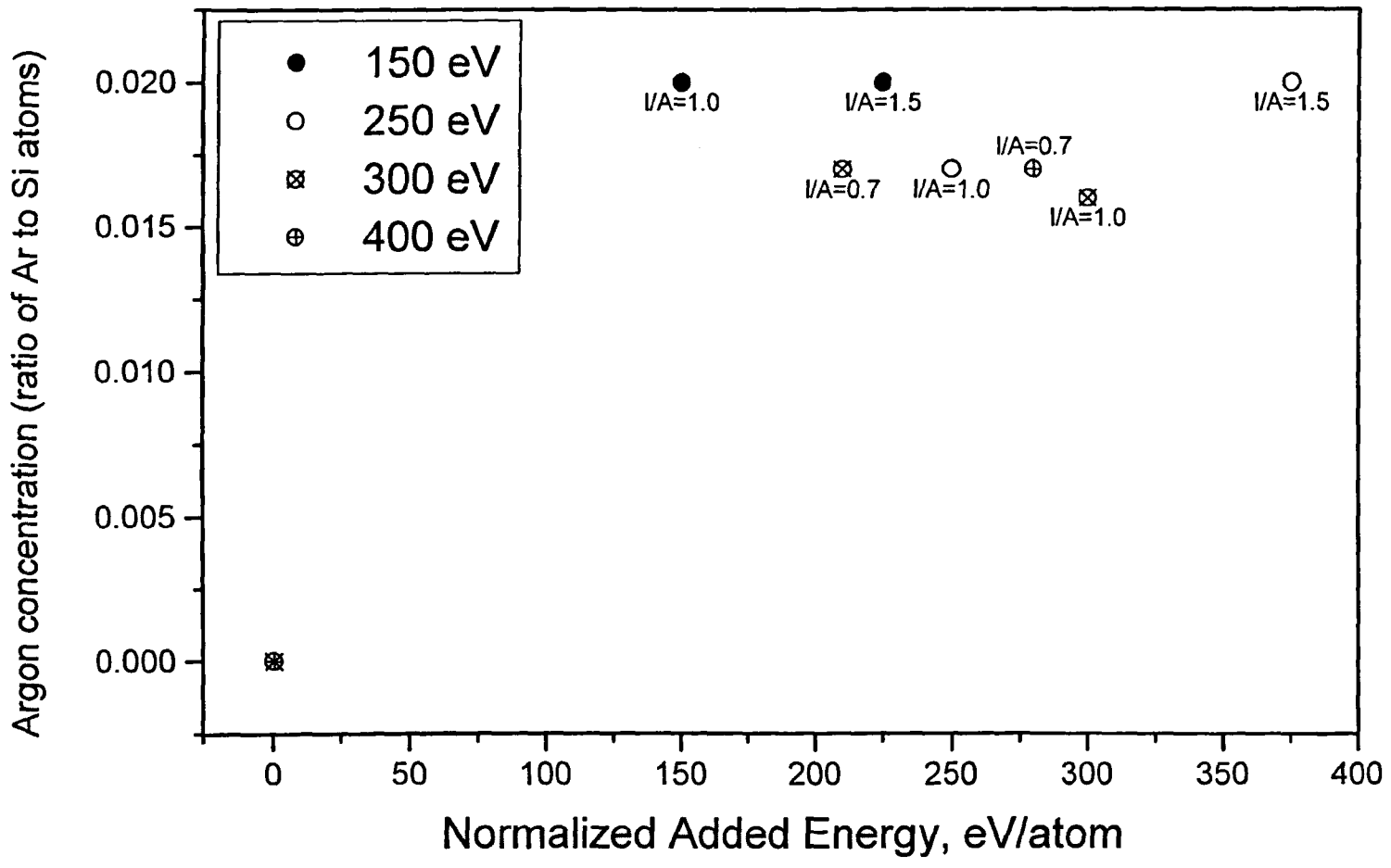

Figure 6.5. Argon incorporation into oxygen-bombarded SiO_2 films.

from the main sputtering source and plasma beam neutraliser. Some of this gas will leak into the secondary source, used for concurrent bombardment. Hence the growing film will be bombarded with a mixture of oxygen and a small amount of argon ions, leading to incorporation of some of the argon into the film.

Ion bombardment can not only lead to variations in film composition or stress levels, but also, depending on the conditions, to re-sputtering of the film material. In this work energetic ions of high doses are used for concurrent ion assistance, so the question of re-sputtering needs to be investigated. If the thickness of the non-assisted film is taken as 100%, then the difference in thickness between this film and ion bombarded film, deposited for the same amount of time, can give an estimate of significance of film re-sputtering. Thus, from Figures 6.6-6.8, it is clear that, for the case of Ta_2O_5, argon bombardment causes up to 54% film re-sputtering. Oxygen bombardment of Ta_2O_5 films leads to a lesser degree of film re-sputtering (up to 43%). For oxygen-bombarded SiO_2 the maximum re-sputtering is 63%. Therefore, it should be noted that all bombardment conditions chosen in this research lead to some film re-sputtering. The total effect on the film will depend on the bombardment gas, energy and dose and also on the sputtering yield of film material. Silicon dioxide films are expected to be affected more by re-sputtering in comparison with tantalum pentoxide films due to the comparable masses of elements involved in the collisions (Si, O and Ar) and thus much more effective energy transfer.

6.1.2. Transmission Electron Microscopy (TEM) Measurements

The results of RBS experiments showed, that argon is incorporated into the ion-bombarded films. Generally, inert gas can be present in the form of single atoms, embedded into the film bulk, atomic clusters or in the form of gas bubbles. Depending on the state of gas in the film, different models have been proposed for estimation of stress levels caused by inert gas incorporation [Was et al, 1996]. In order to determine the state of incorporated argon in the films, studied in this work, cross-section transmission electron microscopy (TEM) was used. Several films of both materials with different concentrations of argon, measured by RBS, were studied. The results are presented in Figure 6.9 for a Ta_2O_5 film and Figure 6.10 for a SiO_2 film.

The sample in Figure 6.9 is a tantalum pentoxide film bombarded with 600 eV Ar^+ ions and ion-to-atom arrival ratio of 1.4. These conditions lead to the maximum level of argon (0.128 Ar/Ta) incorporated into the film. The image in Figure 6.9 is captured in

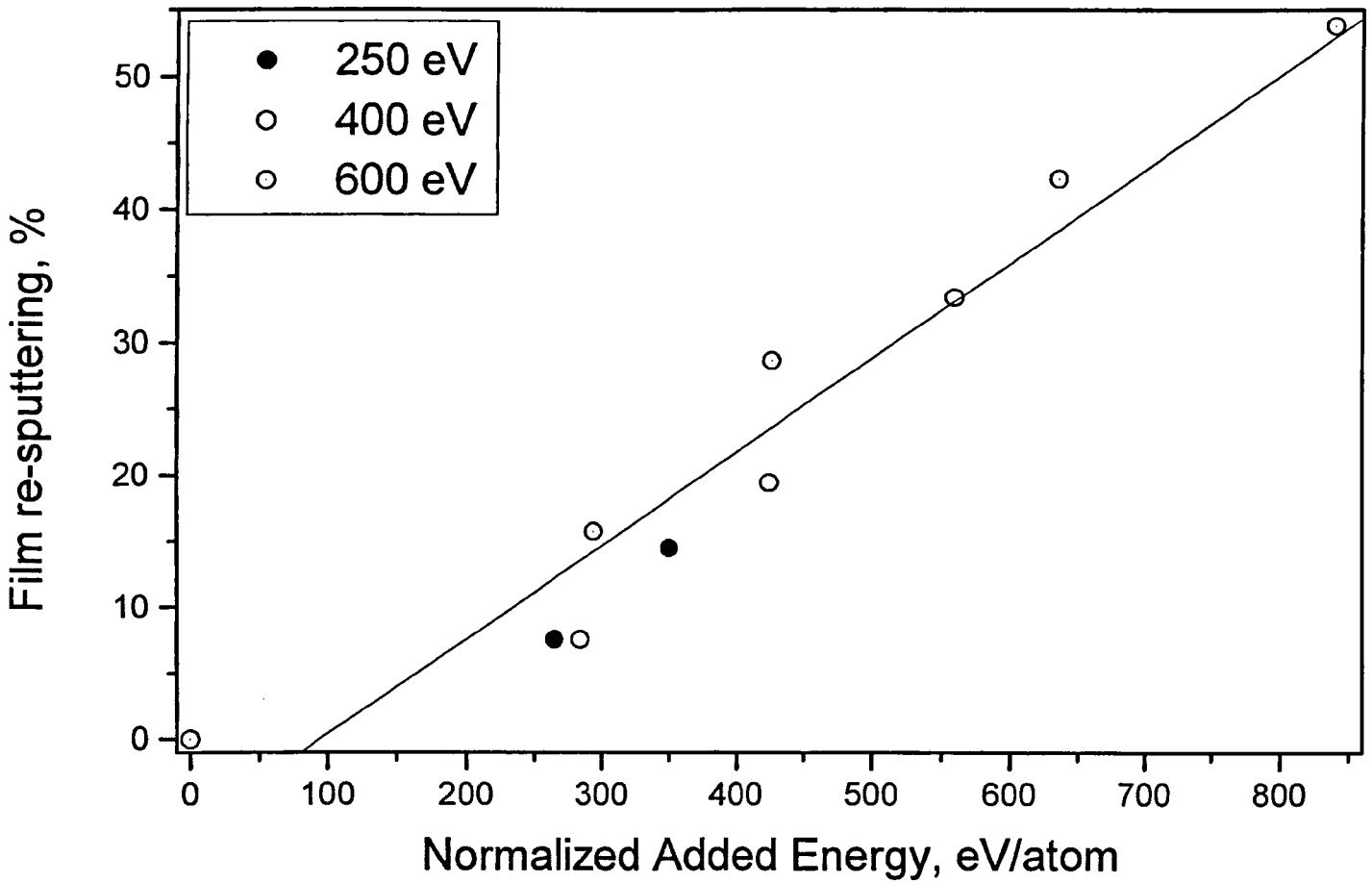

Figure 6.6. Amount of Ta_2O_5 film re-sputtering by argon bombardment. Line represents linear fitting of the experimental results.

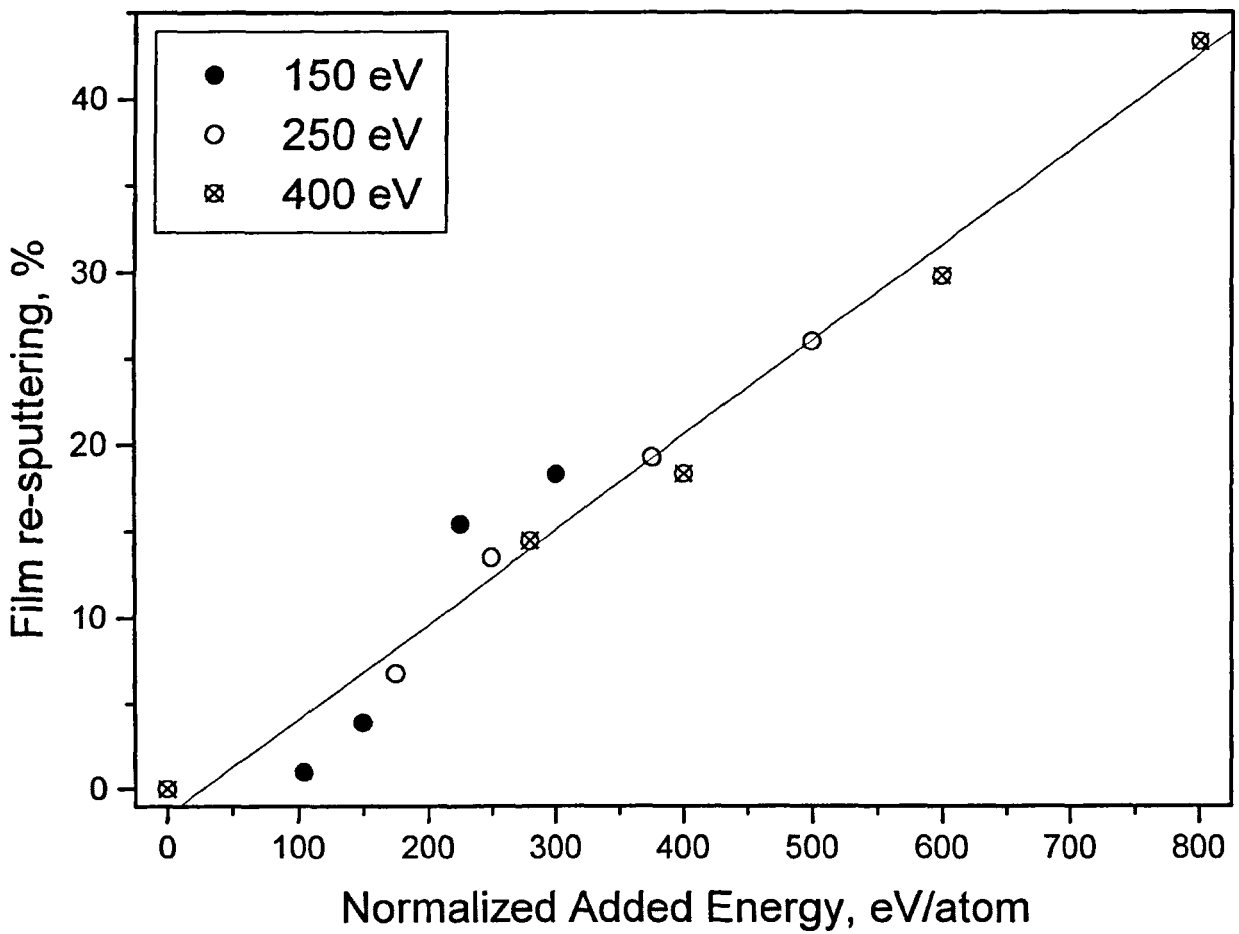

Figure 6.7. Amount of Ta_2O_5 film re-sputtering by oxygen bombardment. Line represents linear fitting of the experimental results.

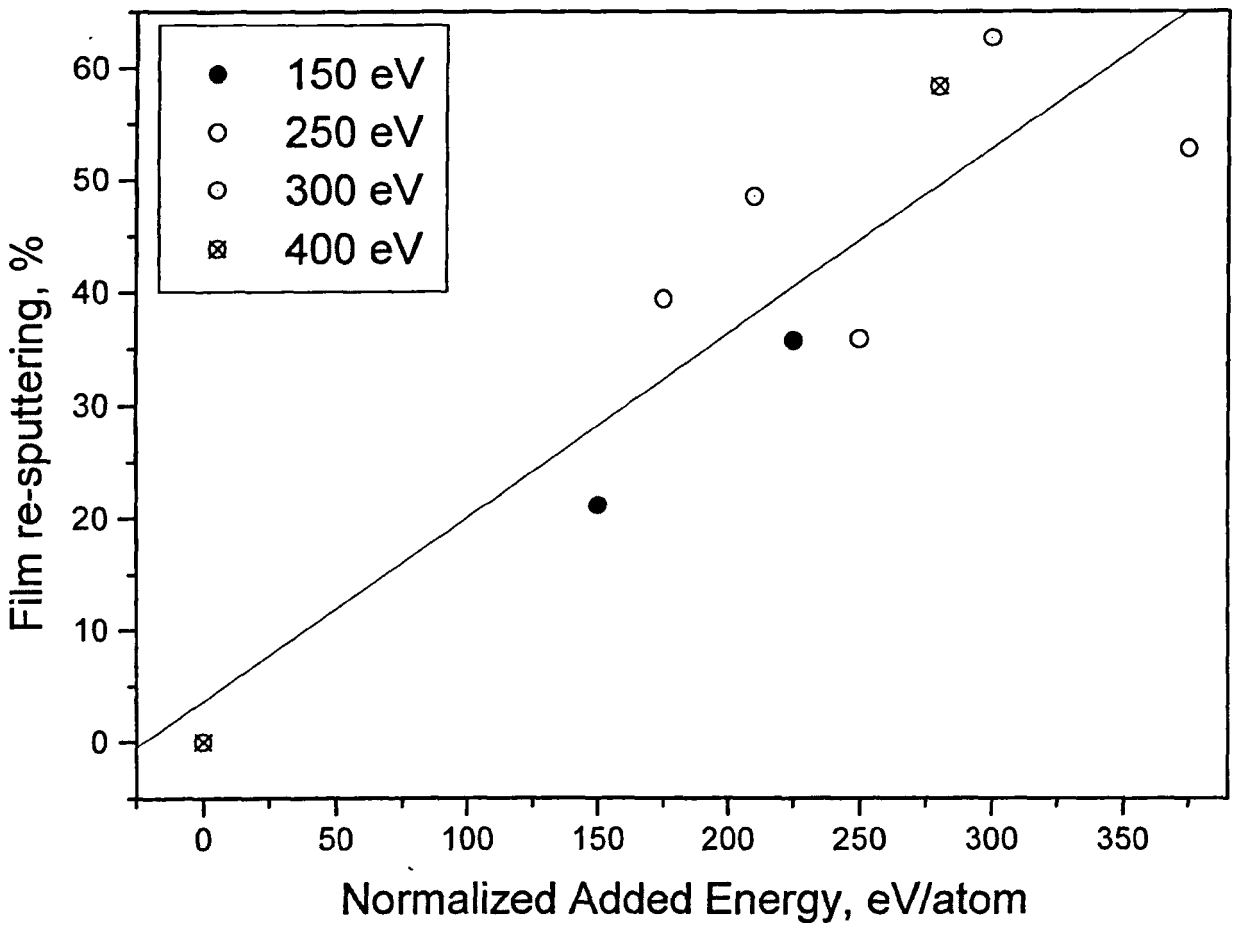

Figure 6.8. Amount of SiO_2 film re-sputtering by oxygen bombardment. Line represents linear fitting of the experimental results.

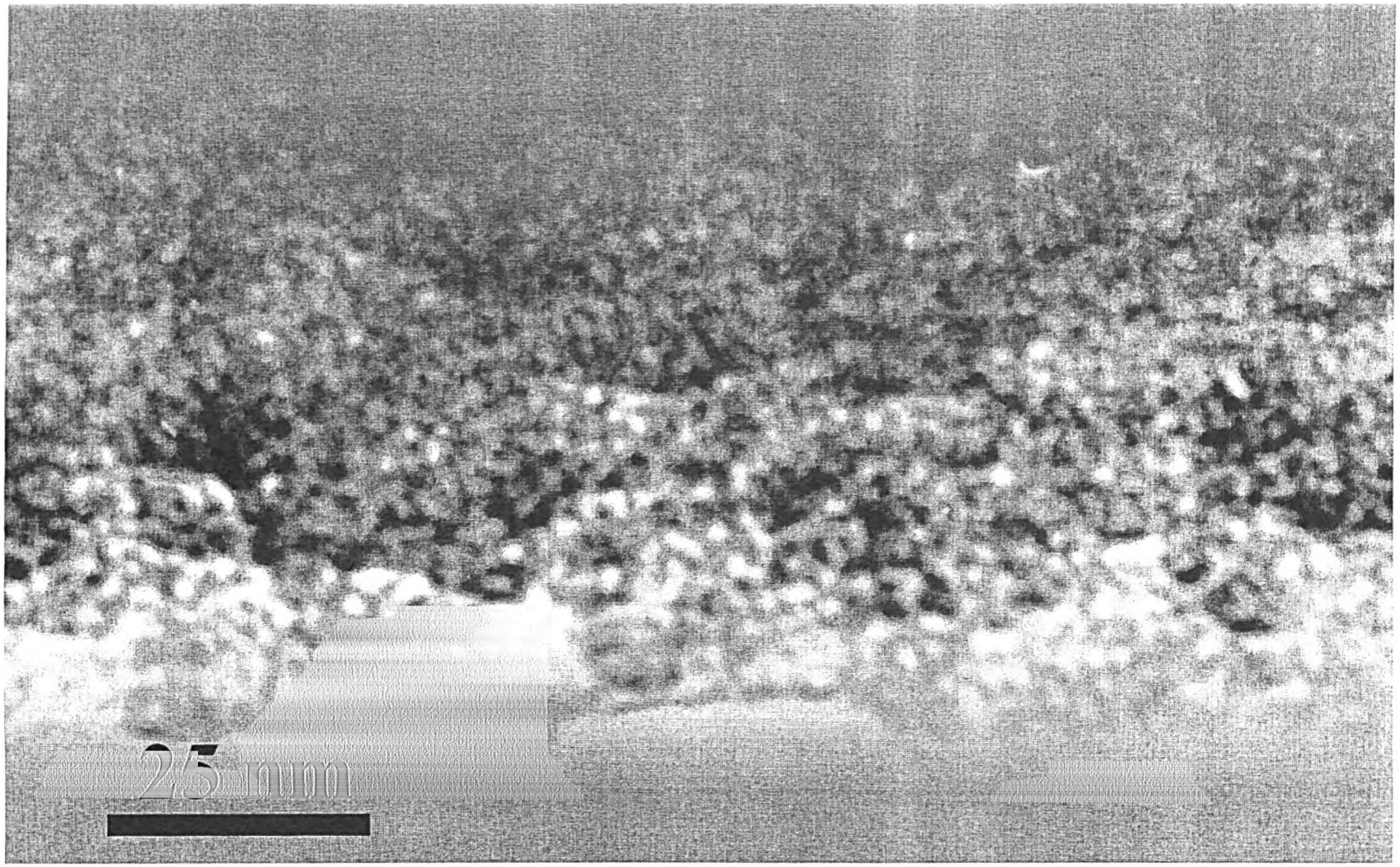

Figure 6.9. Digitally enhanced cross-section TEM underfocus image of Ta_2O_5 film, deposited under concurrent 600 eV Ar bombardment (I/A=1.4).

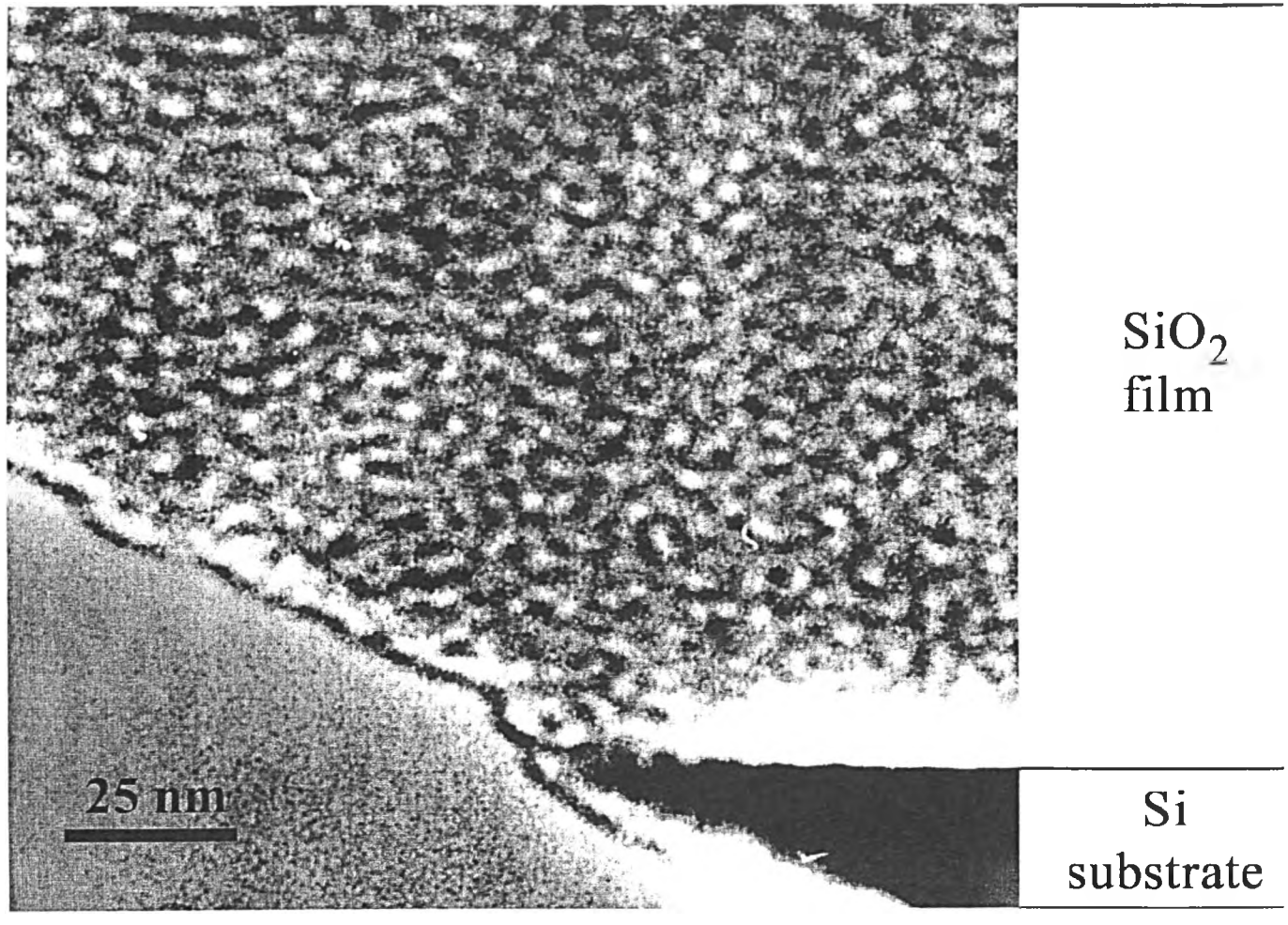

Figure 6.10. Digitally enhanced cross-section TEM overfocus image of SiO_2 film, deposited under concurrent 250 eV Ar bombardment (I/A=1.4).

under-focus conditions, therefore, regions with higher concentration of lighter elements will appear to be brighter. Thus, in the case of a tantalum pentoxide film in under-focus conditions argon gas bubbles will appear as bright areas. Figure 6.9 clearly shows the presence of such areas of approximate average diameter of 1.8 nm, leading to the conclusion that argon in the Ta_2O_5 film is present in the form of bubbles.

Figure 6.10 represents an over-focus image of silicon dioxide film, deposited under concurrent bombardment with 250 eV Ar^+ ions at an ion-to-atom arrival ratio of 1.4. The concentration of argon in this case, measured by RBS, is 0.04 Ar/Si atoms. As the image is captured in over-focus conditions, areas with high concentration of heavier elements will appear lighter. Thus, in this case argon bubbles should appear as bright regions on a darker background. Such areas of approximate average diameter of 2.8 nm can be seen in Figure 6.10, therefore, it is concluded that in SiO_2 films, as well as in Ta_2O_5 films, argon is present in the form of gas bubbles.

No gas bubbles have been observed in films, deposited at lower levels of ion bombardment. This can, probably, be explained as follows: as the energy and dose of ion bombardment decrease, the argon concentration in films of both materials decreases and the size of the gas bubbles becomes lower than the detection limit of the microscope.

In general, it can be proposed that, at low bombardment energies and doses, argon is incorporated into the film matrix in the form of single atoms or atomic clusters. As the bombardment of the film increases, argon starts to form atomic clusters of a size which is below the detectable limits. With further increase in ion bombardment these atomic clusters grow bigger and become what is known to be gas bubbles, which can be detected by TEM.

6.1.3. X-ray Photoelectron Spectroscopy (XPS) measurements

As already mentioned, RBS does not give information on the chemical state of the film elements. Therefore, a number of films were studied by XPS and results of the measurements were analysed at the Institute of Chemistry of Solid States, Urals Branch of Russian Academy of Sciences. These results are quoted below.

First, the results of analysis of Ta_2O_5 films will be reviewed. Here three samples have been studied. The first sample is a non-ion-assisted film with thickness of 310 nm and impurity incorporation of 0.01 Fe/Ta and 0.1 Ar/Ta. The second sample is an Ar^+-bombarded film (600 eV, I/A=1.4) of 215 nm thickness and impurity incorporation of

0.015 Fe/Ta and 0.128 Ar/Ta. The last film is an oxygen-bombarded sample (400 eV, I/A=2.0) of 295 nm thickness and impurity incorporation of 0.03 Fe/Ta and 0.14 Ar/Ta. XPS-spectra from the untreated surface of all of the films (first 3-5 nm) show the presence of Ta, O and C. Signals from each of the elements were studied in detail. No signals from film impurities (Fe and Ar) have been observed. This can be partially explained by the low XPS-method sensitivity to such small concentrations of impurities. For argon impurity detection another problem exists: the signal from Ar, expected in the region of the 240-250 eV, could be overshadowed by the much more intense signal from Ta.

The aim of the XPS-analysis of Ta_2O_5 films is to find out the chemical state of tantalum and verify the presence/absence of tantalum sub-oxides. However, the analysis is complicated by the fact that tantalum and tantalum sub-oxide surfaces oxidise fully to Ta_2O_5 upon contact with air. Usually the thickness of such a surface layer is about 1-2 nm. Therefore, if tantalum/tantalum sub-oxides are present in the film, their signals should be present in the spectra along with the signal from stoichiometric oxide (observed at 26.3 eV in this research, see Figure 6.11). The exact position of the signals from tantalum sub-oxides is unknown. For many metals, signals from their sub-oxides would be situated on the energy scale between the signal from the pure metal (lower boundary) and fully oxidised metal (upper boundary). However, tantalum sub-oxides do not show this tendency, and, on the energy scale, their signals can also be observed above the signal of the fully oxidised tantalum. This should lead to peak broadening and loss of resolution, which is not observed in the spectra. Thus it can be concluded that no sub-oxides are present in the film surface layer.

In XPS analysis it is a common practice to remove the surface layers of the samples, often contaminated with hydrocarbons and oxygen, by Ar^+ ion etching. The benefits of such procedure in the case of oxides are, however, doubtful, as it can lead to surface modification by preferential sputtering of light elements (for example, preferential oxygen sputtering in Ta_2O_5 films). Nevertheless, such a procedure can also give an insight into the changes, which are experienced by a film, deposited under concurrent ion bombardment. XPS-spectra of the films, bombarded for 10 minutes by Ar^+ ions, show a series of various sub-oxide signals (see Figure 6.11). It was not possible to resolve the obtained spectra, but it can be said that, under Ar^+ ion bombardment, stoichiometric Ta_2O_5 can be decomposed to a solid solution of oxygen in tantalum. Comparison of the spectra from all three films shows that the level of tantalum oxide dissociation increases when going from a non-bombarded sample to an argon and then

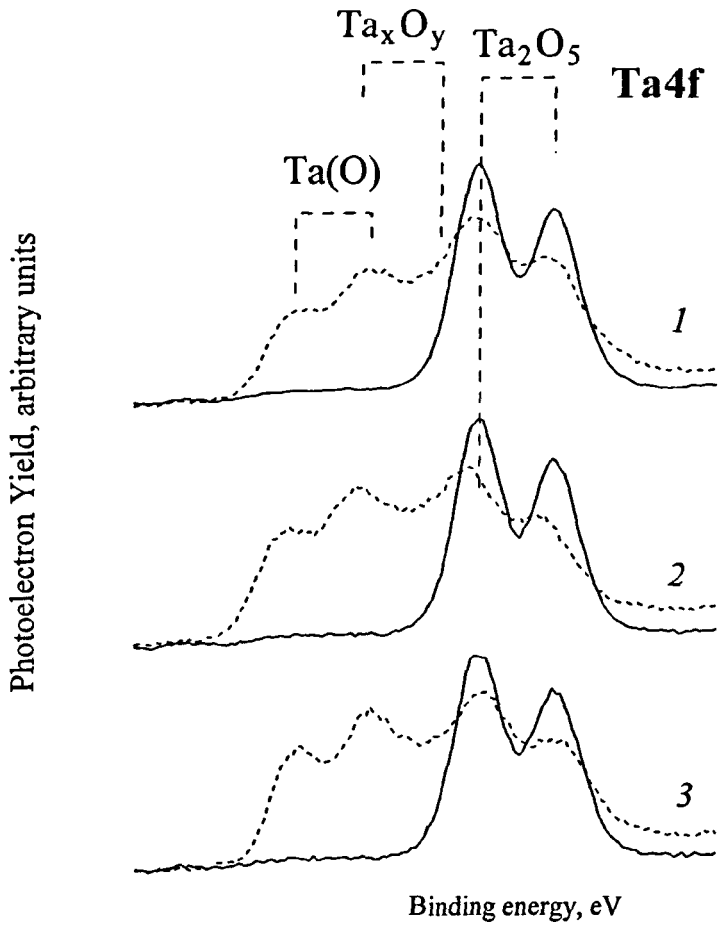

Figure 6.11. XPS Ta4*f* spectra for tantalum in Ta_2O_5 films. 1 corresponds to sample 1 – non-assisted film; 2 corresponds to sample 2 – Ar-assisted film, 3 corresponds to samle 3 – oxygen-assisted film. Solids lines represent spectra from the un-treated film surfaces, dotted lines represent spectra from the film surfaces, etched for 10 minutes with 6 keV Ar^+ beam of 15 μA beam current.

an oxygen-bombarded sample. It is unclear, whether this fact can be attributed to the differences in the nature of the original films or to the differences caused by the ion etching procedure.

Analysis of oxygen signals (see Figure 6.12) showed two peaks, one at 530.5 eV and one at 532.3 eV. These peaks correspond to oxygen in Ta_2O_5 and in surface contamination, and are in agreement with published values (530.3 eV for Ta_2O_5 in [Ho et al, 1987]). Figure 6.12 also shows the development of a feature at the high-energy edge (531-532 eV) of the oxygen peak of the film, deposited under concurrent Ar ion bombardment. At the moment the nature this feature is unclear.

A signal from carbon showed similarity for all three samples, therefore, only the spectra of a non-assisted sample is shown in Figure 6.13. The observed peak (285.0 eV) corresponds to C present only in organic hydrocarbon contamination on the film surface. Ion etching leads to almost complete removal of such contamination. However, after etching a very small peak at 282.5 eV is observed. This peak is related to C in tantalum carbide or a solid solution in the metal. It is possible that carbon impurity is present in the film bulk. However, the peak is not observed in spectra from non-etched samples. Therefore, most probably, this peak is due to changes in the film during etching and results from forward recoil implantation of carbon atoms into the film bulk.

Film composition can be judged not only from the position and characteristics of the peaks in XPS spectra, but also calculated using relevant peak areas. Here peaks, corresponding to surface contamination, should not be taken into account. Film composition (i.e. the ratio of the oxygen to tantalum concentrations C_O/C_{Ta}) can be calculated as

$$\frac{C_O}{C_{Ta}} = A\frac{I_O}{I_{Ta}}\frac{\sigma_{Ta}}{\sigma_O}, \tag{6.2}$$

where A is a proportionality constant, I_O and I_{Ta} are peak areas of oxygen at 530.5 eV and tantalum (26.3 eV), respectively, and $\sigma_{Ta} = 907$ and $\sigma_O = 285$ are photoexcitation cross-sections. The elemental ratios C_O/C_{Ta} have been calculated as 2.15 A, 2.08 A and 2.10 A for non-bombarded, argon-assisted and oxygen-assisted Ta_2O_5 films, respectively. Assuming that all three films are stoichiometric, the proportionality coefficient A can be calculated (A is approx. 1.2). Then, from the above three ratios it can be concluded that the composition of all of three films is within the accuracy limit of such a method (± 0.1). Using the calculated A value, the composition of the etched film surfaces can be

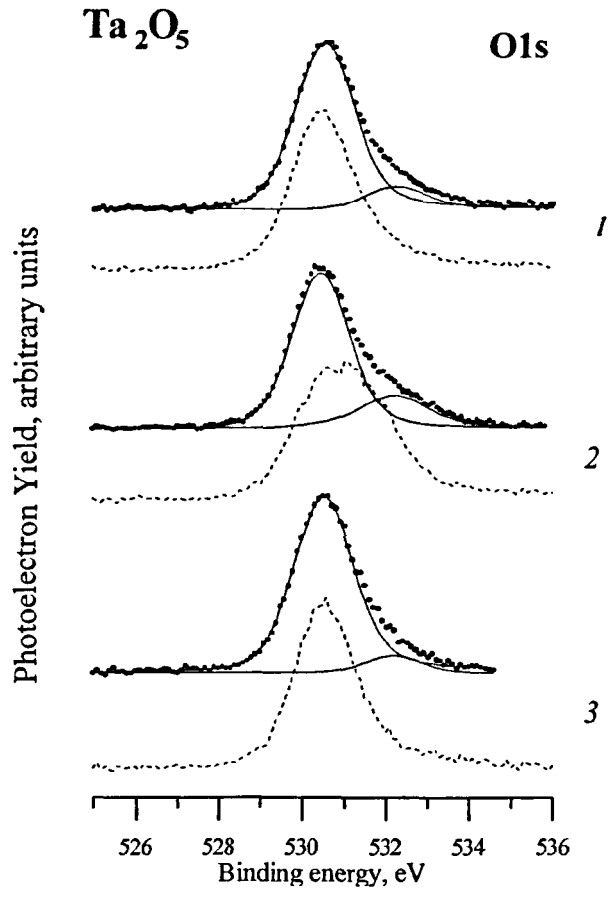

Figure 6.12. XPS O1*s* spectra for oxygen in Ta_2O_5 films. 1 corresponds to sample 1 – non-assisted film; 2 corresponds to sample 2 – Ar-assisted film, 3 corresponds to sample 3 – oxygen-assisted film. Solids lines represent spectra from the un-treated film surfaces, dotted lines represent spectra from the film surfaces, etched for 10 minutes with 6 keV Ar^+ beam of 15 μA beam current.

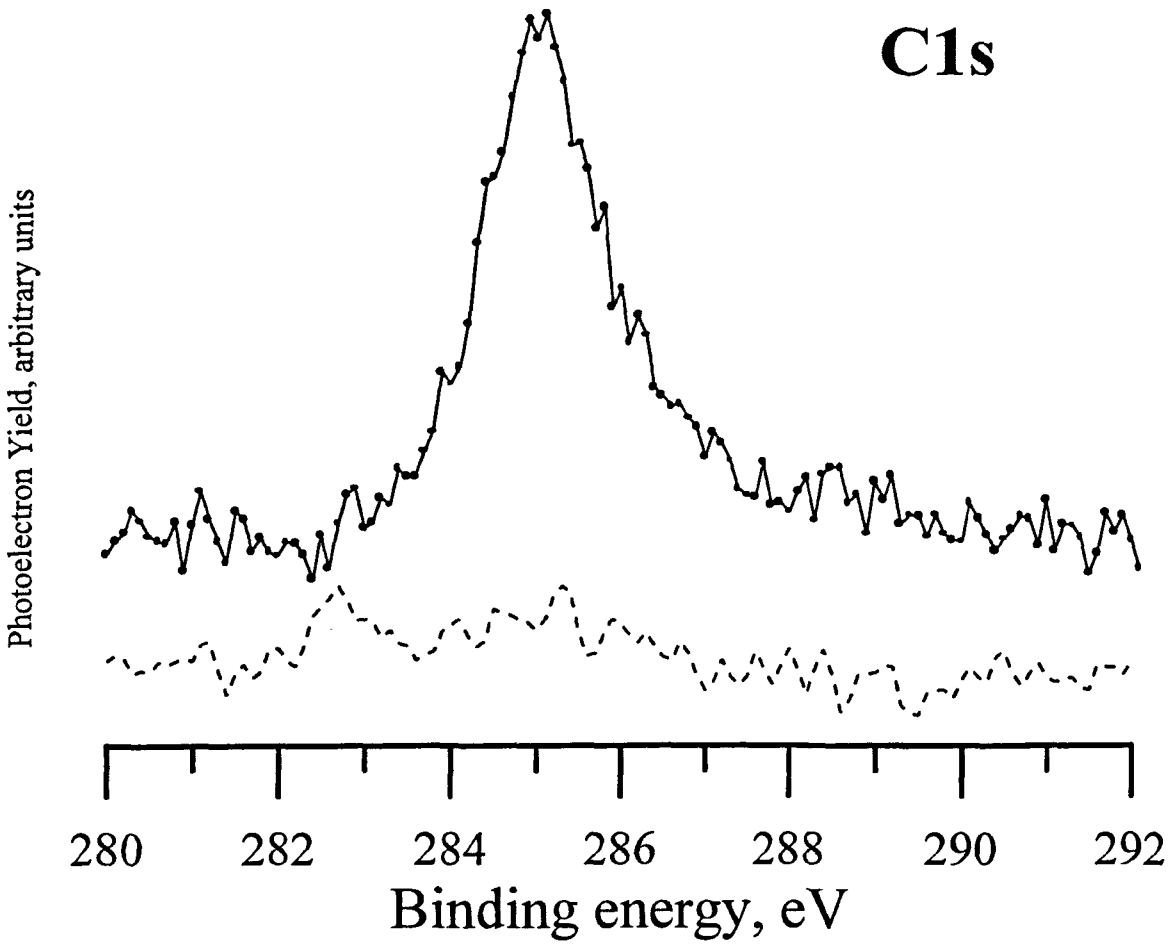

Figure 6.13. XPS C1*s* spectra for carbon in non-ion-assisted Ta_2O_5 film. Solids lines represent spectra from the un-treated film surfaces, dotted lines represent spectra from the film surfaces, etched for 10 minutes with 6 keV Ar^+ beam of 15 μA beam current.

estimated as $TaO_{1.64}$, $TaO_{1.50}$ and $TaO_{1.13}$ for non-assisted, argon-assisted and oxygen-assisted films, respectively. This trend is unexpected but it is unclear whether such variation is caused by small irregularities in the etching conditions or by intrinsic film properties (for example, morphology changes due to a difference in deposition conditions).

Analysis of valence band spectra (see Figure 6.14) of Ta_2O_5 films can also yield important information, namely the dielectric forbidden gap width. If the position of the Fermi level is taken as the middle of the forbidden gap zone, the distance between the filled and free zones is estimated to be 6-7 eV.

Thus, for Ta_2O_5 films it can be concluded that there are no differences in the chemical state of tantalum and oxygen in the films, deposited without ion bombarded and with concurrent argon or oxygen bombardment.

XPS-investigations of four silicon dioxide films have also been performed. The first sample was a SiO_2 (O/Si=2.1) film deposited without ion assistance using a SiO_2 sputter target. The second sample was a SiO_2 (O/Si=2.05) film, deposited under 400 eV Ar^+ ion bombardment (I/A=0.35) using a Si sputter target. Impurities of iron (0.012 Fe/Si), argon (0.035 Ar/Si), and tantalum (0.003 Ta/Si) have been registered in this film by RBS. The third film was a non-ion assisted SiO_2 film, deposited from a Si target with oxygen fed into the chamber through the secondary (assist) source (O/Si=2.25). Impurities of iron (0.02 Fe/Si), tantalum (0.002 Ta/Si) and molybdenum (0.01 Mo/Si) have been registered by RBS in this film. The last film was deposited from a Si target under concurrent 300 eV oxygen ion bombardment (I/A=0.7) (O/Si=2.25). Impurities of Ta, Fe, Mo and Ar have been registered by RBS in this film.

General XPS-spectra of SiO_2 films (Figure 6.15) showed the presence of signals from Si, O and C. In the region of 730-790 eV peaks from Auger-transitions can be also seen. No impurities have been observed in the films by XPS. Again, this can, probably, be related to the low sensitivity of the measurements.

Details of Si and O peaks before and after film surface etching with an Ar^+ beam are presented in Figures 6.16 and 6.17, respectively. It can be seen, that, for most samples, ion etching does not modify the oxygen (532.5 eV) and silicon (103.4 eV) peaks. The only exception is the O line of the non-ion-assisted film, deposited from the Si target. Comparison of these results with the results for Ta_2O_5 films show, that SiO_2 films are less effected by Ar^+ etching. In the case of SiO_2 films the composition is not uniquely defined by peak positions. The oxygen line is registered at approximately the same energy for both the monoxide and dioxide of silicon. The silicon line is registered at

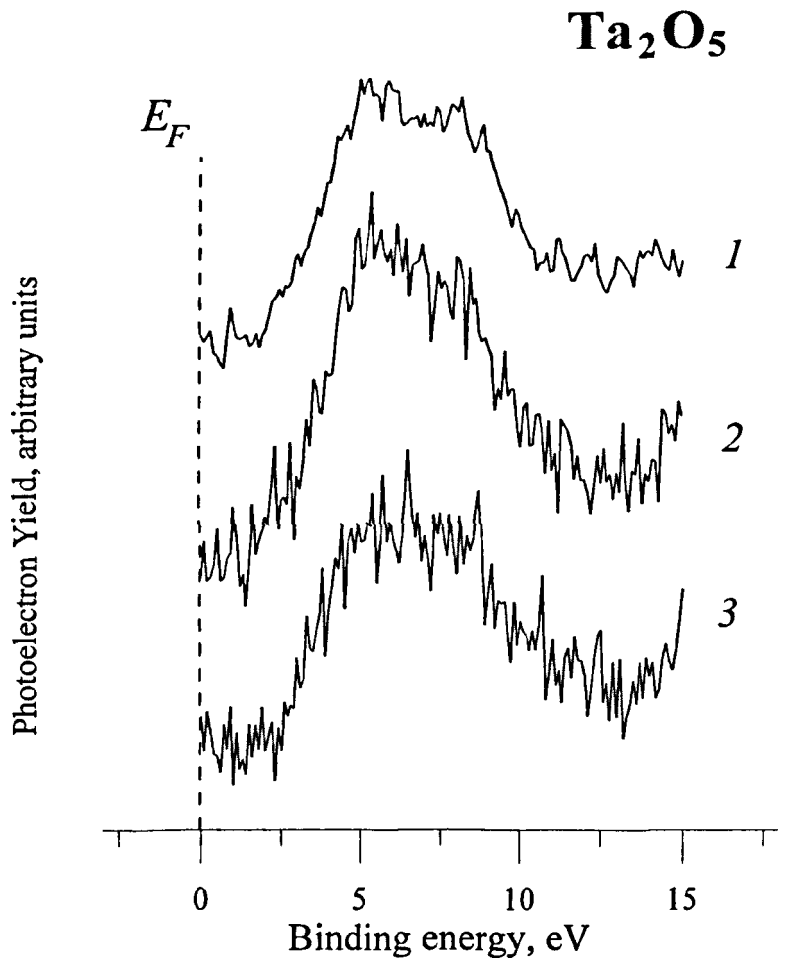

Figure 6.14. XPS of valence bands of Ta_2O_5 films. 1 corresponds to sample 1 – non-assisted film; 2 corresponds to sample 2 – Ar-assisted film, 3 corresponds to samle 3 – oxygen-assisted film.

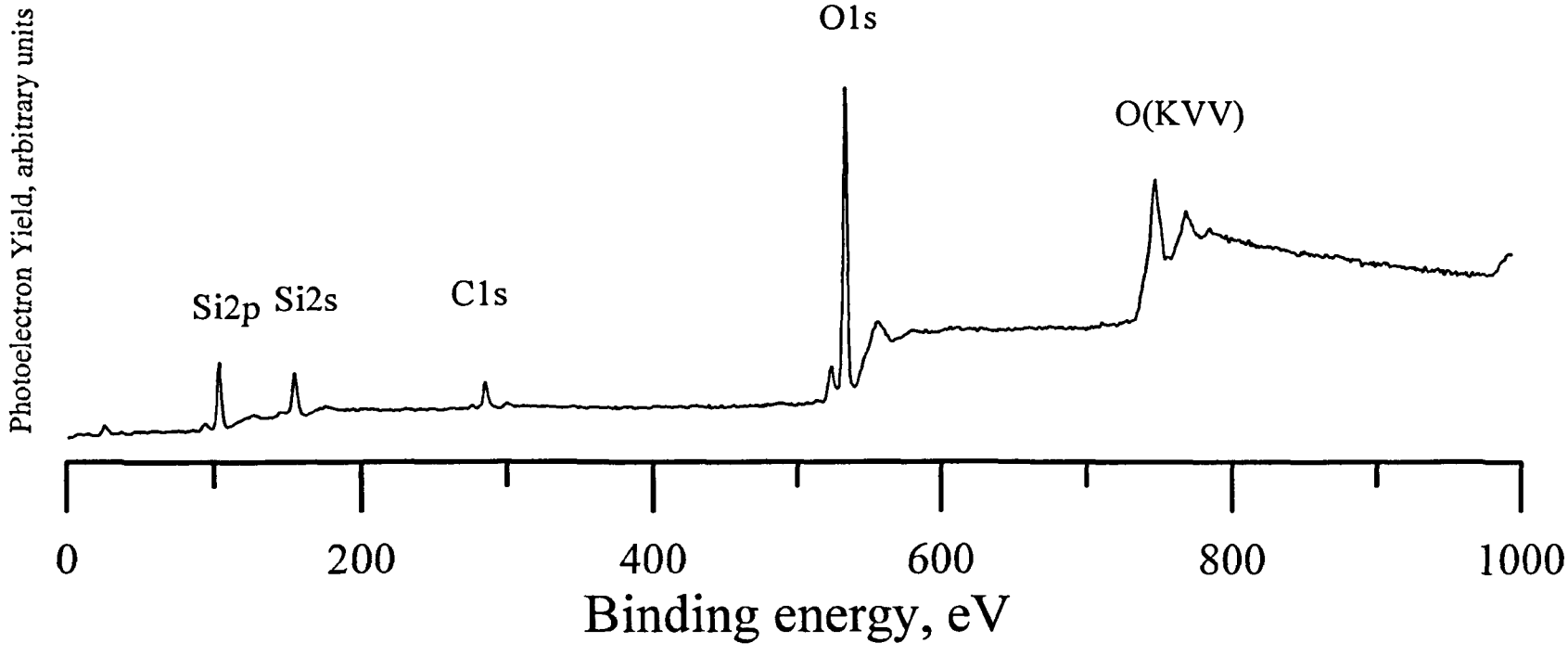

Figure 6.15. XPS spectra from the –treated surface of SiO_2 film, deposited by non-assisted sputtering of SiO_2 target (sample 1).

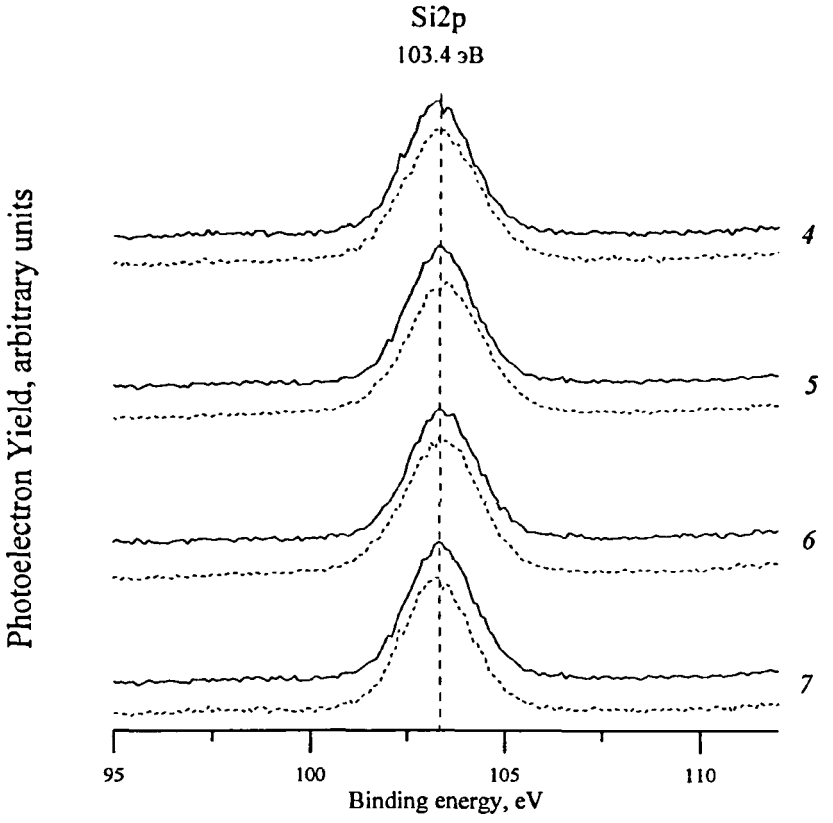

Figure 6.16. XPS Si2*p* spectra for silicon in SiO_2 films. 4 corresponds to sample 1 – non-assisted film sputtered from SiO_2 target; 5 corresponds to sample 2 – Ar-assisted film, 6 corresponds to samle 3 – non-assisted film sputtered from Si target, 7 corresponds to sample 4 – oxygen-assisted film. Solids lines represent spectra from the un-treated film surfaces, dotted lines represent spectra from the film surfaces, etched for 10 minutes with 6 keV Ar^+ beam of 15 μA beam current.

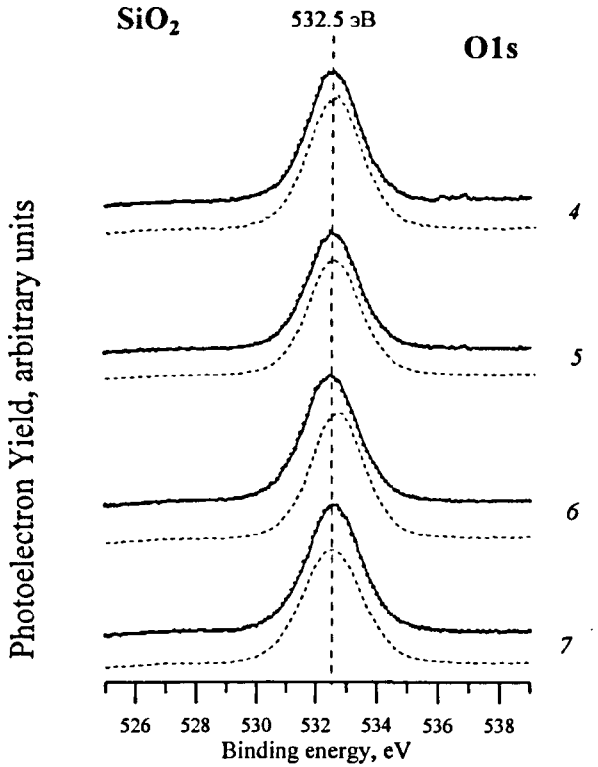

Figure 6.17. XPS O1*s* spectra for oxygen in SiO_2 films. 4 corresponds to sample 1 – non-assisted film sputtered from SiO_2 target; 5 corresponds to sample 2 – Ar-assisted film, 6 corresponds to samle 3 – non-assisted film sputtered from Si target, 7 corresponds to sample 4 – oxygen-assisted film. Solids lines represent spectra from the un-treated film surfaces, dotted lines represent spectra from the film surfaces, etched for 10 minutes with 6 keV Ar^+ beam of 15 μA beam current.

102.7 eV or 102.0 eV for silicon monoxide and at 103.5 eV for silicon dioxide. As the measured position of the silicon peak for the films in this research is 103.4 eV, it is highly likely that the films are stoichiometric SiO_2.

Film atomic concentration cannot be calculated from the results of measurements on untreated surfaces, as in this case the peak from oxygen in surface contamination coincides with the peak from oxygen in SiO_2. However, surface contamination can be removed by Ar^+ etching (proved by the disappearance of the C line from the spectra in Figure 6.18). The effect of preferential sputtering in this case is not expected to be significant due to comparable masses of the elements involved. Thus, after etching, the film composition can be calculated from the peak areas. Using Equation (6.2) the atomic concentration C_O/C_{Si} was estimated as 1.35 *B*, 1.42 *B*, 1.55 *B* and 1.55 *B* (*B* is the proportionality constant) for samples 1-4, respectively. Films 3 and 4 have the highest oxygen concentration. The oxygen content in films 1 and 2 is, respectively, 13% and 8.4% lower than that of the samples 3 and 4. Such values are in agreement with the data, obtained by RBS (a difference of 7-11% was measured). Exact film composition cannot be calculated, as the value of the proportionality coefficient *B* is not known.

Analysis of the spectra (Figure 6.19) of the valence band (located in the area 5-17 eV) of SiO_2 films allowed an estimate of the dielectric forbidden gap value of 10-12 eV to be made.

In conclusion, it can be said, that the SiO_2 film composition depends on the deposition method. It is not possible to identify the exact film composition, as the proportionality coefficient *B* is not known.

6.2. Stress measurements in non ion-assisted films

6.2.1. Tantalum Pentoxide Films: Film Composition

Several experiments on Ta_2O_5 films were performed in order to establish conditions for deposition of films with reproducible stoichiometry and stress values. The results of these experiments are presented in Figures 6.20 and 6.21. Changes in film composition, measured by RBS, with increase in oxygen content in the deposition chamber are shown in Figure 6.20. It is expected that, due to the presence of oxygen in the chamber, oxidation at the surface of the Ta target and the film will begin to occur and with increase in oxygen partial pressure oxygen incorporation into the film will increase up

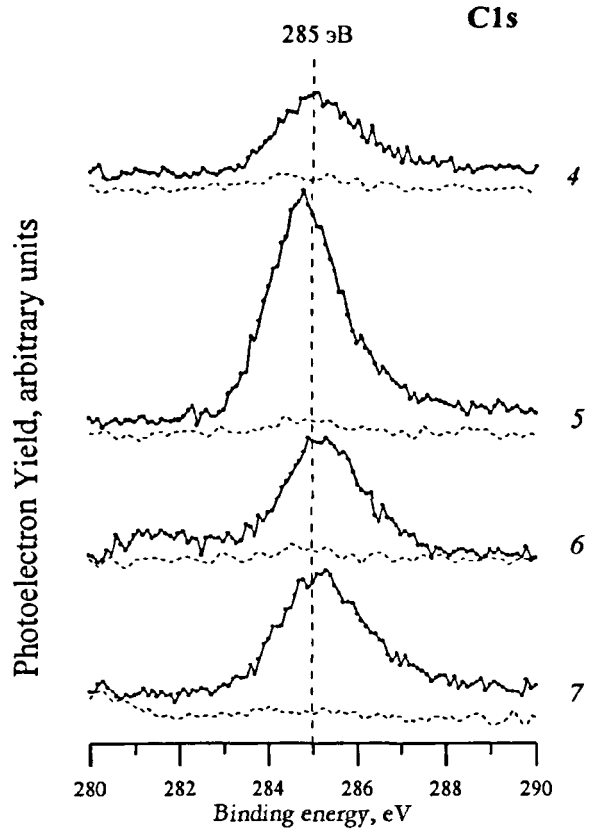

Figure 6.18. XPS C1*s* spectra for carbon in SiO_2 films. 4 corresponds to sample 1 – non-assisted film sputtered from SiO_2 target; 5 corresponds to sample 2 – Ar-assisted film, 6 corresponds to samle 3 – non-assisted film sputtered from Si target, 7 corresponds to sample 4 – oxygen-assisted film. Solids lines represent spectra from the un-treated film surfaces, dotted lines represent spectra from the film surfaces, etched for 10 minutes with 6 keV Ar^+ beam of 15 μA beam current.

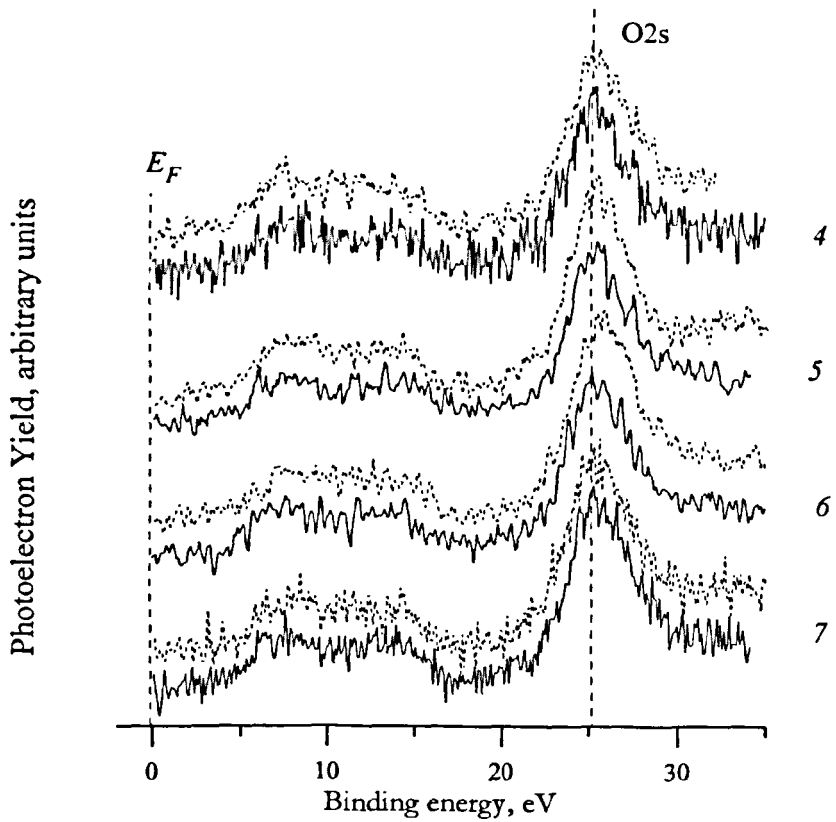

Figure 6.19. XPS valence band and O2*s* spectra of SiO_2 films. 4 corresponds to sample 1 – non-assisted film sputtered from SiO_2 target; 5 corresponds to sample 2 – Ar-assisted film, 6 corresponds to sample 3 – non-assisted film sputtered from Si target, 7 corresponds to sample 4 – oxygen-assisted film. Solids lines represent spectra from the un-treated film surfaces, dotted lines represent spectra from the film surfaces, etched for 10 minutes with 6 keV Ar^+ beam of 15 μA beam current.

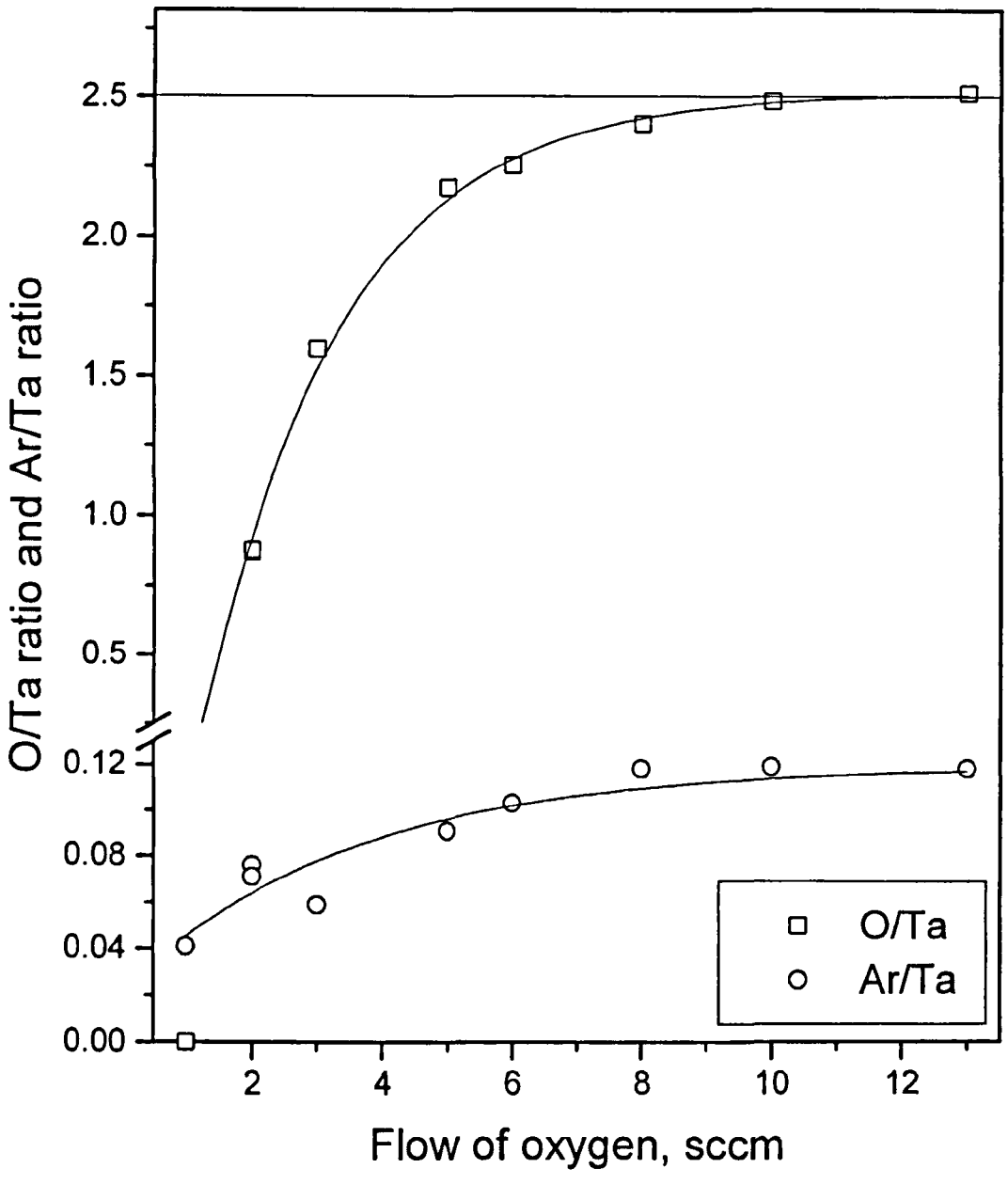

Figure 6.20. Dependence of tantalum oxide film composition on the amount of oxygen gas, present in the chamber. Solid lines represent exponential fitting of the experimental data.

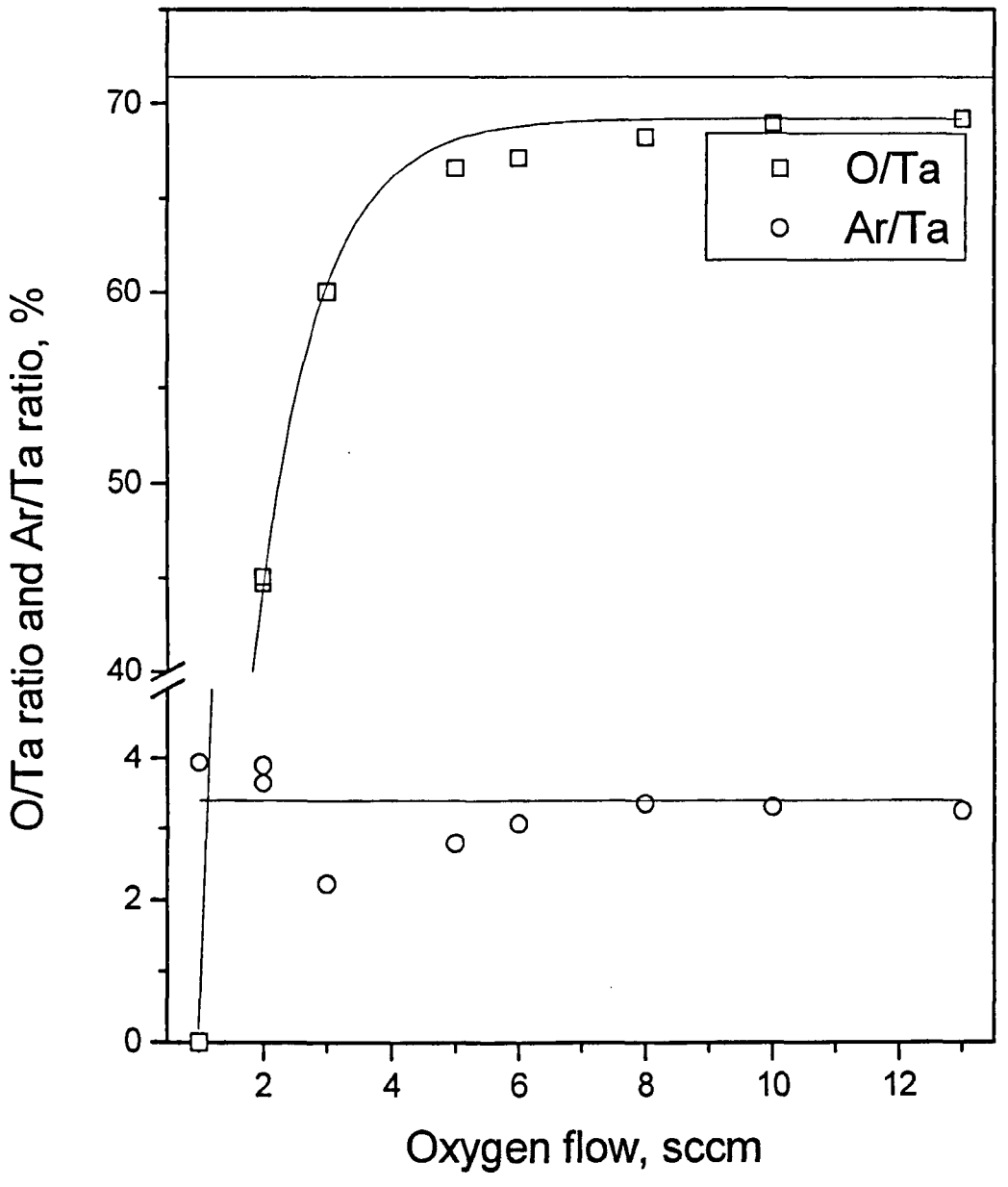

Figure 6.21. Dependence of tantalum oxide film composition in percents on the amount of oxygen gas, present in the chamber. Solid lines represent exponential fitting of the experimental data.

to the point when an oxide is formed on the target surface and a stable stoichiometric oxide film is deposited on the substrate. From Figure 6.20 it can be concluded that, with increase in the oxygen supply to the chamber, oxygen content of the films increases and films change from metallic to fully stoichiometric oxide. This change can also be noticed by sample observation where, with variation of the deposition conditions, films change from absorbing metallic-coloured layers to transparent layers with a bright colour, which depends on the film thickness. If, in addition, incorporation of Ar into the total film volume (see Figure 6.21) is considered, it can be noted that this parameter changes only very little and is in the region of 2-4%.

Initial experiments, performed at 8.0 sccm oxygen flow into the chamber, resulted in films with non-reproducible stress values and deviations from expected composition and film thickness. The reason of such behaviour can be understood from the data in Figure 6.20. It can be clearly seen that, at the point of 8.0 sccm oxygen flow, small changes in deposition conditions will lead to changes in the O/Ta ratio in the film. Small changes in composition can, in turn, lead to changes in film thickness and stress values. Figure 6.20 also shows that for 10.0 sccm oxygen flow this effect is not as high, so parameters of resulting coatings are expected to vary less. Indeed, it was experimentally found that deposition under 10 sccm oxygen flow leads to Ta_2O_5 films with reproducible properties.

Stress, measured in these films was found to be compressive. Stress values are plotted in Figure 6.22. It can be seen that films, deposited under different conditions, have different thickness. The difference in thickness of films, deposited during the same time interval, can be explained by a combined effect of target surface oxidation, decrease in sputtering yield and increase in molar volume V_m of an oxide material (V_m=54 cm^{-3} for Ta_2O_5) relative to pure metal (V_m=10.9 cm^{-3} for Ta). However, initial experiments showed that stress in these type of films does not depend on film thickness, thus stress values, presented in Figure 6.22, can be used in the subsequent analysis of data. It can be concluded that, with an increase in oxygen flow into the chamber, the film compressive stress decreases and, finally, reaches its saturation value of 400 MPa for a reactive gas flow of 5.0 sccm and higher. From the comparison of Figures 6.20-6.21 with Figure 6.22 it can be concluded that stress is strongly dependent on the film composition and stoichiometry and for an increase in oxygen concentration in the film and the formation of an amorphous oxide instead of a polycrystalline metal film the stress magnitude decreases.

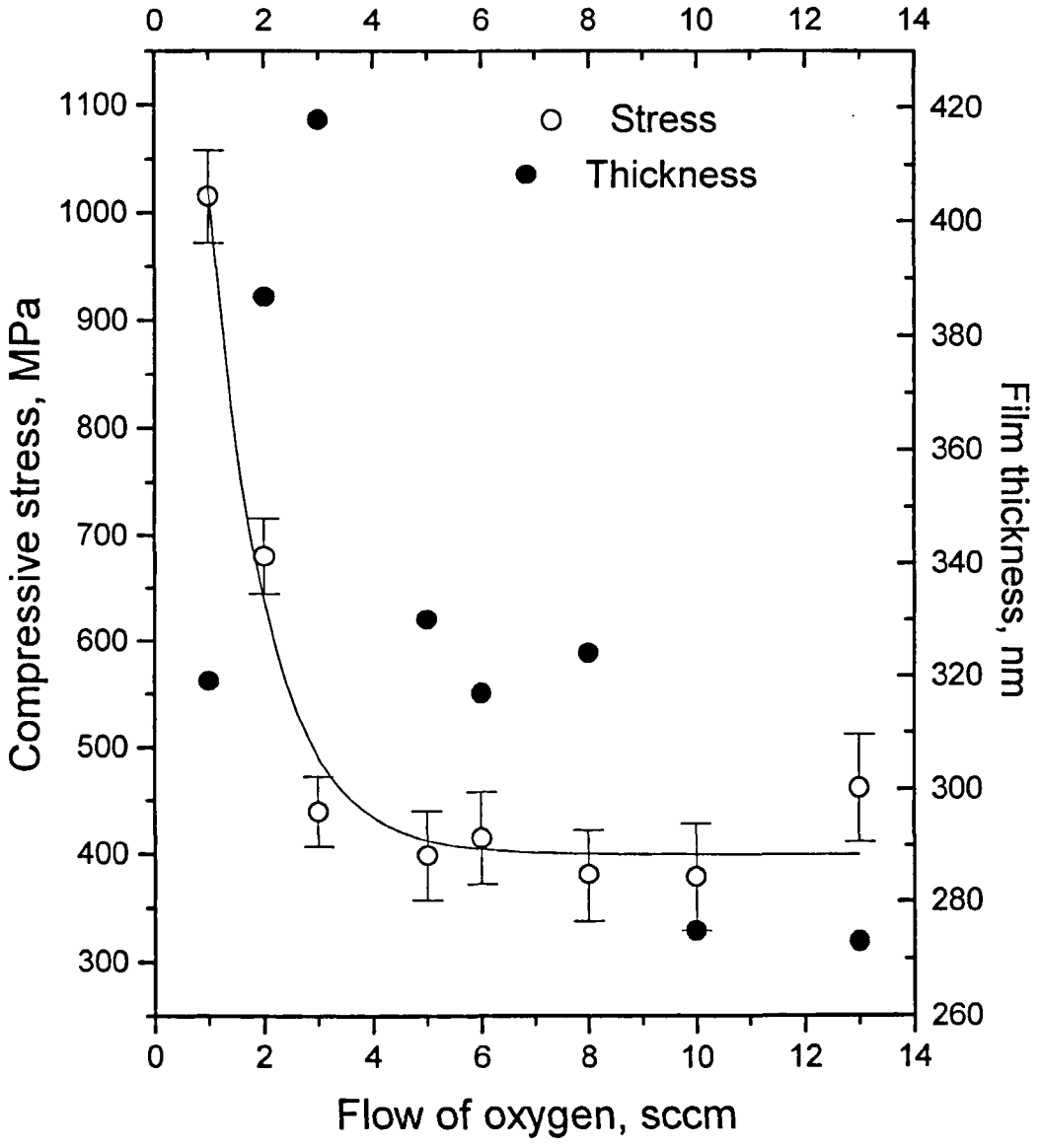

Figure 6.22. Stress and thickness of tantalum oxide films, deposited under various levels of oxygen flow into the chamber. Solid line represents exponential fitting of the experimental data.

6.2.2. Tantalum Pentoxide Films: Film Thickness Measurements

It is known that film thickness can be measured using various techniques, results of the two of which, namely, profilometry and RBS, have been compared in this research programme. Values of thickness of stoichiometric Ta_2O_5 films, measured by both techniques, are presented in Figure 6.23. It can be seen that these values are in a good agreement with each other, especially in the case of longer deposition runs and thus higher film thicknesses. Therefore, the choice of the bulk density value for RBS analysis is justified and it can be concluded that ion-beam sputtered Ta_2O_5 films have good quality and high bulk-like density. It can also be concluded that, for stress calculations, values of stoichiometric film thickness obtained by RBS can be used without introducing significant errors.

6.2.3. Tantalum Pentoxide Films: Substrate Cleaning Effects

In order to investigate the influence of substrate cleaning procedures and thus substrate initial state on stress in Ta_2O_5 thin films several different cleaning procedures have been used. Their detailed description can be found in Chapter V paragraph 2.2. Results of these experiments (see Figure 6.24) showed, that stress in thin tantalum pentoxide films is reproducible and is independent of

- film thickness (for thickness greater than 200 nm);
- deposition interval (1.5 h continuous deposition or 2.5 h interrupted deposition), or
- substrate cleaning procedure.

This stress is compressive, which is shown by the bending direction of the substrate (film is on the convex side) and has a mean value of 350 MPa. Independence of film stress on the deposition interval can be explained by the absence of any significant effect due to stress relaxation, film cooling or contamination during the periods of interruption of the deposition.

The independence of the final stress on substrate pre-cleaning may probably be explained by the material properties. It is known, that below 600 ^{0}C Ta_2O_5 grows in amorphous state (see Chapter II). This is further supported by the results of the Raman backscattering measurements. The Raman spectra from the system substrate/film showed only a peak attributed to the substrate, which suggests that films are indeed amorphous. In this type of material, information on substrate surface conditions

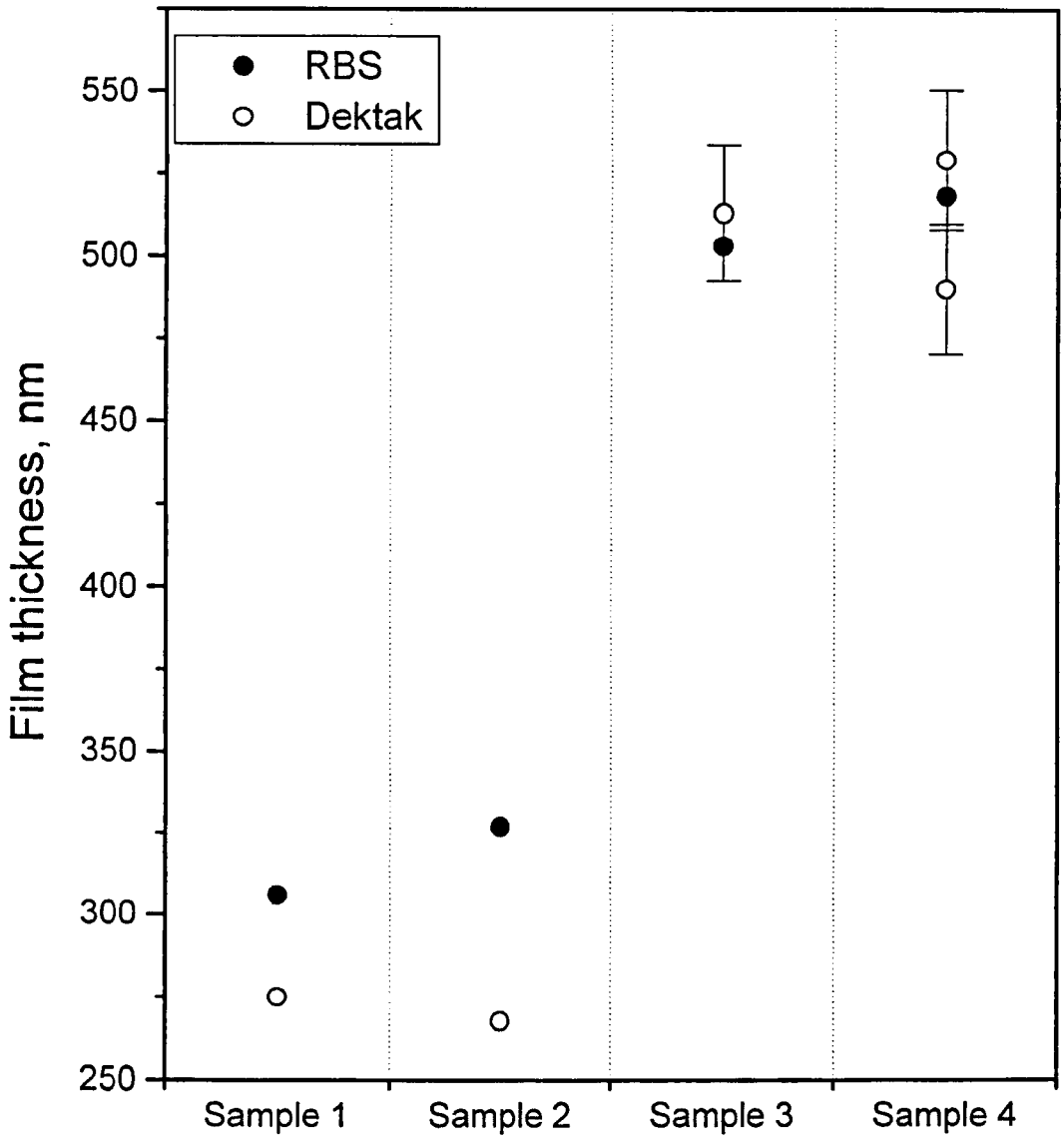

Figure 6.23. Thickness of stoichiometric tantalum oxide films, measured by RBS and DekTak profilometer. Deposition conditions were chosen as follows: O_2 fed near the substrate at 10 sccm, total deposition pressure 4.0×10^{-4} mbar, sputtering of Ta target with 45 mA 1keV Ar^+ ions. Samples 1 and 2 deposited continuously for 1.5 hours, samples 3 and 4 deposited for 2.5 hours with interruption for approx. 0.5 h after every 0.5 h.

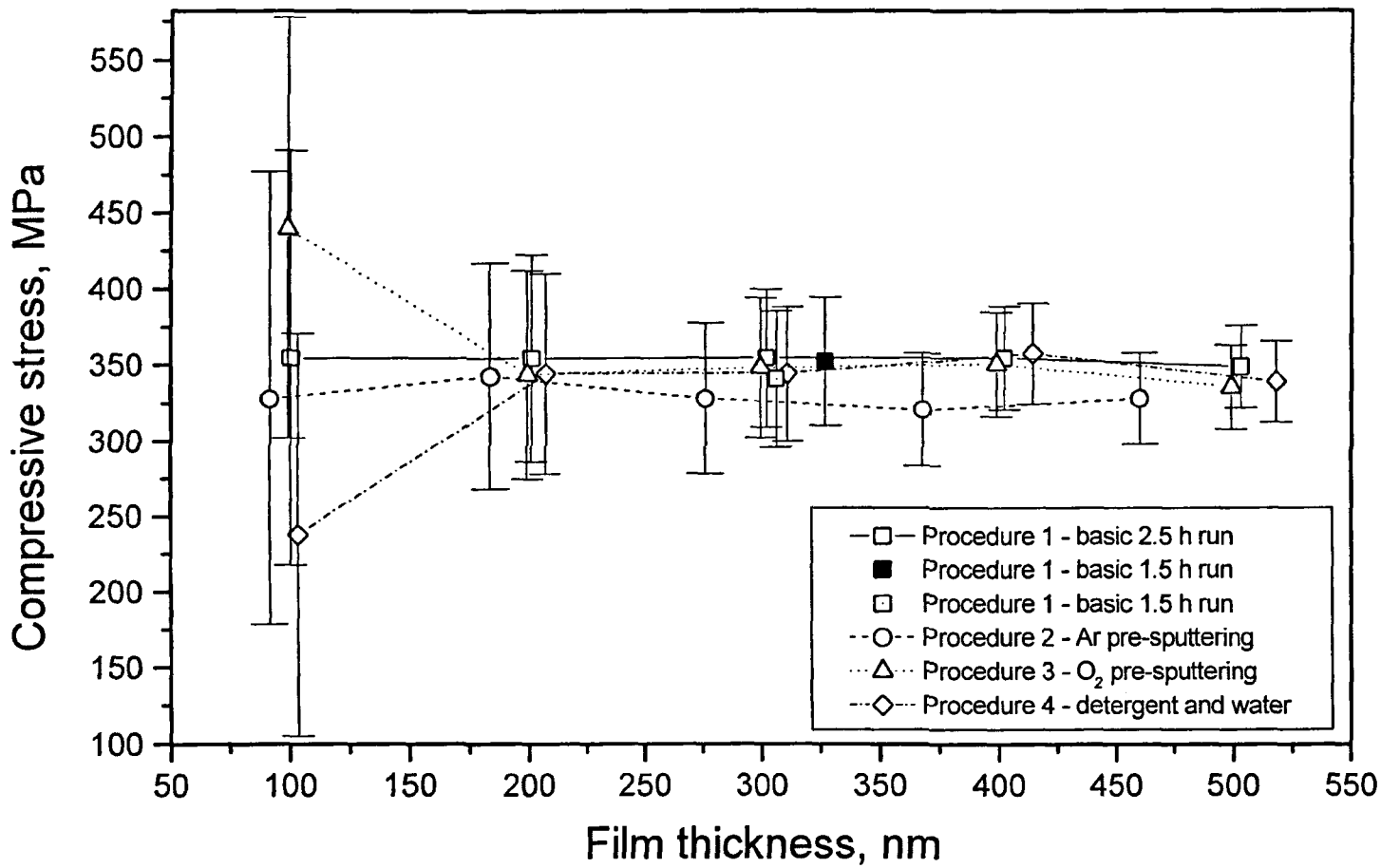

Figure 6.24. Influence of different substrate cleaning procedures on stress in thin stoichiometric Ta_2O_5 films.

and its small variations is not transferred to the succeeding layers of the growing film in the way it would be transmitted in a material possessing a crystal structure. Films are relatively thick, so, most probably, the influence of interfacial stress is low or negligible. This could be the reason for the independence of stress on substrate pre-cleaning procedures.

The amorphous, highly dense, and thus, low voided state of Ta_2O_5 films can also be used for explanation of stress independence on film thickness (for thickness greater than approx. 200 nm). In this case mechanisms, that could influence stress levels, such as preferential grain growth in the case of polycrystalline materials or changes in void size and population during film growth, are absent.

From the results of this research nothing can be concluded about stress in the initial stages of film growth and the influence of the substrate state on very thin films. In the set-up, used in this research, small substrate deflections cannot be measured with the necessary degree of accuracy and, therefore, it is not possible to obtain reliable results for very thin films.

The total stress value of –350 MPa, measured for Ta_2O_5 films, is in a good agreement with stress values, reported in the literature for films with similar properties deposited by various deposition methods (See Chapter II Table 2.4).

6.2.4. Tantalum Pentoxide Films: Sputtering Gas Effect

The influence of sputtering gas may be a factor of importance for stress behaviour in thin films. Therefore, experiments with Ar and Xe as sputtering gases were performed. Results are presented in Figure 6.25. It can be seen that the stress in Xe-sputtered films is also compressive and its value is on average only 150 MPa higher that that of Ar-sputtered films. It is known that, upon hitting the target, some of the ions will be immediately scattered from it. These back-reflected particles can bombard the substrate and growing film and thus influence film properties. Such influence will, in turn, depend on the number of particles, bombarding the film, and on their energy. It is known that the maximum energy E_a transferred to a stationary atom in the collision with an ion of energy E_i can be calculated as

$$E_a = \frac{4E_i m_a m_i}{(m_a + m_i)^2}, \tag{6.3}$$

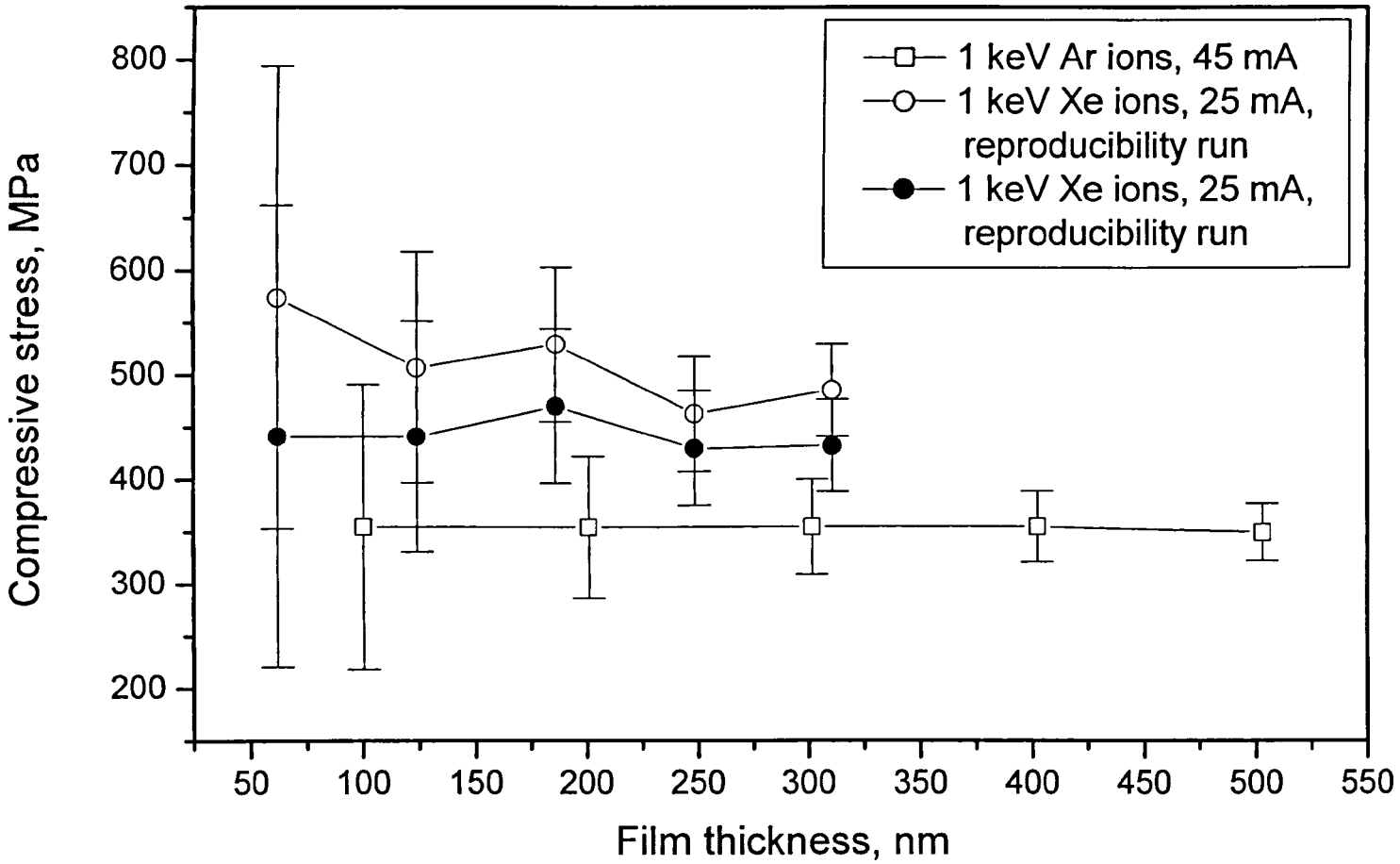

Figure 6.25. Influence of different sputtering gases (Ar and Xe) on stress in thin stoichiometric Ta_2O_5 films.

where m_a and m_i are masses of atom and ion, respectively. In the first collision a 1keV Ar ion gives a maximum of 816 eV to an O atom and only 593 eV to a Ta atom. In the case of a 1keV Xe ion this changes to 387 eV for an O atom and 975 eV for a Ta atom. Thus, if we consider Ta target bombardment with 1keV ions, back-scattered particles will possess an energy of approx. 407 eV for Ar and only 25 eV for Xe. Therefore, films, deposited with Xe sputtering gas, will be exposed to less energetic particle bombardment during growth.

Another insight into this problem can be gained from the analysis of TRIM simulation data, which can give the number of back-scattered particles, their energy and angular distribution. Calculations have been performed for the case of a Ta target bombarded with 1keV Ar or Xe ions (a history of 10000 impacting ions was simulated), directed onto the target at 35^0 to the target normal. It was found that approximately 35% of Ar and 16% of Xe are back-reflected from the target. Their energy distribution is presented in Figure 6.26. It can be seen that, apart from the larger amount of back-reflected particles, on average back-reflected Ar is much more energetic. Thus, it can be concluded that Ar-sputtered films are subjected to a higher degree of bombardment with particles of higher energy.

The picture considered above is, however, simplified. The decrease in growth rate of films with increase in oxygen presence in the chamber, illustrated by the changes in thickness in Figure 6.22, indicates that the target becomes poisoned and an oxide layer is formed on its surface. The thickness of this layer is unknown, as is the composition, because tantalum can form sub-oxides (TaO or TaO_2). All these features complicate the analysis of such cases. It should be noted, that other mechanisms, such as incorporation of sputtering gas into the film bulk, can also be important. RBS experiments clearly show that, for stoichiometric Ar-sputtered films, small amounts (2-3 at.pt.) of argon are present in the film. No argon is detected in Xe-sputtered films, and nothing can be concluded about Xe incorporation, as any signal from the small amount of Xe in the film in the RBS spectra would be overshadowed by the Ta signal from the film. (In RBS the channel numbers are approx. 366.5 for Ta and 354.5 for Xe.)

6.2.5. Tantalum Pentoxide Films: Effect of angle of incidence of sputtering beam to target normal

The results of this experiment for Ta_2O_5 films are presented in Figure 6.27. Although, for a Ta target, changes in angle of incidence of 1 keV Xe ions from 15^0 to 35^0 and then

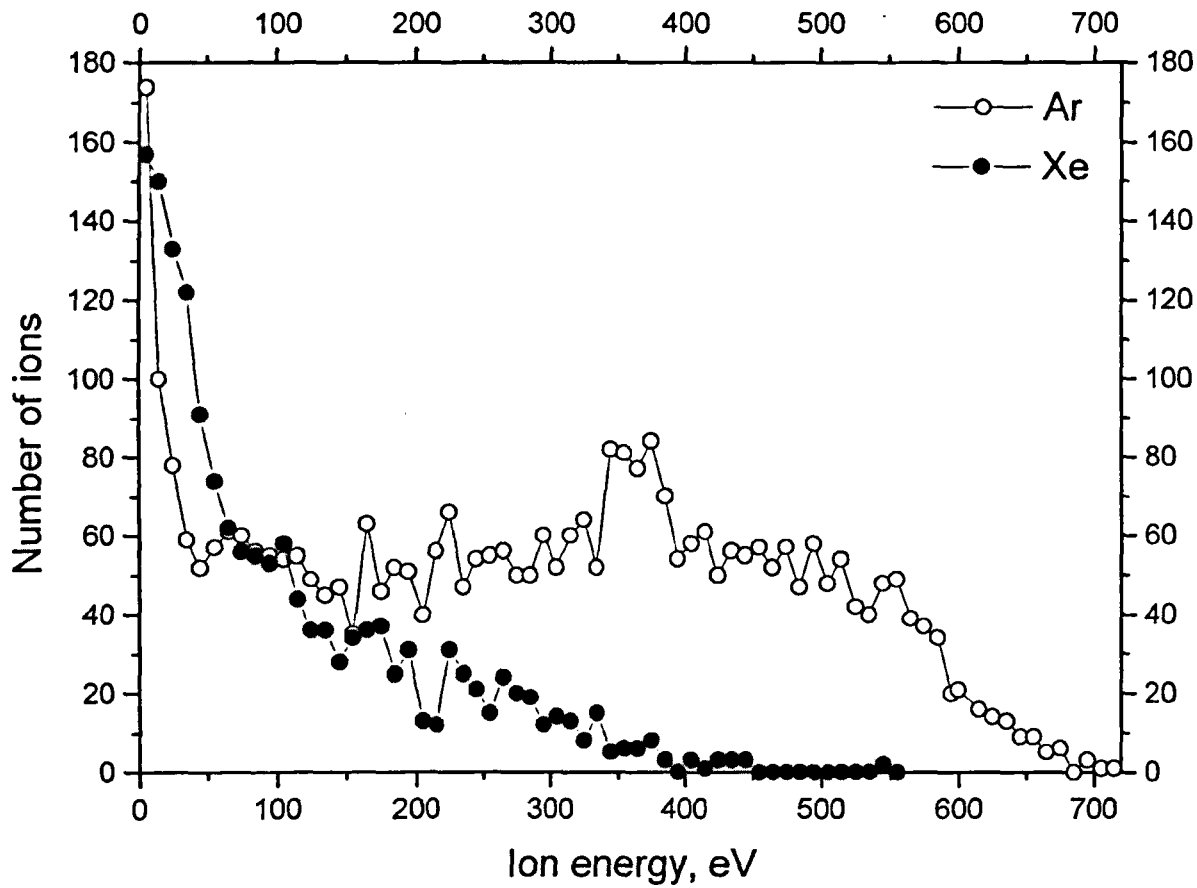

Figure 6.26. Energy distribution of Ar and Xe, back-reflected from Ta target.

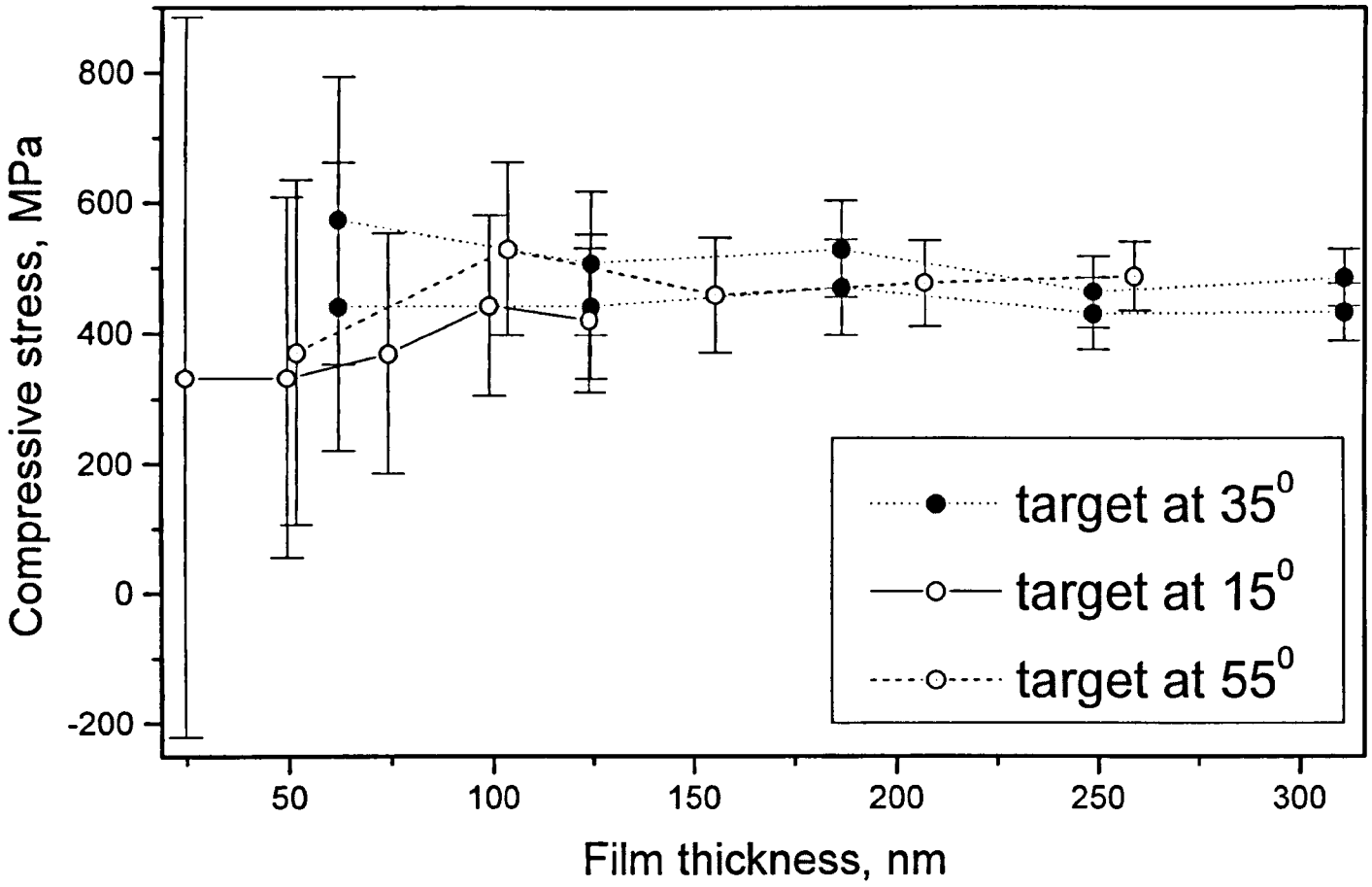

Figure 6.27. Influence of different sputtering beam to target normal angles on stress in thin stoichiometric Ta_2O_5 films.

to 55^0 result in changes in the amount of back-reflected Xe from approx. 10% to 16% and then to 31%, respectively, the stress does not depend on the angle. It can probably be assumed that the change in the ion-to-energetic back-scattered particle arrival ratio due to change in beam-to-target normal angle is not high enough to cause any significant variation of stress levels.

6.2.6. Tantalum Pentoxide Films: Effect of angle of arrival of sputtering flux onto the substrate

It can be seen from Figure 6.28 that stress also does not depend on this parameter. Again, this can, probably, be explained by the dense amorphous nature of ion-beam sputtered Ta_2O_5 films. In this case no morphological changes (for example, changes in the angle of column growth relative to the substrate due to changes in sputtering flux angle, observed for low-density films [see, e.g., Müller, 1989]), which may lead to the stress changes, are expected to take place.

6.2.7. Tantalum Pentoxide Films: Effect of Other Deposition Conditions

To minimise the effect of deposition conditions on stress in Ta_2O_5 films the total working pressure in the deposition chamber was kept constant for all ion-assisted experiments. Therefore, it was necessary to feed in oxygen near the substrate for argon ion bombardment experiments and through the secondary (assisting) ion source for oxygen bombardment experiments. An additional experiment showed that the stress results were dependent on the location of the entry point of the reactive gas, the value being 68 MPa higher when gas is not introduced near the substrate (see Figure 6.29). A further experiment showed that the stress in films was not dependent on the type of grids used in the ion source (carbon grids were used in experiments on the effect of cleaning procedures and molybdenum grids were used in all other experiments, presented in Figure 6.29). It also showed that the stress in films was not dependent on the neutraliser used (Immersed wire neutraliser was used for experiments on the effect cleaning procedures and for one experiment where oxygen was fed in thorough the secondary source. In all other experiments, presented in Figure 6.29, plasma-bridge neutraliser was used.)

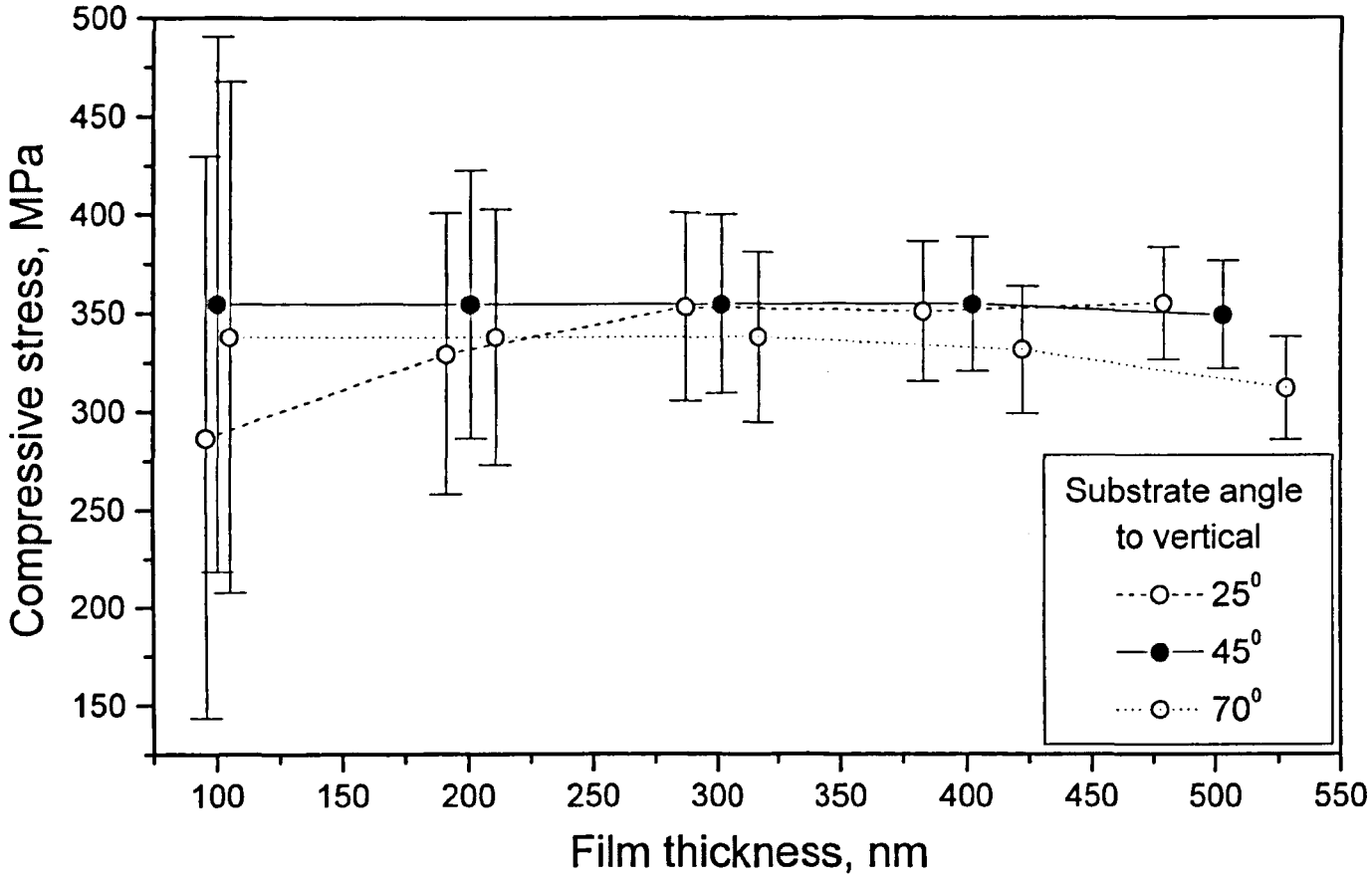

Figure 6.28. Influence of different substrate angles on stress in thin stoichiometric Ta_2O_5 films.

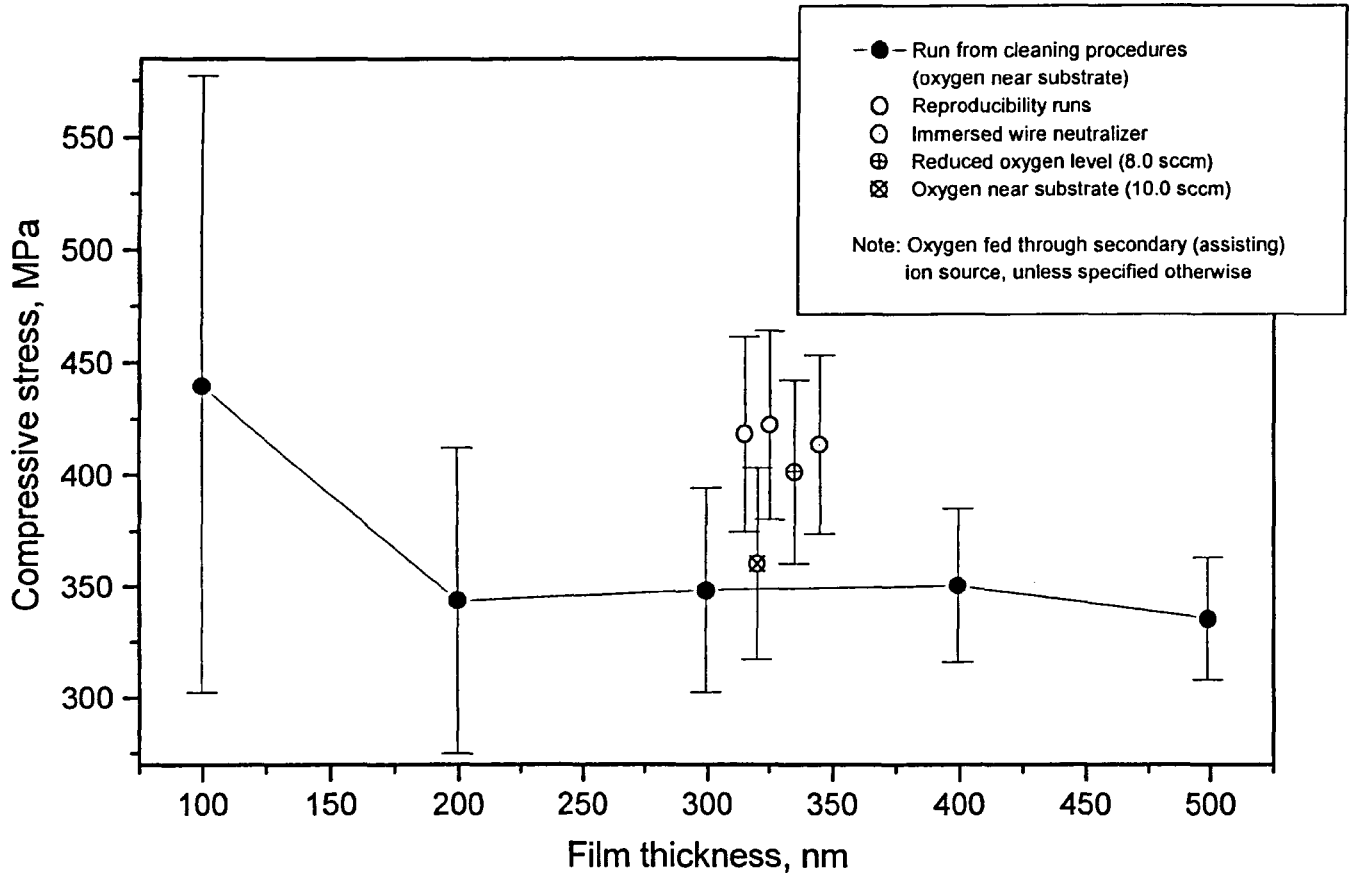

Figure 6.29. Influence of main source grid material (run from cleaning procedures was deposited with C grids, all other runs were deposited with Mo grids), neutralisation type and oxygen feeding method on stress in thin non-assisted Ta_2O_5 films.

6.2.8. Silicon Dioxide Films: Film Composition

The second material studied in this work is silicon dioxide. Some thin films of SiO_2 were deposited from SiO_2 target and others using Si targets. For both targets, conditions for deposition of stoichiometric oxide with reproducible properties were checked in a manner, similar to that employed for the Ta_2O_5 films.

6.2.9. Silicon Dioxide Films: Substrate Cleaning Effect

The results for SiO_2 films are presented in Figure 6.30. Stress in SiO_2 was found to be compressive with its value varying in the region of 658 MPa to 968 MPa for films thinner than approx. 175 nm. With increase in film thickness the stress magnitude saturated to a constant value of approx. 735 MPa. The magnitude of stress does not depend on the type of procedure used for substrate cleaning. For an explanation of such behaviour it is possible to use the same argument, as for Ta_2O_5 films. As for Ta_2O_5 films, SiO_2 films are amorphous and have a high quality, which is shown by the absence of measurable water-absorption-induced stress component upon exposure of the SiO_2 films to ambient air. These amorphous film properties, as well as the known fact that the influence of interfacial stress in SiO_2 films becomes negligible if the film thickness is greater than approx. 23 nm [Jia et al, 2000], can then be used to explain the independence of stress on substrate pre-cleaning procedures. If, in addition, the high density of these films is taken into account, the independence of film stress on thickness can also be explained. Once again, it should be noted that, for low film thickness (in this case less than approx. 175 nm), the deflection of the cantilever substrate is small and measured curvatures and thus calculated stress values contain very large errors in them. Therefore, nothing conclusive can be said about the stress in very thin films.

Stress values, shown in Figure 6.30 are calculated from measurements in the single beam non-scanning stress measurement system configuration and are about 735 MPa. For the film on an oxygen pre-treated substrate the scanning configuration was also used. In this case the mean stress value was calculated as 564 MPa. The difference in the measured stress values clearly shows the deficiency of stress measurement systems of the non-scanning type. Here a small movement of the clamped end of the sample and the sample's initial curvature cannot be measured and taken into account, which leads to errors in results. Therefore, other stress values, reported in this thesis, are calculated from the measurements using the scanning technique.

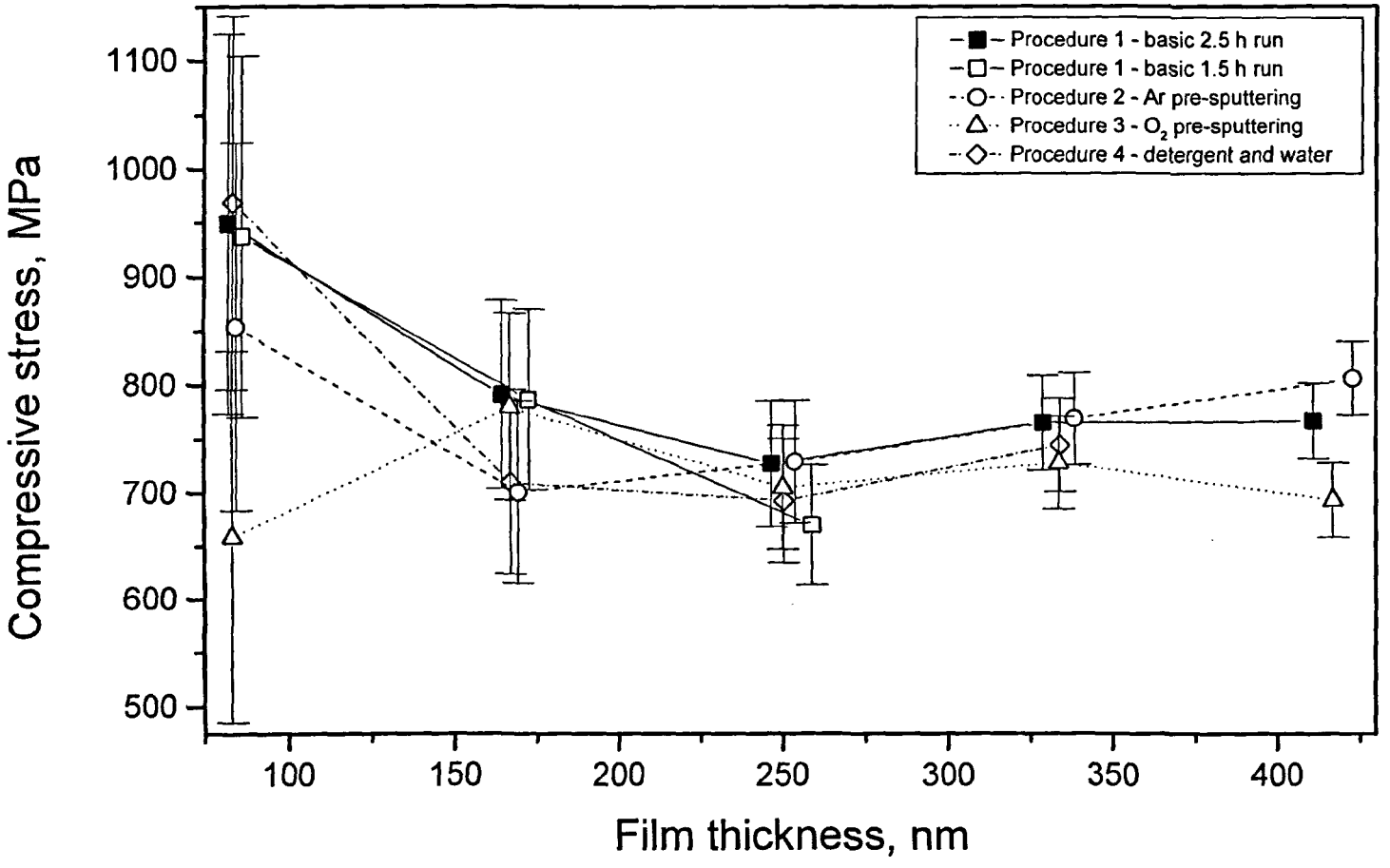

Figure 6.30. Influence of different substrate cleaning procedures on stress in thin stoichiometric SiO_2 films.

It is interesting to compare stress levels in non-ion-assisted Ta_2O_5 and SiO_2 films (350 MPa and 564 MPa, respectively). In their work Strauss et al [Strauss et al, 1997] attributed higher stress levels in SiO_2 films relative to Ta_2O_5 films to more efficient momentum transfer between the energetic gas particles and the film and thus, a better degree of densification. However, in this research films of both materials already have bulk-like density, so the effect of densification is not expected to be significant. Moreover, according to the TRIM simulations for a 1 keV 35^0 beam, only 0.6% of Ar is back-reflected from a SiO_2 target in comparison with 35% from a Ta target, so the growing Ta_2O_5 film will be subjected to a higher degree of bombardment. Therefore, although bombardment and bombardment-induced densification may play some part in the difference between the stress values of SiO_2 and Ta_2O_5 films, other origins, intrinsic to films (e.g., difference in argon incorporation) or indeed basic properties (e.g, molar volume 53.9 cm^3 for Ta_2O_5 and 2.27 cm^3 for SiO_2) of the materials, should, probably, be taken into account.

6.2.10. Silicon Dioxide Films: Effect of angle of arrival of sputtering flux onto the substrate

The influence of the angle of arrival of sputtered particles to substrate on film stress was checked in the next experiment, the results of which are plotted in Figure 6.31. It can be seen that the angle of arrival of the flux of sputtered particles does not have any significant influence on the stress in SiO_2 films. This result is in agreement with the work of Leplan et al [Leplan et al, 1996] (see Chapter II), who found that, even for the case of evaporated SiO_2 the stress does not depend on evaporation flux angle or film thickness. Again, the explanation of this behaviour can be similar to that for Ta_2O_5 films, i.e. the stress does not change because there are no significant morphological changes in the dense amorphous nature of the SiO_2 films.

6.2.11. Silicon Dioxide Films: Effect of total working pressure

The analysis of experimental results, available from the published literature (see Chapter II) showed, that film stress can strongly depend on the pressure in the deposition chamber. Increase in total deposition pressure leads to a decrease in the mean free path of the sputtered atoms, so these atoms experience more collisions on their way to the substrate. This mechanism not only leads to a decrease in the film growth rate,

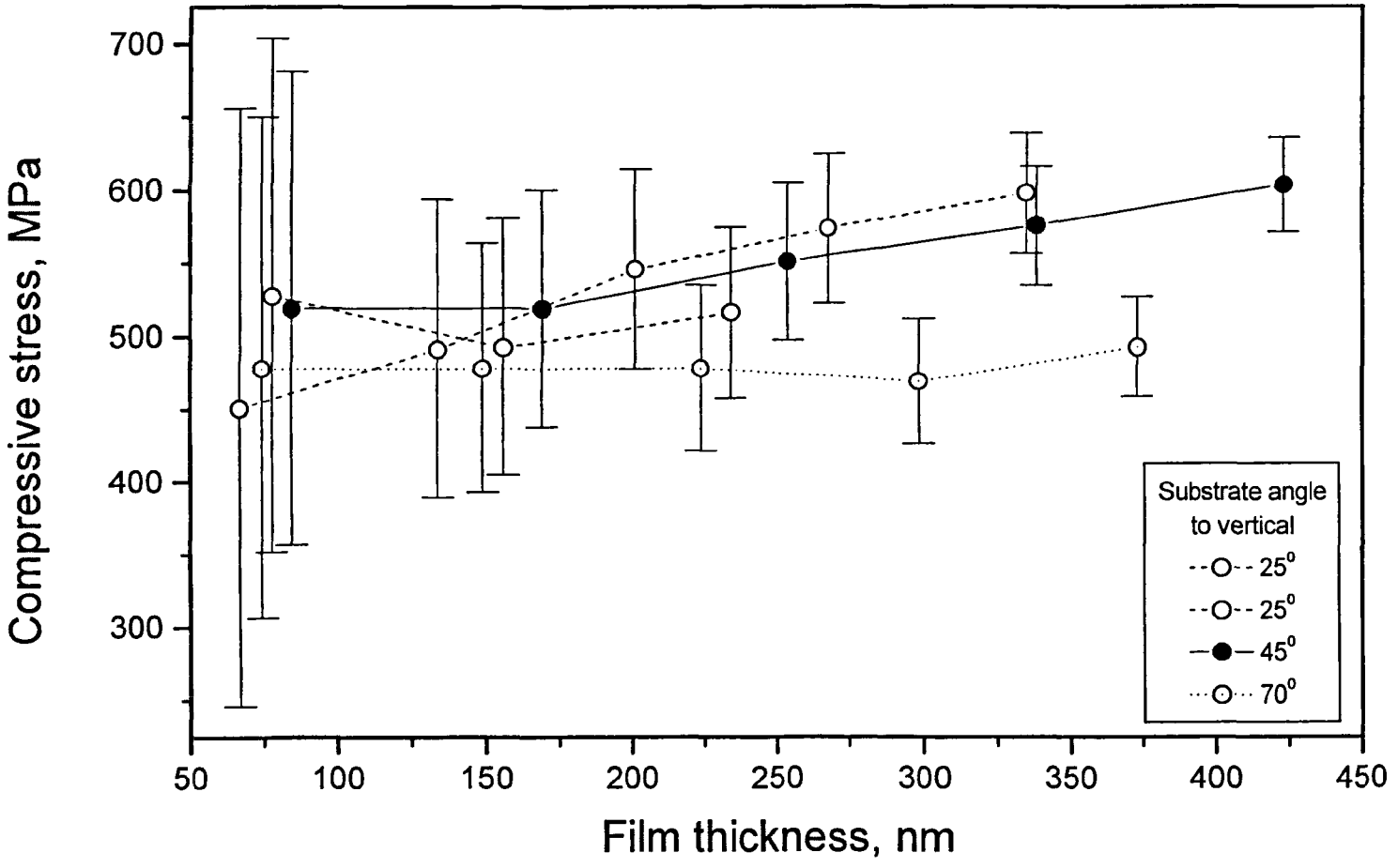

Figure 6.31. Influence of different substrate angles on stress in thin stoichiometric SiO_2 films.

but also results in a decrease in the energy and mobility of arriving atoms, leading to a porous film structure and, often, a decrease in compressive stress levels. It is known that the average mean free path at $1x10^{-3}$ mbar is approximately 50 mm. In this study the pressure was varied from $1.2x10^{-4}$ mbar to $1.0x10^{-3}$ mbar. The resulting influence on the mean free path is presented in Figure 6.32. It can be clearly seen that, for the first three values of total deposition pressure, the mean free path is larger than the target-to-substrate distance, therefore, no significant changes in the atomic energy and mobility and, thus, in stress levels in the films, are expected. For the highest pressure value the mean free path is smaller than the target-to-substrate distance, therefore, many sputtered atoms would experience collisions on their way to the substrate and thus lose some of their energy. In this case an effect on film stress is possible. Compressive stress values, measured in SiO_2 films, deposited under various total deposition pressures, are presented in Figure 6.33. From this figure it can be concluded that the stress level in SiO_2 films does not depend on the deposition pressure in the range studied. Although no effect on stress value was observed, some effect of the deposition pressure on film thickness can be noted in Figure 6.33. Indeed, a film, deposited at $1.0x10^{-3}$ mbar pressure exhibits a lower thickness value than films, deposited at lower pressures, which is in agreement with the argument on the mean free path, presented above.

6.3. Stress measurements in ion-assisted films

So far, it was found that, apart from sputtering gas and location of reactive gas entry, none of the studied deposition parameters (cleaning procedures, angle of incidence of ions or atoms, deposition pressure, type of neutralisation or ion source grid material) have any measurable influence on stress levels in ion-beam sputtered stoichiometric non ion-assisted films of both materials. The influence of energetic oxygen or argon ion bombardment during deposition onto stress levels in evaporated and ion-beam sputtered films was studied next. The results of these studies for ion-assisted SiO_2 films (evaporation and ion assistance) are presented in Figure 6.34. The results for dual ion-beam sputtered films (sputtering and ion assistance) of Ta_2O_5 films are presented in Figure 6.35 (argon bombardment) and Figure 6.36 (oxygen bombardment). In the case of dual ion-beam sputtered SiO_2 films results are presented in Figure 6.37 and Figure 6.38 for bombardment with argon and oxygen ions, respectively.

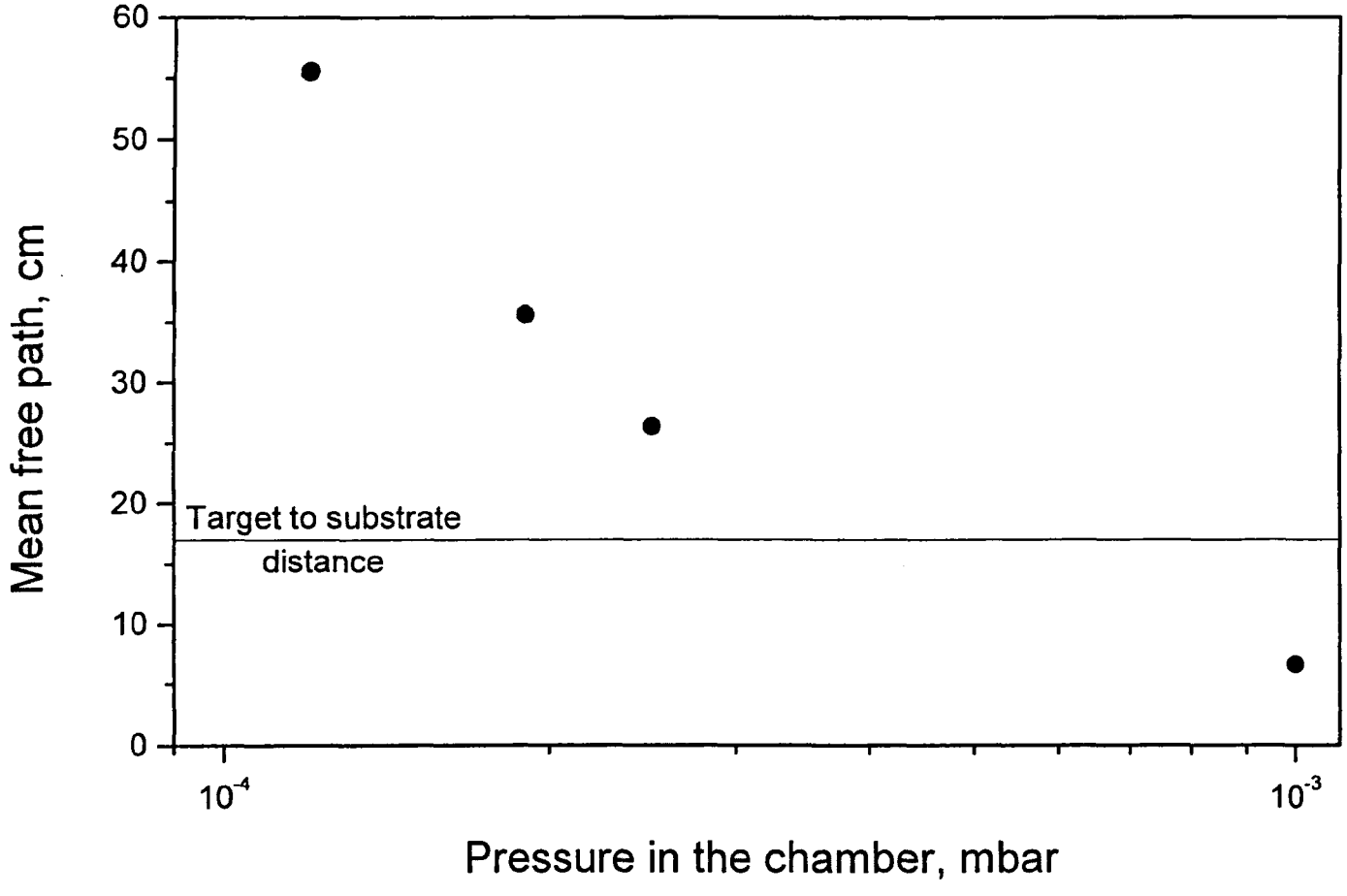

Figure 6.32. Mean free path in the deposition chamber at different total pressure values.

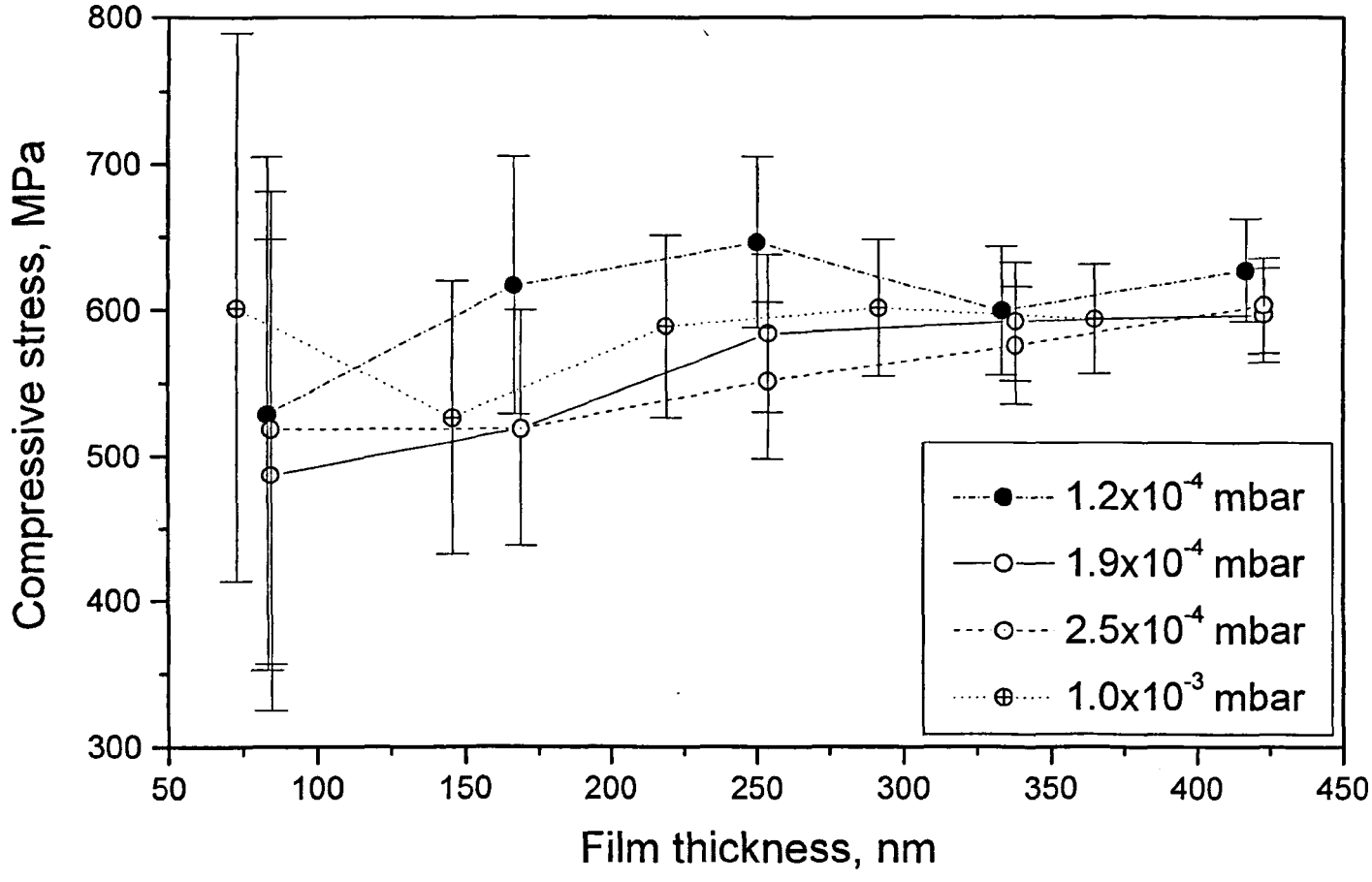

Figure 6.33. Influence of different total deposition pressure values on stress in thin stoichiometric SiO_2 films.

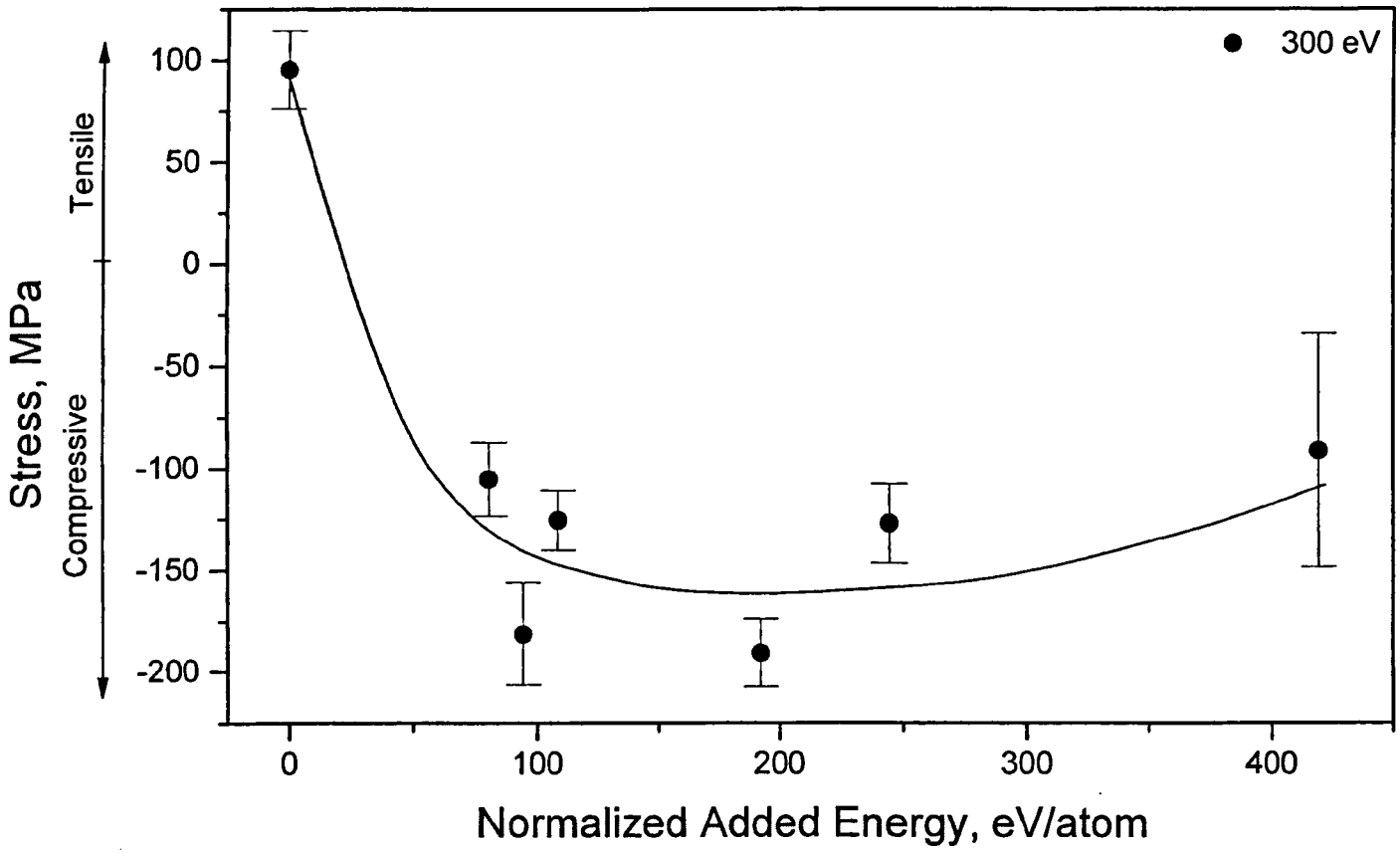

Figure 6.34. Influence of argon ion bombardment on stress in thin evaporated stoichiometric SiO_2 films. Circles represent experimentally measured values. Line is drawn to guide the eye only.

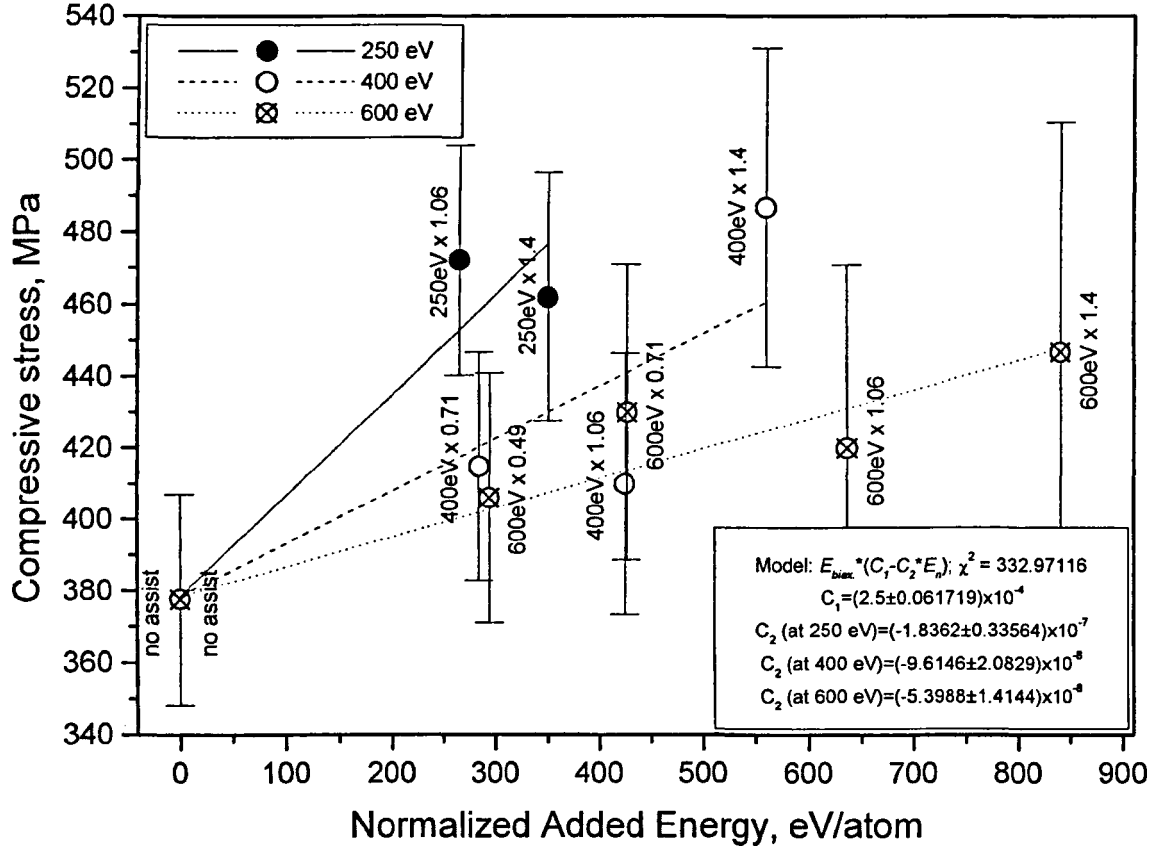

Figure 6.35. Influence of argon ion bombardment on stress in thin stoichiometric Ta_2O_5 films. Circles represent experimentally measured values. Lines represent stress values, obtained by model fitting procedure. Numbers after multiplication sign are the ion-to-atom arrival ratios used.

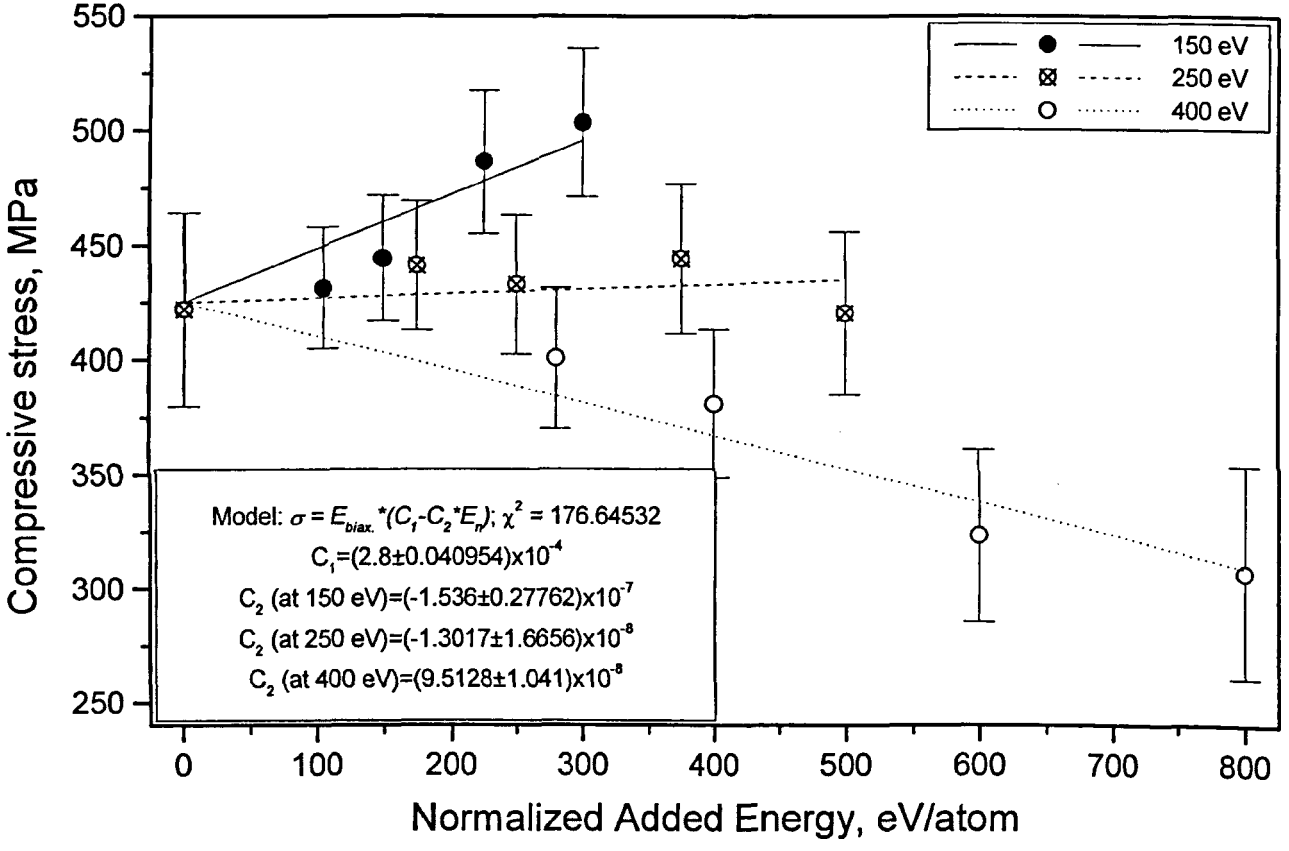

Figure 6.36. Influence of oxygen ion bombardment on stress in thin stoichiometric Ta_2O_5 films.

Circles represent experimentally measured values. Lines represent stress values, obtained by model fitting procedure.

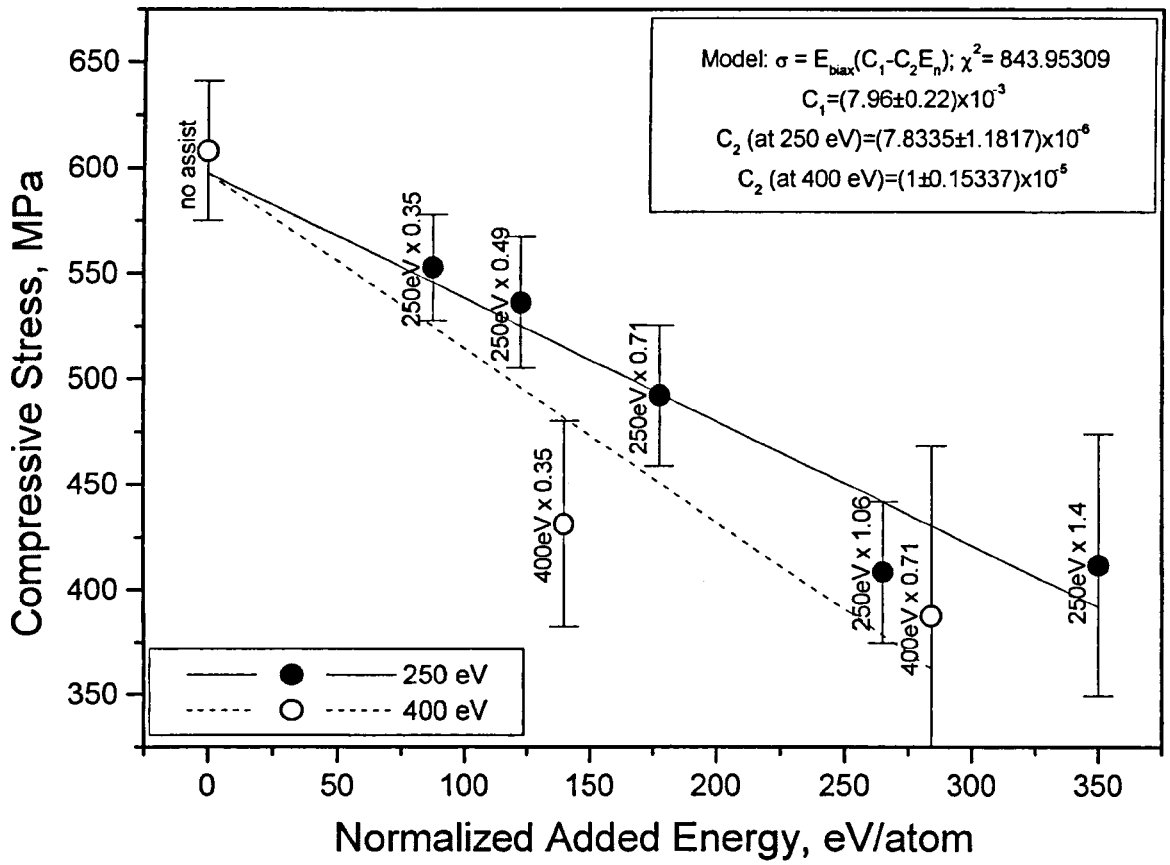

Figure 6.37. Influence of argon ion bombardment on stress in thin stoichiometric SiO_2 films. Lines represent model fitting of the experimental data. Numbers after multiplication sign are the ion-to-atom arrival ratios used.

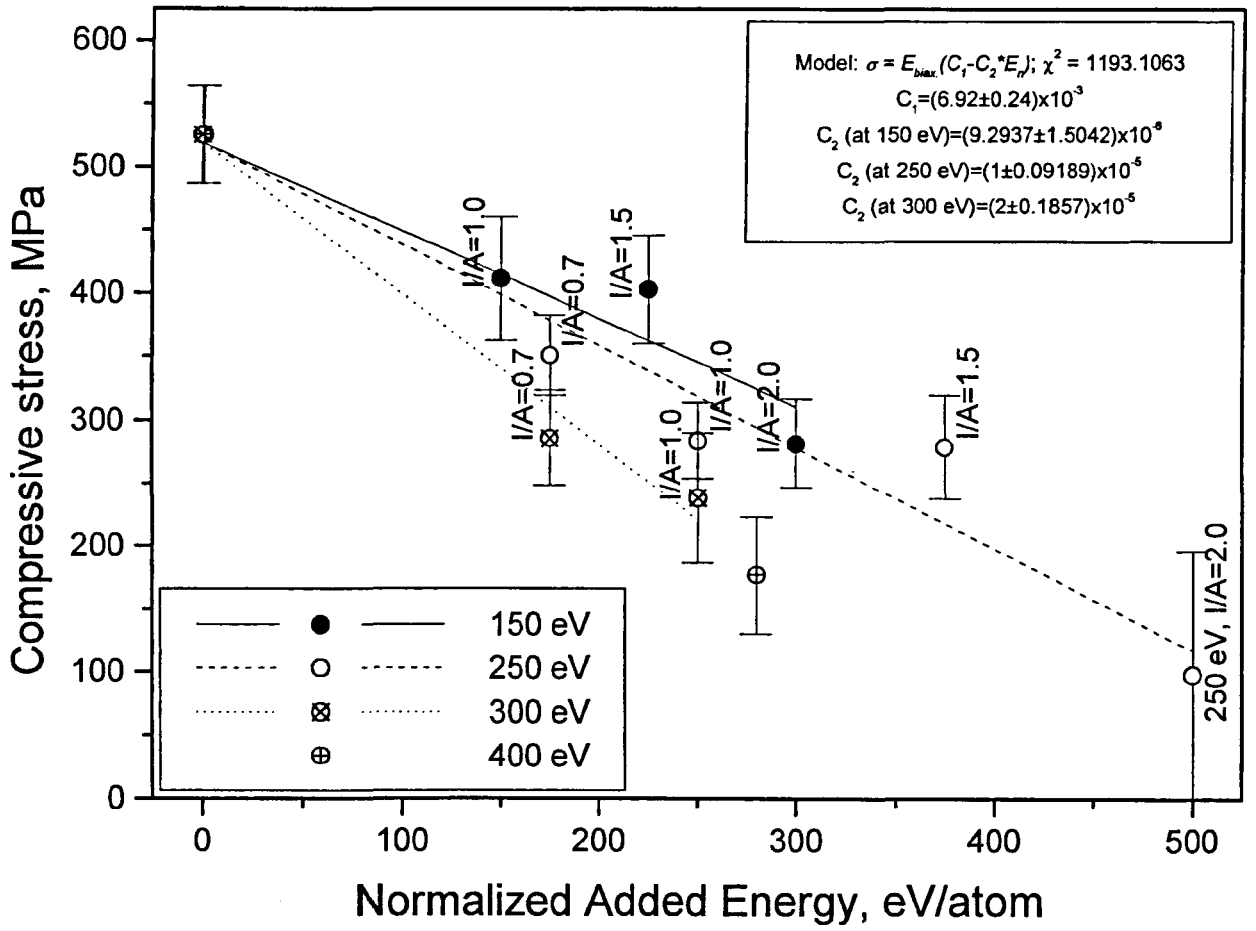

Figure 6.38. Influence of oxygen ion bombardment on stress in thin stoichiometric SiO_2 films. Lines represent model fitting of the experimental data.

6.3.1. Argon-assisted Evaporated SiO_2 films

The results of stress measurements on purely evaporated silicon dioxide films show the presence of low-level (100 MPa) tensile stress in the film (see Figure 6.34). Ion bombardment with 300 eV Ar^+ ions leads to a transition of film stress from tensile to compressive. All evaporated films, deposited under concurrent ion bombardment in this research, show compressive stress with a maximum level of 200 MPa. From the measured values it is unclear whether the stress saturates or slowly decreases with increase in normalized added energy of bombardment. However, further experimental research into this problem is prevented by high film re-sputtering rates, leading to low film thickness and thus very large measurement errors, which is clearly demonstrated in Figure 6.34. Film stress values are within reasonable agreement with other values, reported in the literature (see Chapter II).

At this point it is useful to briefly recall the known facts of stress behaviour in ion-assisted films. Tensile film stress under no ion assistance and stress transition from tensile to compressive regions with ion bombardment are commonly observed in evaporated and ion-assisted films. At the moment, it is generally agreed that, during evaporation onto an unheated substrate, the mobility of atoms forming the film is low. Thus, a purely evaporated film will have low density and a high number of voids, which favours the formation of tensile stress. In addition, such films will not be able to sustain stresses of high magnitude. Ion bombardment brings additional energy to the growing film, so that the mobility of film atoms increases. This leads to film densification, disappearance of voids and forward recoil implantation, which favours tensile stress relaxation/compressive stress generation. In addition, films of higher density become able to sustain high levels of stress in them. On this basis, it can be predicted that evaporated films will exhibit low tensile stress, which decreases and becomes compressive with increase in ion bombardment. Indeed, such behaviour was clearly demonstrated by argon-assisted evaporated silicon dioxide films in this research programme.

6.3.2. Argon-assisted Sputtered Tantalum Pentoxide Films

The results of measurements on argon-bombarded Ta_2O_5 films (Figure 6.35) show that the film stress is compressive (determined by the direction of sample bending). The stress magnitude slowly increases with increase in normalised energy of bombarding

argon and is in the region of 380 to approx. 490 MPa. It can also be said that with increase in ion-to-atom arrival ratio the film stress increases. Bombardment with ions of lower energy but higher dose also leads to an increase in stress magnitude.

The similarities in the behaviour of stress and argon incorporation into the film should be mentioned. In agreement with the stress trends in Figure 6.35, the amount of argon, present in Ta_2O_5 films of this experiment (see Figure 6.1), increases with increase in normalised energy. At this stage, it is unclear whether such behaviour is simply a consequence of the increase in ion bombardment or one of the causative factors of stress generation.

XPS studies showed that both preferential oxygen sputtering and formation of sub-oxides do occur in the film subjected to Ar ion bombardment. Conditions in the deposition chamber differ from those in the XPS chamber by the presence of oxygen gas in the former, which could lead to immediate film re-oxidation. No systematic or significant changes in film composition due to concurrent Ar bombardment were observed by RBS, but these facts cannot lead to the total elimination of the hypothesis that the formation of sub-oxides happens on a scale below the detection limit of the measurements. However, initial stress/composition analysis of Ta_2O_5 films (Figures 6.20-6.22) showed that film stress rapidly reaches a saturation value with increase in oxygen concentration in the coating, therefore, very small compositional changes (if indeed taking place) are highly unlikely to cause significant stress variations.

It would be interesting to estimate the influence of densification and atomic peening on film stress. However, it is not clear if a simple model by Windischmann [Windischmann, 1987], which predicts stress increase proportional to ion dose and square root of ion energy, can be applied in this case. Figure 6.6 clearly shows significant film re-sputtering due to ion bombardment. This places these Ar-assisted Ta_2O_5 films above the upper limit of the Windischmann formula applicability (see Chapter III).

6.3.3. Oxygen-assisted Sputtered Tantalum Pentoxide Films

The effect of preferential sputtering is expected to be less important for concurrent oxygen bombardment of Ta_2O_5 films. In this case oxygen will still be preferentially removed from the coating, but at the same time additional oxygen ion implantation should lead to tantalum oxidation leading to a fully stoichiometric film. The results of stress measurements in this case are presented in Figure 6.36. Film stress is compressive

and varies in the region of approx. 300 to 500 MPa. It can be seen that ion energy is a very important parameter in governing stress behaviour. Film bombardment with 150 eV oxygen ions of different ion-to-atom arrival ratio leads to an increase in compressive stress. If 250 eV ions are chosen for bombardment the stress levels are found to be almost constant. Further increase in ion energy up to 400 eV leads to a decrease in stress levels with increase in normalised energy of bombardment and ion-to-atom arrival ratio. Again, it would be interesting to compare stress behaviour to the film composition. Figure 6.4 shows that, with an increase in normalised energy, argon incorporation into the films, bombarded with 400 eV oxygen ions, increases. For other films (except the film, deposited at 250 eV, I/A=2.0 bombardment) argon levels do not exhibit significant changes. Thus, for argon-assisted films both the stress magnitude and argon content in the film increase with increase in normalised energy of bombardment. In 400 eV oxygen-assisted films with increase in normalised energy the argon incorporation increases and the stress decreases. This difference in the behaviour of stress and argon content leads to the conclusion that inert gas incorporation into Ta_2O_5 films is not the main mechanism behind stress generation and thus cannot solely explain stress behaviour.

6.3.4. Argon-assisted Sputtered Silicon Dioxide Films

The results of experiments on argon bombardment of SiO_2 films (Figure 6.37) show that, with increase in normalised energy of bombardment, the compressive stress decreases. For a fixed energy with increase in ion-to-atom arrival ratio the stress decreases. For a fixed ion-to-atom arrival ratio an increase in the energy of bombarding ions leads to a decrease in stress magnitude. Results of compositional analysis (Figure 6.2) show that with the increase in normalised energy of argon bombardment, argon incorporation into the film increases and reaches a saturation value of approx. 0.045 Ar/Si. However, saturation in stress is not observed. It can also be seen that, for less energetic ions, the Ar content increase is more rapid than for higher energy ions.

6.3.5. Oxygen-assisted Sputtered Silicon Dioxide Films

The last experiment on ion-beam sputtered ion-beam assisted films was performed for oxygen-bombarded SiO_2 films. It was found (Figure 6.38) that the stress in all films is compressive. With increase in normalised energy of ion bombardment the stress

decreases from approx. 525 MPa to the levels below the resolution of the stress measurement system. It is hard to perform accurate stress measurements for ion bombardment at normalised energies greater than approx. 350 eV due to significant film re-sputtering, which leads to extremely low growth rates, small deflections and high errors. However, some points (for example, stress for 250 eV, I/A=2.0 bombarded films) are shown on the graph for clear representation of the trends in stress behaviour. It was found that oxygen bombardment leads to the appearance of an argon impurity in SiO_2 films (Figure 6.5). Argon incorporation in this case is small (0.02 Ar/Si). As in the case of Ta_2O_5 films, it is believed that such impurity is due to the back-streaming of Ar into the secondary (assisting) source.

Thus, it can be summarised that, in the case of SiO_2 films, bombardment with both argon and oxygen ions leads to a decrease in stress levels. Argon bombardment leads to an increase in argon incorporation into the coating. Oxygen bombardment leads to a lower level of argon incorporation into the coating. Again, it can be said that from the analysis of these results it can be concluded that Ar incorporation has a negligible (if any) effect on film stress and it is the energy and ion-to-atom arrival ratio of bombarding ions, which is the predominant factor governing stress behaviour.

6.3.5. Proposed Model of Stress Behaviour with Ion Bombardment

The complex stress behaviour with normalised energy in case of Ta_2O_5 films and stress relaxation with ion bombardment in case of SiO_2 films, lead to the conclusion that there is not just one simple mechanism of stress generation, but rather there are two competing mechanisms: one is responsible for stress generation and the other is responsible for stress relaxation. The balance between the two mechanisms will depend on the film properties and the amount of ion bombardment and will determine the stress magnitude under each set of deposition conditions. The only model which accounts for such an effect is the Davis model [Davis, 1993]. This model is not only qualitatively based on the hypothesis of competing mechanisms, but also gives a formula for quantitative evaluation. The mechanism, responsible for stress generation in this model, is atomic peening. Stress relaxation is the effect of atomic re-arrangements during thermal spikes, caused by ion bombardment. In recent studies of thermal spikes [Cheng, 1990], however, it is stated that "thermal spikes cannot form in low atomic number (Z) solids". It is stated that, in order for the thermal spike to form, the atomic number Z

should be more than 20. Silicon dioxide, with its components having atomic numbers of 14 and 8 for Si and O, respectively, does not satisfy this condition. Therefore, thermal spikes are not expected to form in silicon dioxide, so stress relaxation cannot be explained by atomic re-arrangements due to thermal spikes. This argument leads to the conclusion that, in the case of ion-assisted silicon dioxide coatings, the Davis model is not applicable. However, it cannot be denied that some film atoms will acquire additional energy due to ion bombardment. It was shown by Koster and Urbassek [Koster and Urbassek, 2002] that movements of such "energised" atoms can also lead to film stress changes. The Davis model has another deficiency. According to the prediction by the Davis model, as the normalised energy of bombardment tends to zero the stress sharply decreases to zero. However, in the present study it was found that, in the absence of additional ion bombardment, films of both materials are compressively stressed.

The study of stress in films of both materials due to argon and oxygen bombardment shows three main features:

1. all ion-sputtered films are in a state of non-zero compressive stress in the absence of additional ion bombardment;
2. ion bombardment can lead to an increase in compressive stress in the coating (for example, in argon-assisted Ta_2O_5 films), and
3. ion bombardment can also lead to a decrease in compressive stress levels in the coatings (for example, in SiO_2 films or in Ta_2O_5 films, assisted with 400 eV oxygen ions).

All these features have to be accounted for in a model of stress evolution with ion bombardment. Features 2 and 3, most probably, mean that two competing mechanisms are acting in the film. One mechanism is responsible for compressive stress generation, while the other one is responsible for stress relaxation. Such hypothesis is not unique and is used, for example, in the Davis model.

The mechanism behind compressive stress generation is well-established. Compressive stress is the result of forward sputtering of surface atoms into the film bulk, or atomic peening. However, Koster and Urbassek [Koster and Urbassek, 2002] showed, that conditions exist, when forward-sputtered atoms can lead to stress relaxation. These conditions include the initial stress state of the bombarded object (forward sputtered atoms can relax stress in an initially compressively stressed specimen) and the energy of bombarding ions (energy, transferred to the forward sputtered atom, has to be high

enough to allow relaxation of the atom surroundings). Thus, only a fraction of forward-sputtered atoms will lead to compressive stress generation.

Ion bombardment does not only produce forward sputtered recoils. Ions of sufficient energy generate displacements on their way into the film bulk, which can cause interstitial recoils to move into normal sites. Vacancies and backward-sputtered recoils can also be generated. It is not unreasonable to assume that, in already compressively stressed amorphous material, production of backward-sputtered recoils will lead to removal of some of the excess atoms from the film bulk towards the film surface, thus the compressive stress will be relaxed. Indeed, such hypothesis is again supported by the studies of ion-bombarded amorphous silicon performed by Koster and Urbassek [Koster and Urbassek, 2002]. The effect of compressive stress-generating recoils in any film, subjected to ion bombardment, will compete with the effect of stress-relaxing forward and backward recoils. Total stress in the film would be a result of such competition. Steady-state total recoil density can be calculated as [Carter, 1994]

$$\frac{N_R}{N} = \alpha \frac{0.42}{E_d} \frac{I}{A} E_i, \tag{6.4}$$

where α is a proportionality factor and E_d is the displacement energy. In the case of significant film re-sputtering this equation takes the form of [Carter, 1994]

$$\frac{N_R}{N} = \beta \frac{0.42}{E_d} \frac{I}{A} \left(1 - \frac{I}{A} Y_f\right)^{-1} E_i, \tag{6.5}$$

where β is a proportionality factor and Y_f is the sputtering yield of the film material. The density of recoils, which lead to changes in stress magnitude $\left(\frac{N_R}{N}\right)'$ can then be assumed to be

$$\left(\frac{N_R}{N}\right)' = C(E_i) \frac{N_R}{N}, \tag{6.6}$$

where $C(E_i)$ is the proportionality coefficient, which depends on ion energy.

Experiments showed that, even under zero bombardment conditions, films of both materials exhibit compressive stress. The value of this initial stress is hard to predict but, generally, it will depend on the materials of film and substrate, film state, deposition technique and conditions. All these conditions will lead to some balance of the positions of the atoms in the film bulk. Denote this initial film state, leading to compressive stress under zero ion bombardment, as C_1'. Ion bombardment leads to the formation of forward and backward recoils. The amount of the recoils, which change the initial film state and also have an effect on film stress, is $\left(\frac{N_R}{N}\right)'$. Thus, the state of the ion-bombarded film can be expressed as $C_1' - \left(\frac{N_R}{N}\right)'$. Strain ε in the film will be proportional to this quantity, i.e. $\varepsilon \propto C_1' - \left(\frac{N_R}{N}\right)'$. Assuming that stress σ and strain in the film are related as $\sigma = \frac{E_f}{1-\nu_f}\varepsilon$, where E_f and ν_f are the Young's modulus and Poisson ratio of the film material, it can be said that

$$\sigma = \frac{E_f}{1-\nu_f}\left(C_1 - C(E_i)\alpha\frac{0.42}{E_d}\frac{I}{A}E_i\right) = \frac{E_f}{1-\nu_f}(C_1 - C_2(E_i)E_n). \qquad (6.7)$$

Here C_1 and $C_2(E_i)$ are proportionality factors, related to the initial film state and the modification of stress by ion bombardment, respectively.

Thus, compressive stress in ion-bombarded films depends on the initial stress for a non-assisted film and the balance of the effect of forward and backward recoils. If the stress magnitude only is considered, formula (6.7) predicts that, in the case of zero ion bombardment ($E_n = 0$), stress is proportional to the initial state of atoms in the film. The effect of ion assistance depends on the energy of bombarding ions. If the bombardment conditions are such, that $C_2 > 0$, film stress relaxes. For conditions, leading to the values of $C_2 < 0$ additional compressive stress in the film is generated.

Such an approach is, however, simplistic, as there are many parameters, which are not taken into account to by the formula (6.7). For example, the effect of incorporated inert gas species (if this exists) and the effect of compositional changes, that can take place during compound bombardment due to preferential sputtering, are neglected. Thus, the

formula (6.7) has several applicability limits. In addition to the limitations already mentioned, it should be taken into account that the film is assumed to be amorphous and dense, and that the effect of densification can be neglected. Although the formula (6.7) is based on only one variable E_n, it should not be forgotten that additional normalized energy is the product of bombarding ion energy and ion-to-atom arrival ratio. Thus, the formula (6.7) would not be applicable for ion bombardment with energy below the threshold (or atomic displacement energy) limit. Plasticity effects will not be accounted for by this model, thus film stress should be within limits which satisfy the linear law of elasticity.

Performance of this simple model, presented above, was tested by least-squares fitting of the formula (6.7) to the experimental values of stress, obtained in this research. Unknown proportionality factors C_i (i=1,2) were used as fitting parameters in the Levenberg-Marquardt fitting routine, built into the MicroCal Origin software. The values of elastic constants were taken as 1549.4 GPa [Tien et al, 2000] for Ta_2O_5 films and as 75 GPa for SiO_2 films. The results of the model fitting are presented in Figures 6.35-6.38. It can be seen that in all cases the agreement between the model and the experimental values is reasonable. The model correctly shows an increase in stress values for argon-assisted Ta_2O_5 films and complicated behaviour for stress in oxygen-assisted Ta_2O_5 films. The model also correctly shows stress relaxation in argon and oxygen bombarded SiO_2 films.

Thus, it can be concluded that the effect of ion bombardment on stress in thin films depends on the film material and ion nature, ion energy and ion-to-atom arrival ratio and on the stress state of the original non ion-assisted film. All effects, ranging from compressive stress generation to compressive stress relaxation, have been experimentally observed. In close agreement with the results of numerical simulations by Koster and Urbassek [Koster and Urbassek, 2002], stress behaviour can be explained by a simple model. This model presumes that, under conditions of zero ion bombardment, film stress is compressive. Film stress can be relaxed by backward recoils. Film stress can also be relaxed by forward recoils, generated by bombardment with ions of energy above some threshold value. Bombardment with low (below threshold value) energy ions will lead to compressive stress producing forward recoils. The net stress value, observed in the films will depend on initial stress state and ion energy (via the balance of the effects of recoils). It can be said that for ion-beam sputtered films in this research the proposed model can correctly show the trends in stress behaviour under ion bombardment. Quantitative predictions are complicated by

the fact, that model parameters are unknown. These parameters can be determined by least-squares fitting of the model to experimental data. However, more research and analysis is needed in order to verify the model performance for films of different materials deposited by different techniques.

6.4. Optical properties of ion-assisted films

Optical properties of both Ta_2O_5 and SiO_2 films, assisted during growth with a beam of argon or oxygen ions, were studied. Analysis of reflectance curves yield not only data on film thickness, but also information on film refractive index and extinction coefficient and their dispersion behaviour. For the ease of analysis of the optical constants behaviour with ion bombardment and clear presentation of the results of both stress and optical constants measurements it was chosen not to use full dispersion curves, but to plot n and k values at a fixed wavelength versus normalised energy of bombardment. It was found that trends in refractive index behaviour do not change with the wavelength, so only data for 500 nm wavelength are shown in the figures.

Several mechanisms can influence film optical behaviour and calculated values of film optical constants. One of such mechanisms is the variation in surface roughness. As the roughness increases, scattering of the incident light from the film surface also increases. This light is scattered in various directions, which can lead, for example, to lower intensity readings for the reflected beam. Analysis of data, obtained from samples of different roughness, will lead to different values of film optical constants. Thus, the possibility of influence of such a mechanism needs to be taken into account.

In this research film surface roughness was measured by using atomic force microscopy (AFM). Only four tantalum pentoxide films were analysed. These films were a non ion-beam assisted Ta_2O_5 sample, and samples of argon-assisted Ta_2O_5 coatings, deposited under 400 eV (I/A=0.71 and I/A=1.4) and 600 eV (I/A=0.71) argon bombardment. The results of these measurements are presented in Figure 6.39. It can be seen that, for the non ion-assisted film no surface pattern is observable. Ion bombardment leads to the appearance of a characteristic ripple pattern on the film surface (the best example is the 600 eV I/A=0.71 Ar^+ bombarded film). The average film roughness also changes with changing deposition conditions (the values are 3.28 ± 0.3 nm for the non-assisted film, 2.69 ± 0.3 nm for 400 eV I/A=0.71; 3.95 ± 0.11 nm for 400 eV I/A=1.4 and 4.69 ± 0.12 nm for 600 eV I/A=0.71 Ar bombarded films). It is therefore possible that the film

a) non ion-assisted film

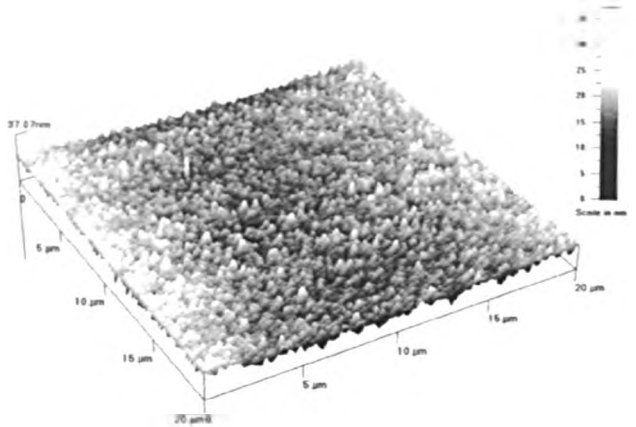

b) Ar^+ 400 eV I/A=0.71

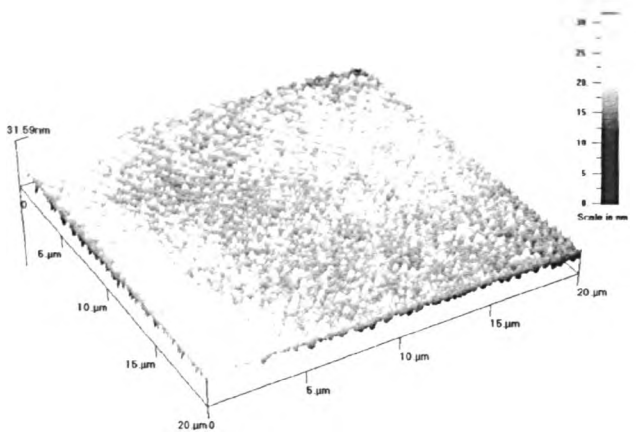

c) Ar^+ 400 eV I/A=1.4

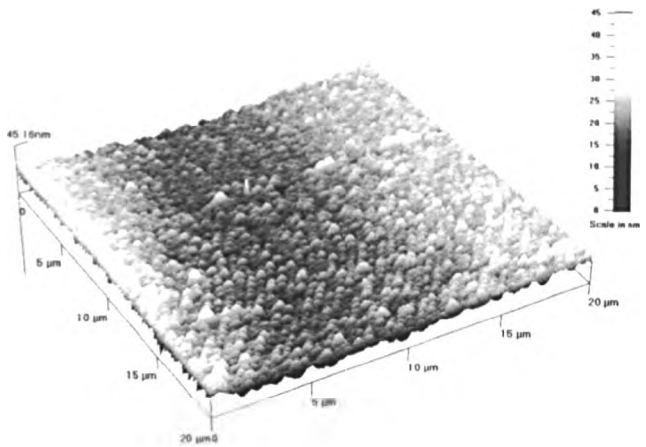

d) Ar^+ 600 eV I/A=0.71

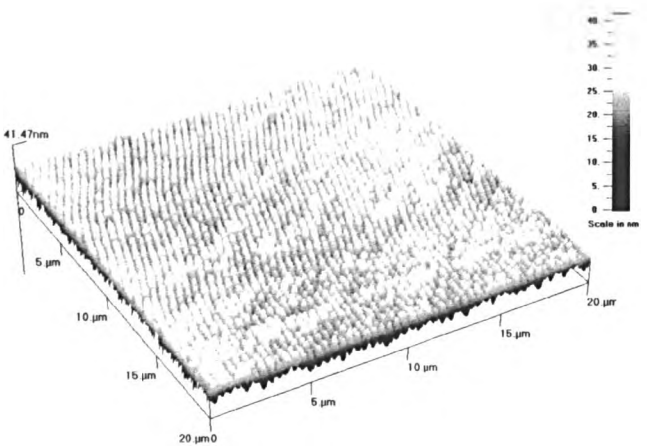

Figure 6.39. AFM images of the surface of selected Ta_2O_5 films.

surface roughness may have some influence on the measured film optical properties in this work. However, at the moment it is unclear how to estimate the magnitude and influence of this parameter on the measured values of optical constants.

Probably the most important mechanism, which can effect the values of optical constants, is film composition. For example, not fully oxidised films often show an increase in the extinction coefficient due to the high absorbance by excess metal or silicon atoms. If impurities are present in the film, the refractive index can also change significantly. For films, composed of different materials, the refractive index n_{comp} can be calculated using one of the well-known models [Feldman et al, 1986; Cevro, 1994]

$$n_{comp} = An_A + Bn_B, \tag{6.8}$$

$$n_{comp}^2 = An_A^2 + Bn_B^2 \text{ or} \tag{6.9}$$

$$\frac{n_{comp}^2 - 1}{n_{comp}^2 + 2} = A\frac{n_A^2 - 1}{n_A^2 + 2} + B\frac{n_B^2 - 1}{n_B^2 + 2}. \tag{6.10}$$

Here n_A and n_B are the refractive indices and A and B are atomic fractions of materials a and b. The first model is known as the linear model, the second is the Drude model and the third is the Lorentz-Lorentz model.

First consider an example of a not fully oxidised silicon dioxide film. A crude approximation would be a film, which consists of some SiO_2 and a small fraction of pure silicon. Calculations by the linear model using values of refractive index of 1.46 for SiO_2 and 4.446 for Si (measured at the 500 nm value for the silicon substrate used in this research) show that a change in the film refractive index of 0.01 would be caused by changes in film composition of approx. 0.9%.

Now consider an example of impurity influence on film refractive index. Let the film of silicon dioxide contain a small amount of iron oxide FeO. Pure silicon dioxide has a refractive index of 1.46. Iron oxide has a refractive index of 2.32 [Weast, 1974]. If the linear model is used, it can be easily shown that a change in the refractive index of 0.01 would be caused by a change in the FeO concentration as small as 0.012 (1.2% of the total film bulk).

Here only estimates of the influence of impurities on values of film optical constants are provided. Films in this research are known to contain impurities of Ar, Fe and Mo in the case of Ta_2O_5 and of Ar, Fe, Mo and Ta in the case of SiO_2. It is not unreasonable to assume that Fe, Mo and Ta are incorporated into the films in the form of oxides. Each

element can form several oxides (FeO, Fe_2O_3, Fe_3O_4; MoO_2, Mo_2O_5, Mo_2O_3, MoO_3; TaO_2, Ta_2O_5 [Weast, 1974]). Each oxide, in turn, has a different refractive index. No information is available on the exact type of impurity oxide in the film. The influence of ion-assistance on the composition of impurity oxide is also unknown. The absence of such information makes it impossible to perform an accurate quantitative calculation of the influence of impurity incorporation on the refractive index of the studied films. Therefore, in this research results of optical analysis will be discussed only qualitatively.

Another important mechanism, which can influence the value of film refractive index is densification. If the film is highly voided, its refractive index is usually lower than that of the bulk material. This is easily understood, considering that the voids, filled with air, will have a refractive index of 1 and the refractive indices of film materials are higher. As the film is densified, the fraction of voids decreases, leading to an increase in the measured film refractive index.

Finally, changes in stress can also lead to changes in material refractive index. This effect, called the photo-elastic effect, is well known. Mathematically, it can be expressed as [Kuske and Robertson, 1974]

$$\begin{aligned}(n_x - n_0) &= a\sigma_x + b(\sigma_y+\sigma_z)\\ (n_y - n_0) &= a\sigma_y + b(\sigma_x+\sigma_z),\\ (n_z - n_0) &= a\sigma_z + b(\sigma_y+\sigma_x)\end{aligned} \qquad (6.11)$$

where n_i and σ_i are principle refractive indices and stresses, n_0 is the refractive index of the non-stressed material and a and b are material-dependent constants. In the case of a residually stressed thin film, changes in the refractive index Δn due to stress σ can be calculated as

$$\Delta n = B\sigma, \qquad (6.12)$$

where B is the stress-optical coefficient, measured in Brewsters (1 Brewster = 10^{-13} cm^2/dyne = 10^{-12} Pa^{-1}) [Hirsch, 1980; Condon and Odishaw, 1958]. According to [Condon and Odishaw, 1958] the order of coefficient B for many materials is 1-10 Brewsters. If a change in stress of approx. 200 MPa is observed (as indeed is the case in this research), the changes in the refractive index are of the order of (2-20)x10^{-4}. For silica the stress-optical coefficients have been measured by [Primak and Post, 1959]. If

the residual stress is relaxing, the refractive index in silica decreases and, for a stress change of 200 MPa, the refractive index change is approx. $8.4x10^{-4}$ (see, for example, Kim et al, 2001).

The results of the measurements of optical properties of Ta_2O_5 and SiO_2 argon and oxygen assisted films, studied in this work, are presented in Figures 6.40-6.44.

6.4.1. Argon-assisted evaporated silicon dioxide films

According to the measurements, presented in Figure 6.40, purely evaporated SiO_2 film has the highest refractive index and the lowest extinction coefficient. Refractive index decreases and extinction coefficient increases with increase in the normalized added energy of 300 eV Ar^+ bombardment. Such behaviour cannot solely be attributed to the influence of additional argon incorporation. Moreover, if the microstructural changes, used to explain stress behaviour, are believed to take place, film density should increase with increase in normalized added energy of ion bombardment. Increase in film density always leads to increase in refractive index, which does not agree with the observed refractive index behaviour.

It is known that film composition may have an influence on film optical properties. Indeed, it was found that purely evaporated films have a composition of $SiO_{1.9}$, while ion-assisted films are SiO_2. Excess of silicon in purely evaporated film could indeed explain the behaviour of refractive index. However, it is also known that, due to higher absorbance, excess of metal in the film leads to increase in extinction coefficient. Thus, a purely evaporated film should have a higher extinction coefficient than ion-assisted films, which is in disagreement with the observed behaviour.

Attempts to correlate the refractive index behaviour gave the stress-optical coefficient equal to 263 Brewster, which is an order of magnitude higher than the expected value. Therefore, it is highly unlikely that film optical behaviour is governed by its stress.

Thus, it can be concluded that, at the moment, no reasonable explanation of film optical properties behaviour can be found and more research is needed to clarify this question.

6.4.2. Argon-assisted sputtered tantalum pentoxide films

Figure 6.41 shows the *n* and *k* behaviour for Ar-assisted Ta_2O_5 films. It can be seen that for 400 and 600 eV argon bombardment *n* decreases with increase in normalised energy. The refractive index of 250 eV bombarded films initially increases, but then also

a) Refractive index

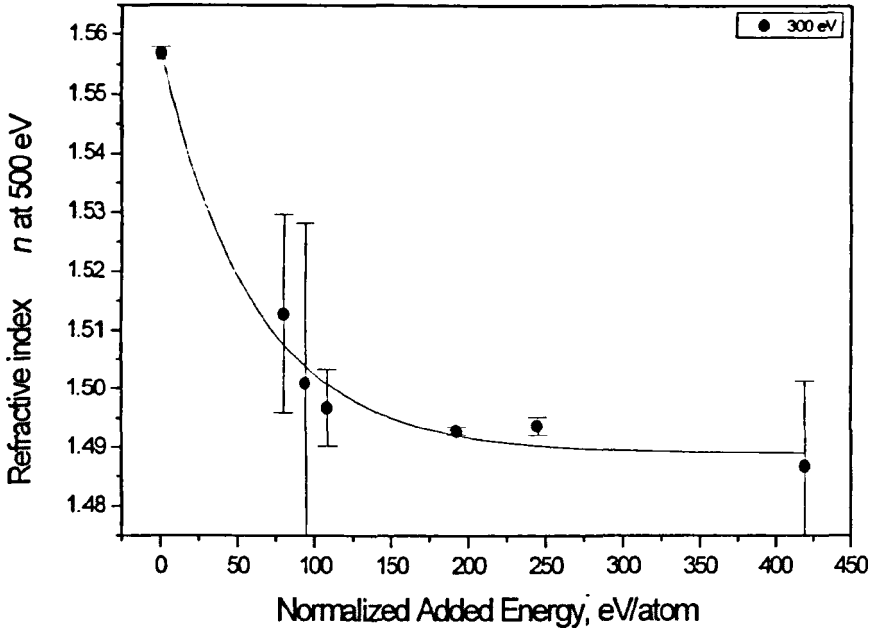

b) Extinction coefficient

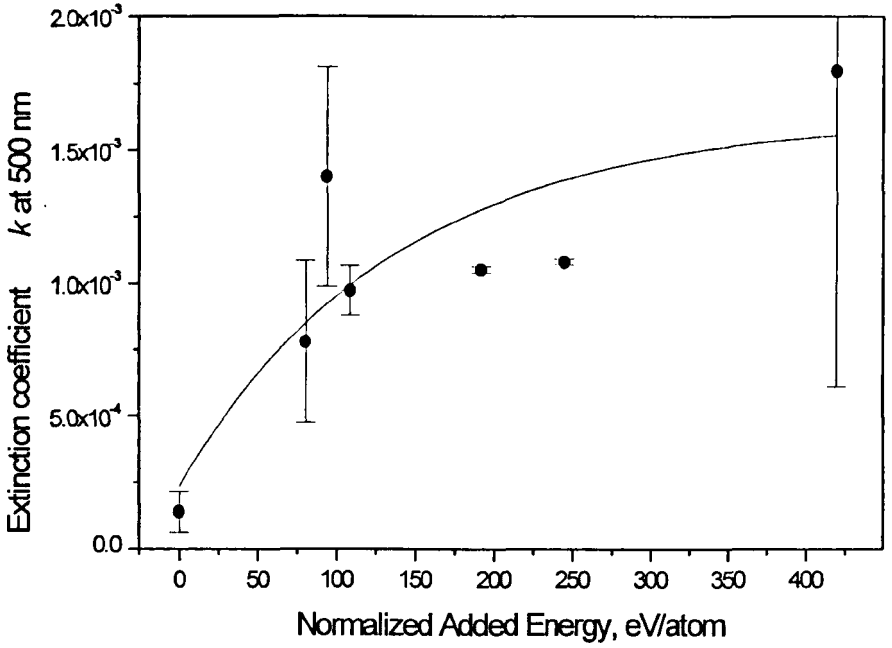

Figure 6.40. Optical properties of evaporated SiO_2 films, deposited under concurrent argon ion bombardment. Lines are drawn to guide the eye only.

a) Refractive index

b) Extinction coefficient

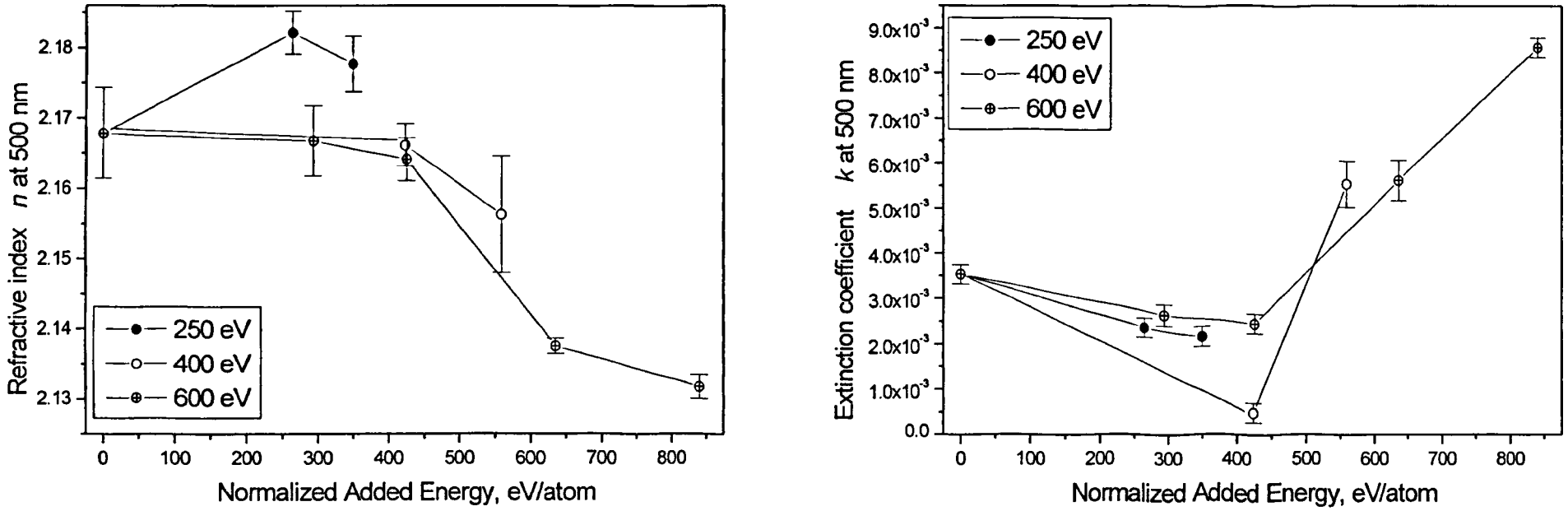

Figure 6.41. Optical properties of argon-bombarded Ta_2O_5 films. Lines are drawn to guide the eye only.

a) Refractive index

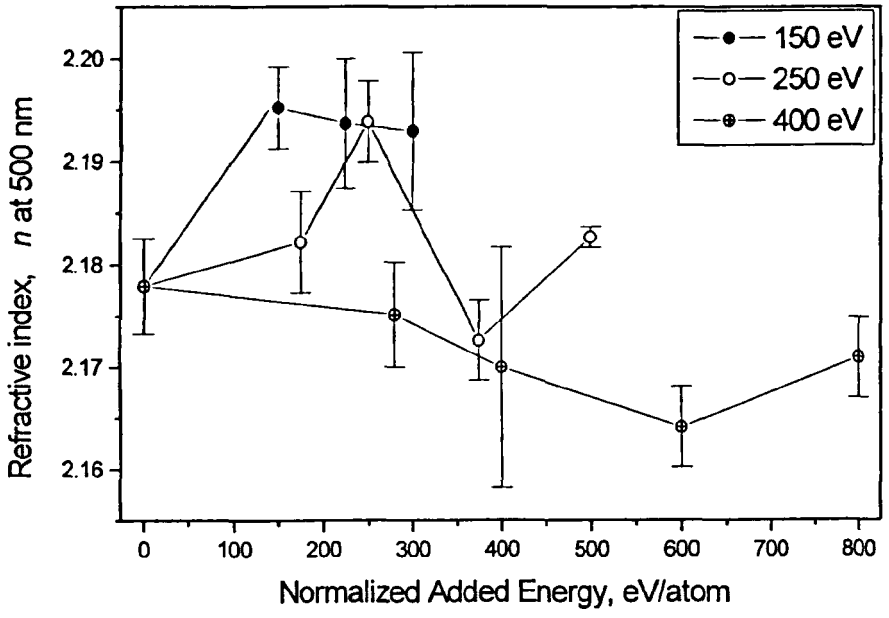

b) Extinction coefficient

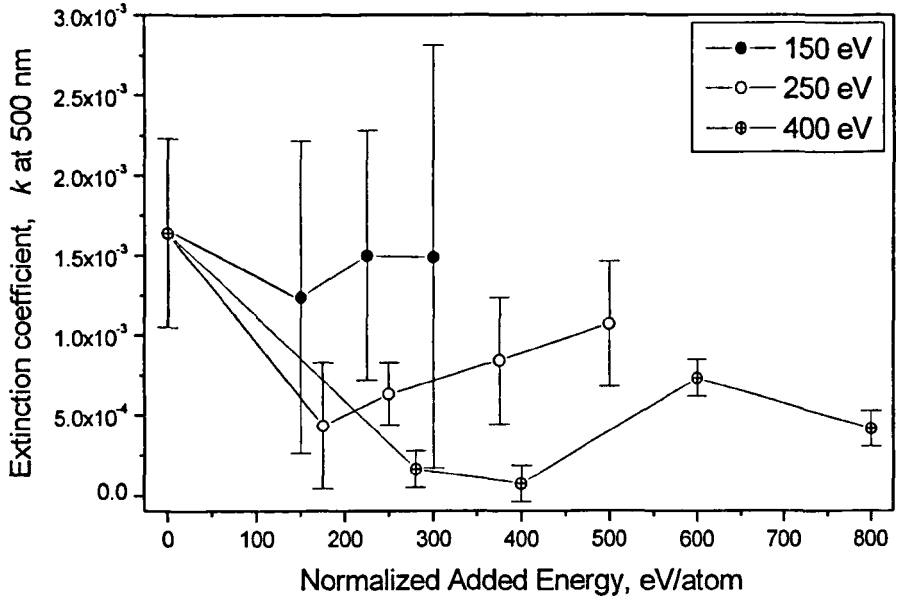

Figure 6.42. Optical properties of oxygen-bombarded Ta_2O_5 films. Lines are drawn to guide the eye only.

a) Refractive index

b) Extinction coefficient

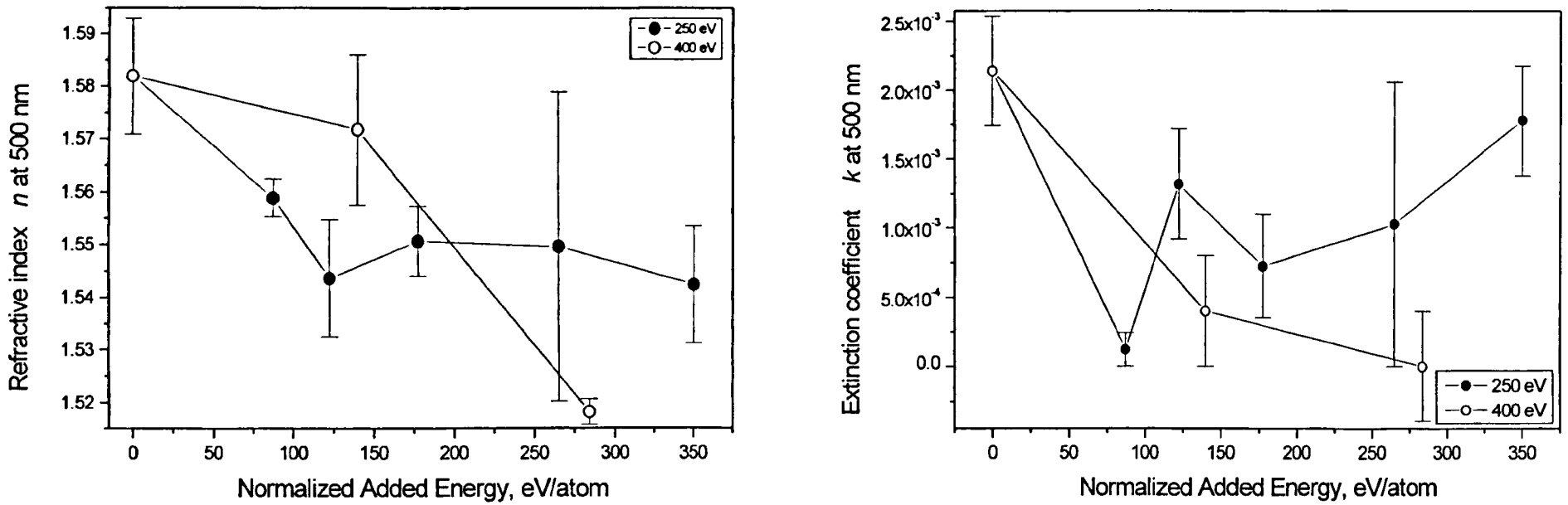

Figure 6.43. Optical properties of argon-bombarded SiO_2 films. Lines are drawn to guide the eye only.

a) Refractive index

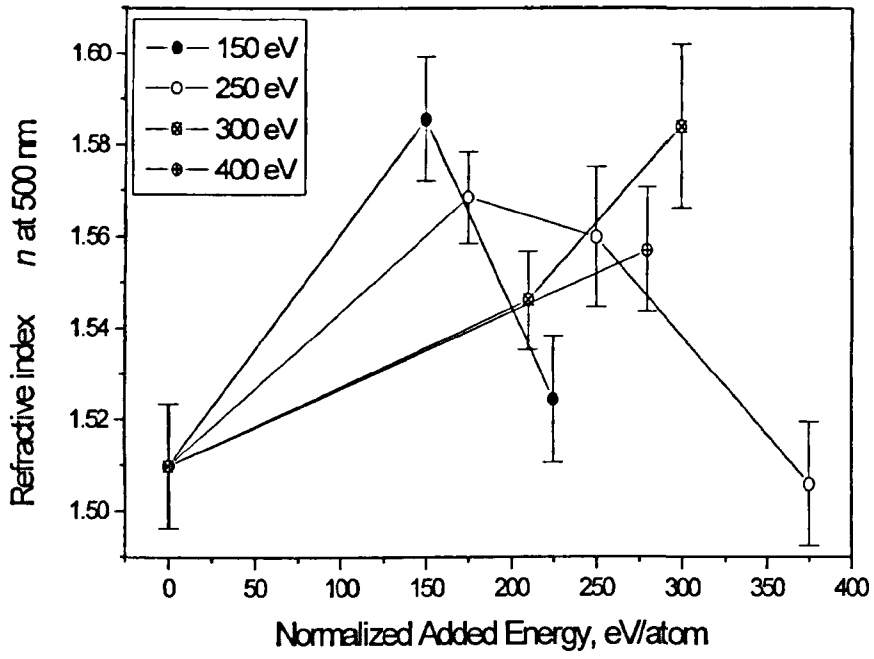

b) Extinction coefficient

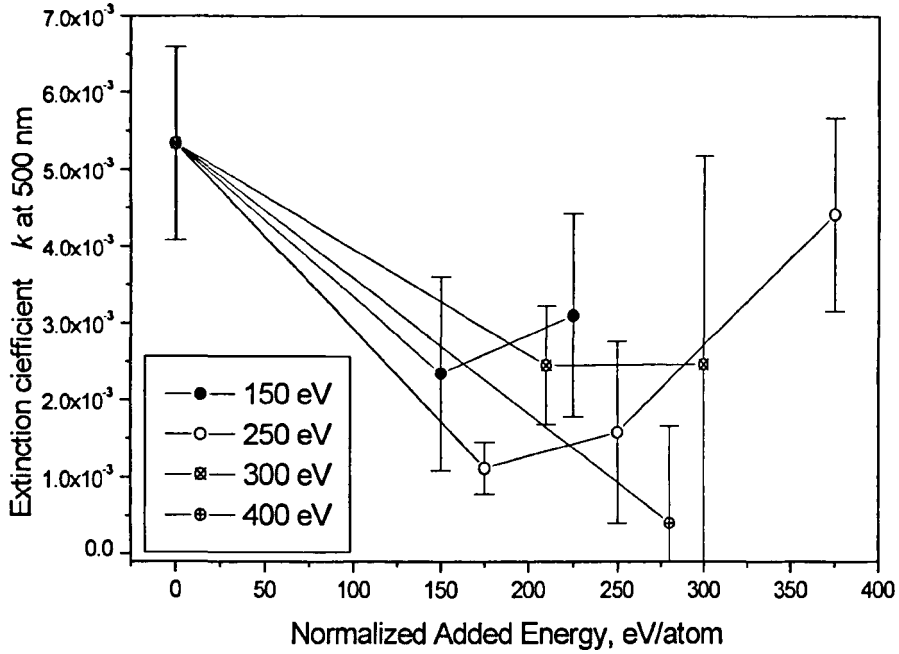

Figure 6.44. Optical properties of oxygen-bombarded SiO_2 films. Lines are drawn to guide the eye only.

decreases with increase in normalised energy. For a fixed ion-to-atom arrival ratio the film refractive index decreases with increase in the energy of ion bombardment. The plot of extinction coefficient shows an initial decrease of k value with increase in normalised energy up to 300-400 eV/atom, where the extinction coefficient reaches a minimum. After that k increases with further increase in normalised energy. It is unclear what are the reasons for such complex behaviour of optical constants. Variation in the values of refractive index can mainly be explained by the increase in the argon concentration in the films (refractive index of Ar is approx. 1, so Ar incorporation leads to a decrease in film refractive index) and changes in iron content (refractive indices of iron oxides vary between 2.32 and 3.01 [Weast, 1974], so iron oxide incorporation leads to an increase in film refractive index). However, other mechanisms (small compositional changes, undetected by RBS, density, surface roughness and stress changes) can also contribute to the optical constants behaviour.

6.4.3. Oxygen-assisted sputtered tantalum pentoxide films

Values of refractive index of oxygen-assisted Ta_2O_5 films at 500 nm are presented in Figure 6.42. It can be seen that the behaviour of refractive index n with normalised energy depends on the energy of assisting oxygen ions. Thus, for 150 eV ion assistance the refractive index increases and then decreases slightly with increase in normalised energy of bombardment. At 250 eV the refractive index behaviour could, probably, be well approximated by a slowly increasing straight line. The deviation, observed for I/A=1.0 and I/A=1.5 is, most probably, related to the amount of film impurities and their effect. At 400 eV the refractive index decreases with increase in normalised energy of bombardment. The extinction coefficient of the oxygen-assisted Ta_2O_5 films shows similar behaviour with normalised energy for all energies of bombardment. With increase in normalised energy k decreases, passes through a minimum and then increases.

It should be noted that, for oxygen-assisted Ta_2O_5 films, the behaviour of film refractive index bears some similarity to the behaviour of the film stress. However, calculations show that, if all changes in the refractive index are attributed to the photoelastic effect, the value of film stress-optic coefficient should be approx. 240 Brewster. Such a value is significantly higher than the expected value (order of 1-10 Brewster). Moreover, although oxygen-assisted films exhibit changes in refractive index, which are in agreement with the stress changes, argon assisted films show a decrease in n values with

increase in normalised energy of bombardment for 400 and 600 eV ions. Thus, although it cannot be denied that stress has some effect on film optical properties, it is not the main reason, governing observed refractive index behaviour.

In general, it was found that the optical constants of argon-assisted Ta_2O_5 films are in a region of 2.13-2.18 for n and (0.5-8.5)x10^{-3} for k at 500 nm. For oxygen-bombarded Ta_2O_5 films the values are 2.16-2.20 for n and <1.7x10^{-3} for k at 500 nm. Such values are in agreement with the results of other research, available in the published literature (see Chapter II). On average, oxygen-assisted Ta_2O_5 films have a higher refractive index and lower extinction coefficient in comparison with argon-bombarded films. This effect may be due to a difference in levels of impurities in the films, as well as a difference in chemical activity of oxygen and argon ions and their energy transfer to the film.

6.4.4. Argon-assisted sputtered silicon dioxide films

Results of refractive index measurements on argon-bombarded SiO_2 films are presented in Figure 6.43. It can be seen that, with an increase in normalised energy the film refractive index decreases. Such behaviour would be expected on the basis of compositional changes in the film. Increase in argon incorporation, for example, (see Figure 6.2) can lead to a decrease in film refractive index. Such behaviour would also be expected on the basis of stress behaviour. However, as shown for oxygen-assisted Ta_2O_5 films, if changes in film refractive index are attributed only to the photoelastic effect, the magnitude of the stress-optic coefficient should be approx. 236 Brewster, which does not agree with the expected values. Moreover, if the results of the measurements on ion-assisted evaporated and sputtered SiO_2 films are compared, another discrepancy can be noticed. In evaporated films with increase in normalised added energy of bombardment compressive stress increases and film refractive index decreases. In sputtered films with increase in normalised energy of bombardment compressive stress decreases, but the refractive index also decreases. Therefore, changes in n are, most probably, related not to the stress changes, but to the film compositional variations.

The film extinction coefficient does not exceed 2.2x10^{-3}. For 250 eV bombardment k initially decreases, passes through a minimum and then increases with increase in normalised energy. For bombardment with 400 eV ions only an initial decrease is

registered. The complicated behaviour of the extinction coefficient of argon-bombarded SiO_2 films agrees well with the behaviour of argon-bombarded Ta_2O_5 films.
The value of film extinction coefficient is in a reasonable agreement with the values of the extinction coefficient reported in literature for SiO_2 films (see Chapter II). Values of film refractive index, varying from 1.52 to 1.58 for 500 nm wavelength, although higher than the value of the thermal oxide, are not unusual, as, for example, seen by Takahashi et al [Takahashi et al, 1996] who quoted values of 1.47-1.62 at 633 nm for RF sputtered films. The increase in the total value of the refractive index for films in this work relative to the thermal oxide can be related to the difference in film composition and density, impurity incorporation or measurement error.

6.4.5. Oxygen-assisted sputtered silicon dioxide films

Oxygen-assisted SiO_2 films (see Figure 6.44) showed refractive indices in the region of 1.5-1.59 and extinction coefficients less than $5.5x10^{-3}$. Again, such values of optical constants are in agreement with other results, available in the literature (see Chapter II). From a comparison of Figure 6.43 and 6.44 it can be seen that two different values are quoted for the non-assisted SiO_2 film. XPS analysis showed that these films have different levels of oxygen, incorporated in them. Therefore, this difference in the refractive index can be related to the difference in the film composition. Figure 6.44 also shows that, with increase in normalised energy of ion bombardment, the extinction coefficient initially decreases, goes through a minimum and then increases. Such behaviour again agrees well with the behaviour of oxygen-assisted Ta_2O_5 films.
In general, it was found that optical constants of argon-assisted SiO_2 films are in a region of 1.52-1.58 for n and $<2.2x10^{-3}$ for k at 500 nm. For oxygen-bombarded SiO_2 films the values are 1.5-1.59 for n and $<5.5x10^{-3}$ for k at 500 nm. Thus, contrary to the results found for Ta_2O_5 films, no significant difference is observed in the values of optical constants of argon-assisted and oxygen-assisted SiO_2 films.

To summarise the above it can be said that both refractive index and extinction coefficient of the studied films exhibit complex behaviour with ion bombardment. Measured values of refractive index of SiO_2 films are higher than the values for the thermal oxide, but not unusually high. Extinction coefficient values of SiO_2 films are in agreement with the published values. Measured values of Ta_2O_5 films optical constants

are in a good agreement with the published values. Oxygen-assisted Ta_2O_5 films have higher refractive index and lower extinction coefficient than argon-assisted Ta_2O_5 films. For films of both materials, bombarded during growth by argon or oxygen ions, the extinction coefficient initially decreases, passes through a minimum and then increases with increase in normalised energy. At the moment the origins of such behaviour are unclear and more research is needed in order to find out the reasons for observed dependences.

References

Carter G., J. Phys. D: Appl. Phys., **27**, 1046, (1994)

Cevro M., *A Study of the Deposition of Oxide Thin Films by Ion Beam Techniques*, Ph.D. thesis, Dept. of Electronic and Electrical Engineering, University of Salford, Salford, U.K., 1994

Cheng Y.-T., Materials Scinece Reports, 5(2), 1990, p. 45

Davis C.A., Thin Solid Films, **226**, 30, (1993)

Feldman A., Farabaugh E.N., and Haller W.K., Sanders D.M., Stempniak R.a., J. Vac. Sci. Technol., **A 4 (6)**, 2969, (1986)

Handbook of Chemistry and Physics 55th edition, ed. by Weast R.C., CRC Press, Inc., 1974

Handbook of Physics, ed. by Condon E.U., and Odishaw H., McGraw-Hill Book Company, Inc., New York, 1958

Hirsch E.H., J. Phys. D: Appl. Phys., **13**, 2081, (1980)

Ho S.F., Contarini S., Rabalais J.W., *J. Phys. Chem.* **91**, 4779 (1987)

Hudson C., and Somekh R.E., J. Vac. Sci. Technol., **A 14 (4)**, 2169, (1996)

Jia Y., Liang Y., Liu Y., Liu Y., Shen D., Thin Solid Films, **370**, 199 (2000)

Kim B.H., Park Y., Ahn T.-J., Kim D.Y., Lee B.H., Chung Y., Paek U.C., and Han W.-T., Optics Letters, **26 (21)**, 1657, (2001)

Koster M., Urbassek H. M., Surf. Science, **496**, 196, (2002)

Kuske A. and Robertson G., *Photoelastic Stress Analysis*, John Wiley and Sons Ltd., London, New York, Sydney, Toronto, 1974

Leplan H., Robic J.Y., Pauleau Y., J. Appl. Phys., **79 (9)**, 6926, (1996)

Martin P.J., Bendavid A., Swain M., Netterfield R.P., Kinder T.J., Sainty W.G., Drage D., and Wielunski L., Thin Solid Films, **239**, 181, (1994)

Müller K.-H., in *Handbook of Ion Beam Processing Technology: Principles, Deposition, Film Modification and Synthesis*/ed. by Cuomo J.J. and Rossnagel S.M., Kaufman H.R.,, Noyes Publications, U.S.A., 1989

Parfitt L., Goldiner M., Junes J.W., and Was G.S., J. Appl. Phys., **77 (7)**, 3029, (1995)

Petrov I., Adibi F., and Greene J.E., Hultman L., and Sundgren J.-E., Appl. Phys. Lett., **63 (1)**, 36, (1993)

Primak W., and Post D., J. Appl. Phys., **30 (5)**, 779, (1959)

Strauss G.N., Danh N.Q., Pulker H.K., J. Non-Cryst. Solids, **218**, 256, (1997)

Takahashi H., Nagata H., and Kataoka H., Takai H., J. appl. Phys., **75 (5)**, 2667, (1994)

Takahashi H., Nishiguchi A., Nagata H., and Kataoka H., Fujishima M., J. Appl. Phys., **79 (5)**, 2787, (1996)

Tien C.-L., Jaing C.-C., Lee C.-C., and Chuang K.-P., J. Mod. Opt., **47** (10), 1681, (2000)

Was G.S., Jones J.W., Parfitt L.J., Goldiner M. and Kalnas C.E., Proc. Mater. Res. Soc., MRS, Pittsburgh, **396**, 479 (1996)

Windischmann H., J. Appl. Phys. **62 (5)**, 1800, (1987)

Chapter VII

Conclusions and Plans for Future Research

In this chapter conclusions, following from the results presented in Chapter VI, will be drawn and plans for future research will be proposed.

7.1. Film composition

For the experimental system, used in this research programme, it is possible to find conditions of deposition of stoichiometric (verified by RBS) SiO_2 and Ta_2O_5 films. Purely evaporated SiO_2 films are slightly understoichiometric with the oxygen fraction being 1.9. They contain no argon and a small level of Ta impurity of about 0.1 at %. Argon bombardment of these evaporated films leads to an increase in oxygen content to the stoichiometric level but the films then contain up to 1 at % of argon.

Sputtered SiO_2 films contain small levels of iron (max. 1.4 at %), tantalum (max. 0.15 at %) and, in some cases, molybdenum (max 0.3 at %). The stoichiometry of sputtered SiO_2 films varies slightly (approx. 8 %), which is related to the difference in deposition conditions and nature and levels of impurities. Bombardment with both argon and oxygen ions does not measurably change film stoichiometry, but leads to incorporation of argon into the coatings to about 1.5 at %.

Sputtered Ta_2O_5 films were found by RBS to contain impurities of argon (2.4 at %) and iron (max 1.4 at %). No significant changes in film stoichiometry due to ion bombardment with either oxygen and argon ions can be observed by RBS, but increase in argon content of Ta_2O_5 films to 3 at % was measured.

The film composition could not be conclusively verified by other methods (XPS) due to the presence of contamination on the film surface and compositional deviations induced by preferential re-sputtering during surface cleaning by ion etching.

TEM studies showed that both SiO_2 and Ta_2O_5 films with the highest amount of argon, incorporate it in the form of gas bubbles. It is possible that at lower levels of argon concentration in the films, argon is incorporated as atomic clusters, which cannot be

detected as their size is below the TEM resolution limits, or even single atoms, dispersed in the film.
In all cases ion bombardment leads to a significant level of film re-sputtering.

7.2. Film stress

From the results, presented in Chapter VI, it can be concluded, that an experimental *in-situ* stress measurement method has been successfully developed and applied to the studies of stress behaviour in evaporated and sputtered, as well as ion-beam and dual ion-beam assisted SiO_2 and Ta_2O_5 films. The single stationary laser beam stress measurement configuration leads to inaccurate stress values. The inaccuracy stems from inability of accounting for the initial substrate curvature and small sample movements during deposition and measurement. Thus, for accurate results the scanning stress measurement configuration should be used.
It was found that evaporated SiO_2 films are in a state of tensile stress of 100 MPa in magnitude. Ion bombardment of evaporated films with 300 eV Ar^+ ions leads to stress transition from tensile to compressive up to a value of -200 MPa. Such behaviour corresponds to that, expected on the basis of morphological changes known to occur in ion-assisted films.
Stress magnitude and stress value reproducibility are strongly dependent on the exact film composition and stoichiometry. For example, using a silicon substrate, compressive stress changes from approx. 1000 MPa for pure Ta films to approx. 350-400 MPa for stoichiometric Ta_2O_5 films. Small changes in film composition can lead to significant variations in the measured stress values. Thus, deposition conditions, which have significant influence on the film composition (in this work the main factors were found to be the partial pressure of oxygen in the chamber and metal target pre-cleaning), have to be accurately established and carefully controlled.
A thorough study of various deposition conditions during ion-beam sputtering showed that, for Ta_2O_5 films formed by sputtering, the stress is compressive and does not depend on film thickness, deposition interval, substrate cleaning procedure, angle of incidence of the sputtering beam to the target normal, angle of arrival of sputtered atoms onto the substrate, the material forming the grids in the ion source and the type of neutralizer used. For SiO_2 films formed by sputtering, it was observed that film stress is compressive and has a mean value of approx. 564 MPa if measured using the scanning configuration. Stress does not change with film thickness, deposition interval, substrate

cleaning procedure, angle of arrival of sputtered atoms onto the substrate or total deposition pressure in the range studied. Mainly, such stress behaviour in films of both materials is believed to be the result of the consistent dense amorphous nature of the films.

For the ion beam sputtered Ta_2O_5 films under all sputtering conditions studied, only the nature of the sputtering gas (Ar and Xe) and entry point of reactive gas (O_2) into the chamber have been found to be factors of importance governing film stress levels. Stress in Xe-sputtered films is on average 150 MPa higher that in Ar-sputtered ones, which may be related to the number and energy of back-scattered particles, difference in impurity incorporation or momentum transfer. However, with the data currently available, it is hard to conclude on the exact mechanism, governing stress behaviour in this case.

Ion-assist parameters do however have a strong influence on stress levels in ion-bombarded sputtered SiO_2 and Ta_2O_5 films. Thus, Ar assistance (250-600 eV, I/A=0.59-1.4) during Ta_2O_5 film deposition leads to an increase in compressive stress levels from 380 to 490 MPa. The effect of oxygen bombardment (I/A=0.7-2.0) depends on ion energy. For 150 eV ions compressive stress increases, for 250 eV stress is almost constant, while for 400 eV stress levels decrease. Stress in ion bombarded (argon 250-400 eV, I/A=0.35-1.4; oxygen 150-400 eV, I/A=0.7-2.0) SiO_2 films exhibit somewhat different behaviour with stress magnitudes decreasing for both argon (approx. -625 to -325 MPa) and oxygen bombardment (-525 MPa to below the detectable limit). Such complicated stress behaviour can be explained by a simple linear model proposed in this thesis, which links stress with the normalized energy of bombardment (a parameter, proportional to the total recoil density in the film). Ion bombardment produces forward and backward recoils in the film. Backward recoils always relax existing compressive stress, while the effect of forward recoils (compressive stress generation or relaxation) depends on their energy. The total resultant stress, measured in the film arises from a balance of the effects of stress-generating and stress-relaxating recoils. As the model contains unknown coefficients, one of which is energy-dependent, it cannot be used for stress prediction. However, the coefficients can be found by numerically fitting the model to the experimental data. Results of numerical fitting showed that the model gives results which are in a reasonable agreement with the measured values. This model can therefore be used to explain stress behaviour in sputtered thin films under ion bombardment over the range of ion-assist parameters for the materials studied in this research programme.

7.3. Film optical properties

Evaporated and ion-assisted SiO_2 films show increasing refractive index and extinction coefficient with increase in normalized energy of argon ion bombardment. More data are is needed in order to explain these trends.

For all sputtered ion-assisted films there is seen to be a complex relation between deposition conditions and the film optical quality, which cannot be resolved at this stage. It is unlikely that such behaviour is governed by changes in stress or in film density and the effect is, most probably, related to small compositional changes below the resolution of the RBS, small variations in the amount of film impurity and variation in the film surface roughness.

Oxygen-assisted Ta_2O_5 films show higher refractive index and lower extinction coefficient relative to argon-assisted films, which can be related to the effect of preferential sputtering, governed by the difference in the momentum transfer between Ta, O and Ar. No significant difference is observed for argon and oxygen-assisted SiO_2 films, which can be related to more effective momentum transfer between Si, O and Ar.

Extinction coefficient of all dual ion beam sputtered films initially decreases with increase in normalized energy of ion bombardment, passes through a minimum and then increases. At the moment, no explanation of such behaviour can be offered, so further studies are required to resolve this question.

7.4. Plans for Future Research

Some of the unresolved questions, requiring further investigation, have already been mentioned above. However, several other possible research trends should be mentioned.

Stress in thin SiO_2 and Ta_2O_5 films, deposited by sputtering, evaporation and ion-assisted variations of these techniques, often puts important mechanical constraints onto the design and performance of many optical products. Although in this research attempts have been made to find out the levels of stress, stress behaviour and variation with deposition conditions, further research is needed for a full understanding of mechanisms of stress generation and evolution. For immediate practical application in industry results of research in the following directions can be of a particular importance:

- A thorough study of the influence of deposition conditions on stress and optical properties of purely evaporated thin films has to be performed. Although for some

conditions (for example, total working pressure), film property behaviour can be reasonably well predicted, the importance and extent of the influence of other parameters (such as, for example, angle of incidence of vapour flux onto the substrate) has to be verified. This information may be useful in the future design of vacuum systems for deposition of films with optimal characteristics.

- A study of ion-assisted films, where the influence of various parameters of the assisting beam (ion energy and ion current, ion angle of incidence and ion nature, i.e. Ne, Ar, Xe, etc.) can be performed. This, again, would allow production of films with desired characteristics and thus, optimisation of the deposition process.
- Dual ion-beam sputtered films can be studied in the similar manner. This would enable improvements not only in the processing and performance of optical coatings, but also in the general understanding of film characteristics behaviour with ion bombardment.
- Common dielectric optical coatings normally consist not of a single, but of multiple layers. Characteristics and performance of a stack of layers (for example, stress) can deviate significantly from the simple summation of the characteristics of single layers. Thus, a study of multilayer properties is also important.
- In this research, only properties of as-deposited (where possible) films were studied. However, real optical products have to be reliable over a range of ambient conditions and over a certain extent of time. Therefore, it would be interesting to study the ageing and ambient-dependent behaviour of the above-mentioned coatings.

All of this information will facilitate a successful search for a "recipe" for an optical coating, ideally suited for a particular application.

For general use, it would also be interesting to verify the validity and applicability of the proposed model of stress behaviour for other dense, amorphous, initially compressively stressed films, deposited under various concurrent ion bombardment conditions. The origins and possible form of an energy-dependent parameter in the model should also be studied.

Appendix I

Thin Film Analysis Methods

In addition to the main stress measurement method used in this work and thoroughly described in chapter II, several other analytical techniques were used to evaluate the properties of the thin films. These methods include Rutherford Backscattering Spectrometry (RBS), spectrophotometry, Raman spectrometry and DekTak profilometry, atomic force (AFM) and tunnelling electron (TEM) microscopy and X-ray photoelectron spectroscopy (XPS). In this chapter the basics of these techniques will be briefly described.

A1.1. Rutherford Backscattering Spectrometry (RBS)

Rutherford Backscattering Spectrometry is a technique, routinely used in this study to determine composition and to estimate thickness of deposited films. This technique was also used to establish the depth distribution of the film elements as well as the amounts and depth distribution of impurities in the coatings. All this information can be obtained without physically destroying the sample (for example, by sputtering the surface layer), but still, some amount of damage will be introduced. RBS does not provide information on the chemical state of a compound and has several other disadvantages, including restrictions on detection of light elements and the requirement that the sample has a high degree of surface uniformity.

Rutherford Backscattering Spectrometry is reviewed in many works devoted to thin film technology [Townsend et al, 1976; Eckertova, 1986; Ohring, 1992; Cervo, 1994; Earwaker, 1994]. Probably, one of the best treatments of this topic is presented in the book by Chu, Mayer and Nicolett [Chu et al, 1978], whose approach to questions on RBS is adopted here.

In RBS a beam of monoenergetic accelerated ions (in our case 2MeV $^4He^+$) is directed onto the surface of the sample. Most of the ions will become implanted into the sample, but some of them will undergo elastic collisions with the nuclei of target atoms and

subsequently will be deflected by the Coulombic force, acting during such collisions. The energy E_1, retained by the ion after the collision, can be calculated from the laws of energy and momentum conservation, and in laboratory coordinates

$$E_1 = E_0 k = E_0 \left(\frac{\sqrt{M_2^2 - M_1^2 \sin^2 \theta} + M_1 \cos\theta}{M_1 + M_2} \right)^2, \qquad \text{(A1.1)}$$

where k is called the kinematic factor, E_0 is the energy of the ion before collision, M_1 and M_2 are masses of ion and target atom, respectively, and θ is the scattering angle, i.e. the angle of deflection of the ion from its initial trajectory. If the mass and the energy of the ion before collision are known, and the energy of the ions, which have undergone elastic collisions, is measured by the detector, positioned at a known steep backward angle, the information on the atoms, constituting the target, can be obtained.

Only few ions undergo collisions with the atoms at the sample surface. Others penetrate into the target and are slowed down along their way before experiencing an elastic collision with the target atom. After the collision, ions travel back through the target to the detector, which will further reduce their energy. Thus ions, scattered at some depth in the target, are registered at lower energies than the ions scattered from the same type of atoms at the target surface. This energy loss is usually described with the help of the stopping cross section ε

$$\varepsilon = \frac{1}{N} \frac{dE}{dx}, \qquad \text{(A1.2)}$$

which is independent of the target density. Here N is target atomic density, expressed in atoms/m^3 and $\frac{dE}{dx}$ is energy loss per unit length for a particular ion-target combination.

In case of a compound $A_n B_m$, Bragg's rule is used:

$$\varepsilon^{A_n B_m} = n\varepsilon^A + m\varepsilon^B, \qquad \text{(A1.3)}$$

where $\varepsilon^{A_n B_m}$, ε^A and ε^B are stopping cross sections of the compound and its elements A and B. Generally, energy loss is an unknown function of ion energy, so approximations of its value are used (surface $dE/dx = dE/dx(E_0)$ and mean energy

approximations). Thus, knowing the initial energy of the incoming ions, detected energy of an ion and the stopping cross-section, it is possible to calculate the distance from the target surface, at which the scattered ion originated. For example, the thickness t of a thin single element film can be calculated as

$$t = \frac{\Delta E}{N\left(\frac{k}{\cos\theta_1}\varepsilon(E_0) + \frac{1}{\cos\theta_2}\varepsilon(kE_0)\right)} \tag{A1.4}$$

if the surface energy approximation is valid. Here ΔE is the difference in energy of ions, reflected from the surface atoms of the film and from the atoms at the film-substrate interface; θ_1 and θ_2 are angles between the target normal and incoming ion beam direction and target normal and scattered ions direction, respectively.

When a backscattered ion hits the detector surface, an electric pulse is generated, which is then amplified and analysed according to its height as belonging to one of the channels. So, as a result of RBS experiment a spectrum is generated, where the number of ions registered with the energy corresponding to a certain channel, is plotted against the channel number. An example of such a spectrum for thin film of silicon dioxide on a silicon and carbon substrates is shown in Figure A1.1. Each of the elements (C, O and Si) generates a signal on the spectrum.

In addition to quantities, mentioned above, two other parameters can be determined from the experimental spectrum, i.e. height of the signal and area under the peak. Both of these quantities are dependent on the number of atoms of a certain element present in the target and thus are often used for calculations of a compound composition. In the case where two signals overlap, as indeed is the case of oxygen and silicon signals for SiO_2 film on Si substrate in Figure A1.1, a rule of additivity is used

$$H(E) = H_A(E) + H_B(E), \tag{A1.5}$$

where $H(E)$ is the total height of the spectrum at energy E and $H_A(E)$ and $H_B(E)$ are the heights of signals from individual elements A and B at this energy.

It can be shown that, in case of a thin film of compound A_nB_m, compositional information (i.e. the ratio n/m) can be calculated as

$$\frac{n}{m} = \frac{H_A}{H_B}\frac{\sigma_B}{\sigma_A}\frac{\Delta E_A}{\Delta E_B} \tag{A1.6}$$

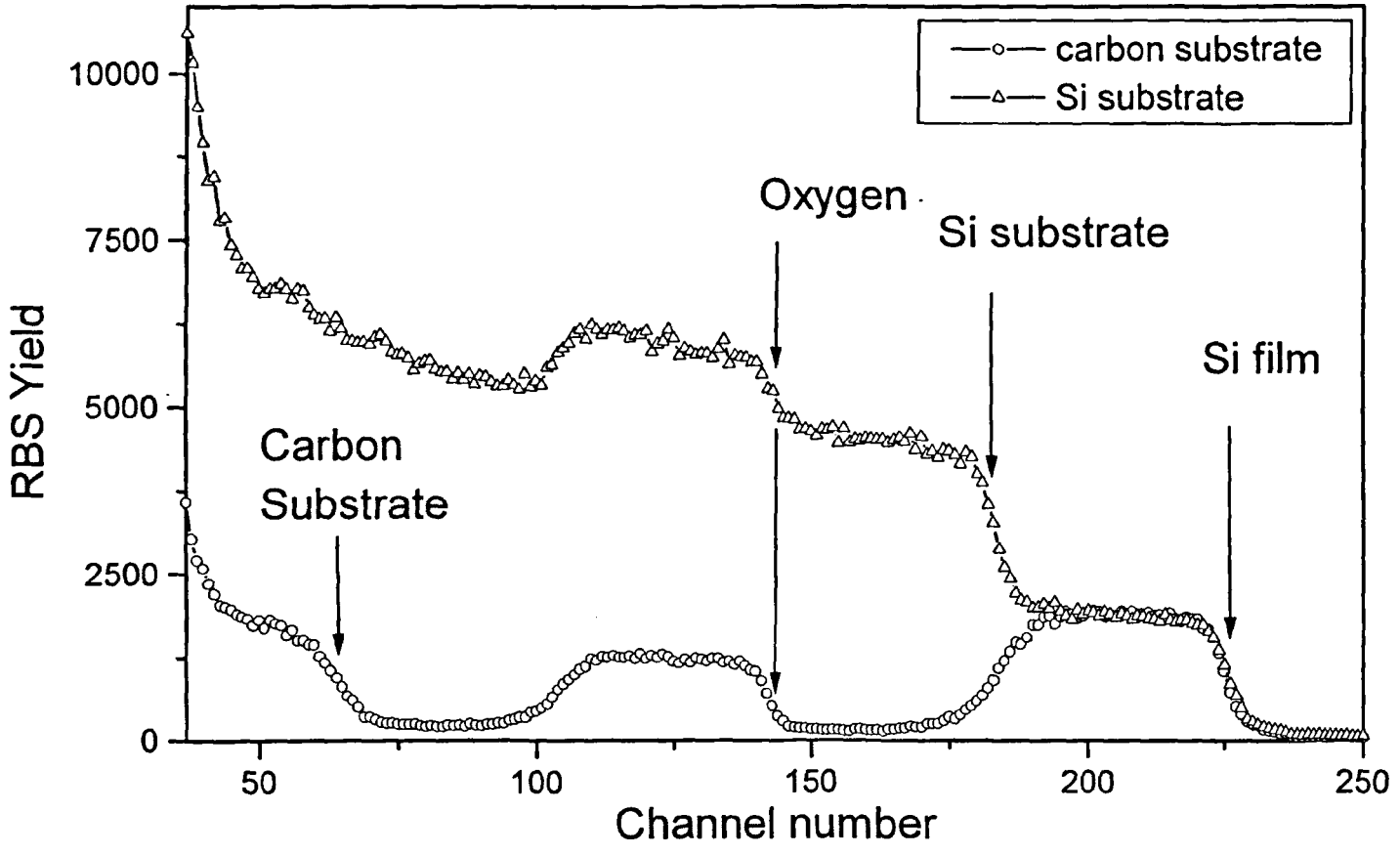

Figure A1.1. Example of RBS spectrum from SiO_2 film on Si substrate and SiO_2 film on C substrate.

when peak height information is used, and as

$$\frac{n}{m} = \frac{A_A \sigma_B}{A_B \sigma_A} \tag{A1.7}$$

when the area under the peak data is utilised. Here H_A, H_B, A_A and A_B are heights and areas under peaks from elements A and B, respectively, ΔE_A and ΔE_B are widths of peaks from elements A and B, respectively, taken at half-maximum height. Quantities σ_A and σ_B are known as scattering cross-sections for elements A and B, respectively and, for a known detector solid angle Ω, can be calculated as

$$\sigma = \frac{1}{\Omega} \iint_{\Omega} \left(\frac{d\sigma}{d\Omega} \right) d\Omega, \tag{A1.8}$$

where for $M_1 << M_2$

$$\frac{d\sigma}{d\Omega} = \left(\frac{Z_1 Z_2 e^2}{4E} \right)^2 \left[\sin^{-4}\left(\theta/2\right) - 2\left(\frac{M_1}{M_2}\right)^2 + \ldots \right]. \tag{A1.9}$$

Here Z_1 and Z_2 are atomic numbers of ion and target atom respectively, e is the electronic charge and E is the energy of the ion just before the scattering event. The latter expression is called the Rutherford formula, which gives the differential scattering cross-section, i.e. the probability of an ion being back-scattered from a target atom at an angle θ into a unit solid angle $d\Omega$.

In practice, it is possible not only to directly calculate film properties from the measured spectrum, but also to extract the information by fitting a computer-generated spectrum to an experimentally obtained one.

A1.2. Spectrophotometry

Two main parameters, defining the behaviour of a thin film as a part of an optical device, are its complex index of refraction N and thickness d. The first quantity is used to describe the behaviour of light in a medium and is defined as

$$N = n - ik, \tag{A1.10}$$

where n is a refractive index of a medium and k is its extinction coefficient. The refractive index is simply the ratio of the velocity of the light wave in vacuum to the

velocity of the light wave in this medium. The extinction coefficient describes the absorption of light in the medium and can be expressed as

$$k = \alpha\lambda/4\pi, \tag{A1.11}$$

where λ is the wavelength of radiation, α is the absorption coefficient, which can be found from the relation between the intensities of incident light I_0 and of light I at a certain depth x in the medium $I/I_0 = e^{-\alpha x}$. Absorption is mainly governed by the electronic transitions in the medium and light scattering, as the intensity of a light beam can be effected by scattering of some part of it into different directions. Scattering can occur due to impurities in the bulk of the film or due to surface and interface roughness. Therefore, k is also sensitive to impurity incorporation into the film and to the film structure.

In general, contrary to their designation as optical constants, both n and k are functions of wavelength, i.e. $n = n(\lambda)$, $k = k(\lambda)$, and are dependent on the composition of the medium, its density and structure.

When the beam of light is incident onto the sample, some part of it will be reflected, some part will be absorbed and some part will be transmitted. This can be expressed as

$$R + T + z = 1, \tag{A1.12}$$

where R is total reflectance, T is total transmittance and z is absorbance of the sample. In thin films a light beam can be reflected or transmitted not only at the film-air interface, but also at the film-substrate interface (see Figure A1.2). These multiple reflections, which occur if the film thickness is comparable with the wavelength of the incident light, combine together to give rise to interference effects, which can be clearly seen on the plot of R against wavelength, as in Figure A1.3 (a sample of SiO_2 film on Si substrate and *s*-polarised light were used to obtain this spectum). Transmittance and reflectance of a thin layer on a substrate can be calculated theoretically and are complex functions of wavelength, film thickness and optical properties of the materials used, i.e.

$$R = R(\lambda, N_s, N_f, d), \quad T = T(\lambda, N_s, N_f, d), \tag{A1.13}$$

where $N_f = n_f - ik_f$ and $N_s = n_s - ik_s$ are the complex refraction indexes of film and substrate, respectively. Exact forms of these functions for each specific case can be

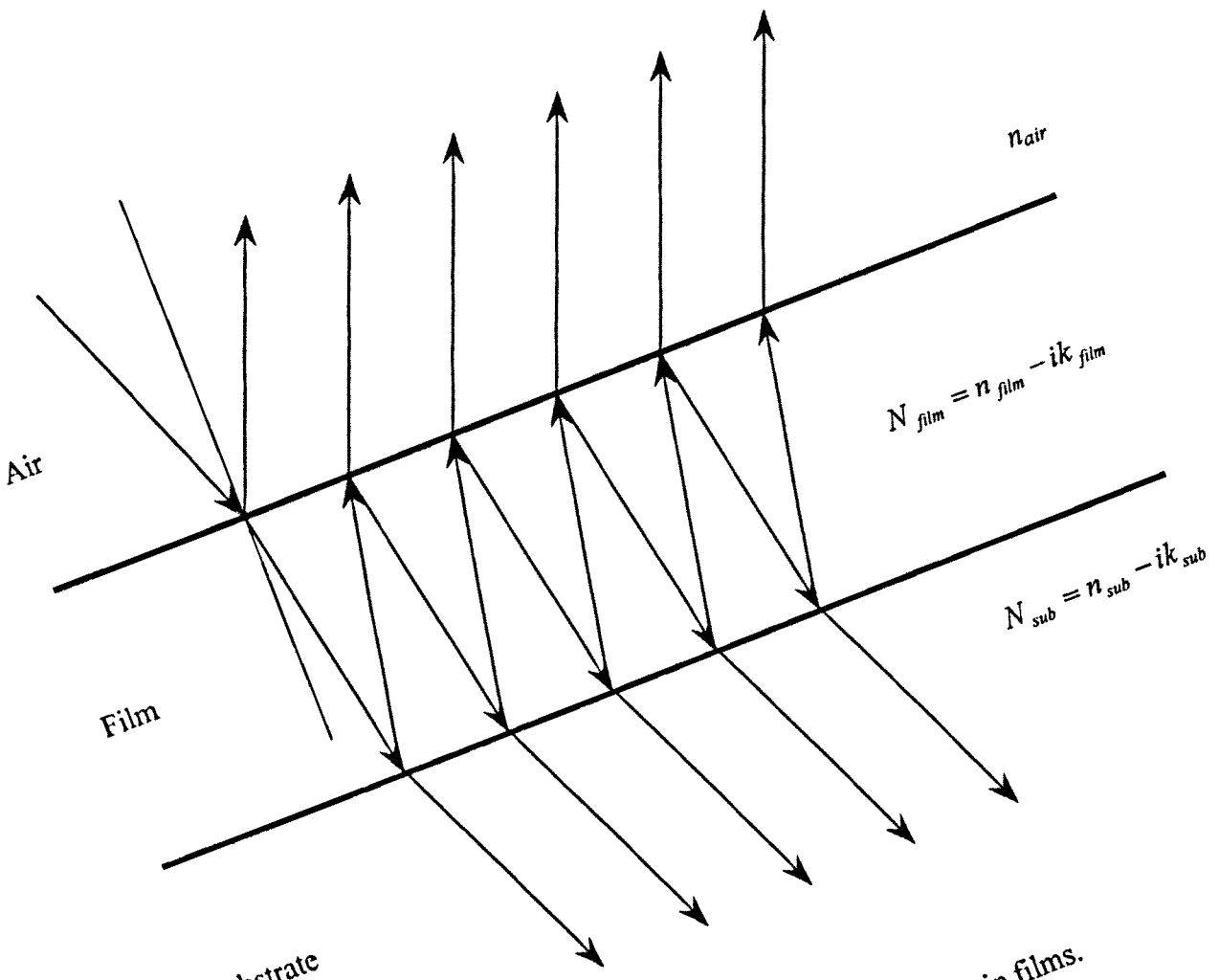

Figure A1.2. Behaviour of light in thin films.

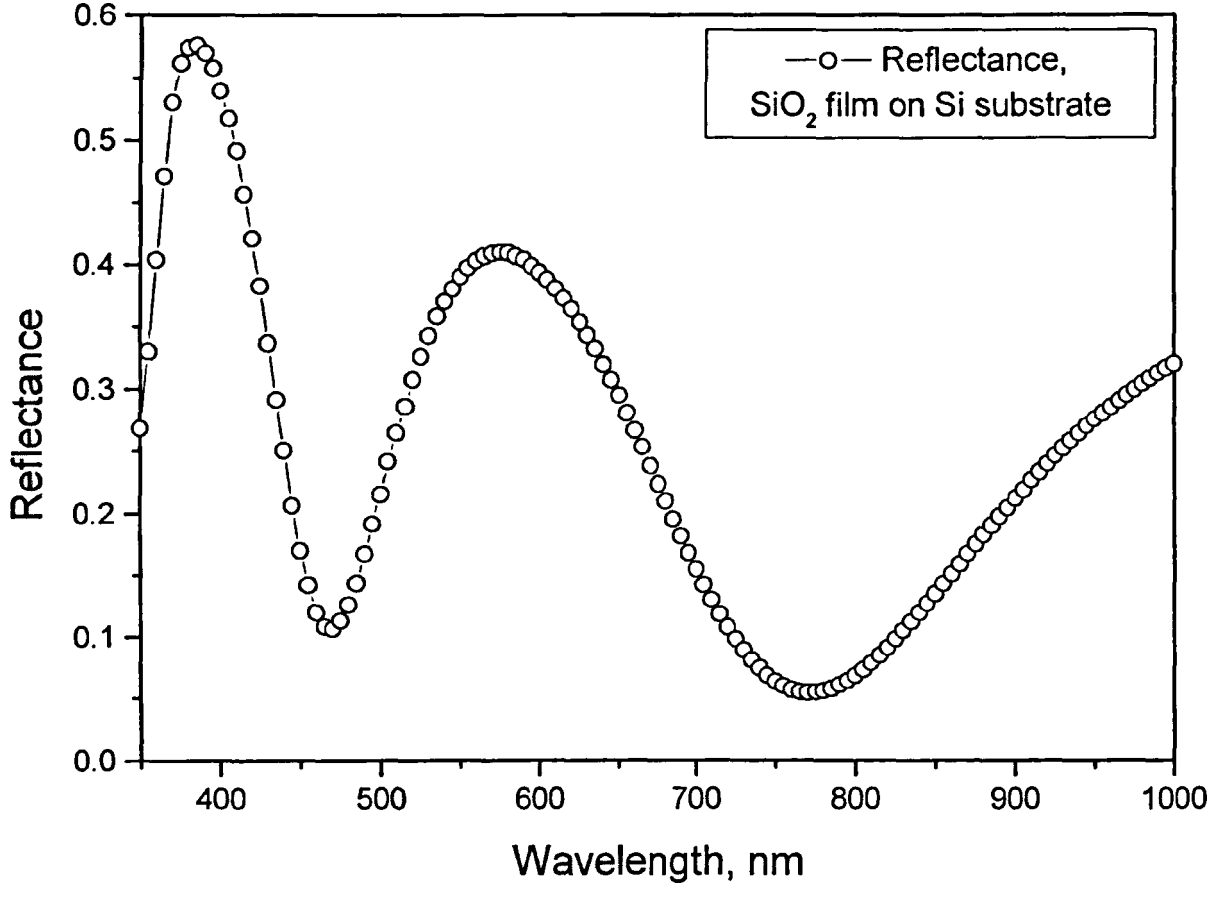

Figure A1.3. Example of a reflectance curve from the SiO_2 film on Si substrate.

found in the literature, for example, for an absorbing film on a transparent substrate [see Kubinyi et al, 1996] or for an absorbing film on a partly absorbing substrate [Mullerova and Mudron, 2000].

T and R can not only be calculated theoretically, but measured using a spectrophotometer. In this device a beam of light is directed onto the sample surface and reflected and transmitted beams are measured. As a result, a plot of transmittance and reflectance (for a transparent sample) or reflectance (for an opaque sample) versus wavelength is obtained (see, for example, Figure A1.3).

It is known that extrema in T and R occur when $2n_f d = m\lambda$ (m=1,2,3,...) and this information was originally used for calculations of optical properties and film thickness from the experimentally obtained spectra. This method has been named an "envelope method", as it relies on the data, obtained from the envelopes (smooth lines, connecting extrema points on the spectra). This is usually done by hand or by a special curve fitting method (see, for example, [Minkov and Swanepoel, 1993 and references in this work]). Optical properties are calculated then according to the method, outlined in [Manifacier et al, 1976]. The "envelope method" is the basis of successful calculations of optical properties in many modern software products. However, as it uses information on the extrema points but not on the whole spectrum, film thickness should be high enough to allow at least several points of minimum and maximum to be measured, which was not always possible with the films in this study.

The deficiencies of the envelope method can be often overcome by using "inverse synthesis" or fitting methods. In this type of method the structure of the measured sample and the substrate properties are presumed to be known. The dependence of refractive index and extinction coefficient of a film on the wavelength is usually expressed with the help of the various dispersion relations. The choice of a particular dispersion relation is based on the expected behaviour of the optical constants and material of the film. Probably the most often used dispersion functions are the Cauchy relation or the Forouhi and Bloomer relation [Forouhi and Bloomer, 1986]. There are several ways of determining the initial values of unknown fitting parameters for these equations [see, for example, Gauthier-Manuel, 1998; Nenkov and Pencheva, 1998]. Thus, with all parameters known in the zero-order approximation, T and R can be calculated. The last step of the method is fitting the simulated spectra to the measured one by a least-squares fitting procedure [see, for example, Marquardt, 1963].

A1.3. Raman Spectrometry

Raman spectrometry is a technique, which is based on the phenomenon of Raman scattering of light by materials [Long, 1977]. As mentioned above, incident light can be reflected, transmitted, absorbed or scattered by a material. In Raman spectrometry scattered light and its properties are studied and related to the properties of the scattering material.

Generally scattering can occur with or without changes in frequency (wavelength) of radiation. The latter case constitutes of two types of scattering: Rayleigh scattering due to the presence of small scattering centres (such as molecules, small in comparison with the wavelength of the incident radiation) and Mie scattering due to the presence of large scattering centres (e.g., dust). The former case includes Brillouin scattering, resulting in very small changes in wavelength, and Raman scattering. In a Raman experiment all the mentioned types of scattering may be observed.

If a system with energy E_1 is irradiated with light of wavelength λ, it can acquire enough energy to move to another energy level E_2. The process can be represented as annihilation of the incident photon of energy hc/λ and creation of a photon of energy $hc\left(\lambda^{-1} \pm \lambda_M^{-1}\right)$. This leads to observation of scattered radiation with wavelengths, corresponding not only to the incident radiation, but also of radiation with different frequencies, forming Raman spectrum. If the registered photon has energy less than the energy of incident photon, its signal is called a Stokes Raman band, otherwise an anti-Stokes Raman band is observed. As wavelength shift depends on the energy, acquired by the system, and this energy in turn is related to the permitted transitions between the energy levels of the system, it is possible to draw conclusions on the properties of the material under consideration.

Another approach is to treat the Raman effect as an electromagnetic radiation, produced by a dipole. This dipole is a result of interaction of an incident photon with a molecule of the scattering system. If molecule vibrations result in changes in polarisability of a dipole, Raman scattering is observed.

Raman scattering is sensitive not only to the internal vibrations and structure of a molecule, but also to the environment of this molecule. For example, vibrations of the crystal lattice can also give rise to Raman spectra and information on the crystal structure of the solid under consideration can be obtained from Raman peaks and their broadening [Virtual Raman Tutorial].

A1.4. Atomic Force Microscopy (AFM)

Atomic force microscopy (AFM) is a relatively new technique, which has grown from scanning tunnelling microscopy (STM) (information on STM can be found in [Wilson, 1994]). Contrary to STM, AFM can be used for measurements on insulators and this, together with ease of use and good resolution, makes AFM one of the most popular methods in studies of surface topography [for example, see AFM on the Web].

The principle of AFM operation is simple: a probe, or tip, is mounted onto the end of a cantilever and this assembly is positioned very close to the sample. The sample surface is then scanned, which results in changes in interactomic force acting between the atomically sharp tip and the sample and in the deflection of the cantilever. Over the years, several ways of sensing cantilever deflection have been proposed, for example, measurements of tunnelling current between the cantilever and the probe, positioned above it. However, a laser beam reflection method, similar to that used for stress measurements, seems to be one of the most popular choices. Depending on the mode of operation during scanning either the cantilever tip is maintained at constant height above the sample surface or the force between the tip and sample are kept constant. This yields either deflecting force or height information. For each position of the tip corresponding height of the sample is plotted and thus a topographical image of the sample surface is obtained.

It is common to classify AFM according to the way the probe makes contact with the surface. In contact mode the tip is in close contact with the sample surface and repulsive forces between the tip and the surface are maintained at a known level. This method often suffers from excessive force application, which is necessary in order to overcome ambient-induced attractive forces (for example, surface tension due to the presence of absorbed water vapour) and results in creation of damaging friction forces. In non-contact mode the tip is positioned several tens of Angstrom away from the sample surface and attractive forces of Van der Waals type are measured. This method also suffers from the influence of surface contaminants and generally has low resolution. In tapping mode the cantilever is made to oscillate with high amplitude and frequency. On contact with the sample surface, the amplitude of cantilever oscillations changes and this is related to the surface topography. As the probe does not have constant contact with the surface, many problems, encountered by contact and non-contact methods are avoided without the loss of resolution.

AFM can be used not only to image the surface, but also to quantitatively measure surface roughness. Traditionally surface roughness was expressed as RMS (route-mean square roughness)

$$RMS = \sqrt{\frac{1}{n}\left(y_1^2 + y_2^2 + ... + y_n^2\right)} \qquad \text{(A1.14)}$$

where n is the number of measured points and y_i, $i = \overline{1,n}$ is the distance of the i measured point from the mean surface line, which satisfies condition $\sum_i y_i = 0$ and for roughness measurements has a form of a straight line. In more recent research another parameter, called arithmetical mean roughness, is often used. It is simply an average of all profile deviations from the mean line, i.e. $\frac{1}{n}\sum_i y_i$, $i = \overline{1,n}$. Several other parameters can be calculated from the measured profile, but those mentioned above are most often used in description of surface roughness [Sander, 1991].

A1.5. Profilometry

Another method, used to measure surface roughness, is profilometry. In this method a sharp stylus is moved along the surface of the sample and the height information is recorded, thus the profile of the surface is obtained. This method can also be used for film thickness measurements. In this case a good quality step between the uncoated substrate and the film (usually obtained by masking part of the sample during the deposition) is needed. Care should be taken in stylus force selection, as excessive or deficient force will lead to erroneous results.

A1.6. Transmission Electron Microscopy (TEM)

Transmission electron microscopy is a technique, providing information on structure of very thin samples, through which electrons can be transmitted [Ohring, 1992]. The popularity of this technique is often based on the high level of resolution of the microscope (theoretically below 2Å). The reason for this lies in the very small

wavelengths λ (Å) utilised. (The de Broglie relation states, that $\lambda = 12.26/\left(\sqrt{E}\sqrt{1+0.9788\times10^{-6}E}\right)$, where E is the electron accelerating potential, therefore, at E=200kV, the wavelength is only 0.0251 Å. [Thomas and Goringe, 1979])

In TEM electrons are generated by an electron gun, accelerated to the required level (usually a few hundred keV) and then focused on the sample (see Figure A1.4). On their way through the sample, electrons can interact elastically with the potential fields of the atomic nuclei of the sample or inelastically with the electrons of the sample. Depending on the type of interaction, two kinds of information can be obtained. Elastic interactions in crystals or polycrystalline materials give rise to diffraction patterns in the form of spots or rings, formed in the back focal plane of the objective lens. The instrumental settings, suitable for this case, are shown in Figure A1.4. Inelastic interactions comprise energy losses and adsorption, which lead to variations in the intensity of the electron beam. Thus, a magnified image can be formed in the image plane and microstructures, present in the sample, can be viewed.

Two ways of image formation exist. In the first method the transmitted and one or more of the diffracted beams, emerging from the sample, are recombined with both their amplitude and phase preserved. This method is called phase contrast imaging and is used when diffracting planes or individual atoms are to be identified. The second method is called amplitude contrast imaging and uses only one of all the available beams. Here two types of images are possible. If the transmitted beam is used, the formed image will be called bright-field image. If only one of the diffracted beams is utilised, with all other beams blocked, the resulting image is called dark-field image. It should be noted that for effective characterisation of complex microstructures, both diffraction pattern and bright and dark-field images are important.

Thus, it can be seen that TEM is a powerful tool for visualisation and characterisation of sample structure. However, stringent requirements on sample preparation for TEM often make this technique extremely time-consuming.

A1.7. X-Ray Photoelectron Spectroscopy (XPS)

X-Ray Photoelectron Spectroscopy (XPS), also called electron spectroscopy for chemical analysis (ESCA), is a well-established technique for chemical analysis of materials. Contrary to RBS, XPS not only provides information on the material components and their ratios, but also on the chemical bonding in the material, thus

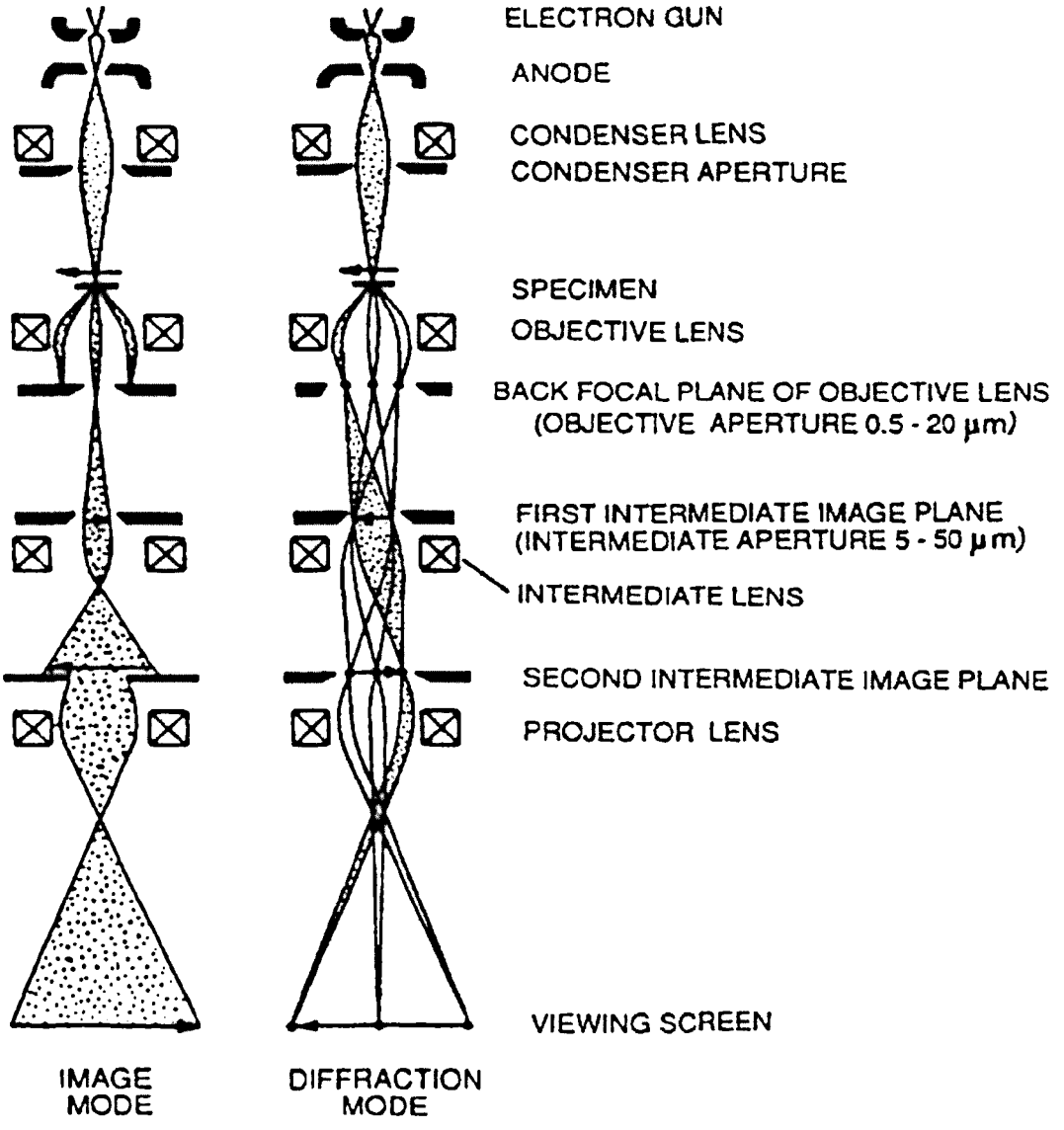

Figure A1.4. Principles of TEM operation in image and diffraction modes [Thomas and Goringe, 1979].

allowing to establish, for example, which particular compounds constitute the thin film under analysis. XPS is a true surface technique with the upper limit for sampling depth usually cited at 2-5 nm [Watts, 1994]. The spatial resolution in XPS depends on the design of the experimental equipment and varies between a few micrometers to a few millimetres with the resulting spectra being averaged out along the sampling area.

The technique of XPS is based on the interaction of X-ray photons with a sample. During the experiment, the sample under analysis is irradiated by X-ray photons with energy $h\nu$ (usually produced by an MgKα or AlKα source). These photons transfer their energy to the electrons of the surface atoms, which leads to ejection of photoelectrons. This process is illustrated in Figure A1.5. The ejected photoelectrons are then detected and their energy E is measured. It is known, that

$$E = h\nu - E_b - \varphi - \delta E, \tag{A1.15}$$

where E_b is the binding energy of electron, φ is the spectrometer work function. XPS analysis can be applied to insulators, therefore another term, i.e. electrostatic charging of the sample δE, is introduced. Electrostatic charging causes signals from photoelectrons to be shifted up the energy scale. The common practice of accounting for this shift is to calibrate using the C1s signal at 285.0 eV [Watts, 1994].

The binding energy of the electron depends on the species and the atomic level, from which this electron originates. The correlation between these parameters is unique, which facilitates the chemical analysis by XPS. Chemical bonding of the elements causes shifts in energy levels of electrons in atoms. This makes it possible to distinguish between different types of compounds, present in the sample. For example, it is possible to observe changes in the signal position for photoelectrons emitted from atoms of a pure metal and its oxide.

In practice, the XPS instrument is often equipped with ion-beam gun, so that removal of surface contaminants or depth profiling of the sample will be possible. However, one should use this facility with caution to avoid the problem of distinguishing between real sample features and bombardment-induced effects.

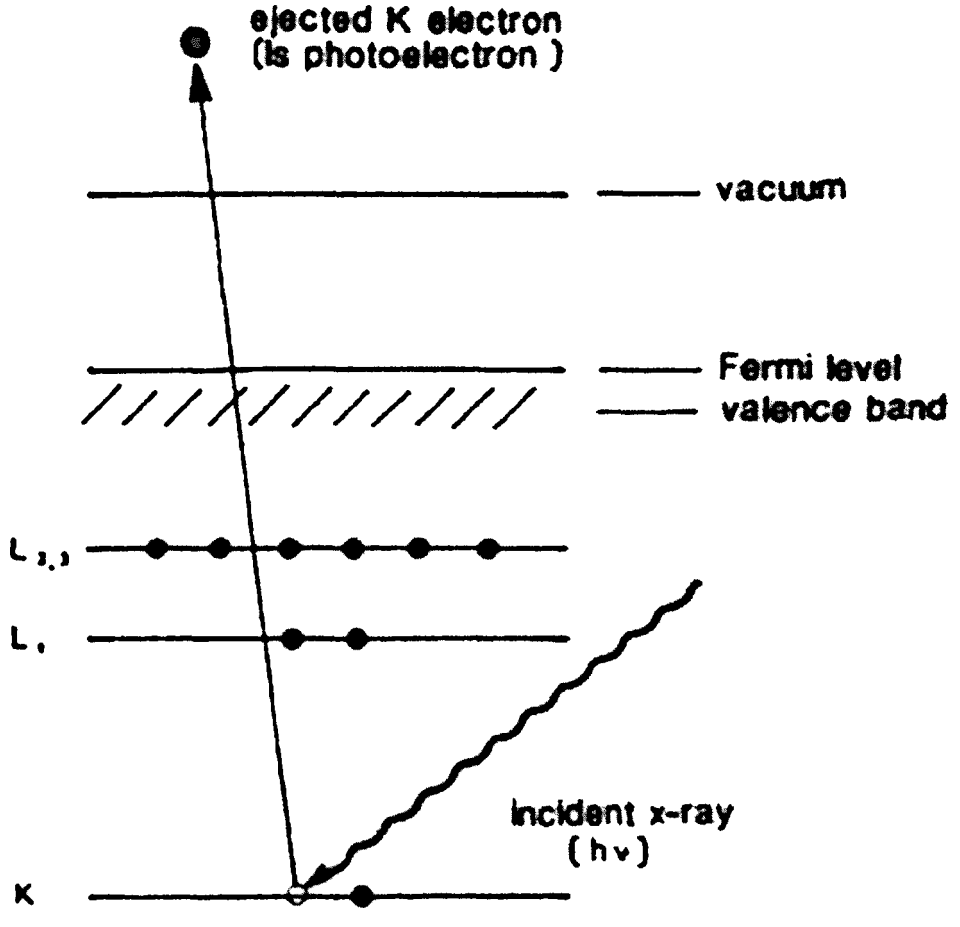

Figure A1.5. Principles of XPS – electron photoemission [Watts, 1994].

References

AFM on the Web – see, for example,

http://www.chembio.uoguelph.ca/educmat/chm729/afm/princip.htm

http://stm2.nrl.navy.mil/how-afm/how-afm.html

http://www.thermomicro.com/spmguide

http://www.di.com/appNotes/AmLab/AL-SPMmain.html

Cervo M., *A Study of the Deposition of Oxide Thin Films by Ion Beam Techniques,* PhD Thesis, The University of Salford, 1994

Chu W.-K., Mayer J.W. and Nicolett M.-A., *Backscattering Spectrometry*, Academic Press, Inc., New York, 1978

Earwaker L.G., *Rutherford Backscattering and Nuclear Reaction Analysis*, in *Surface Science Techniques*, ed. by J.M. Walls and R. Smith, Pergamon, 1994

Eckertova L., *Physics of Thin Films*, Plenum Press, New York and London, 1986

Forouhi A.R., Bloomer I., Phys.Rev. B, *34(10)*, (1986), 7018

Gauthier-Manuel B., Meas. Sci, Technol., *9*, (1998), 485

Ion Implantation, Sputtering and Their Applications, ed. by P.D. Townsend, J.C. Kelly, N.E.W. Hartley, Academic Press Inc. (London) Ltd., 1976

Kubinyi M., Benko N., Grofcsik A., Jones W. Jeremy, Thin Solid Films, *286*, (1996), 164

Long D.A., *Raman Spectroscopy*, McGraw-Hill, Inc., 1977

Manifacier J.C., Gasiot J. and Fillard J.P., J. of Phys. E: Sci. Instr., *9*, (1976), 1002

Marquardt D.W., J. Soc. Indust. Appl. Math., *11(2)*, (1963), 431

Minkov D. and Swanepoel R., Optical Engineering, *32(12)*, (1993), 3333

Mullerova J., Mudron J., Acta Physica Slovaca, *50(4)*, (2000), 477

Nenkov M. and Pencheva T., J. Opt. Soc. Am. A, *15(7)*, (1998), 1852

Ohring M., *The Materials Science of Thin Films,* Academic Press, Inc., 1992

Sander M., *A Practical Guide to the Assessment of Surface Texture*, Feinpruf GmbH, Gottingen, Germany, 1991

Thomas G., Goringe M.J., *Transmission Electron Microscopy of Materials*, A Wiley-Interschience Publication, 1979

Virtual Raman Tutorial, Kaiser Optical Systems, Inc., 1996-2002
http://www.kosi.com/raman/applications/ramantutorial/index.html

Watts J.F., *X-ray Photoelectron Spectroscopy*, in *Surface Science Techniques*, ed. by J.M. Walls and R. Smith, Pergamon, 1994

Wilson I.H., *Scanning Tunelling Microscopy*, in *Surface Science Techniques*, ed. by J.M. Walls and R. Smith, Pergamon, 1994